



# UCAM

UNIVERSIDAD CATÓLICA  
DE MURCIA

ESCUELA INTERNACIONAL DE DOCTORADO

Programa de Doctorado en Ciencias de la Salud

TESIS DOCTORAL

**Development of improved methodologies for the discovery  
of novel bioactive compounds and their application to  
problems of biomedical relevance**

Autora:

Dña. Helena den Haan Alonso

Directores:

Dr. D. Horacio Emilio Pérez Sánchez

Dr. D. José Manuel Villalgordo Soto

Dr. D. Alfonso Pérez Garrido

Murcia, 23 de septiembre 2019





# UCAM

UNIVERSIDAD CATÓLICA  
DE MURCIA

ESCUELA INTERNACIONAL DE DOCTORADO

Programa de Doctorado en Ciencias de la Salud

TESIS DOCTORAL

**Development of improved methodologies for the discovery  
of novel bioactive compounds and their application to  
problems of biomedical relevance**

Autora:

Dña. Helena den Haan Alonso

Directores:

Dr. D. Horacio Emilio Pérez Sánchez

Dr. D. José Manuel Villalgordo Soto

Dr. D. Alfonso Pérez Garrido

Murcia, 23 de septiembre 2019





# UCAM

UNIVERSIDAD CATÓLICA  
DE MURCIA

## AUTHORIZATION OF THE DIRECTORS OF THE THESIS FOR SUBMISSION

Prof. Dr. Horacio Emilio Pérez Sánchez, Prof. Dr. D. José Manuel Villalgordo Soto and Prof. Dr. D. Alfonso Pérez Garrido as Directors<sup>1</sup> of the Doctoral Thesis “Development of improved methodologies for the discovery of novel bioactive compounds and their application to problems of biomedical relevance”, by Mrs. Helena den Haan Alonso in the Escuela Internacional de Doctorado (EIDUCAM), **authorize for submission** as a compendium Thesis since it has the conditions necessary for its defense.

We sign, to comply with the Reales Decretos 99/2011, 1393/2007, 56/2005 and 778/98, in Murcia, 20th September 2019.

Prof. Dr. Horacio Pérez Sánchez

Prof. Dr. José Manuel Villalgordo Soto

Prof. Dr. Alfonso Pérez Garrido

---

<sup>1</sup>If the Thesis is directed by more than one Director, all of them must be indicated and they all have to sign.



*to my family,*





## Acknowledgements

It seems like only yesterday I started this road. Looking back, I am happy with the work done and the trajectory followed, and I feel an enormous gratitude to all the people who have supported me all this time.

I would like to begin by thanking the Catholic University San Antonio of Murcia and the company Eurofins-Villapharma for trusting me and giving me the opportunity to work in this thesis, providing not only the necessary funding during the three years, but also an exceptional working environment.

The directors of this thesis, José Manuel, Alfonso and Horacio, deserve a special acknowledgement. Thank you all very much for your advice and for teaching me so much. No doubt this work would not have been possible without your guidance and experience. Although all of them have been the driving force behind this thesis, I would especially like to thank Horacio who has also been the rudder. Thank you for the encouragement, for your optimism (and realism when it was needed), thank you for letting me in on so many projects and for how much you have taught me about research.

I cannot forget to thank my office colleagues and, after so much, friends. Ricardo, thank you for your patience and enthusiasm that you put in helping me with programming. Cerón, I never thought I would encounter anyone more absent-minded than me. Thank you for your advice, for the laughter and for everything you have taught me. Thanks especially to Jorge, my life partner, none of this would have been possible without his work. It has been difficult, but thanks to you, it has been possible.

To Frederik for the always fruitful work meetings. For giving me new points of view and making me part of his projects.

To be also grateful to those who put up with you when nobody else does it, who understand you, who make you laugh and disconnect from everything. Thanks to



my friends and family.

To my mother, for her affection, her effort, her generosity and her discipline. To my younger brother, who has become my older brother, my backing. To my aunts and grandmother, my second mothers, and to my uncles, thank you very much for loving me so much, helping me so much. To my cousins, the "little ones" of the house. To my babies, my shelter.

To my father, the jewel. For teaching me that, even in adversity, even without hope, you can find reasons to smile. I carry your rock'n roll, I carry it in my heart.

I'm sorry for all those colleagues at work, at school, at leisure, whom I haven't named because I haven't gone on too long, but who have undoubtedly brought me here. Thank you for everything.

To all of you, I owe a lot, I love you more.



## Abstract

Cheminformatics is a discipline that has positioned itself both in the world of academic research and in the industrial field as a fundamental tool given its high efficiency/cost ratio. However, it also has certain limitations that have been addressed in the development of this industrial thesis.

The principal objective on which this work is based is fundamentally to apply methodological improvements in cheminformatic techniques for the discovery of new bioactive compounds against different therapeutic targets, both in an academic and industrial context.

The computational techniques used are based on both ligand structure (pharmacophore modeling, QSAR, three-dimensional similarity) and protein structure (docking and molecular dynamics). Some of the therapeutic targets studied have been Zika virus protease NS2B-NS3, acetyl and butyrylcholinesterase enzymes, the  $\alpha$ -galactosidase enzyme and various proteins involved in diabetes.

The first contribution of this thesis (which is presented as a compendium of publications) investigated the discovery of a pharmacological chaperone for the enzyme  $\alpha$ -galactosidase with the ability to bind to the enzyme in a region other than the active site of the enzyme so that it would stabilize its three-dimensional structure and recover its functionality without inhibiting it at high concentrations as Migalastat (the only drug approved by the Food and Drug Administration for the treatment of Fabry disease) does. Using a combined strategy of virtual screening based on the three-dimensional shape of the chemical compounds and the modeling of the molecular coupling we discovered a compound, 2,6-ditiopurine, which after laboratory tests was found to be able to stabilize and promote the maturation of the enzyme.

In the following three contributions, docking techniques were used to describe the potential mechanism of action as acetyl and butyrylcholinesterase inhibitors of N-acetyl-tryptophan compounds, different classes of tanshinones, rosmarinic acid, hyperforin and hyguanin C. In all these cases, our simulation results predict that

more stable binding of these compounds with enzymes takes place in the active site of the same, so that the compounds would block the entry of the substrate, which would explain their activity as inhibitors.

In the penultimate contribution we screened Drugbank (Law et al., 2013), a public database containing FDA-approved drugs and compounds used in clinical research) for searching compounds suitable for the treatment of Zika virus infection. In this case, protease NS2B-NS3 was selected as a therapeutic target for which 8 enzyme-inhibiting compounds were found by means of structure based virtual screening. Of these, the Novobiocin compound proved to inhibit both the protein *in vitro* and *in vivo*, obtaining 100% survival of the animal models used for the experiment.

An on-line platform was finally developed for the identification of new anti-diabetic compounds. This thesis presents a work derived from the use of this platform to carry out an inverse screening and identify the potential therapeutic target of different natural compounds. We have found bibliographic evidences of experimental validation for eight of the compounds for which the computational method predicted a possible therapeutic target confirming the they have certain activity.

**Keywords:** *Docking, pharmacophore modeling, cheminformatics, Fabry disease, cholinesterase, Zika, diabetes.*

## Resumen

La quimioinformática es una disciplina que se ha posicionado tanto en el mundo de la investigación académica como en el ámbito industrial como una herramienta fundamental dado su alto ratio de eficacia/coste. Aunque también tiene ciertas limitaciones que se han abordado en el desarrollo de esta tesis industrial.

El objetivo fundamental en el que se basa este trabajo son fundamentalmente aplicar mejoras metodológicas de las técnicas quimioinformáticas para el descubrimiento de nuevos compuestos bioactivos frente a distintas dianas terapéuticas, tanto en un contexto académico como industrial.

Las técnicas computacionales empleadas se basan tanto en la estructura del ligando (modelado farmacofórico, QSAR, similitud tridimensional) como en la de la proteína (modelado del acoplamiento molecular (*docking*) y dinámica molecular). Algunas de las dianas terapéuticas objeto de estudio han sido la proteasa NS2B-NS3 del virus Zika, las enzimas acetil y butirilcolinesterasa, la enzima  $\alpha$ -galactosidasa y diversas proteínas involucradas en la diabetes.

En la primera contribución de esta tesis (que se presenta como un compendio de publicaciones) se investigó el descubrimiento de una chaperona farmacológica para la enzima  $\alpha$ -galactosidasa con capacidad de unirse a la enzima en una región distinta al sitio activo de la enzima de manera que estabilizase su estructura tridimensional y recuperase la funcionalidad de la misma sin inhibirla a elevadas concentraciones como lo hace Migalastat (único fármaco aprobado por la *Food and Drug Administration* para el tratamiento de la enfermedad de Fabry). Usando una estrategia combinada de cribado virtual basado en la forma tridimensional de los compuestos químicos y el modelado del acoplamiento molecular descubrimos un compuesto, 2,6-ditiopurina, que una vez realizadas las pruebas de laboratorio se observó que era capaz de estabilizar y promover la maduración de la enzima.

En las siguientes tres contribuciones se emplearon técnicas de *docking* para describir el potencial mecanismo de acción como inhibidores de acetil y butirilcolinesterasa de los compuestos N-Acetil-triptófano, distintas clases de *tanshinones*, ácido

rosmarínico, hiperforina e *hyguanin C*. En todos estos casos los resultados de nuestra simulación predicen que la unión más estable de estos compuestos con las enzimas tiene lugar en el sitio activo de la misma, de manera que bloquearían la entrada del sustrato de las mismas, lo que explicaría su actividad como inhibidores.

En la penúltima contribución se filtró la base de datos Drugbank (Law et al., 2013) (base de datos pública que contiene tanto fármacos aprobados para su uso clínico como compuestos actualmente en fases de investigación) en busca de un compuesto adecuado para el tratamiento de la infección por virus Zika. En este caso se seleccionó la proteasa NS2B-NS3 como diana terapéutica para la que, mediante técnicas de cribado virtual basado en estructura, se encontraron 8 compuestos inhibidores de la enzima. De todos ellos el compuesto Novobiocina demostró inhibir la proteína tanto *in vitro* como *in vivo*, obteniendo un 100 % de supervivencia de los modelos animales empleados para el experimento.

Finalmente se participó en el desarrollo de una plataforma *web*, *DIA-DB* para la identificación de nuevos compuestos antidiabéticos. En esta tesis se presenta un trabajo derivado del uso de esta plataforma para llevar a cabo un cribado inverso e identificar la potencial diana terapéutica de distintos compuestos naturales. Para ocho de los compuestos para los que el método computacional predijo una posible diana terapéutica se han encontrado evidencias experimentales en la bibliografía.

**Palabras clave:** *Simulación del acoplamiento molecular, modelado farmacofórico, quimioinformática, enfermedad de Fabry, colinesterasa, Zika, diabetes.*



# Index

<b>1</b>	<b>Introduction</b>	<b>1</b>
1.1	Objectives . . . . .	3
1.2	Structure of the Dissertation . . . . .	4
<b>2</b>	<b>Articles that are part of the doctoral thesis</b>	<b>7</b>
2.1	Fundamentals of the doctoral thesis . . . . .	7
2.2	Identification of an Allosteric Binding Site on Human Lysosomal Alpha-Galactosidase Opens the Way to New Pharmacological Chaperones for Fabry Disease . . . . .	9
2.3	Selective <i>in vitro</i> and <i>in silico</i> butyrylcholinesterase inhibitory activity of diterpenes and rosmarinic acid isolated from <i>Perovskia atriplicifolia Benth.</i> and <i>Salvia glutinosa L.</i> . . . . .	25
2.4	Acetylcholinesterase inhibitory assessment of isolated constituents from <i>Salsola grandis</i> Freitag, Vural & Adıgüzel and molecular modeling studies on N-acetyltryptophan . . . . .	38
2.5	Profiling Auspicious Butyrylcholinesterase Inhibitory Activity of Two Herbal Molecules: Hyperforin and Hyuganin C . . . . .	45
2.6	Selective <i>in vitro</i> and <i>in silico</i> cholinesterase inhibitory activity of isoflavones and stilbenes from <i>Belamcandae chinensis rhizoma</i> . . . . .	54
2.7	Structure-based discovery of clinically approved drugs as Zika virus NS2B-NS3 protease inhibitors that potently inhibit Zika virus infection <i>in vitro</i> and <i>in vivo</i> . . . . .	67
2.8	Exploring African Medicinal Plants for Potential Anti-Diabetic Compounds with the DIA-DB Inverse Virtual Screening Web Server . . . . .	79

---

<b>3</b>	<b>Industrial part of the thesis</b>	<b>111</b>
3.1	Introduction . . . . .	111
3.2	Discovery and optimization of bioactive compounds in the context of Cancer . . . . .	112
3.3	Discovery of bioactive compounds enhancers of the cystic fibrosis transmembrane regulating protein (CFTR) . . . . .	114
<b>4</b>	<b>Conclusions and outlook</b>	<b>117</b>
4.1	Conclusions . . . . .	117
4.1.1	Discovery of a novel pharmacological chaperone for the treat- ment of Fabry disease . . . . .	117
4.1.2	Description of the mode of action of cholinesterase-inhibiting bioactive compounds . . . . .	118
4.1.3	Repositioning of an antibiotic as a NS2B-NS3 protease in- hibitor for the treatment of Zika virus infection. . . . .	120
4.1.4	Development of a virtual screening platform for the identifi- cation of new anti-diabetic compounds . . . . .	121
4.2	Outlook . . . . .	122
<b>5</b>	<b>Publications, collaborations and quality of journals</b>	<b>125</b>
5.1	Collaborations and other publications . . . . .	125
5.1.1	Publications in journals indexed in ISI . . . . .	125
5.1.2	Editorials . . . . .	127
5.1.3	Preprints . . . . .	127
5.1.4	Congresses . . . . .	127
5.1.5	Patents . . . . .	128
5.2	Data on quality of publications . . . . .	128
5.2.1	Identification of an allosteric binding site on human lysoso- mal alpha-galactosidase opens the way to new pharmacolog- ical chaperones for Fabry disease - <i>PLOS ONE</i> . . . . .	129

---

5.2.2	Selective <i>in vitro</i> and <i>in silico</i> butyrylcholinesterase inhibitory activity of diterpenes and rosmarinic acid isolated from <i>Perovskia atriplicifolia</i> Benth. and <i>Salvia glutinosa</i> L. - <i>Phytochemistry</i> . . . . .	130
5.2.3	Acetylcholinesterase inhibitory assessment of isolated constituents from <i>Salsola grandis</i> Freitag, Vural & Adıgüzel and molecular modeling studies on N-acetyltryptophan - <i>Phytochemistry Letters</i> . . . . .	131
5.2.4	Profiling Auspicious Butyrylcholinesterase Inhibitory Activity of Two Herbal Molecules: Hyperforin and Hyuganin C - <i>Chemistry &amp; Biodiversity</i> . . . . .	133
5.2.5	Selective <i>in vitro</i> and <i>in silico</i> cholinesterase inhibitory activity of isoflavones and stilbenes from <i>Belamcandae chinensis rhizoma</i> - <i>Phytochemistry letters</i> . . . . .	134
5.2.6	Structure-based discovery of clinically approved drugs as Zika virus NS2B-NS3 protease inhibitors that potently inhibit Zika virus infection <i>in vitro</i> and <i>in vivo</i> - <i>Antiviral Research</i> . .	135
5.2.7	Exploring African Medicinal Plants for Potential Anti-Diabetic Compounds with the DIA-DB Inverse Virtual Screening Web Server - <i>Molecules (MDPI)</i> . . . . .	137
	<b>References</b>	<b>139</b>



# Chapter 1

## Introduction

At present, one of the most important challenges in the field of health and social security is the discovery of novel bioactive compounds to deal with problems of pharmacological relevance or where previously known compounds are not sufficiently effective (Drews, 2000). Traditionally the Pharma industry has dealt with the study of such challenges, due to the great expense this implies and the technical difficulties involved (Khanna, 2012).

However, for the last two decades new methodologies based on computational chemistry and cheminformatics have been developed to speed up these discoveries, which can be carried out efficiently in an academic environment at a much lower cost (Kola and Landis, 2004). Cheminformatics is a discipline that consists in the use of computers and computer programs (Jorgensen, 2004) to look for solutions to problems related to the field of chemistry. The relationship between computer science and chemistry has been going on for more than 50 years, being the decades of the 70's and 80's when the field was born (Brown et al., 1998). However, it was not until the 90's when the first references to this discipline appeared by its name. Since then this field has been gaining importance both in industry and in academic research as inferred from the impact it has on publications in recent years. There is no single definition that can be used to describe this area. David Wild defined it as "the field that studies all aspects related to the representation and use of chemical

and biological information related to it by means of the computers” (Wild and Wiggins, 2006). Perhaps one of the broadest definitions was stated by Frank Brown Brown et al. (1998) who defined it as “the combination of those technological and management resources used to transform data into information and information into knowledge for the purpose of making better decisions more rapidly in the field of discovery and optimization of new drugs”.

This thesis is based on the following core objectives; a) the use of cheminformatic techniques for the discovery of novel bioactive compounds, and b) the use of these same techniques to identify the parts of the compounds that are potentially responsible for this activity as well as the type of interactions that are established between the compound and the therapeutic target at the binding site (Schenone et al., 2013). However, this methodology and others used by a large number of scientists continue to have certain limitations in terms of predictive capacity and data processing speed (Schneider, 2010), two extremely important factors for successfully carrying out this type of project. In this thesis, some relevant limitations in these methods have been identified and we proposed some solutions. The improvements in both processing speed and predictive quality studied in this thesis have been applied at the same time to different contexts of pharmacological relevance. For this purpose, different computational techniques have been used that can be grouped into techniques based on the chemical structure of the ligands (Ripphausen et al., 2011) and techniques based on the structure of the therapeutic targets (Lyne, 2002).

In this thesis, therefore, the practicability of cheminformatics techniques has been demonstrated by applying a multidisciplinary research process (chemistry, biology, physics) with the exploitation of high-performance parallel computational architectures such as supercomputers, grids, clusters, etc. (Banegas-Luna et al., 2019).

Finally, it should be noted that this work has been carried out both in academic contexts, where all the results obtained have been published and which form the skeleton of this compilation, and in industrial contexts, where, due to reasons of

confidentiality, none of the results obtained could be published.

## 1.1 Objectives

The objectives on which the dissertation is based are listed and summarized below. These objectives have been oriented towards three main lines of work: *a)* the methodological improvement of chemoinformatic techniques, *b)* the application of these improvements to contexts of pharmacological relevance in the academic world, and *c)* the exploitation of the aforementioned improvements in industrial drug discovery projects.

- **Objective 1. To improve chemoinformatic techniques methodologies.** This objective aims to propose methodological improvements to deal with some limitations in cheminformatics techniques. Specifically, the aim is to work on methods for proposing allosteric pharmacological chaperones (Leidenheimer and Ryder, 2014), on improving the strategies and analytical capacity of virtual screening techniques based on both the protein structure (Ghosh et al., 2006) and the ligands (Banegas-Luna et al., 2018), and on the exploitation of chemical information in polypharmacological contexts.
- **Objective 2. Apply the resulting improvements in the context of Fabry disease.** Different techniques from Objective 1 will be applied to discover allosteric molecular chaperones in the context of Fabry disease (Germain, 2010).
- **Objective 3. To use the improved methods for describing the mode of action of bioactive compounds that inhibit acetylcholinesterase.** Advances and improvements in the objective 1 will be implemented to analyze experimental results obtained in the context of cholinesterase-inhibiting bioactive compounds (Birks, 2006) to better describe their modes of action.
- **Objective 4. To apply the obtained improvements in the discovery of inhibitors against the Zika virus.** We will apply the methodological novelties

of the objective 1 to the discovery of novel inhibitors in the context of the Zika virus (Mlakar et al., 2016).

- **Objective 5. Exploiting the improvements mentioned in industrial projects.** The methodological improvements obtained in the objective 1 will be used to work in a variety of pharmaceutical drug discovery industrial projects bound by confidentiality agreements (Gray, 2006).

## 1.2 Structure of the Dissertation

In this section and with the purpose of facilitating the reading of this doctoral thesis, its composition is briefly indicated according to the chapters that make it up.

- *Chapter 1: Introduction.*

It is a presentation and contextualization of the main problem from which this thesis derives, the attack approaches that are addressed and the main objectives that are intended to be achieved are enumerated.

- *Chapter 2: Articles that are part of the doctoral thesis.* The rationale of this thesis is explained in relation to the main published scientific papers and how these articles form the compendium, connecting them to the initial proposed objectives.

- *Chapter 3: Projects with company intellectual property results.*

The industrial projects worked within Eurofins-Villapharma are briefly discussed due to confidentiality reasons.

- *Chapter 4: Conclusions and outlook.*

In this part, the main conclusions obtained as a result of the work on the stated objectives are mentioned. It also lists directions for potential future work.

- *Chapter 5: Publications, collaborations and quality of journals.*



The most important quality indexes of the publications that make up the compendium of this dissertation are detailed in this last section. Other results obtained in this Industrial PhD thesis are also indicated.

- *Bibliography.*

This section includes bibliographical details about the most relevant works cited in this thesis by compendium.



## Chapter 2

# Articles that are part of the doctoral thesis

### 2.1 Fundamentals of the doctoral thesis

The following sections of this chapter include scientific publications in high-impact indexed international journals that justify this doctoral thesis by compendium, and that fulfill the initially proposed objectives.

In the first publication (section 2.2) we worked on the design of methodological improvements in the context of Fabry disease (Citro et al., 2016). In this lysosomal storage disease, patients have mutations in the enzyme alpha-galactosidase which affects the structure of the enzyme which prevents it from performing its biological function correctly. Work was conducted to discover new allosteric pharmacological chaperones that could stabilize the enzyme.

The context of the detailed analysis of the modes of action of cholinesterase-inhibiting bioactive compounds led to four of the publications in this compendium (Senol et al., 2017; Orhan et al., 2017, 2019; Ślusarczyk et al., 2019), as it can be seen in the sections 2.3, 2.4, 2.5 and 2.6. In these cases some methodologic improvements were developed in order to propose which parts of these molecules interacted with the active sites of the implicated cholinesterase enzymes.

The following publication (section 2.7) details how drugs already approved by the FDA were repositioned as potent inhibitors of the Zika virus (Yuan et al., 2017) thanks to the methodological advances that were made. At the same time, an international patent was filed for one of these compounds.

In the last of the publications, section 2.8, efforts were made to process different sources of chemical data, both based on protein structure and ligands, in order to study the anti-diabetic potential of a wide variety of bioactive compounds from African medicinal plants (Pereira et al., 2019).

## 2.2 Identification of an Allosteric Binding Site on Human Lysosomal Alpha-Galactosidase Opens the Way to New Pharmacological Chaperones for Fabry Disease

<b>Title</b>	<i>Identification of an Allosteric Binding Site on Human Lysosomal Alpha-Galactosidase Opens the Way to New Pharmacological Chaperones for Fabry Disease</i>
<b>Authors</b>	Valentina Citro, Jorge Peña García, Helena den Haan, Horacio Pérez Sánchez, Rosita Del Prete, Ludovica Liguori, Chiara Cimaruta, Jan Lukas, Maria Vittoria Cubellis, Giuseppina Andreotti
<b>Journal</b>	<i>Plos One</i>
<b>Year</b>	2016
<b>State</b>	Published

### PhD candidate contribution

Helena den Haan Alonso, declares to be the co-author and contributor of the article *Identification of an Allosteric Binding Site on Human Lysosomal Alpha-Galactosidase Opens the Way to New Pharmacological Chaperones for Fabry Disease* in the section on computational chemistry.

## RESEARCH ARTICLE

# Identification of an Allosteric Binding Site on Human Lysosomal Alpha-Galactosidase Opens the Way to New Pharmacological Chaperones for Fabry Disease

Valentina Citro<sup>1</sup>✉, Jorge Peña-García<sup>2</sup>✉, Helena den-Haan<sup>2</sup>, Horacio Pérez-Sánchez<sup>2\*</sup>, Rosita Del Prete<sup>1</sup>, Ludovica Liguori<sup>1,3</sup>, Chiara Cimmaruta<sup>1,3</sup>, Jan Lukas<sup>4</sup>, Maria Vittoria Cubellis<sup>1\*</sup>, Giuseppe Andreotti<sup>3</sup>

**1** Dipartimento di Biologia, Università Federico II, Napoli, 80126, Italy, **2** Bioinformatics and High Performance Computing Research Group (BIO-HPC), Computer Engineering Department, Universidad Católica San Antonio de Murcia (UCAM), Spain, **3** Istituto di Chimica Biomolecolare—CNR, Pozzuoli, 80078, Italy, **4** Albrecht-Kossel-Institute for Neuroregeneration, Medical University Rostock, Rostock, Germany

✉ These authors contributed equally to this work.

\* [cubellis@unina.it](mailto:cubellis@unina.it) (MVC); [hperes@ucam.edu](mailto:hperes@ucam.edu) (HPS)


 OPEN ACCESS

**Citation:** Citro V, Peña-García J, den-Haan H, Pérez-Sánchez H, Del Prete R, Liguori L, et al. (2016) Identification of an Allosteric Binding Site on Human Lysosomal Alpha-Galactosidase Opens the Way to New Pharmacological Chaperones for Fabry Disease. PLoS ONE 11(10): e0165463. doi:10.1371/journal.pone.0165463

**Editor:** Stephan N. Witt, Louisiana State University Health Sciences Center, UNITED STATES

**Received:** May 10, 2016

**Accepted:** October 12, 2016

**Published:** October 27, 2016

**Copyright:** © 2016 Citro et al. This is an open access article distributed under the terms of the [Creative Commons Attribution License](https://creativecommons.org/licenses/by/4.0/), which permits unrestricted use, distribution, and reproduction in any medium, provided the original author and source are credited.

**Data Availability Statement:** All data are included in the paper and in its Supporting Information files.

**Funding:** Funding was provided by Telethon - Italy (Grant no. GGP12108). This work was partially supported by the Fundación Séneca del Centro de Coordinación de la Investigación de la Región de Murcia under Project 18946/JLI/13. Powered@NLHPC: This research was partially supported by the supercomputing infrastructure of the NLHPC (ECM-02). The funders had no role in

## Abstract

Personalized therapies are required for Fabry disease due to its large phenotypic spectrum and numerous different genotypes. In principle, missense mutations that do not affect the active site could be rescued with pharmacological chaperones. At present pharmacological chaperones for Fabry disease bind the active site and couple a stabilizing effect, which is required, to an inhibitory effect, which is deleterious. By *in silico* docking we identified an allosteric hot-spot for ligand binding where a drug-like compound, 2,6-dithiopurine, binds preferentially. 2,6-dithiopurine stabilizes lysosomal alpha-galactosidase *in vitro* and rescues a mutant that is not responsive to a mono-therapy with previously described pharmacological chaperones, 1-deoxygalactonojirimycin and galactose in a cell based assay.

## Introduction

Fabry disease (FD) is a rare pathology, but accounts for 8.8% of the patients affected by inherited disorders of metabolism [1]. It is caused by mutations in the gene *GLA*, which is located on the X chromosome and encodes lysosomal alpha-galactosidase (AGAL) [2]. Enzyme replacement (ERT) is the only approved specific therapy for FD; it is well tolerated and safe [3]. The large phenotypic and genotypic spectrum of the disease poses several problems and the cost-effectiveness of ERT is still debated, in particular for patients who have residual enzyme activity [4]. In FD, about 40% of all missense mutations are associated with a biochemically mildly damaged enzyme [5]. A therapy with sub-inhibitory concentrations of 1-deoxygalactonojirimycin (DGJ) was first proposed by Suzuki and co-workers [6] and then tested in cells [7–13], in mouse models of FD [14] [15] and in clinical trials [16] [17]. Such therapy is suitable

study design, data collection and analysis, decision to publish, or preparation of the manuscript.

**Competing Interests:** The authors have declared that no competing interests exist.

**Abbreviations:** FD, Fabry disease; AGAL, lysosomal alpha-galactosidase; ERT, Enzyme replacement therapy; DGJ, 1-deoxygalactonojirimycin; DTP, 2,6-dithiopurine; GLA, alpha-D-galactose; GAL, beta-D-galactose.

only for patients carrying specific mutations (40%-60% of missense mutants tested in cell based assays [11, 12]) and requires fine-tuning of the dosage regimen because DGJ is an inhibitor of AGAL. The approach with small molecules for FD is promising, but DGJ is not yet the ideal drug. Molecules that either substitute DGJ or act in synergy with it to enable reduced dosage of DGJ should be sought, in particular for mutants that do not respond to a monotherapy with DGJ. Analogues of DGJ have been developed [18] [19]. A new family of arylthioureas showed a better balance between the stabilizing effect, which is required, and the inhibitory effect, which is detrimental [20]. However, these molecules bind the active site, as demonstrated by x-ray crystallography, and enhance enzymatic activity only at micromolar concentration, not dissimilarly from DGJ, when administered to eukaryotic cells expressing AGAL mutants [20].

Ambroxol, a mucolytic agent used in the treatment of respiratory diseases, proved to be useful in association with DGJ to rescue some AGAL mutants [21]. Its mechanism of action is not clear since ambroxol is not specific for AGAL, but it is effective also on lysosomal beta-glucocerebrosidase [22] and alpha-glucosidase mutants [21].

Discovery of chaperones directed against the active site is facilitated by focusing on molecules with structural similarity to galactose, a natural product of AGAL. Conversely, the discovery allosteric ligands, i.e. ligands that bind AGAL at sites outside the active site, is complicated by the fact that they may not chemically resemble any known substrates or products. We performed *in silico* molecular docking (virtual screening) of over ten thousand low molecular weight structurally diverse compounds previously filtered from ZINC database [23], by looking for molecules that bind preferentially at a site different from the active site. Among the top ranking hits we found one molecule, 2,6-dithiopurine (DTP). This molecule was chosen for further studies since it has already passed some safety tests, is a known chemopreventive agent [24] [25] and it is safe when administered to mice [26]. DTP is able to stabilize AGAL against thermal and urea-induced denaturation and is able to rescue a mutant that is not sensitive to DGJ. It acts *in vivo* in synergy with galactose and with very low concentrations of DGJ.

## Methods and Materials

### Virtual screening

We selected a random subset of 9 million molecules (including FDA-approved drugs) from the ZINC database [23] for performing the virtual screening calculations in this study. Molecular docking calculations were carried out on the structure deposited in the PDB with the code 3S5Z [27] with the Leadfinder [28] docking program using default parameters. Protein structure 3S5Z contains 2 ligands: alpha-D-galactose (GLA) bound at the active site through D92, D93, K168, E203, R227, D231 (GLA site) and beta-D-galactose (GAL) bound at a different site through D255 and K374 (GAL site). Thus, two boxes (x, y, z dimensions 40 Å), centered on the position occupied by either GLA or GAL, were set for docking. Using the global shape similarity tool WEGA [29] alpha-D-galactose (the natural substrate of AGAL) was processed against the selected compound library and those molecules with the highest values for similarity score, ranging from 0.8 to 0.95, were selected for posterior docking studies. In total ten thousand purchasable molecules obtained after filtering with WEGA were selected for docking.

### Thermal unfolding

Thermal shift assay [30, 31] was adapted as described [32] using commercially available wt-AGAL, Fabrazyme<sup>®</sup> (Genzyme, Cambridge, MA). Melting profiles were recorded under different conditions by thermal shift assay with the StepOne Real-Time PCR System (Applied Biosystems). The protein (0.5–1 mg/mL final concentration) was equilibrated in Na-Hepes 20

mM, NaCl 150 mM, pH 7.4 with Sypro Orange 2.5X (Invitrogen Molecular Probes, lifetechnologies.com), either without ligands or in the presence of ligands (6 mM DTP, 0.040 mM DGJ (SIGMA, Milan, Italy)). The samples were distributed in 48-well PCR plates (0.025 mL in each well), sealed and heated from 20 to 90° at 1°C/min with increments of 0.6°C. The excitation wavelength of 490 nm and the emission wavelength of 575 nm, which are optimal for fluorescein, were adapted to detect Sypro Orange. Melting profiles of recombinant human phosphomannomutase2 were recorded similarly, the only exception was the presence of 1mM MgCl<sub>2</sub> in the buffer. Phosphomannomutase 2 had been expressed and purified as described [33].

In order to verify the reversibility of the effect of DTP on Fabrazyme<sup>®</sup>, the enzyme equilibrated in Na-Hepes 20 mM, NaCl 150 mM, pH 7.4 was incubated for 1 hour at 4°C in the presence of 6 mM DTP dissolved in DMSO, then the sample was dialysed by ultrafiltration (by using Centrifugal ultrafiltration unit 15-mL MWCO 10 kDa, Merck-Millipore). A control experiment was also conducted incubating the enzyme with DMSO and dialysing it. Each dialysed sample was analysed by enzymatic assay (at pH 7.5) and by TSA (the experiment was conducted either in the presence of 6 mM DTP or with only DMSO) as described above.

### Urea-induced unfolding

The experiment was carried out with a method firstly described by Kim et al [34] and adapted as described [35]. In brief, Fabrazyme<sup>®</sup> (0.32 mg/mL) was induced to unfold by urea in Hepes buffer at pH 7.4, with or without DTP 6 mM, in a final volume of 0.028 mL. The enzyme was incubated in the presence of urea concentrations ranging from 0 to 5 M. The samples were incubated at 10°C overnight, then each sample was treated with the appropriate amount of thermolysin necessary to obtain a 1:5 protease to protein ratio in the presence of CaCl<sub>2</sub> (10 mM final concentration). After 1 min incubation at 37°C the reaction was stopped by the addition of EDTA (40 mM final concentration). The samples were separated by SDS-PAGE and coloured by Coomassie Blue Staining, then undigested proteins (Fabrazyme<sup>®</sup> and thermolysin) were quantified with a ChemiDoc XRS (Bio-Rad Laboratories, Hercules, CA-USA). Two rectangular boxes were used to define specific protein bands, one for Fabrazyme<sup>®</sup> and one for thermolysin as shown in [S1 File](#). The intensity of bands was corrected subtracting the appropriate background (adjusted volumes), the ratio between the corrected values was calculated for Fabrazyme<sup>®</sup> and thermolysin in each lane and was plotted against urea concentration.

### Transfection into COS-7 cells

COS-7 cells were cultured in DMEM containing 10% FBS at 37°C and 5% CO<sub>2</sub>. The cells were transfected with individual plasmids containing mutant AGAL-encoding ORF using the LipofectAMINE2000 cationic lipid reagent in suspension [36].

67.5 micrograms of plasmid DNA in 13.5 mL Opti-MEM (Invitrogen) were mixed with 0.135 mL LipofectAMINE2000 reagent (Invitrogen) and incubated for 30 min at room temperature. COS-7 cells were harvested by trypsin treatment and resuspended in DMEM containing 10% FBS.

COS-7 in suspension (40.5 mL) were added to the transfection mix solution, distributed into 27 wells of six-well plates at 60% confluency and allowed to adhere for 5h.

The medium was substituted by fresh DMEM, 10% FBS, 1% DMSO (used to solubilize DTP and ambroxol) (1 mL), and drugs were added either in monotherapy or in binary combination as indicated in the specific figure legends. After 48 h incubation, the cells were washed in PBS (5 times), scraped and harvested by centrifugation. Dry pellets were resuspended in 0.030 mL of water and lysed by freeze-thawing. Three independent transfections were carried out for A230T, C56Y, C63Y, two for the other mutants, E341D, A37T, P40S, M42T, M42V, S126C,



C172G, R118C, Q280K, L300F, L310F and G360C. Water-soluble extracts were used for enzyme assays or western blot. The Bradford colorimetric assay was used for protein quantification [37] using the Bio-Rad Protein Assay with bovine serum albumin as standard.

### Alpha-galactosidase assay

Tests on transfected mutants were carried out as described in [36]. Briefly: cell lysates (1–2 microliters) were added to 38 microliters of AGAL assay buffer (sodium citrate 27 mM-sodium phosphate dibasic 46 mM, 4-methylumbelliferyl- $\alpha$ -D-galactopyranoside 5 mM and N-acetyl-D-galactosamine 100 mM, pH 4.5) and incubated for 0.5–1 h at 37°C. All chemicals were obtained from Sigma. The reaction was stopped by adding 0.360 mL of 1 M sodium carbonate buffer [10]. Fluorescence was detected using a fluorescence spectrophotometer (Cary Eclipse-Varian) at 355 nm excitation and 460 nm emission.

A 4-methylumbelliferone standard curve ranging from 5 nM to 0.025 mM was run in parallel for conversion of fluorescence data to AGAL activity expressed as nmol/mg protein per min.

In order to measure the enzymatic activity in the presence of DTP 6 mM a spectrophotometric assay was run. Fabrazyme (1–2 microliters 0.25 mg/ml) were added to 0.038 mL of AGAL assay buffer (4-Nitrophenyl  $\alpha$ -D-galactopyranoside 17 mM in Hepes 40 mM pH 7.4) and incubated for 3–15 min at 37°C. The reaction was stopped by adding 0.360 mL of 1 M sodium carbonate and the absorbance at 405nm was measured. The assay was conducted in the presence of DTP 6 mM (previously dissolved in DMSO) or DMSO.

### Western blot analysis

Western blot analysis for the detection of AGAL was performed using rabbit polyclonal antibodies (Abcam 70520) and HRP-coniugated anti-rabbit IgG antibody produced in goat (Bio-Rad 1706515). After SDS-PAGE (15% acrylamide), proteins were transferred to a PVDF membrane. The membrane was blocked with 5% (w/v) non-fat dried skimmed milk in blot solution at 4°C overnight, then treated with the primary antibody diluted in a blot solution 1:500 for 1 hour at room temperature. After washing, the detection was performed by using the Precision Plus Protein™ (Bio-Rad). GAPDH was revealed with mouse monoclonal anti lapine GAPDH (AbD seroTec (cat:4699–9555) 1:2000. All other chemicals were from Bio-Rad. Uncropped images of the gels are provided as [S1 File](#).

### Deglycosylation

Deglycosylation of A230T expressed in COS7 cells (treated or untreated with DTP 6 mM) (10  $\mu$ g f each) was performed according to the producer's instructions. wt-AGAL was processed at the same way as a control. Briefly, EDTA and SDS were added to the proteins (final concentrations were 20 mM and 0.1% respectively). The samples were then boiled for 5 min, immediately cooled before the addition of NP-40 to a final condition of 0.7% and N-Glycosidase F (0.5 unit) and incubated overnight at 37°C. A parallel experiment was conducted avoiding the denaturation step (SDS and heating) before adding NP-40. The samples was analysed by western blotting as described elsewhere.

### Bioinformatic and Statistical analysis

Standard deviations and p values (paired two-tailed Student's t-test) were obtained using Microsoft Excel (Microsoft Office professional 2010).

The effect of mutation on protein stability was predicted either running SDM on-line [38] or running MUPRO1.1 [39] locally. Secondary structure was assigned with SEGNO [40]. Accessibility to solvent was calculated by SDM. Active site residues were identified with DrosP [41]. Molecular dynamics was run with Yasara program under default conditions for 50 nsec [42] and flexibility assessed as described [43]. Protein damaging scores based on sequence conservation were derived using PolyPhen-2 software [44] or Fabry\_CEP [45].

## Results

Molecular docking calculations were carried out on the AGAL structure deposited in the pdb with the code 3S5Z [27]. In this model AGAL binds two ligands per chain: alpha-D-galactose at the active site through D92, D93, K168, E203, R227 and D231 (GLA site) and beta-D-galactose at a different site through D255 and K374 (GAL site). This structure offers a good target to identify molecules that have little inhibitory activity and/or act in synergy with drugs directed against the active site. In proximity to the GAL site, we identified a hot-spot for binding that will be referred to as the allosteric site. It comprises residues A37, R38, T39, P40, T41, M42, E87, Y88 and does not overlap with the active site that is lined by W47, D92, D93, Y134, C142, K168, D170, E203, L206, Y207, R227, D231, S297 (Fig 1). The allosteric site is different from the GAL binding site.

We looked for molecules that bind the allosteric site with a high score, but bind the active site with a very low score. Drug repositioning, which should always be considered as the first choice when developing new therapies for rare diseases [46], could not be used because none of the approved drugs tested (FDA database) bound specifically the allosteric site (results not shown).

As a second choice we selected DTP, which is not an approved drug, but is a good candidate because it is safe when tested on human skin cells [25] and on mice [24] [26]. Even if the docking simulations started at GAL site DTP contacted the allosteric site. As a control we carried out a simulation limiting the search to a box centred on the active site as described in the methods. We show the interactions of DTP with the allosteric site in Fig 1B, and the corresponding energetic contributions in Fig 2A, the potential interactions of DTP with the active site (GLA site) in Fig 1C and the corresponding energetic contributions in Fig 2B. Docking simulations calculated a binding affinity at GLA's binding site 52% lower (absolute value) than at the allosteric site (Fig 2). Scores calculated with Leadfinder [28] are reported as kcal/mol in Fig 2, but are meant only for rank-ordering different docking poses of DTP and cannot provide accurate binding energy predictions.

DTP does not inhibit AGAL (Fabrazyme<sup>®</sup>, Genzyme) when tested at 6 mM concentration using 4-Nitrophenyl  $\alpha$ -D-galactopyranoside 17 mM in Hepes 40 mM pH 7.4, whereas DGJ blocks completely the enzyme (1% residual activity) at concentration as low as 0.001 mM. Thermal shift assay was used to evaluate the ability of DTP (6mM) to stabilize wt-AGAL, (Fabrazyme<sup>®</sup>, Genzyme) in the presence or in the absence of DGJ. DTP is able to stabilize the enzyme against thermal denaturation alone or in synergy with the iminosugar (Fig 3A), without forming covalent bonds. To prove the reversibility of this stabilising effect, DTP (6 mM) was incubated with enzyme and subsequently removed by dialysis before thermal shift assay. Results are indicated in Fig 3B (filled squares DTP/DTP; open squares DMSO/DTP; filled circles; DTP/DMSO; open circles DMSO/DMSO) where the first word of the label corresponds to the pretreatment and the second part corresponds to the presence of the compound during the thermal scan. The specificity of effect of DTP was tested running thermal shift assay on phosphomannomutase2, an enzyme structurally and functionally unrelated to AGAL in the presence of DTP 6 mM or a positive control, glucose 1–6 biphosphate 0.5 mM (S1 Fig).

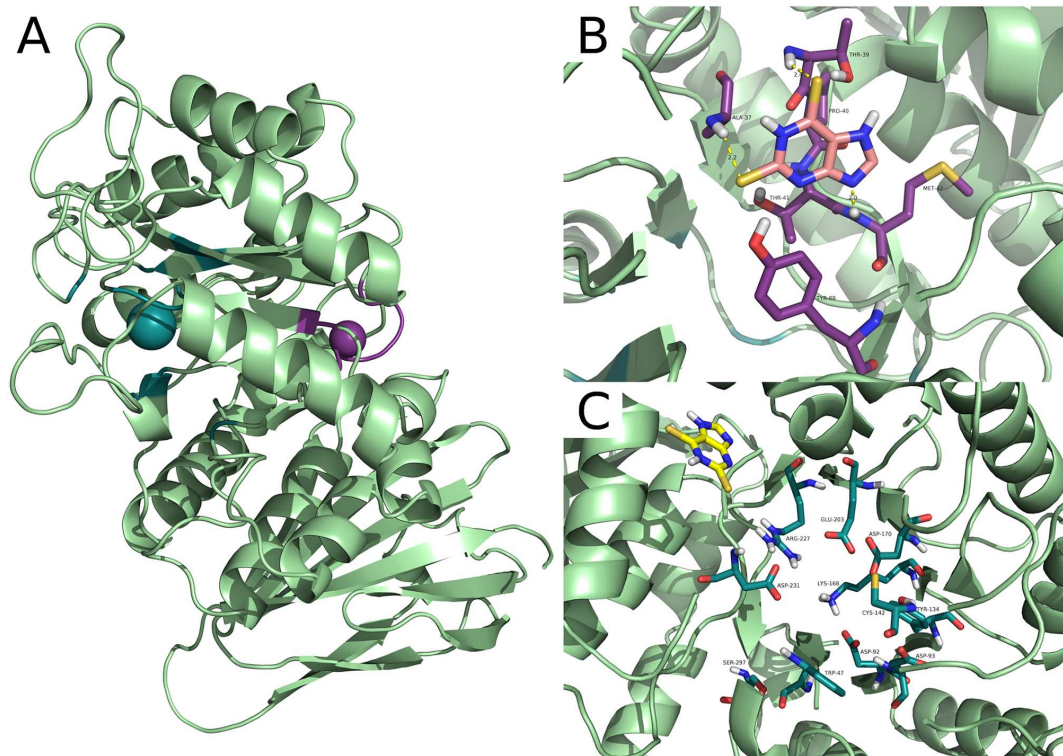


**Fig 1. The active site and the allosteric binding site in human lysosomal alpha-galactosidase.** The structure of lysosomal alpha-galactosidase is shown as a cartoon. In Panel A the active site (GLA site) is pinpointed by a blue sphere while the allosteric binding site is pinpointed by a violet sphere. Residues involved in the 2,6-dithiopurine allosteric and alpha-galactose binding site respectively are shown as sticks in Panel B or C respectively along with docked DTP. Predicted hydrogen bonds between DTP and AGAL within the allosteric binding site are shown as yellow dashed lines in Panel B. Best ranked pose of DTP in the alpha-galactose binding site area is shown in Panel C.

doi:10.1371/journal.pone.0165463.g001

The stability of AGAL in the presence or in the absence of DTP was tested by unfolding induced by a range of urea concentrations, followed by limited proteolysis. The enzyme unfolds at 2.7 M urea in the absence of DTP, and at 3 M urea in the presence of DTP (Fig 4). A minor band, which might represent a differently glycosylated form of AGAL, is observed in Fig 4. Its intensity correlates with that of the major band (data not shown).

AGAL mutants were expressed transiently in COS-7 cells. We tested the effect of DTP on the mutant A230T [47], which is non-responsive to DGJ [36], but eligible for PC therapy [48].

After transfection of A230T into COS-7 cells, specific bands were revealed by Western blot (WB) and the total alpha-galactosidase activity was measured in cell extracts. In order to interpret results it is worth remembering that AGAL is synthesized as a precursor of 50 kDa, but it is converted into a mature form of 46 kDa. A detailed analysis of Ishii and co-workers [49] demonstrated that when AGAL mutants are correctly processed into a 46 kDa form, they are also transferred into lysosomes. In Fig 5A we show the migration of transfected wt-AGAL (90 ± 9 U/mg activity in the lysates) as a reference. A230T shows a faint band corresponding to the precursor form of AGAL. This is not induced by the treatment with acknowledged PCs, DGJ,

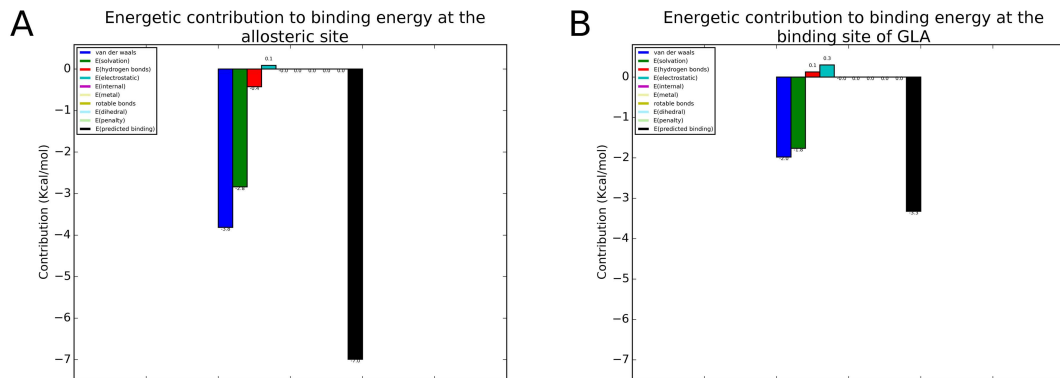


**Fig 2. Energetic contributions to the binding of 2–6 dithiopurine to the allosteric site and the active site of human lysosomal alpha-galactosidase.** Depicted energetic contributions are: van der Waals interactions (dark blue), volume-based free energy of solvation (green), hydrogen bonds (red), electrostatic energy (cyan), internal energy (pink), metal interactions (light yellow), energy of entropic losses associated with ligand's rotatable bonds (dark yellow), dihedral energy (light blue), internal energy penalty (light green) and total predicted binding affinity (black). A) Decomposition for the allosteric site, and B), decomposition for the active site.

doi:10.1371/journal.pone.0165463.g002

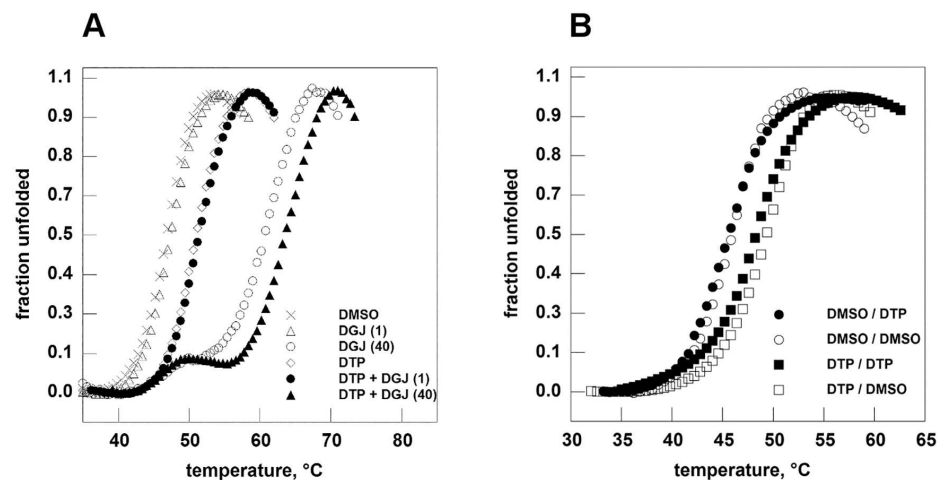


**Fig 3. 2–6 dithiopurine stabilizes human lysosomal alpha-galactosidase in thermal shift assay.** Panel A. Fabrazyme<sup>®</sup> (in Na-Hepes 20 mM, NaCl 150 mM, pH 7.4) was equilibrated in the presence of ligands dissolved in DMSO 20%: DGJ 1 microM (empty triangle) or 40 microM (empty circle); DTP 6 mM (empty diamond); DTP 6 mM plus DGJ 1 microM (filled circle); DTP 6 mM plus DGJ 40 microM (filled triangle). A control (with only DMSO) was also shown (x). Panel B. Fabrazyme<sup>®</sup> (in Na-Hepes 20 mM, NaCl 150 mM, pH 7.4) was incubated in the presence of DTP 6 mM for 1 hour at 4°C then DTP was eliminated by dialysis. A control experiment was conducted by incubating the enzyme only with DMSO. Both the aliquots of Fabrazyme<sup>®</sup> were analysed by thermal shift assay in the presence of DTP 6 mM or in the presence of DMSO. Filled squares: DTP/DTP; open squares: DMSO/DTP; filled circles: DTP/DMSO; open circles: DMSO/DMSO where the first word of the label corresponds to the pretreatment and the second part corresponds to the presence of the compound during the thermal scan. The protein samples were heated from 20 to 90° at 1°C/min in the presence of Sypro Orange 2.5x. Data were shown as normalized curves.

doi:10.1371/journal.pone.0165463.g003

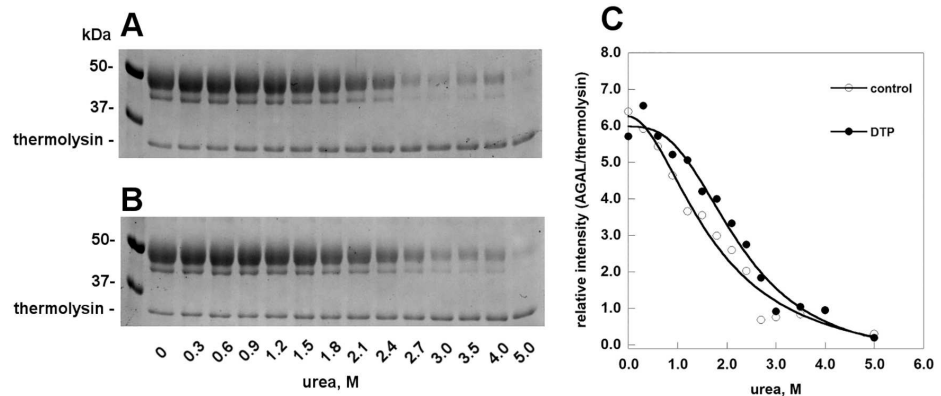


**Fig 4. 2–6 dithiopurine protects human alpha-galactosidase against urea-induced unfolding.** Fabrazyme<sup>®</sup> was incubated in the presence of urea (from 0 to 5 M), with (B) or without (A) DTP 6 mM, at 10 °C over night, then each sample was treated for 1 min at 37 °C with thermolysin (1:5 protease to protein ratio). Folded undigested proteins were visualized by SDS-PAGE. The intensity of the bands was quantified and the relative intensity of major band of Fabrazyme<sup>®</sup> and thermolysin in each lane was plotted against urea concentration (C).

doi:10.1371/journal.pone.0165463.g004

galactose [50] or ambroxol [21], at the dosages commonly used to measure their chaperoning effect on transfected mutants, 0.020 mM, 100 mM or 0.040 mM respectively. However, DTP 6 mM promotes the maturation of A230T. Moreover, its effect is potentiated by galactose and DGJ, even at very low concentration (0.001mM), but not by ambroxol (Fig 5A, 5B and 5C).

The lowest concentration at which DTP promotes A230T maturation is 2 mM (Fig 5D and 5E). The different bands visualised on WB represent different glycosylated forms, as demonstrated by treatment of A230T or wt-AGAL with N-Glycosidase F Fig 5F.

We tested the effect of DTP 6 mM on further mutants expressed in COS-7 cells: C56Y (Fig 6A), C63Y (Fig 6B) and E341D (Fig 6C). In these cases, enzymatic activity was not recovered (Fig 6D), possibly because the proteins are not catalytically active, but increased protein processing was detectable. C63Y and E341D are not responsive to DGJ [12, 13]. C56Y activity increases in the presence of DGJ although it does not meet the criteria chosen by Lukas *et al* [13] to define responsiveness.

We tested four mutations affecting residues in the allosteric site, A37T, P40S, M42T, M42V. None of these mutants responds to DTP (Fig 7). A37T [12], M42T [13] and M42V [8, 9, 12] are responsive to 0.020 mM DGJ, whereas P40S is not [10, 11, 13]. This finding supports the idea that DTP binds the allosteric site found *in silico*, although it does not prove it, because the same molecule has no effect on mutations that do not affect the allosteric site. An example is provided by S126C, C172G, and R118C which are not responsive to DGJ, [10–12, 51] (S2 Fig) and by Q280K, L300F, L310F and G360C (S3 Fig), which are responsive to DGJ [12] [36].

## Discussion

The catalytic domain of AGAL is formed by a TIM-barrel and the active site is located at the carboxyterminal end of beta-strands, as expected [52].

We identified a different druggable pocket located at the opposite side of the TIM-barrel of AGAL. Some molecules resulting from our virtual screening bind better to the allosteric site than to the active site. One of these molecules, a chemopreventive 2,6-dithiopurine DTP, appeared particularly promising because it is actively transported into mammalian cells where it accumulates at millimolar concentration [25] and it is safe [24] [26].

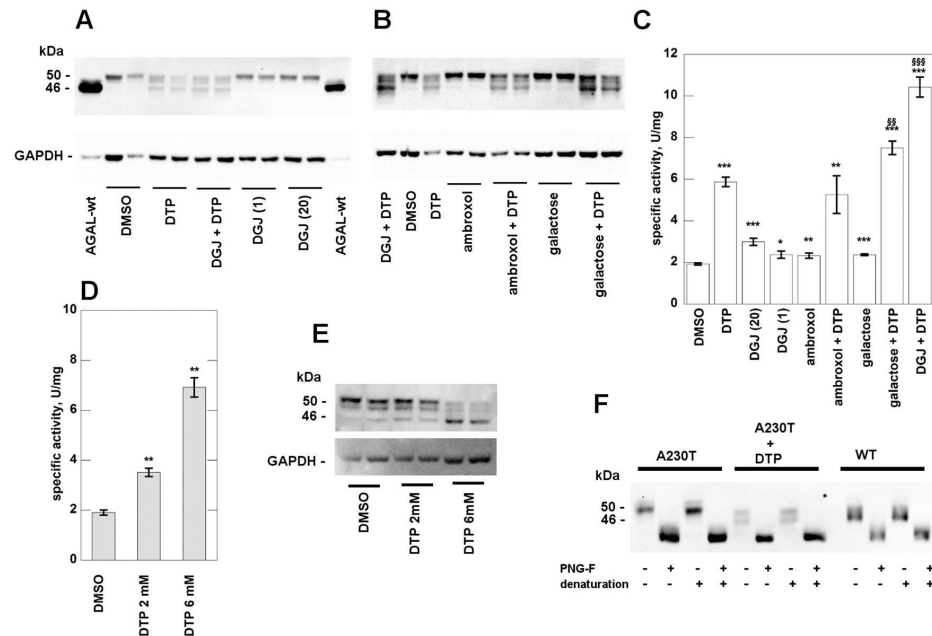


**Fig 5. 2–6 dithiopurine rescues mutant human alpha-galactosidase in monotherapy or in synergy.** COS-7 cells were cultured in conventional medium and transfected with plasmid containing A230T mutant. Cells were treated with: DTP 6 mM, DGJ 1 microM, DGJ 20 microM, ambroxol 40 microM, ambroxol 40 microM plus DTP 6 mM, galactose 100 mM, galactose 100 mM plus DTP 6 mM, DGJ 1 microM plus DTP 6 mM. All the molecules were dissolved in DMSO and an appropriate control was realized. After 48 h incubation, the cells were scraped and lysed then water-soluble extracts were analysed by western blotting (A and B) and enzyme assay (C). The effect of DTP 2 mM is shown in D and E. Cell extracts were treated with N-Glycosidase F and then analysed by WB (F). Standard deviations is indicated by bars and differences that are statistically significant are flagged by \* when compared to the control with DMSO ( $p < 0.05$ :\*;  $p < 0.01$ :\*\*;  $p < 0.001$ :\*\*\*), are flagged by § when compared to DTP ( $p < 0.01$ :§§;  $p < 0.001$ :§§§).

doi:10.1371/journal.pone.0165463.g005

DTP promotes the processing of some mutants of AGAL that are not responsive to DGJ and in one case, A230T, enhances its activity in monotherapy as well as in synergy with DGJ or galactose.

Not all missense mutations associated with FD are responsive to PC and we have not yet found molecular features that are necessary and sufficient to determine responsiveness. Mutations occurring at non conserved sites are generally less severe and responsive to PC, but there are exceptions to this rule. The best example we encountered is A230T, a mutation occurring at a non conserved site. A230 is exposed to solvent and exhibits moderate flexibility (Root mean square fluctuation, RMSF, of alpha carbon  $0.74 \pm 0.02 \text{ \AA}$ ). A230 is not directly implicated in catalysis, but it flanks D231, a proton donor that is essential for the hydrolysis of the substrate and belongs to a short stretch in polyproline II conformation. Its mutation to Threonine is classified as mildly destabilizing by MUPRO [39] or SDM [38]. The position specific substitution score, which measures the tolerability of the mutation in orthologous sequences and correlates with responsiveness to DGJ, is benign [48]. A230T is classified as possibly damaging or benign by HumDiv- and HumVar-trained PolyPhen-2 models respectively [44]. To summarize, A230T is eligible for PC therapy and does respond to DTP, although it does not respond to DGJ. Although DTP might be active only on a minority of AGAL missense mutations, we

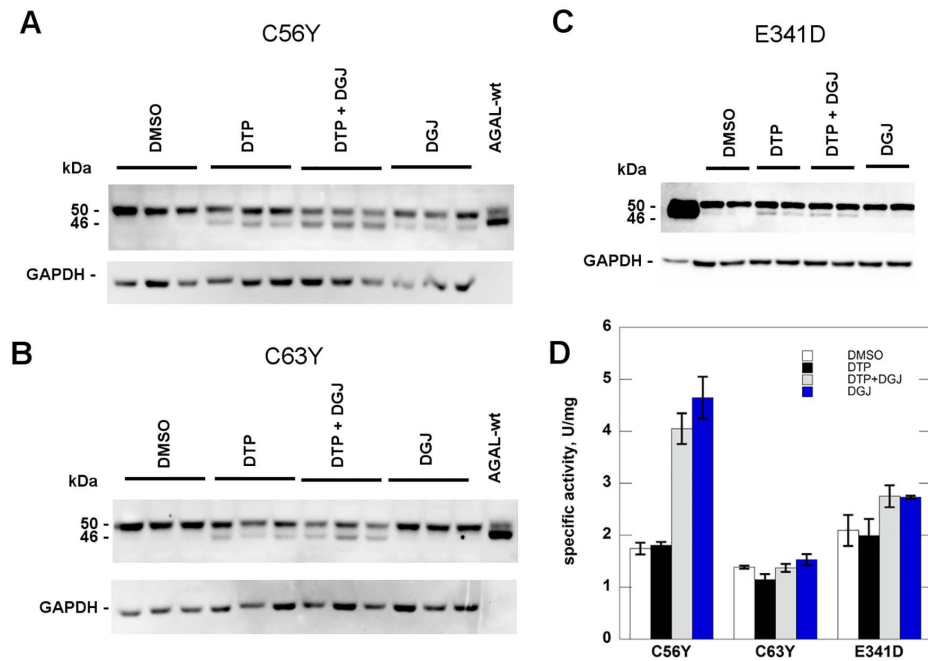


**Fig 6. 2–6 dithiopurine promotes processing of some mutant human alpha-galactosidase.** COS-7 cells were cultured in conventional medium and transfected with plasmid containing C56Y, C63Y and E341D mutants. Cells were treated with: DTP 6 mM, DGJ 1 microM, DGJ 1 microM plus DTP 6 mM. All the molecules were dissolved in DMSO and an appropriate control was realized. After 48 h incubation, the cells were scraped and lysed then water-soluble extracts were analysed by western blotting (A, B and C) and enzyme assay (D). Standard deviations are indicated by bars.

doi:10.1371/journal.pone.0165463.g006

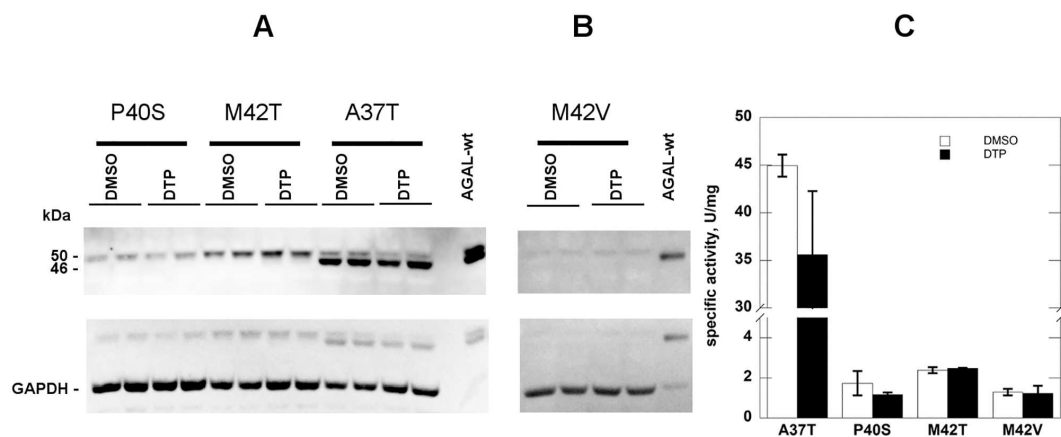


**Fig 7. 2–6 dithiopurine has no effect on mutations affecting the allosteric site.** COS-7 cells were cultured in conventional medium and transfected with plasmid containing A37T, P40S, M42T, M42V mutants. Cells were treated with DTP 6 mM dissolved in DMSO and an appropriate control was realized. After 48 h incubation, the cells were scraped and lysed then water-soluble extracts were analysed by western blotting (A and B) and enzyme assay (C). Standard deviations are indicated by bars.

doi:10.1371/journal.pone.0165463.g007

suggest that it should be tested in the cases that receive a positive score with Fabry\_CEP [45], but fail to respond to DGJ. We are aware that the interaction of DTP with AGAL, which occurs in vitro only at high concentration, cannot exclude non specific off-target effects of the drug on protein homeostasis. Derivatives of DTP obtained by techniques of lead optimization and medicinal chemistry might prove to be effective at lower doses and more specific.

### Supporting Information

**S1 Fig. 2–6 dithiopurine does not stabilize human lysosomal phosphomannomutase2 in thermal shift assay.** Human Phosphomannomutase2 (in Na-Hepes 20 mM, NaCl 150 mM, MgCl<sub>2</sub> 1mM pH 7.4) was equilibrated in the presence of ligands dissolved in DMSO 20%: DTP 6 mM (empty circle) and glucose 1, 6 bisphosphate (G16) 0.5 mM (filled squares) as a positive control. A control (with only DMSO) was also shown (filled circles).  
(TIF)

**S2 Fig. 2–6 dithiopurine has no effect on some mutations that are not responsive to DGJ.** COS-7 cells were cultured in conventional medium and transfected with plasmid containing R118C, S126C and C172G mutants. Cells were treated with: DTP 6 mM, DGJ 1 microM, DGJ 1 microM plus DTP 6 mM. All the molecules were dissolved in DMSO and an appropriate control was realized. After 48 h incubation, the cells were scraped and lysed then water-soluble extracts were analysed by western blotting (A, B and C) and enzyme assay (D). Standard deviations are indicated by bars.  
(TIF)

**S3 Fig. 2–6 dithiopurine has no effect on some mutations that are responsive to DGJ.** COS-7 cells were cultured in conventional medium and transfected with plasmid containing L310F, L300F, Q280K and G360C mutants. Cells were treated with DTP 6 mM. All the molecules were dissolved in DMSO and an appropriate control was realized. After 48 h incubation, the cells were scraped and lysed then water-soluble extracts were analysed by western blotting (A, B) and enzyme assay (C). Standard deviations are indicated by bars.  
(TIF)

**S1 File. Uncropped gels.** Images are relative to gels shown in Figs 4, 5, 6 and 7.  
(PDF)

### Acknowledgments

The authors gratefully acknowledge the computer resources and the technical support provided by the Plataforma Andaluza de Bioinformática of the University of Málaga. We thank E. Castelluccio, V.Mirra, A.Paone and A.Siciliano for technical assistance. We thank D.J.G. Mackay for copyediting the manuscript. This work is dedicated to our friend and colleague Dr Maria Malanga.

### Author Contributions

**Conceptualization:** VC HP-S GA.

**Data curation:** HP-S MVC.

**Formal analysis:** VC GA.

**Funding acquisition:** HP-S MVC GA.

**Investigation:** JP-G Hd-H RDP LL CC.



**Methodology:** JP-G Hd-H RDP LL CC.

**Project administration:** GA.

**Resources:** HP-S JL MVC GA.

**Software:** JP-G Hd-H HP-S.

**Supervision:** HP-S MVC GA.

**Validation:** VC RDP LL CC.

**Visualization:** VC HP-S.

**Writing – original draft:** MVC GA.

**Writing – review & editing:** JL MVC GA.

## References

1. Sirrs S, Hollak C, Merkel M, Sechi A, Glamuzina E, Janssen MC, et al. The Frequencies of Different Inborn Errors of Metabolism in Adult Metabolic Centres: Report from the SSIEM Adult Metabolic Physicians Group. *JIMD Rep.* 2015. Epub 2015/10/10. doi: [10.1007/8904\\_2015\\_435](https://doi.org/10.1007/8904_2015_435) PMID: [26450566](https://pubmed.ncbi.nlm.nih.gov/26450566/).
2. Germain DP. Fabry disease. *Orphanet J Rare Dis.* 2010; 5:30. PMID: [21092187](https://pubmed.ncbi.nlm.nih.gov/21092187/). doi: [10.1186/1750-1172-5-30](https://doi.org/10.1186/1750-1172-5-30)
3. Beck M, Hughes D, Kampmann C, Larroque S, Mehta A, Pintos-Morell G, et al. Long-term effectiveness of agalsidase alfa enzyme replacement in Fabry disease: A Fabry Outcome Survey analysis. *Mol Genet Metab Rep.* 2015; 3:21–7. Epub 2016/03/05. [pii]. PMID: [26937390](https://pubmed.ncbi.nlm.nih.gov/26937390/); PubMed Central PMCID: [PMC4750577](https://pubmed.ncbi.nlm.nih.gov/PMC4750577/).
4. Rombach SM, Hollak CE, Linthorst GE, Dijkgraaf MG. Cost-effectiveness of enzyme replacement therapy for Fabry disease. *Orphanet J Rare Dis.* 2013; 8:29. Epub 2013/02/21. [pii]. PMID: [23421808](https://pubmed.ncbi.nlm.nih.gov/23421808/); PubMed Central PMCID: [PMC3598841](https://pubmed.ncbi.nlm.nih.gov/PMC3598841/).
5. Lukas J, Scalia S, Eichler S, Pockrandt AM, Dehn N, Cozma C, et al. Functional and Clinical Consequences of Novel alpha-Galactosidase A Mutations in Fabry Disease. *Hum Mutat.* 2016; 37(1):43–51. Epub 2015/09/30. doi: [10.1002/humu.22910](https://doi.org/10.1002/humu.22910) PMID: [26415523](https://pubmed.ncbi.nlm.nih.gov/26415523/).
6. Fan JQ, Ishii S, Asano N, Suzuki Y. Accelerated transport and maturation of lysosomal alpha-galactosidase A in Fabry lymphoblasts by an enzyme inhibitor. *Nat Med.* 1999; 5(1):112–5. PMID: [9883849](https://pubmed.ncbi.nlm.nih.gov/9883849/). doi: [10.1038/4801](https://doi.org/10.1038/4801)
7. Shin SH, Kluepfel-Stahl S, Cooney AM, Kaneski CR, Quirk JM, Schiffmann R, et al. Prediction of response of mutated alpha-galactosidase A to a pharmacological chaperone. *Pharmacogenet Genomics.* 2008; 18(9):773–80. PMID: [18698230](https://pubmed.ncbi.nlm.nih.gov/18698230/). doi: [10.1097/FPC.0b013e32830500f4](https://doi.org/10.1097/FPC.0b013e32830500f4)
8. Shimotori M, Maruyama H, Nakamura G, Suyama T, Sakamoto F, Itoh M, et al. Novel mutations of the GLA gene in Japanese patients with Fabry disease and their functional characterization by active site specific chaperone. *Hum Mutat.* 2008; 29(2):331. PMID: [18205205](https://pubmed.ncbi.nlm.nih.gov/18205205/). doi: [10.1002/humu.9520](https://doi.org/10.1002/humu.9520)
9. Park JY, Kim GH, Kim SS, Ko JM, Lee JJ, Yoo HW. Effects of a chemical chaperone on genetic mutations in alpha-galactosidase A in Korean patients with Fabry disease. *Exp Mol Med.* 2009; 41(1):1–7. PMID: [19287194](https://pubmed.ncbi.nlm.nih.gov/19287194/). doi: [10.3858/emm.2009.41.1.001](https://doi.org/10.3858/emm.2009.41.1.001)
10. Benjamin ER, Flanagan JJ, Schilling A, Chang HH, Agarwal L, Katz E, et al. The pharmacological chaperone 1-deoxygalactonojirimycin increases alpha-galactosidase A levels in Fabry patient cell lines. *J Inher Metab Dis.* 2009; 32(3):424–40. PMID: [19387866](https://pubmed.ncbi.nlm.nih.gov/19387866/). doi: [10.1007/s10545-009-1077-0](https://doi.org/10.1007/s10545-009-1077-0)
11. Wu X, Katz E, Della Valle MC, Mascioli K, Flanagan JJ, Castelli JP, et al. A pharmacogenetic approach to identify mutant forms of alpha-galactosidase A that respond to a pharmacological chaperone for Fabry disease. *Hum Mutat.* 2011; 32(8):965–77. PMID: [21598360](https://pubmed.ncbi.nlm.nih.gov/21598360/). doi: [10.1002/humu.21530](https://doi.org/10.1002/humu.21530)
12. Lukas J, Giese AK, Markoff A, Grittner U, Kolodny E, Mascher H, et al. Functional characterisation of alpha-galactosidase A mutations as a basis for a new classification system in fabry disease. *PLoS Genet.* 2013; 9(8):e1003632. Epub 2013/08/13. [pii]. PMID: [23935525](https://pubmed.ncbi.nlm.nih.gov/23935525/); PubMed Central PMCID: [PMC3731228](https://pubmed.ncbi.nlm.nih.gov/PMC3731228/).
13. Lukas J, Scalia S, Eichler S, Pockrandt AM, Dehn N, Cozma C, et al. Functional and Clinical Consequences of Novel alpha-Galactosidase A Mutations in Fabry Disease. *Hum Mutat.* 2015. Epub 2015/09/30. doi: [10.1002/humu.22910](https://doi.org/10.1002/humu.22910) PMID: [26415523](https://pubmed.ncbi.nlm.nih.gov/26415523/).

14. Ishii S, Chang HH, Yoshioka H, Shimada T, Mannen K, Higuchi Y, et al. Preclinical efficacy and safety of 1-deoxygalactonojirimycin in mice for Fabry disease. *J Pharmacol Exp Ther*. 2009; 328(3):723–31. PMID: [19106170](#). doi: [10.1124/jpet.108.149054](#)
15. Khanna R, Benjamin ER, Pellegrino L, Schilling A, Rigat BA, Soska R, et al. The pharmacological chaperone isofagomine increases the activity of the Gaucher disease L444P mutant form of beta-glucosidase. *Febs J*. 2010; 277(7):1618–38. PMID: [20148966](#). doi: [10.1111/j.1742-4658.2010.07588.x](#)
16. Germain DP, Giugliani R, Hughes DA, Mehta A, Nicholls K, Barisoni L, et al. Safety and pharmacodynamic effects of a pharmacological chaperone on alpha-galactosidase A activity and globotriaosylceramide clearance in Fabry disease: report from two phase 2 clinical studies. *Orphanet J Rare Dis*. 2012; 7:91. PMID: [23176611](#). doi: [10.1186/1750-1172-7-91](#)
17. Giugliani R, Waldek S, Germain DP, Nicholls K, Bichet DG, Simosky JK, et al. A Phase 2 study of migalastat hydrochloride in females with Fabry disease: Selection of population, safety and pharmacodynamic effects. *Mol Genet Metab*. 2013; 109(1):86–92. PMID: [23474038](#). doi: [10.1016/j.ymgme.2013.01.009](#)
18. Tsukimura T, Chiba Y, Ohno K, Saito S, Tajima Y, Sakuraba H. Molecular mechanism for stabilization of a mutant alpha-galactosidase A involving M511 amino acid substitution by imino sugars. *Mol Genet Metab*. 2011; 103(1):26–32. PMID: [21353612](#). doi: [10.1016/j.ymgme.2011.01.013](#)
19. Jenkinson SF, Fleet GW, Nash RJ, Koike Y, Adachi I, Yoshihara A, et al. Looking-glass synergistic pharmacological chaperones: DGJ and L-DGJ from the enantiomers of tagatose. *Org Lett*. 2011; 13(15):4064–7. Epub 2011/07/13. doi: [10.1021/ol201552q](#) PMID: [21744786](#).
20. Yu Y, Mena-Barragan T, Higaki K, Johnson JL, Drury JE, Lieberman RL, et al. Molecular basis of 1-deoxygalactonojirimycin arylthiourea binding to human alpha-galactosidase a: pharmacological chaperoning efficacy on Fabry disease mutants. *ACS Chem Biol*. 2014; 9(7):1460–9. Epub 2014/05/03. doi: [10.1021/cb500143h](#) PMID: [24783948](#).
21. Lukas J, Pockrandt AM, Seemann S, Sharif M, Runge F, Pohlers S, et al. Enzyme enhancers for the treatment of fabry and pompe disease. *Mol Ther*. 2015; 23(3):456–64. Epub 2014/11/21. doi: [10.1038/mt.2014.224](#) [pii]. PMID: [25409744](#).
22. Bendikov-Bar I, Maor G, Filocamo M, Horowitz M. Ambroxol as a pharmacological chaperone for mutant glucocerebrosidase. *Blood Cells Mol Dis*. 2013; 50(2):141–5. Epub 2012/11/20. doi: [10.1016/j.bcmd.2012.10.007](#) [pii]. PMID: [23158495](#); PubMed Central PMCID: [PMC3547170](#).
23. Irwin JJ, Shoichet BK. ZINC—a free database of commercially available compounds for virtual screening. *J Chem Inf Model*. 2005; 45(1):177–82. Epub 2005/01/26. doi: [10.1021/ci049714+](#) PMID: [15667143](#); PubMed Central PMCID: [PMC1360656](#).
24. Boulware S, Fields T, McIvor E, Powell KL, Abel EL, Vasquez KM, et al. 2,6-Dithiopurine, a nucleophilic scavenger, protects against mutagenesis in mouse skin treated in vivo with 2-(chloroethyl) ethyl sulfide, a mustard gas analog. *Toxicol Appl Pharmacol*. 2012; 263(2):203–9. Epub 2012/06/27. doi: [10.1016/j.taap.2012.06.010S0041-008X\(12\)00269-4](#) [pii]. PMID: [22732900](#); PubMed Central PMCID: [PMC3422404](#).
25. Powell KL, Boulware S, Thames H, Vasquez KM, MacLeod MC. 2,6-Dithiopurine blocks toxicity and mutagenesis in human skin cells exposed to sulfur mustard analogues, 2-chloroethyl ethyl sulfide and 2-chloroethyl methyl sulfide. *Chem Res Toxicol*. 2010; 23(3):497–503. Epub 2010/01/07. doi: [10.1021/tx9001918](#) PMID: [20050631](#); PubMed Central PMCID: [PMC2838951](#).
26. Qing WG, Powell KL, Stoica G, Szumlanski CL, Weinshilboum RM, MacLeod MC. Toxicity and metabolism in mice of 2,6-dithiopurine, a potential chemopreventive agent. *Drug Metab Dispos*. 1995; 23(8):854–60. Epub 1995/08/01. PMID: [7493553](#).
27. Guce AI, Clark NE, Rogich JJ, Garman SC. The molecular basis of pharmacological chaperoning in human alpha-galactosidase. *Chem Biol*. 2011; 18(12):1521–6. PMID: [22195554](#). doi: [10.1016/j.chembiol.2011.10.012](#)
28. Stroganov OV, Novikov FN, Stroylov VS, Kulkov V, Chilov GG. Lead finder: an approach to improve accuracy of protein-ligand docking, binding energy estimation, and virtual screening. *J Chem Inf Model*. 2008; 48(12):2371–85. Epub 2008/11/15. doi: [10.1021/ci800166p](#) PMID: [19007114](#).
29. Yan X, Li J, Liu Z, Zheng M, Ge H, Xu J. Enhancing molecular shape comparison by weighted Gaussian functions. *J Chem Inf Model*. 2013; 53(8):1967–78. Epub 2013/07/13. doi: [10.1021/ci300601q](#) PMID: [23845061](#).
30. Pantoliano MW, Petrella EC, Kwasnoski JD, Lobanov VS, Myslik J, Graf E, et al. High-density miniaturized thermal shift assays as a general strategy for drug discovery. *J Biomol Screen*. 2001; 6(6):429–40. Epub 2002/01/15. doi: [10.1089/108705701753364922](#) PMID: [11788061](#).
31. Lo MC, Aulabaugh A, Jin G, Cowling R, Bard J, Malamas M, et al. Evaluation of fluorescence-based thermal shift assays for hit identification in drug discovery. *Anal Biochem*. 2004; 332(1):153–9. Epub 2004/08/11. doi: [10.1016/j.ab.2004.04.031](#) [pii]. PMID: [15301960](#).

32. Andreotti G, Monticelli M, Cubellis MV. Looking for protein stabilizing drugs with thermal shift assay. *Drug Test Anal.* 2015. Epub 2015/04/08. doi: [10.1002/dta.1798](https://doi.org/10.1002/dta.1798) PMID: [25845367](https://pubmed.ncbi.nlm.nih.gov/25845367/).
33. Andreotti G, Pedone E, Giordano A, Cubellis MV. Biochemical phenotype of a common disease-causing mutation and a possible therapeutic approach for the phosphomannomutase 2-associated disorder of glycosylation. *Mol Genet Genomic Med.* 2013; 1(1):32–44. doi: [10.1002/mgg3.3](https://doi.org/10.1002/mgg3.3) PMID: [24498599](https://pubmed.ncbi.nlm.nih.gov/24498599/)
34. Kim MS, Song J, Park C. Determining protein stability in cell lysates by pulse proteolysis and Western blotting. *Protein Sci.* 2009; 18(5):1051–9. PMID: [19388050](https://pubmed.ncbi.nlm.nih.gov/19388050/). doi: [10.1002/pro.115](https://doi.org/10.1002/pro.115)
35. Andreotti G, Citro V, Correr A, Cubellis MV. A thermodynamic assay to test pharmacological chaperones for Fabry disease. *Biochim Biophys Acta.* 2014; 1840(3):1214–24. Epub 2013/12/24. doi: [10.1016/j.bbagen.2013.12.018](https://doi.org/10.1016/j.bbagen.2013.12.018) [pii]. PMID: [24361605](https://pubmed.ncbi.nlm.nih.gov/24361605/); PubMed Central PMCID: [PMC3909460](https://pubmed.ncbi.nlm.nih.gov/PMC3909460/).
36. Andreotti G, Citro V, De Crescenzo A, Orlando P, Cammisa M, Correr A, et al. Therapy of Fabry disease with pharmacological chaperones: from in silico predictions to in vitro tests. *Orphanet J Rare Dis.* 2011; 6:66. Epub 2011/10/19. doi: [10.1186/1750-1172-6-66](https://doi.org/10.1186/1750-1172-6-66) [pii]. PMID: [22004918](https://pubmed.ncbi.nlm.nih.gov/22004918/); PubMed Central PMCID: [PMC3216245](https://pubmed.ncbi.nlm.nih.gov/PMC3216245/).
37. Bradford MM. A rapid and sensitive method for the quantitation of microgram quantities of protein utilizing the principle of protein-dye binding. *Anal Biochem.* 1976; 72:248–54. Epub 1976/05/07. S0003269776699996 [pii]. PMID: [942051](https://pubmed.ncbi.nlm.nih.gov/942051/).
38. Worth CL, Preissner R, Blundell TL. SDM—a server for predicting effects of mutations on protein stability and malfunction. *Nucleic Acids Res.* 2011; 39(Web Server issue):W215–22. PMID: [21593128](https://pubmed.ncbi.nlm.nih.gov/21593128/). doi: [10.1093/nar/gkr363](https://doi.org/10.1093/nar/gkr363)
39. Cheng J, Randall A, Baldi P. Prediction of protein stability changes for single-site mutations using support vector machines. *Proteins.* 2006; 62(4):1125–32. PMID: [16372356](https://pubmed.ncbi.nlm.nih.gov/16372356/). doi: [10.1002/prot.20810](https://doi.org/10.1002/prot.20810)
40. Cubellis MV, Cailliez F, Lovell SC. Secondary structure assignment that accurately reflects physical and evolutionary characteristics. *BMC Bioinformatics.* 2005; 6 Suppl 4:S8. PMID: [16351757](https://pubmed.ncbi.nlm.nih.gov/16351757/). doi: [10.1186/1471-2105-6-S4-S8](https://doi.org/10.1186/1471-2105-6-S4-S8)
41. Cammisa M, Correr A, Andreotti G, Cubellis MV. Identification and analysis of conserved pockets on protein surfaces. *BMC Bioinformatics.* 2013; 14 Suppl 7:S9. Epub 2013/07/17. doi: [10.1186/1471-2105-14-S7-S9](https://doi.org/10.1186/1471-2105-14-S7-S9) [pii]. PMID: [23815589](https://pubmed.ncbi.nlm.nih.gov/23815589/); PubMed Central PMCID: [PMC3633052](https://pubmed.ncbi.nlm.nih.gov/PMC3633052/).
42. Krieger E, Darden T, Nabuurs SB, Finkelstein A, Vriend G. Making optimal use of empirical energy functions: force-field parameterization in crystal space. *Proteins.* 2004; 57(4):678–83. PMID: [15390263](https://pubmed.ncbi.nlm.nih.gov/15390263/). doi: [10.1002/prot.20251](https://doi.org/10.1002/prot.20251)
43. Cubellis MV, Baaden M, Andreotti G. Taming molecular flexibility to tackle rare diseases. *Biochimie.* 2015; 113:54–8. Epub 2015/04/07. doi: [10.1016/j.biochi.2015.03.018](https://doi.org/10.1016/j.biochi.2015.03.018) [pii]. PMID: [25841341](https://pubmed.ncbi.nlm.nih.gov/25841341/); PubMed Central PMCID: [PMC4441037](https://pubmed.ncbi.nlm.nih.gov/PMC4441037/).
44. Adzhubei IA, Schmidt S, Peshkin L, Ramensky VE, Gerasimova A, Bork P, et al. A method and server for predicting damaging missense mutations. *Nat Methods.* 2010; 7(4):248–9. Epub 2010/04/01. doi: [10.1038/nmeth0410-248](https://doi.org/10.1038/nmeth0410-248) [pii]. PMID: [20354512](https://pubmed.ncbi.nlm.nih.gov/20354512/); PubMed Central PMCID: [PMC2855889](https://pubmed.ncbi.nlm.nih.gov/PMC2855889/).
45. Cammisa M, Correr A, Andreotti G, Cubellis MV. Fabry\_CEP: a tool to identify Fabry mutations responsive to pharmacological chaperones. *Orphanet J Rare Dis.* 2013; 8:111. Epub 2013/07/26. doi: [10.1186/1750-1172-8-111](https://doi.org/10.1186/1750-1172-8-111) [pii]. PMID: [23883437](https://pubmed.ncbi.nlm.nih.gov/23883437/); PubMed Central PMCID: [PMC3729670](https://pubmed.ncbi.nlm.nih.gov/PMC3729670/).
46. Hay Mele B, Citro V, Andreotti G, Cubellis MV. Drug repositioning can accelerate discovery of pharmacological chaperones. *Orphanet J Rare Dis.* 2015; 10:55. Epub 2015/05/08. [pii]. PMID: [25947946](https://pubmed.ncbi.nlm.nih.gov/25947946/); PubMed Central PMCID: [PMC4429356](https://pubmed.ncbi.nlm.nih.gov/PMC4429356/).
47. Ashton-Prolla P, Tong B, Shabbeer J, Astrin KH, Eng CM, Desnick RJ. Fabry disease: twenty-two novel mutations in the alpha-galactosidase A gene and genotype/phenotype correlations in severely and mildly affected hemizygotes and heterozygotes. *J Investig Med.* 2000; 48(4):227–35. PMID: [10916280](https://pubmed.ncbi.nlm.nih.gov/10916280/).
48. Andreotti G, Guarracino MR, Cammisa M, Correr A, Cubellis MV. Prediction of the responsiveness to pharmacological chaperones: lysosomal human alpha-galactosidase, a case of study. *Orphanet J Rare Dis.* 2010; 5:36. PMID: [21138548](https://pubmed.ncbi.nlm.nih.gov/21138548/). doi: [10.1186/1750-1172-5-36](https://doi.org/10.1186/1750-1172-5-36)
49. Ishii S, Chang HH, Kawasaki K, Yasuda K, Wu HL, Garman SC, et al. Mutant alpha-galactosidase A enzymes identified in Fabry disease patients with residual enzyme activity: biochemical characterization and restoration of normal intracellular processing by 1-deoxygalactonojirimycin. *Biochem J.* 2007; 406(2):285–95. PMID: [17555407](https://pubmed.ncbi.nlm.nih.gov/17555407/). doi: [10.1042/BJ20070479](https://doi.org/10.1042/BJ20070479)
50. Okumiya T, Ishii S, Takenaka T, Kase R, Kamei S, Sakuraba H, et al. Galactose stabilizes various missense mutants of alpha-galactosidase in Fabry disease. *Biochem Biophys Res Commun.* 1995; 214(3):1219–24. Epub 1995/09/25. S0006-291X(85)72416-3 [pii] doi: [10.1006/bbrc.1995.2416](https://doi.org/10.1006/bbrc.1995.2416) PMID: [7575533](https://pubmed.ncbi.nlm.nih.gov/7575533/).

51. Spada M, Pagliardini S, Yasuda M, Tukul T, Thiagarajan G, Sakuraba H, et al. High incidence of later-onset fabry disease revealed by newborn screening. *Am J Hum Genet.* 2006; 79(1):31–40. PMID: [16773563](#). doi: [10.1086/504601](#)
52. Vega MC, Lorentzen E, Linden A, Wilmanns M. Evolutionary markers in the (beta/alpha)8-barrel fold. *Curr Opin Chem Biol.* 2003; 7(6):694–701. Epub 2003/12/04. S136759310300139X [pii]. PMID: [14644177](#).

### 2.3 Selective in vitro and in silico butyrylcholinesterase inhibitory activity of diterpenes and rosmarinic acid isolated from *Perovskia atriplicifolia* Benth. and *Salvia glutinosa* L.

<b>Title</b>	<i>Selective in vitro and in silico butyrylcholinesterase inhibitory activity of diterpenes and rosmarinic acid isolated from Perovskia atriplicifolia Benth. and Salvia glutinosa L.</i>
<b>Authors</b>	F Sezer Senol, Sylwester Slusarczyk, Adam Matkowski, Alfonso Pérez-Garrido, Francisco Girón-Rodríguez, José P Cerón-Carrasco, Helena den-Haan, Jorge Peña-García, Horacio Pérez-Sánchez, Krzysztof Domaradzki, Ilkay Erdogan Orhan
<b>Journal</b>	<i>Phytochemistry</i>
<b>Year</b>	2017
<b>State</b>	Published

#### PhD candidate contribution

Helena den Haan Alonso, declares to be the co-author and contributor of the article *Selective in vitro and in silico butyrylcholinesterase inhibitory activity of diterpenes and rosmarinic acid isolated from Perovskia atriplicifolia Benth. and Salvia glutinosa L.* in the section on computational chemistry.



Contents lists available at ScienceDirect

Phytochemistry

journal homepage: [www.elsevier.com/locate/phytochem](http://www.elsevier.com/locate/phytochem)

## Selective *in vitro* and *in silico* butyrylcholinesterase inhibitory activity of diterpenes and rosmarinic acid isolated from *Perovskia atriplicifolia* Benth. and *Salvia glutinosa* L.



F. Sezer Senol <sup>a</sup>, Sylwester Ślusarczyk <sup>b,c</sup>, Adam Matkowski <sup>b</sup>, Alfonso Pérez-Garrido <sup>c</sup>, Francisco Girón-Rodríguez <sup>d</sup>, José P. Cerón-Carrasco <sup>c</sup>, Helena den-Haan <sup>c</sup>, Jorge Peña-García <sup>c</sup>, Horacio Pérez-Sánchez <sup>c,\*\*</sup>, Krzysztof Domaradzki <sup>e</sup>, İlkay Erdogan Orhan <sup>a,\*</sup>

<sup>a</sup> Department of Pharmacognosy, Faculty of Pharmacy, Gazi University, 06330 Ankara, Turkey

<sup>b</sup> Department of Pharmaceutical Biology and Botany, Wrocław Medical University, Wrocław, Poland

<sup>c</sup> Bioinformatics and High Performance Computing Research Group, Universidad Católica San Antonio de Murcia (UCAM), Spain

<sup>d</sup> Department of Food and Nutrition Technology, Universidad Católica San Antonio de Murcia (UCAM), Spain

<sup>e</sup> Department of Weed Science and Soil Tillage Systems, IUNG-Institute of Soil Science and Plant Cultivation, Wrocław, Poland

### ARTICLE INFO

#### Article history:

Received 17 July 2016

Received in revised form

25 October 2016

Accepted 27 October 2016

Available online 3 November 2016

#### Keywords:

*Perovskia atriplicifolia* (Lamiaceae)

*Salvia glutinosa* (Lamiaceae)

Tanshinones

Diterpenes

Cholinesterase inhibition

Butyrylcholinesterase

QSAR

Molecular modeling

### ABSTRACT

Cholinesterase inhibition is one of the most treatment strategies against Alzheimer's disease (AD) where metal accumulation is also strongly associated with pathology of the disease. In the current study, we assessed inhibitory effect against acetyl- (AChE) and butyrylcholinesterase (BChE) and metal-chelating capacity of twelve diterpenes: arucadiol, miltirone, tanshinone IIa, 1-oxomiltirone, cryptotanshinone, 1,2-didehydromiltirone, 1,2-didehydrotanshinone IIa, 1 $\beta$ -hydroxycryptotanshinone, 15,16-dihydrotanshinone, tanshinone I, isotanshinone II, 1(S)-hydroxytanshinone IIa, and rosmarinic acid, isolated from *Perovskia atriplicifolia* and *Salvia glutinosa*. The compounds were tested at 10  $\mu$ g/mL using ELISA microtiter assays against AChE and BChE. QSAR and molecular docking studies have been also performed on the active compounds.

All of the compounds showed higher [e.g., IC<sub>50</sub> = 1.12  $\pm$  0.07  $\mu$ g/mL for 1,2-didehydromiltirone, IC<sub>50</sub> = 1.15  $\pm$  0.07  $\mu$ g/mL for cryptotanshinone, IC<sub>50</sub> = 1.20  $\pm$  0.03  $\mu$ g/mL for arucadiol, etc.] or closer [1,2-didehydrotanshinone IIa (IC<sub>50</sub> = 5.98  $\pm$  0.49  $\mu$ g/mL) and 1(S)-hydroxytanshinone IIa (IC<sub>50</sub> = 5.71  $\pm$  0.27  $\mu$ g/mL)] inhibition against BChE as compared to that of galanthamine (IC<sub>50</sub> = 12.56  $\pm$  0.37  $\mu$ g/mL), whereas only 15,16-dihydrotanshinone moderately inhibited AChE (65.17  $\pm$  1.39%). 1,2-Didehydrotanshinone IIa (48.94  $\pm$  0.26%) and 1(S)-hydroxytanshinone IIa (47.18  $\pm$  5.10%) possessed the highest metal-chelation capacity. The present study affords an evidence for the fact that selective BChE inhibitors should be further investigated as promising candidate molecules for AD therapy.

© 2016 Elsevier Ltd. All rights reserved.

### 1. Introduction

Alzheimer's disease (AD) is a progressive neurodegenerative disorder with complex pathology that affects particularly elderly

population. Pathogenesis of the disease still remains indistinct in most parts due to its multifactorial etiology (Guzior et al., 2015). Cholinergic hypothesis is one of the most accepted approaches to explain AD pathology which asserts the deficit in acetylcholine (ACh) amount as an apparent evident in the brains of AD patients. Since ACh is hydrolyzed by acetylcholinesterase (AChE), inhibition of this enzyme has been a popular approach for AD treatment and, in this regard, cholinesterase (ChE) inhibitors such as rivastigmine, tacrin, donepezil, and galanthamine are the most prescribed drug

\* Corresponding author.

\*\* Corresponding author.

E-mail addresses: [hperetz@ucam.edu](mailto:hperetz@ucam.edu) (H. Pérez-Sánchez), [iorhan@gazi.edu.tr](mailto:iorhan@gazi.edu.tr) (I.E. Orhan).

**Abbreviations**

ACh	Acetylcholine
AChE	Acetylcholinesterase
AD	Alzheimer's disease
BCh	Butyrylcholine
BChE	Butyrylcholinesterase
ChE	Cholinesterase
CID	Collision-activated dissociation
CYP	Cytochrome P450
DFT	Density functional theory
DL	Desolvation line
DTNB	5,5'-Dithio-bis(2-nitrobenzoic)acid
EDTA	Ethylenediaminetetraacetic acid
ESI	Electrospray ionization
EtOAc	Ethyl acetate
MRM	Multiple-reaction monitoring
PDB	Protein data bank
PTZ	Pentylentetrazol
QSAR	Quantitative structure-activity relationship
S.E.M.	Standard error of the mean
TLC	Thin layer chromatography

class towards AD (Orhan et al., 2011). Other member of ChE family is butyrylcholinesterase (BChE), which is also considered as promising target for AD drug discovery since its enzymatic activity upsurges in the late stages of AD. In fact, it has been reported that BChE inhibitors can also act in a similar way to those of AChE inhibitors and slows down cognitive decline (Li et al., 2008).

Tanshinones are red to orange-colored nor-abietanoid quinones obtained mainly from *Salvia miltiorrhizae radix* (danshen, roots and rhizomes of *S. miltiorrhiza* Bunge), an important traditional Chinese herb (Chen et al., 2014) and have been reported to exhibit some desired pharmacological activities such as anticancer (Li et al., 2008), anti-aging (Wu et al., 2014), anticonvulsant (Buenafe et al., 2013), etc. Actually, one of them, e.g. tanshinone IIa, is currently under phase-III clinical trial for treatment of cardiovascular conditions (Shang et al., 2013). Besides *S. miltiorrhiza*, several other species of the genus *Salvia*, along with a few other genera from the Lamiaceae contain tanshinones in various proportions. *Salvia glutinosa* L. is a common plant growing in mountainous deciduous forests throughout Europe and in Caucasus. Notwithstanding, only little information is available on its phytochemical profile up to date. *Perovskia atriplicifolia* Benth. belongs to a small genus of aromatic shrubs growing in arid habitats of Central Asia, which is considered a sister genus to *Salvia* L. and *Rosmarinus* L. from Lamiaceae. Several varieties of *P. atriplicifolia* are cultivated worldwide for ornamental purpose, known as "Russian sage". Although presence of a large number of auspicious ChE inhibitors has been reported from plants, only a few tanshinone derivatives have been investigated for their ChE inhibitory potential (Zhou et al., 2011). Consequently, we undertook the present study in order to test twelve nor-abietanoids - arucadiol (1), miltirone (2), tanshinone IIa (3), 1-oxomiltirone (4), cryptotanshinone (5), 1,2-didehydromiltirone (6), 1,2-didehydrotanshinone IIa (7), 1 $\beta$ -OH-cryptotanshinone (8), 15,16-dihydrotanshinone (9), tanshinone I (10), isotanshinone II (11), 1(S)-OH-tanshinone IIa (12) as well as rosmarinic acid (13) (Fig. 1), isolated by our group from the roots of *P. atriplicifolia* (Ślusarczyka et al., 2015) or *S. glutinosa*, against AChE and BChE as well as their metal-chelating properties *in vitro*.

**2. Results and discussion****2.1. ChE inhibitory activity**

Compounds 1–13 isolated from *Perovskia atriplicifolia* and *Salvia glutinosa* were assayed *in vitro* against AChE and BChE at 10  $\mu$ g/mL. Except compound 12, all of them exerted higher activity against BChE than the reference drug (galanthamine) (Table 1), whereas only compound 9 inhibited AChE moderately. The most potent BChE-inhibiting compound was miltirone 2.

**2.2. Metal-chelation capacity**

All of the compounds tested displayed a lower metal-chelation capacity than 50% (Fig. 2), where only 1,2-didehydrotanshinone IIa (7, 48.94  $\pm$  0.26%) and  $\beta$ -OH-tanshinone IIa (12, 47.18  $\pm$  5.10%) were revealed to have the highest metal-chelation capacity than the rest, which is still below 50%.

**2.3. QSAR modeling**

Following the computational strategies outlined in the methods section, the most stable models obtained are presented in Table 2. We obtained moderately stable models for AChE and for the receptor selectivity. For BChE inhibitory activity stable and predictive models were not obtained due to the low values of  $Q^2_{LOO}$  and  $Q^2_{boot}$ . Noting the sign of the coefficients of each descriptor we can say that high values of HGM and R2m have a positive influence in the AChE inhibitory activity, as well as low values in SpMax7\_Bh(s) and RDF080s have a positive influence in BChE inhibitory activity. Moreover, low values of HATS2u and R3m have an increment in the selectivity between BChE and AChE receptors. Since the model developed for the BChE receptor does not offer conclusive results, we will focus on the model obtained for the selectivity between the two receptors. The descriptors HATS2u and R3m are part of the family of descriptors called GETAWAY that encode information on structural fragments and therefore they seem to be particularly suitable for describing differences in congeneric series of molecules, as in the present case. These two descriptors report high values with the presence in the molecule of external atoms more close to each other in the molecular space. In this regard, we observed that the presence of aliphatic groups such as isopropyl (C2 or C6) (farthest atoms) compared to an aromatic ring such as 3-methyl furan (C3 or C7) (atoms closer) causes a decrease in the values of both descriptors and thus an increase in selectivity for BChE versus AChE receptor. So, we emphasized that the presence of more aliphatic substituents make the molecules more selective for BChE versus AChE receptor, whereas the presence of more aromatic substituents make the molecules more selective for AChE versus BChE receptor.

**2.4. Molecular docking**

Docking calculations for control compounds, e.g. acetylcholine (ACh) and butyrylcholine (BCh) were carried out in order to test capability of the protocol to predict residues that are widely known to interact with these molecules (Bajda et al., 2013). The results obtained for ACh in the cavity of AChE and BCh in the cavity of BChE, respectively, are illustrated in Figs. 3 and 4. In both cases, ACh and BCh lie close to residues from the catalytic triad, in total agreement with the enzymatic mechanisms. Therefore, we can continue forward and analyze the information that docking methods can yield for the compounds reported in this work. For that aim, we have focused on the two most representative compounds from this set, compounds 9 (C9) and 13 (C13). As observed

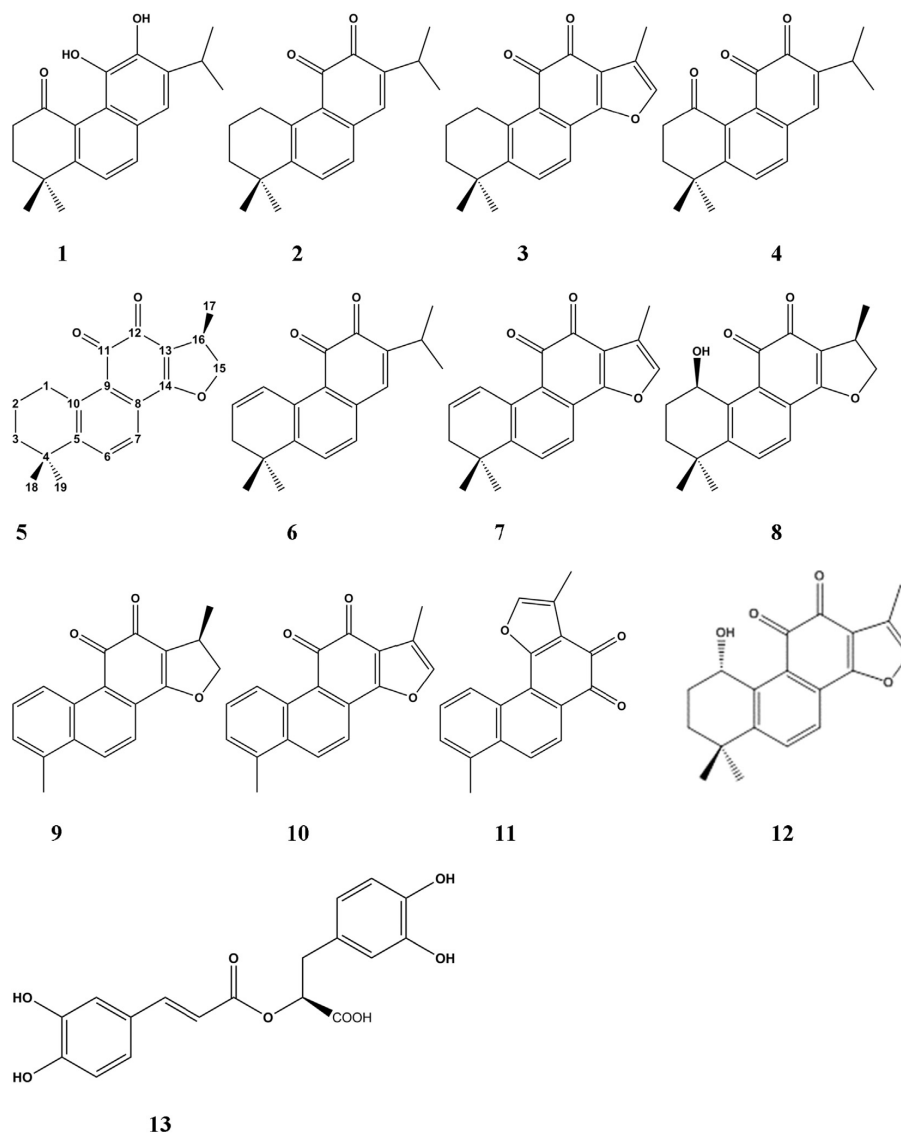


Fig. 1. Structures of compounds 1–13. Example of carbon atom numbering is shown for nor-diterpenoids in compound 5 (cryptotanshinone).

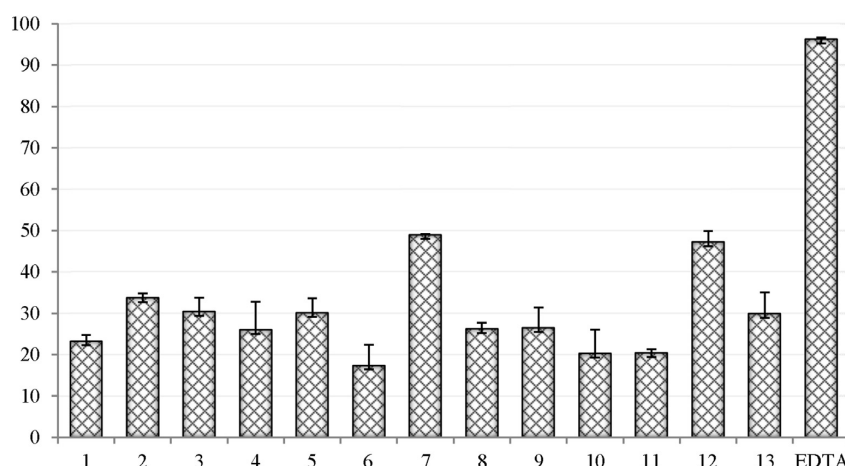
in Table 2, C9 is the one that inhibits AChE the most effectively which has inhibitory activity close to 100% for BChE. Compounds from 1 to 12 share the same chemical scaffold, hence, which directed us to focus first on the docking results obtained for C9 against both enzymes, and later on C13, which is a totally different chemical entity. In Fig. 5, docking results for C9 against AChE are shown. Main interactions are pi-pi stacking with TYR334 and hydrophobic interactions with PHE330, situated at the gorge of the active site of the enzyme. This way, C9 blocks ACh access to the catalytic triad, and thus inhibits the enzyme. In addition, crystallographic pose of drug Aricept<sup>®</sup> is shown in Fig. 6 (purple skeleton) and we can observe that both molecules share same interaction area and, as a result, similar enzyme blocking mechanism. From the other side, docking results for C9 against BChE are shown in Fig. 6.

In this case, main interactions between the compound and enzyme are due to hydrogen bonds formed between oxygen atoms from carbonyl groups of C9 and HIS438 from catalytic triad as well as hydrophobic interactions of C9 with residues TRP82, LEU286 and VAL288. Here, C9 blocks entry of BCh and also interferes with availability of HIS438 for interacting with BCh, which leads to the suggestion that inhibition should be higher here than in the case of AChE, where only the entry of substrate was blocked. Nevertheless, the residues from the active site were still free for interactions. As a final point, interactions of C13 within BChE active site were also studied as revealed in Fig. 7. According to the findings, main interactions are due to hydrogen bonds between hydroxyl groups of the compound and residues TRP82 and TYR128, hence, blocking access of substrate to the catalytic triad.



**Table 1**  
AChE and BChE inhibitory activity (%inhibition  $\pm$  S.E.M.) and IC<sub>50</sub> values of compounds 1–13.

Compound	(% Inhibition $\pm$ S.E.M. <sup>a</sup> ) (at 10 $\mu$ g/mL)		IC <sub>50</sub> values ( $\mu$ g/mL) for BChE inhibition
	AChE	BChE	
1 Arucadiol	– <sup>b</sup>	91.97 $\pm$ 0.08	1.20 $\pm$ 0.03
2 Miltirone	–	98.36 $\pm$ 0.89	0.90 $\pm$ 0.05
3 Tanshinone IIa	45.16 $\pm$ 5.49****	97.41 $\pm$ 0.23	2.79 $\pm$ 0.25
4 1-Oksomiltirone	11.08 $\pm$ 0.38****	77.45 $\pm$ 1.97	5.06 $\pm$ 0.89
5 Cryptotanshinone	28.95 $\pm$ 1.74****	74.37 $\pm$ 3.57	1.15 $\pm$ 0.07
6 1,2-Didehydromiltirone	10.08 $\pm$ 2.22****	97.36 $\pm$ 2.78	1.12 $\pm$ 0.07
7 1,2-Didehydrotanshinone IIa	41.88 $\pm$ 2.05****	67.65 $\pm$ 1.88*	5.98 $\pm$ 0.49
8 1 $\beta$ -OH-Cryptotanshinone	17.70 $\pm$ 3.86****	93.15 $\pm$ 2.31	1.21 $\pm$ 0.10
9 15,16-Dihydrotanshinone	65.17 $\pm$ 1.39**	94.88 $\pm$ 1.88	1.71 $\pm$ 0.23
10 Tanshinone I	6.19 $\pm$ 3.91****	85.84 $\pm$ 4.15	11.24 $\pm$ 0.65
11 Isotanshinone II	5.55 $\pm$ 3.03****	77.81 $\pm$ 1.45*	9.16 $\pm$ 0.11
12 1(S)-OH-Tanshinone IIa	36.32 $\pm$ 1.85****	64.50 $\pm$ 1.50*	5.71 $\pm$ 0.27
13 Rosmarinic acid	28.18 $\pm$ 5.13****	80.74 $\pm$ 4.03	6.59 $\pm$ 0.37
Ref. <sup>c</sup> Galanthamine	85.64 $\pm$ 0.78	67.72 $\pm$ 1.70	12.56 $\pm$ 0.37

[\* $p$  < 0.05; \*\* $p$  < 0.01; \*\*\* $p$  < 0.001, \*\*\*\* $p$  < 0.0001].<sup>a</sup> Standard error mean (n = 3).<sup>b</sup> No inhibition.<sup>c</sup> Reference for AChE and BChE inhibition tested at 12.5  $\mu$ g/mL.**Fig. 2.** Metal-chelation capacity (%  $\pm$  S.E.M.) of the compounds 1–13 and reference (EDTA).**Table 2**

Statistical parameters extracted for QSAR models.

Receptor	Std. Coeff.	Descriptor	Std. Coeff.	Descriptor	R <sup>2</sup>	Q <sup>2</sup> <sub>LOO</sub>	Q <sup>2</sup> <sub>boot</sub>	a(R <sup>2</sup> )	a(Q <sup>2</sup> )	F	s
AChE	0.47	HGM	0.70	R2m	0.95	0.93	0.91	0.23	–0.23	83.64	0.18
BChE	–0.76	SpMax7_Bh(s)	–0.64	RDF080s	0.66	0.54	0.48	0.32	–0.25	8.91	0.34
Selectivity	–1.02	HATS2u	–0.46	R3m	0.91	0.86	0.79	0.28	–0.27	45.13	0.34

The cholinergic hypothesis proposes that AD is caused by a decrease in ACh level in the brain as well as BCh, leading to gradual neurodegeneration. In normal brain signaling, ACh is related to preserving and accessing memory as well as functioning, so increasing level of ACh is now one of the current pharmacotherapies of AD. As mentioned earlier, one of the treatment possibilities has focused on inhibition of the sister enzymes AChE and BChE by natural plant substances. In this regard, a variety of medicinal plants has been reported to show AChE inhibitory activity and, so, may be relevant to the treatment of neurodegenerative disorders such as AD. A list of plants with noteworthy AChE inhibitory activity seems to be long, but also limited by the appearance of central and

peripheral side effects (Mukherjee et al., 2007).

The tanshinones have been already reported to display a wide range of pharmacological activities such as cardioprotective, anti-cancer, antioxidant, mitochondria-protective, etc. (Adams et al., 2006). *S. miltiorrhiza* and some other plant species, i.e. *P. abrotanoides* Kar. (Sairafianpour et al., 2001) and *S. columbariae* Benth. (Adams et al., 2005), are the known sources of these compounds; while the species studied herein (*P. atriplicifolia* and *S. glutinosa*) have also been identified as novel sources for tanshinones. Neuroprotective property of tanshinones, which are lipid-soluble and have ability to pass blood-brain barrier, have been revealed in several studies, e.g. reduction in injured cortex neurons (He et al.,

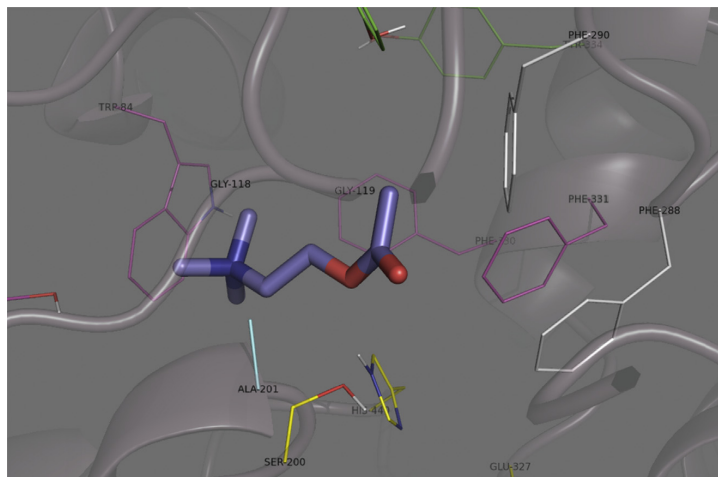


**Fig. 3.** Interactions of acetylcholine with residues within binding site of AChE. Crystal structure used was PDB:1EVE. Residues are colored according to their binding area as yellow (catalytic triad), pink (anionic site), grey (acyl pocket), blue (oxyanion hole) and green (peripheral anionic site). (For interpretation of the references to color in this figure legend, the reader is referred to the web version of this article.)

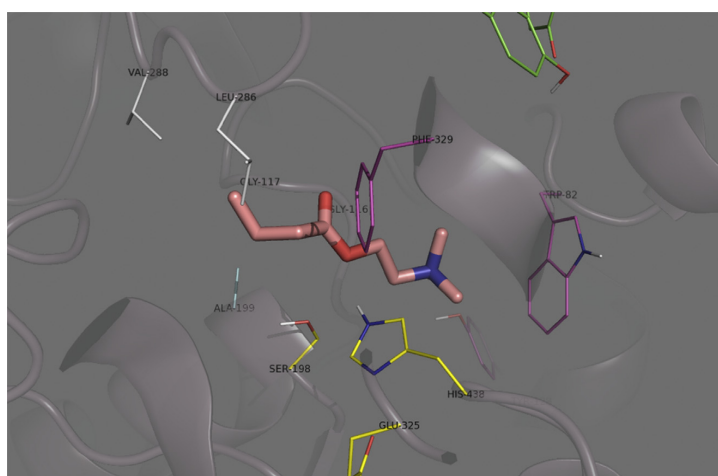


**Fig. 4.** Interactions of butyrylcholine with residues within binding site of BChE. Crystal structure used was PDB:1P0I. Residues are colored according to their binding area as yellow (catalytic triad), pink (anionic site), grey (acyl pocket), blue (oxyanion hole) and green (peripheral anionic site). (For interpretation of the references to color in this figure legend, the reader is referred to the web version of this article.)

2001), decrease in brain injury in tanshinone IIA and IIB-treated mice through reducing brain infarct volume and edema as well as restoration of neurological function in an experimental model of stroke *in vivo* (Lam et al., 2003), anticonvulsant activity *via* inhibiting pentylentetrazol (PTZ)-induced seizure activity in zebrafish larvae (Buenafe et al., 2013), and protecting pyramidal neurons of the hippocampal CA1 region (CA1) after transient cerebral ischemia in gerbils *via* increasing of neurotrophic factors (Park et al., 2014). Moreover, tanshinones isolated from *S. miltiorrhiza* together with phenolic acids have shown protective effect against  $\beta$ -amyloid-induced cytotoxicity and acted as inhibitors of AChE, probably with dual mechanism of action (Zhou et al., 2011). Accordingly, the roots of *P. atriplicifolia* and *S. glutinosa* can play a neuroprotective role due to containing similar active components. Multiple mechanisms of

action of tanshinones and phenolic components as neuroprotective agents relevant to AD have been described such as anti-amyloid- $\beta$ , antioxidant, anti-apoptosis, ChE inhibition, metal-chelation, and anti-inflammation (Bonaccini et al., 2015). Tanshinone I, tanshinone IIA, cryptotanshinone, and 15,16-dihydrotanshinone were demonstrated to reverse scopolamine-induced cognitive impairments using passive avoidance task test in mice by Kim et al. (2007). In the same study, modest inhibitory effect of cryptotanshinone and 15,16-dihydrotanshinone I was found *in vitro* with  $IC_{50}$  values 82 and 25  $\mu$ M, respectively, whereas  $IC_{50}$  value of tacrine (the reference) was 118.66 nM, which is consistent with our data on these compounds (Table 1). On the other hand, dihydrotanshinone, cryptotanshinone, tanshinone I, and tanshinone IIA were also tested by Ren et al. (2004) against AChE and the most potent ones

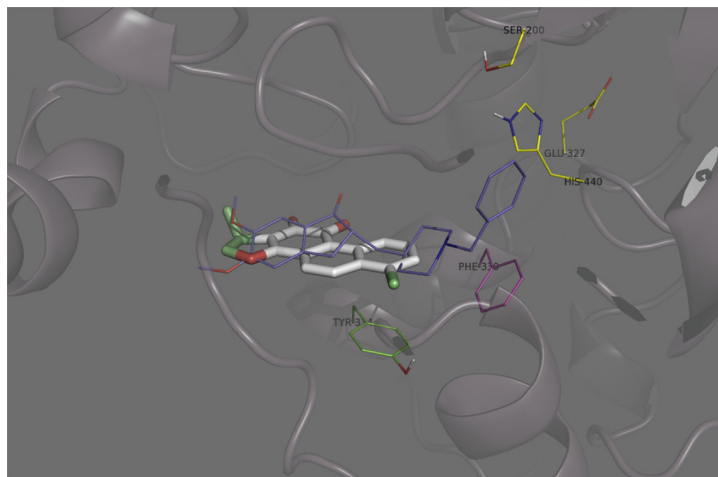


**Fig. 5.** Interactions of 15,16-dihydrotanshinone (9) (white skeleton) with residues within binding site of AChE. Crystal structure used was PDB:1EVE. Residues are colored according to their binding area as yellow (catalytic triad), pink (anionic site) and green (peripheral anionic site). Drug Aricept<sup>®</sup> is depicted with purple skeleton. (For interpretation of the references to color in this figure legend, the reader is referred to the web version of this article.)

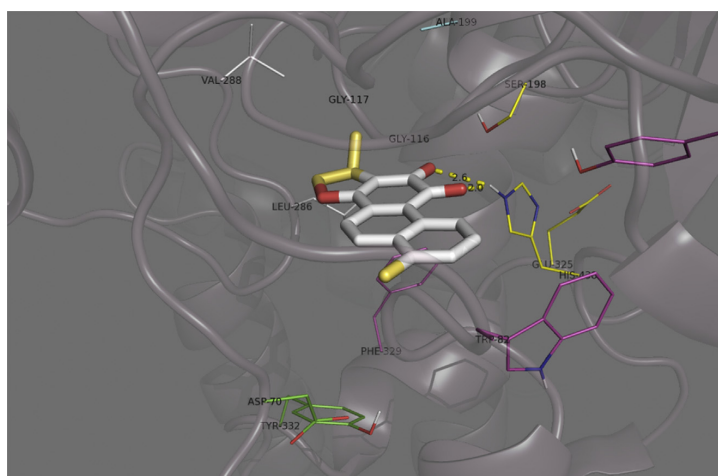


**Fig. 6.** Interactions of 15,16-dihydrotanshinone (9) with residues within binding site of BChE. Crystal structure used was PDB:1P0I. Residues are colored according to their binding area as yellow (catalytic triad), pink (anionic site), grey (acyl pocket), blue (oxyanion hole) and green (peripheral anionic site). (For interpretation of the references to color in this figure legend, the reader is referred to the web version of this article.)

were established as dihydrotanshinone ( $IC_{50} = 1.0 \mu\text{M}$ ) and cryptotanshinone ( $IC_{50} = 7.0 \mu\text{M}$ ). However, tanshinone I and IIA displayed low inhibition in this assay, which is in complete accordance with our current findings. Relevantly, tanshinones exhibited modulating effect on AChE and nitric oxide synthase concentrations in the hippocampus of rats with AD, which was suggestive of a benefit in AD (Yin et al., 2008). We previously reported *in vitro* inhibitory effect of rosmarinic acid from *Rosmarinus officinalis* L. against AChE and BChE ( $47.3 \pm 1.05\%$  and  $85.8 \pm 1.31\%$ , respectively) (Orhan et al., 2008) and found consistent results for rosmarinic acid in the present work isolated from *S. glutinosa*, which was proceeded to *in silico* study herein.

Our current investigation revealed significant inhibitory activity of the isolated tanshinones and rosmarinic acid towards BChE, and

mostly a weak inhibition to AChE. Among them, the most potent compound against AChE was found to be 15,16-dihydrotanshinone (9) with 65.17% of inhibition having affinity toward BChE (94.88%,  $IC_{50} = 1.71 \mu\text{g/mL}$ ) which was even higher than that of galanthamine (67.72%,  $IC_{50} = 12.56 \mu\text{g/mL}$ ). Consequently, it was chosen as a representative model for *in silico* experiments of this study in addition to rosmarinic acid (13).

Molecular docking analysis was used to simulate the binding conformations of tanshinones and rosmarinic acid into the active gorge of AChE and BChE. There is still insufficient information explaining potential SAR and QSAR of tanshinones towards ChEs. It should be noted that this is the first study on BChE inhibitory effect of isolated diterpenes and rosmarinic acid, all of which exerted much stronger inhibition toward BChE rather than AChE.

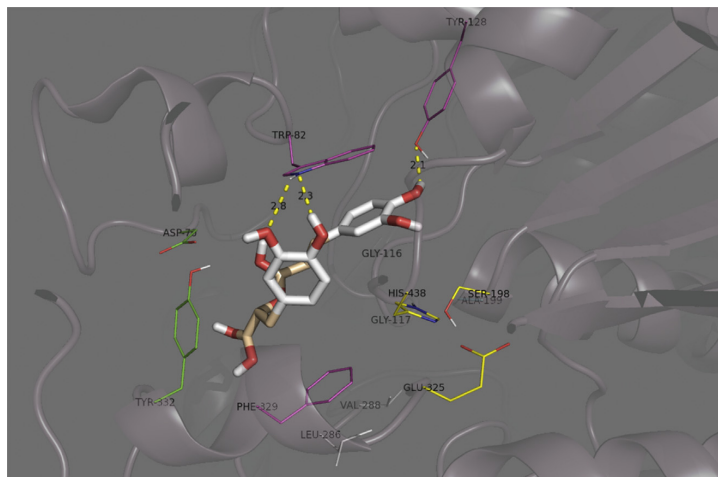


**Fig. 7.** Interactions of rosmarinic acid (13) with residues within binding site of BChE. Crystal structure used was PDB:1POI. Residues are colored according to their binding area as yellow (catalytic triad), pink (anionic site), grey (acyl pocket), blue (oxyanion hole) and green (peripheral anionic site). (For interpretation of the references to color in this figure legend, the reader is referred to the web version of this article.)

Tanshinones were shown to have inhibition of major microsomal cytochrome (CYP) isoforms that metabolize testosterone to hydroxytestosterone in the male rat liver, suggesting potential importance of furan group. The structural difference between 15,16-dihydrotanshinone and tanshinone I at carbon 15 position of furan ring resulted in the different modes of inhibition of CYP3A activity (Wang and Yeung, 2011). Hence, it might bring a possible explanation for affecting BChE and AChE by this compound. Miltirone inhibited BChE by more than 98%, which was the strongest activity among the tested compounds. However, miltirone did not inhibit AChE, what can be explained by possessing of isopropyl group instead of furan rings, and spatial conformation difference of binding in the enzyme active cavity.

Metal-chelation effect of is related to AD pathology as metal ions, i.e.  $\text{Cu}^{2+}$ ,  $\text{Zn}^{2+}$ , and  $\text{Fe}^{3+}$ , accumulates in the brain which causes oxidative damage. Therefore, it might be considered advantageous to have a metal-chelating property for an anti-AD drug candidate besides cholinesterase inhibition or reduction in  $\beta$ -amyloid plaque formation (Rowinska-Zyrek et al., 2015). In this regard, when we tested the compounds **1–13** for their possible metal-chelating effect, all of them exerted capacity to chelate  $\text{Fe}^{3+}$  below 50% (Fig. 2). Only 1,2-didehydrotanshinone **1a** and 1-OH-tanshinone **1a** had a closer effect to 50%.

### 3. Conclusion

In the current study, a number of tanshinones as well as rosmarinic acid isolated from *Perovskia atriplicifolia* and *Salvia glutinosa* have been revealed to exert a strong BChE inhibitory activity and relatively weaker inhibition against AChE. According to our findings, all of the compounds tested could be good precursor models for BChE-inhibiting molecules and among them, 15,16-dihydrotanshinone (**9**) in particular could be more promising since it can display dual inhibition toward both enzymes effectively. Moreover, our *in silico* data well-matched with the *in vitro* outcomes of this study. The *in silico* results indicated that QSAR models developed in this work can yield insights about AChE/BChE selectivity, while molecular docking results revealed that compounds **1–12** share similar interaction patterns, related to

hydrophobic and pi-pi stacking interactions in the case of AChE, thus blocking entry of substrate, and in the case of BChE, main interactions are due to hydrogen bonds with the catalytic triad, or TRP82 and TYR128. In this study, we disclose the first *in silico* study on cholinesterase inhibitory effect of tanshinones and rosmarinic acid, while the first BChE inhibitory data for the tested compounds, which have promising neuroprotective potential particularly for AD treatment.

## 4. Experimental

### 4.1. Chemicals

All solvents used for this work were of analytical grade and purchased from POCh (Gliwice, Poland) and Chempur (Piekary, Poland). HPLC-quality deionized water was obtained using Hydrolab system (Neunhuben, Poland). LC-MS grade acetonitrile; methanol, water, and formic acid were obtained from J.T. Baker, (Deventer, Netherlands).

### 4.2. Plant materials

The root samples of cultivated *P. atriplicifolia* Benth. and *S. glutinosa* L. (both Lamiaceae) were harvested from the certified collection of Botanical Garden of Medicinal Plants in Wrocław, Poland (Ministry of Environment decision No. DOPogiz-4210-26-6024-/05/kl) in the fall season of 2012. The voucher specimens have been preserved in the herbarium of the Botanical Garden under the accession no. "Lamiaceae-Patriplicifolia 2012/1-4" and "Lamiaceae-Sglutinosa-2012-1", respectively.

### 4.3. Instrumentation and chromatographic conditions

#### 4.3.1. Analytical HPLC-MS/MS

The HPLC system (Shimadzu, Japan) consisted of an LC-30ADXR Pump, DGU-20A3 degasser, SIL-20AXR auto sampler, aCTO-10ASVP column heater, and a CBM-20A system controller. For the isolated compounds **1–13**, we used an optimization method (without chromatographic column separation with direction

injection to MS system), which allows selection of collision energy and prominent MS/MS product ions. All data acquisition and peak integration were performed using LabSolution (5.53 SP2) from Shimadzu Ltd.

#### 4.3.2. MS/MS

Mass spectrometric (MS) detection was performed on a Shimadzu triple-quadrupole system LC/MS-8030 with electrospray ionization (ESI). The analytes were determined in positive ionization mode and quantified by multiple-reaction monitoring (MRM). The parameters and conditions were optimized as follows: capillary voltage 4.5 kV, desolvation line (DL) temperature 250 °C, heat block temperature 400 °C, nebulizing gas flow and drying gas flow were 3 L/min and 15 L/min, respectively. The  $[M+H]^+$  ion was selected for collision-activated dissociation (CID) studies as the precursor ion.

#### 4.3.3. NMR spectroscopy

NMR data were acquired at room temperature on a Bruker Avance III<sup>TM</sup> 500 MHz spectrometer (Bruker, Fällanden, Switzerland) operating at 500.13 MHz for  $^1H$ , and 125.77 MHz for  $^{13}C$  experiments. A 1 mm TXI-microprobe with a z-gradient was used for  $^1H$ -detected experiments; whilst  $^{13}C$ -NMR spectra were recorded with a 5 mm BBO-probe head with z-gradient. Structure assignment was achieved by comprehensive analysis of 2D NMR data ( $^1H$ - $^1H$  COSY, HMBC, and HSQC correlation) and by comparison with the literature data. Purity of the isolated substances was 95% as calculated by integration of the  $^1H$ -NMR spectra. Topspin 2.0 software was used for data processing.

#### 4.4. Isolation procedure of compounds 1–13

The dried and ground plant materials from *P. atriplicifolia* (250 g) and *S. glutinosa* (376 g) were extracted in ultrasonic bath (IS-40, Intersonic, Poland) with *n*-hexane (1.4 L) four times in 25 °C for 4 h for each and filtrated. The *n*-hexane phases were evaporated *in vacuo* to dryness which finally yielded 2.87 g of *n*-hexane extract of *P. atriplicifolia*. Isolation of compounds was explained in detail in our recent study (Ślusarczyka et al., 2015) on *P. atriplicifolia*, briefly, the *n*-hexane extract of *S. glutinosa* (1.4 g) was applied on glass column (50 × 5 cm) filled with silica gel 60 (200 g, 60–200 mesh). The column was eluted with dichloromethane-ethyl acetate (EtOAc) step gradient with EtOAc increasing from 5% to 100% (Table 1). The eluted fractions (31 in total) were monitored on thin layer chromatography (TLC, Merck SG-60 F<sub>254</sub>) and combined accordingly to obtain 10 subfractions (Table 3). Then, each subfraction was subsequently purified (Table 2) on flash chromatography column with *n*-hexane-EtOAc stepwise gradient starting from 0.5% EtOAc, then, 2%, 5%, 10%, and 30% of EtOAc and/or preparative TLC on (Silica 20 × 20, thicknesses 2 mm, Merck Germany) with *n*-hexane: EtOAc (9:1 v/v). Details of the isolated compounds are presented in Tables 3 and 4.

**Table 3**  
Step gradient column fractionation of the *n*-hexane extract *S. glutinosa*.

Eluent	Volume [ml]	Obtained fractions F
DCM	500	1–7
5% EtOAc in DCM	1450	8–23
7%	1000	24–25
10%	400	26
20%	200	27
40%	200	28
50% EtOAc in MeOH	200	29–30
100% MeOH	400	31

#### 4.5. Structure assignment of compounds 1–13

All isolated compounds were identified based on their MS/MS and 1D and 2D NMR spectra (NMR details in the Supplemental file, Table S1). Spectral characteristics (see SI) were in agreement with literature data (Nagy et al., 1999; Sairafianpour et al., 2001; Lee et al., 2005; Ślusarczyka et al., 2015). Nine of the isolated diterpenes; arucadiol (1), miltirone (2), tanshinone IIa (3), 1-oxomiltirone (4), cryptotanshinone (5), 1,2-didehydromiltirone (6), 1,2-didehydrotanshinone IIa (7), 1β-OH-cryptotanshinone (8) as well as rosmarinic acid (13) were identified as described in our previous paper (Ślusarczyka et al., 2015) and the references therein), whereas 15,16-dihydrotanshinone (9), tanshinone I (10), isotanshinone II (11) and 1(S)-OH-tanshinone IIa (12) from *S. glutinosa* have been characterized in this study as given below. From this species, we isolated seven compounds, four of which (9–12) were not detected in the *P. atriplicifolia* extract, whereas three other compounds (3, 5, and 6) were common in *P. atriplicifolia*. For compounds 6 and 12, this is a first record of their occurrence in *S. glutinosa*.

**15,16-Dihydrotanshinone (9):** Molecular ion  $m/z$  279  $[M+H]^+$  for compound 9 is a close analog of tanshinone I (10) with only small difference between C15–C16 for lack of double bond and molecular formula C<sub>18</sub>H<sub>14</sub>O<sub>3</sub>. The fragmentation gave minor ions at  $m/z$  261  $[M+H-H_2O]^+$ ,  $m/z$  233  $[M+H-H_2O-CO]^+$  and  $m/z$  205  $[M+H-H_2O-2CO]^+$ , which were attributed to successive losses of H<sub>2</sub>O and CO. Other two product ions at  $m/z$  218  $[M+H-H_2O-CO-CH_3]^+$  and 190  $[M+H-H_2O-2CO-CH_3]^+$  were attributed to losses of CH<sub>3</sub> radical residue from the precursor ions  $m/z$  233 and 218, respectively. For compound 9, H<sup>1</sup>-NMR experiment was done as well.

**Tanshinone I (10):**  $m/z$  277  $[M+H]^+$  generated preferential losses of CO and CH<sub>3</sub> radical cause to product ions at  $m/z$  249  $[M+H-CO]^+$ ,  $m/z$  234  $[M+H-CO-CH_3]^+$ ,  $m/z$  221  $[M+H-2CO]^+$  and  $m/z$  193  $[M+H-3CO]^+$ , respectively. Additionally, in order to confirm its structure,  $^1H$ -NMR experiment was done and results were compared in detail with the available literature data (Lee et al., 2005).

**Isotanshinone II (11):**  $^1H$ -NMR spectrum of compound 11 was very similar to that of compound 10, however signals of proton H6 and H7 in the spectrum appeared as a quartet δ 8.36, δ 8.38 ( $J = 8.8$  Hz) instead of doublet at δ 8.32 H-6, and δ 7.83 H-7 in that of compound 10. MRM fragmentation pathway of 11 was similar as well and we observed molecular ion  $m/z$  277  $[M+H]^+$  and  $m/z$  249  $[M+H-CO]^+$ ,  $m/z$  234  $[M+H-CO-CH_3]^+$ ,  $m/z$  221  $[M+H-2CO]^+$  and  $m/z$  193  $[M+H-3CO]^+$ , respectively. This compound was isolated previously from this species by Nagy et al. (1999).

**1(S)-OH tanshinone IIa (12):** Compound 12 possesses hydroxyl group in C<sub>1</sub> position. The target molecular ion in MRM experiments was  $m/z$  311  $[M+H]^+$ . In positive ion mode, we observed the loss of a H<sub>2</sub>O moiety as dominant ion fragmentation at  $m/z$  293  $[M+H-H_2O]^+$ , followed by CO moiety loss producing ion at  $m/z$  265  $[M+H-H_2O-CO]^+$ , and small abundant fragment corresponding with the loss of two H<sub>2</sub>O molecules  $m/z$  275  $[M+H-2H_2O]^+$ . The structure was confirmed by  $^1H$ -NMR experiments, where OH group in A ring was revealed as resulting from oxidation of methin group in position H-1 δ 5.36 ( $dd, J = 3.4, 3.4$  Hz) δ 5.27 ( $brq, J = 3.5$  Hz) that additionally improved  $^{13}C$ -NMR signal for carbon in this position C-1 δ 64.1 ppm. The other NMR signals were similar to those of tanshinone IIa (3). The stereochemistry of C1 hydroxyl group was confirmed by circular dichroism measurement. Hydroxytanshinone IIa was previously isolated by Sairafianpour et al. (2001) from *Perovskia* roots but was optically inactive and was interpreted as a photooxidation product of non-biosynthetic origin. Therefore, we have also measured circular dichroism using Jasco 1500 CD-

**Table 4**  
Process and amount of compounds isolated from the *n*-hexane extract *S. glutinosa*.

Fraction combination	Amount (mg)	Process of purification	Obtained compounds (mg)
F1–F10	81	Flash chromatography	Tanshinone IIa (16.4)
F11	18	NP <sup>a</sup>	
F12	184.2	Flash chromatography	Cryptotanshinone (23) Tanshinone I (7.2)
F13	63.5	Preparative chromatography	1,2-Dihydrotanshinone (9.5)
F14	74.5	Preparative chromatography	Isotanshinone II (2.4)
F15	32.8	NP	
F16–F17	289.6	Flash chromatography	15,16-Dihydrotanshinone IIa (38.6)
F18–F19	89.4	Flash chromatography	1(S)-OH-Tanshinone IIa (13.1)
F20–F23	172.7	NP	
F24–F31	113.2	NP	

<sup>a</sup> Not purified because of lack of target compounds or too small amount.

spectrophotometer (Jasco, Japan) of **12**, dissolved in 80% MeOH at 1 mM and superimposed the experimental spectrum over the simulated spectrum calculated using TDDFT (see Supplementary information, Fig. S1).

Considering compound **12** isolated from our material, the CD spectrum revealed the evident circular dichroism indicating optical activity that was attributed to hydroxylation of the asymmetric carbon 1 in configuration unambiguously established as 1-*S*. This compound is reported for the first time as a natural product from *S. glutinosa*.

#### 4.6. Microtiter assays for AChE and BChE inhibition

AChE and BChE inhibitory activity of the compounds was determined by modified spectrophotometric method of Ellman et al. (1961). Electric eel AChE (Type-VI-S, EC 3.1.1.7, Sigma) and horse serum BChE (EC 3.1.1.8, Sigma) were used as the enzyme sources, while acetylthiocholine iodide and butyrylthiocholine chloride (Sigma, St. Louis, MO, USA) were employed as substrates of the reaction. 5,5'-Dithio-bis(2-nitrobenzoic)acid (DTNB, Sigma, St. Louis, MO, USA) was used for the measurement of the cholinesterase activity. All the other reagents and conditions were the same as described in our previous publication (Georgiev et al., 2011). In brief, 140  $\mu$ L of 0.1 mM sodium phosphate buffer (pH 8.0), 20  $\mu$ L of 0.2 M DTNB, 20  $\mu$ L of sample solutions and 20  $\mu$ L of 0.2 M acetylcholinesterase/butyrylcholinesterase solution were added by multichannel automatic pipette (Gilson pipetman, France) in a 96-well microplate and incubated for 15 min at 25 °C. The reaction was then initiated with the addition of 10  $\mu$ L of 0.2 M acetylthiocholine iodide/butyrylthiocholine chloride. The hydrolysis of acetylthiocholine iodide/butyrylthiocholine chloride was monitored by the formation of the yellow 5-thio-2-nitrobenzoate anion as a result of the reaction of DTNB with thiocholines, catalyzed by enzymes at a wavelength of 412 nm utilizing a 96-well microplate reader (VersaMax, Molecular Devices, USA). Galanthamine, the anticholinesterase alkaloid-type of drug isolated from the bulbs of snowdrop (*Galanthus* sp.), was purchased from Sigma (St. Louis, MO, USA) and was employed as the reference.

#### 4.7. Data processing for enzyme inhibition assays

The measurements and calculations were evaluated by using Softmax PRO 4.3.2.LS software. Percentage of inhibition of AChE/BChE was determined by comparison of rates of reaction of test samples relative to blank sample (ethanol in phosphate buffer pH = 8). Extent of the enzymatic reaction was calculated based on the following equation:  $E = (C - T)/C \times 100$ , where *E* is the activity of the enzyme. *E* value expresses the effect of the test sample or the positive control on AChE and BChE enzyme activity articulated as

the percentage of the remaining activity in the presence of test sample or positive control. *C* value is the absorbance of the control solvent (blank) in the presence of enzyme, where *T* is the absorbance of the tested sample (plant extract or positive control in the solvent) in the presence of enzyme.

Data are expressed as average inhibition  $\pm$  standard error mean (S.E.M.) and the results were taken from at least three independent experiments performed in triplicate.

#### 4.8. Fe<sup>2+</sup>-ferrozine test system for metal-chelation capacity

The metal-chelating effect of the extracts by Fe<sup>2+</sup>-ferrozine test system was estimated using Chua et al.'s (2008) method. Accordingly, 740  $\mu$ L of ethanol and 200  $\mu$ L of the samples dissolved in ethanol (75%) were incubated with 2 mM FeCl<sub>2</sub> solution. The reaction was initiated by the addition of 40  $\mu$ L of 5 mM ferrozine solution into the mixture, shaken vigorously, and left standing at ambient temperature for 10 min. The absorbance of the reaction mixture was measured at 562 nm. Ethylenediaminetetraacetic acid (EDTA) was employed as the reference in this assay and metal-chelation capacity was calculated as given below and the results were expressed as percent inhibition (%):

$\% = [(A_{\text{blank}} - A_{\text{sample}})/A_{\text{blank}}] \times 100$ , where *A*<sub>blank</sub> is the absorbance of the control reaction (containing all reagents except the test sample), and *A*<sub>sample</sub> is the absorbance of the extracts. Analyses were run in triplicate and the results were expressed as average values with S.E.M. (Standard error of the mean).

#### 4.9. Statistical analysis of data

Data obtained from *in vitro* enzyme inhibition experiments were expressed as the SEM. Statistical differences between the reference and the sample groups were evaluated by ANOVA (one way). Dunnett's multiple comparison tests were used as *post hoc* tests.  $p < 0.05$  was considered to be significant [ $*p < 0.05$ ;  $**p < 0.01$ ;  $***p < 0.001$ ,  $****p < 0.0001$ ].

#### 4.10. QSAR modeling

Assessment of quantitative structure-activity relationship (QSAR) is a technique widely used in medicinal chemistry (Nantasenamat et al., 2009; Roy and Das, 2014). With this technique, we can correlate the observed biological activity with a series of variables called descriptors that codify several aspects of the molecules under study, such as structure, topology, charge distribution, etc. Thus, these methods have predictive abilities and they can also be used in the analysis of structural characteristics that can give rise to the activities of interest.

For this work, the activity values used to develop a QSAR models

42

F.S. Senol et al. / *Phytochemistry* 133 (2017) 33–44

were based on the transformation of the inhibition percentage given in Table 1. The activity was transformed into logarithmic by the equation:

$$I = \log[\%I/(100 - \%I)] \quad (1)$$

Where %I was the inhibition percentage.

We did also study the selectivity between two receptors for the compounds of Table 2, being selectivity a widely used aspect in

drug design and QSAR (Salt et al., 2004; Weber et al., 2006; Helguera et al., 2013). For selectivity models, we used the difference between both activities and for both receptors through the following equation:

$$S = I(\text{BChE}) - I(\text{AChE}) \quad (2)$$

Where I(BChE) and I(AChE) was the activities calculated by Eq. (1) for BChE and AChE inhibition activity, respectively.

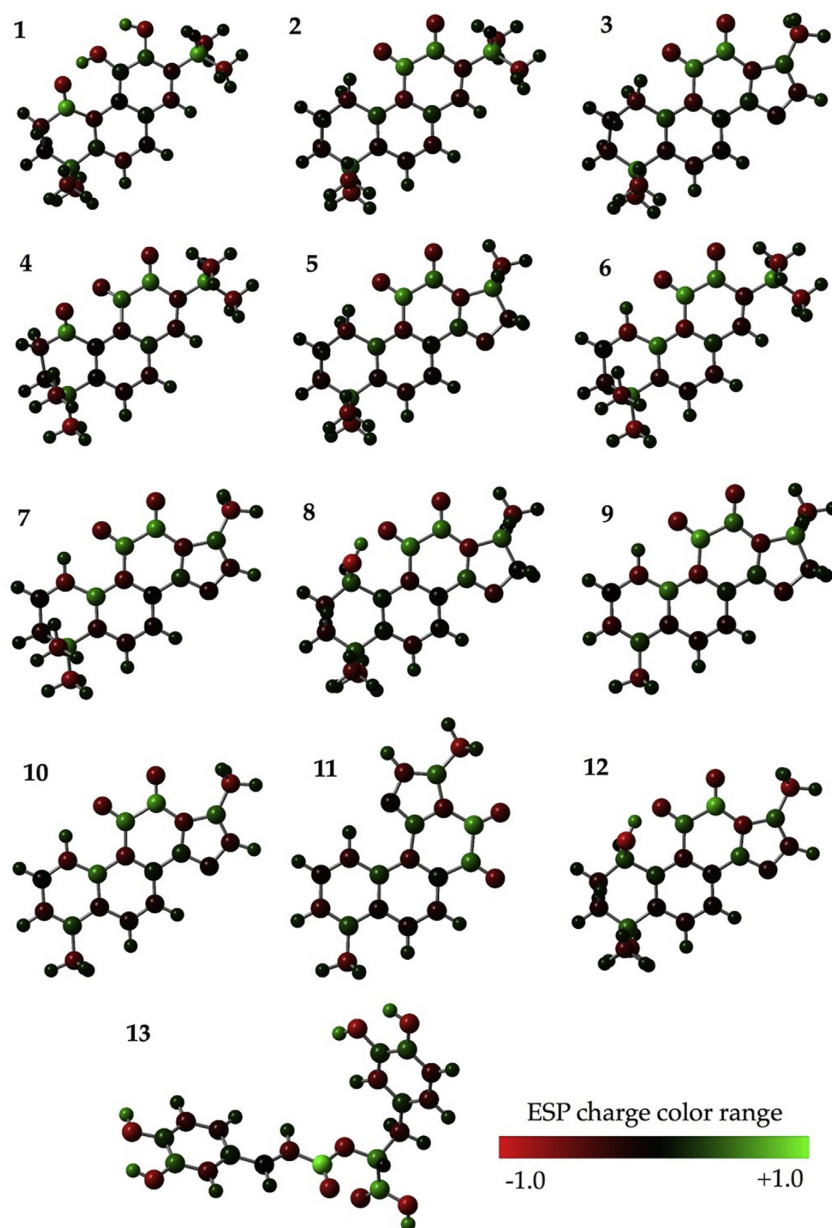


**Fig. 8.** Optimized structures at the selected DFT level of theory. Each atom is colored by the computed ESP charge (see charge color range). (For interpretation of the references to color in this figure legend, the reader is referred to the web version of this article.)

The DRAGON (Todeschini et al., 2004) and MOE (2008) descriptors were used as the variables to correlate with the activities and applied a full search procedure for selecting the variables, as implemented in Mobydigs software ver. 1.0.43. Goodness of fit of the models was assessed by examining the determination coefficient (R<sup>2</sup>), the standard deviation (s), and the Fisher ratio (F). The robustness and predictivity of the models were evaluated by means of cross-validation, basically leave-one-out (LOO) (Cruciani et al., 1992) and bootstrapping testing techniques (Efron, 1987) were calculated with the training set, by looking to the outcome statistics of both techniques (i.e. Q2LOO and Q2boot). Further, the stability under heavy perturbations in the training set was checked by examining the outcome statistics of a response randomization procedure (Y scrambling) for the training and test sets (a(R2) and a(Q2) values) (Lindgren et al., 1996). Good quality of the models is indicated by high F and by low s, as well as by values closed to one for R<sup>2</sup>, Q2LOO and Q2boot and values of a(R2) and a(Q2) close to zero.

#### 4.11. Molecular docking experiments

The geometry of each ligand was fully optimized within the density functional theory (DFT) framework at the B3LYP/6-31G(d) level (Becke, 1993; Lee et al., 2005). Vibrational calculations were subsequently performed to ascertain the nature of every localized structure: a stable structure corresponds to a minimum in the potential energy surface and consequently all frequencies are real. Partial atomic charges were next computed by using the Merz-Singh-Kollman ESP protocol (Singh and Kollman, 1984; Besler et al., 1990) to be used during docking simulations. All quantum chemical calculations were performed with the Gaussian 09 suite of programs (Gaussian, 2009), and partial charges distribution for all compounds that can be seen from Table 2 and Fig. 8.

The molecular structures used in this study were built manually using AutoDock tools (Morris et al., 2009) or derived from experimental data. The structures for AChE and BChE were extracted from the crystal structures of protein data bank (PDB) with codes 1EVE and 1POI, respectively and converted to PDBQT format using default parameters. Molecular docking calculations were carried out using default parameters in AutoDock Vina (Trott and Olson, 2010). Graphical representations of the docking results were prepared using PyMOL (Molecular Graphics System, version 1.3, Schrödinger, LLC).

#### Acknowledgements

This work has been funded by the Fundación Séneca del Centro de Coordinación de la Investigación de la Región de Murcia under Project 18946/JLI/13 and by the Nils Coordinated Mobility under grant 012-ABEL-CM-2014A, in part financed by the European Regional Development Fund (ERDF). The cultivation and analysis of experimental plants is supported by the grant for special research facility [Decision No. 215259/E-394/SPUB/2014/1] and Medical University grant No. ST-909. S. Ślusarczyk contribution was supported by postdoctoral training grant FUGA DEC/2014/12/S/NZ9/00715. We also appreciate help with circular dichroism spectroscopy provided by Dr. Samad Nejad Ebrahimi from Shahid Beheshti University, Department of Phytochemistry (Iran) and Dr. Aleksandra Marciniak from Wrocław Medical University, Department of Inorganic Chemistry (Poland).

#### Appendix A. Supplementary data

Supplementary data related to this article can be found at <http://dx.doi.org/10.1016/j.phytochem.2016.10.012>.

#### References

- Adams Jr., J.D., Wall, M., Garcia, C., 2005. *Salvia columbariae* contains tanshinones. Evid.-Based Complement. Altern. Med. 2, 107–110.
- Adams, J.D., Wang, R., Yang, J., Lien, E.J., 2006. Preclinical and clinical examinations of *Salvia miltiorrhiza* and its tanshinones in ischemic conditions. Chin. Med. 1, Article number 3.
- Bajda, M., Więckowska, A., Hebda, M., Guzior, N., Sottriffer, C.A., Malawska, B., 2013. Structure-based search for inhibitors of cholinesterases. Int. J. Mol. Sci. 14, 5608–5632.
- Becke, A.D., 1993. Density-functional thermochemistry III. The role of exact exchange. J. Chem. Phys. 98, 5648–5652.
- Besler, B.H., Merz, K.M., Kollman, P.A., 1990. Atomic charges derived from semi-empirical methods. J. Comp. Chem. 11, 431–439.
- Bonaccini, L., Karioti, A., Bergonzi, M.C., Bilia, A.R., 2015. Effects of *Salvia miltiorrhiza* on CNS neuronal injury and degeneration: a plausible complementary role of tanshinones and depsides. Planta Med. 81, 1003–1016.
- Buenafe, O.E., Orellana-Paucar, A., Maes, J., Huang, H., Ying, X., De Borggraeve, W., Crawford, A.D., Luyten, W., Esguerra, C.V., De Witte, P., 2013. Tanshinone IIA exhibits anticonvulsant activity in zebrafish and mouse seizure models. ACS Chem. Neurosci. 4, 1479–1487.
- Chen, X., Guo, J., Bao, J., Lu, J., Wang, Y., 2014. The anticancer properties of *Salvia miltiorrhiza* Bunge (danshen): a systematic review. Med. Res. Rev. 34, 768–794.
- Chua, M.T., Tung, Y.T., Chang, S.T., 2008. Antioxidant activities of ethanolic extracts from the twigs of *Cinnamomum osmophleum*. Bioresour. Technol. 99, 1918–1925.
- Cruciani, G., Baroni, M., Clementi, S., Costantino, G., Riganelli, D., Skagerberg, B., 1992. Predictive ability of regression models. I. Standard deviation of prediction errors (SDEP). J. Chemom. 6, 335–346.
- Efron, B., 1987. Better bootstrap confidence intervals. J. Am. Stat. Assoc. 82, 171–200.
- Ellman, G.L., Courtney, K.D., Andres, V., Featherstone, R.M., 1961. A and rapid colorimetric determination of acetylcholinesterase activity. Biochem. Pharmacol. 7, 88–95.
- Frisch, M.J., Trucks, G.W., Schlegel, H.B., Scuseria, G.E., Robb, M.A., Cheeseman, J.R., Scalmani, G., Barone, V., Mennucci, B., Petersson, G.A., et al., 2009. Gaussian 09, Revision A.02. Gaussian, Inc., Wallingford CT.
- Georgiev, M., Alipieva, K., Orhan, I., Abrashev, R., Denev, P., Angelova, M., 2011. Antioxidant and cholinesterase inhibitory activities of *Verbascum xanthophoenicum* Griseb. and its phenylethanoid glycosides. Food Chem. 128, 100–105.
- Guzior, N., Więckowska, A., Panek, D., Malawska, B., 2015. Recent development of multifunctional agents as potential drug candidates for the treatment of Alzheimer's disease. Curr. Med. Chem. 22, 373–404.
- He, L.N., He, S.B., Yang, J., Wang, J., Liu, C., 2001. Protective effect of tanshinones against ischemia injury in cultured primary cortex neurons. Chin. Pharmacol. Bull. 17, 214–217.
- Helguera, A.M., Pérez-Garrido, A., Gaspar, A., Reis, J., Cagide, F., Vina, D., Cordeiro, M.N.D.S., Borges, F., 2013. Combining QSAR classification models for predictive modeling of human monoamine oxidase inhibitors. Eur. J. Med. Chem. 59, 75–90.
- Kim, D.H., Jeon, S.J., Jung, J.W., Lee, S., Yoon, B.H., Shin, B.Y., Son, K.H., Cheong, J.H., Kim, Y.S., Kang, S.S., Ko, K.H., Ryu, J.H., 2007. Tanshinone congeners improve memory impairments induced by scopolamine on passive avoidance tasks in mice. Eur. J. Pharmacol. 574, 140–147.
- Lam, B.Y.H., Lo, A.C.Y., Sun, X., Luo, H.W., Chung, S.K., Sucher, N.J., 2003. Neuroprotective effects of tanshinones in transient focal cerebral ischemia in mice. Phytomedicine 10, 286–291.
- Lee, S., Choi, D., Woo, E., 2005. Inhibition of osteoclast differentiation by tanshinones from the root of *Salvia miltiorrhiza* Bunge. Arch. Pharm. Res. 28, 909–913.
- Li, B., Duysen, E.G., Carlson, M., Lockridge, O., 2008. The butyrylcholinesterase knockout mouse as a model for human butyrylcholinesterase deficiency. J. Pharmacol. Exp. Ther. 324, 1146–1154.
- Lindgren, F., Hansen, B., Karcher, W., Sjöström, M., Eriksson, L., 1996. Model validation by permutation tests: applications to variable selection. J. Chemom. 10, 521–532.
- MOE (Molecular Operating Environment), 2008. Chemical Computing Group, Inc., Montreal, QC, Canada.
- Morris, G.M., Huey, R., Lindstrom, W., Sanner, M.F., Belew, R.K., Goodsell, D.S., Olson, A.J., 2009. AutoDock4 and AutoDockTools4: automated docking with selective receptor flexibility. J. Comp. Chem. 30, 2785–2791.
- Mukherjee, P.K., Kumar, V., Mal, M., Houghton, P.J., 2007. Acetylcholinesterase inhibitors from plants. Phytomedicine 14, 289–300.
- Nagy, Á., Gu, Á., Crabb, T.A., 1999. Diterpenoids from *Salvia glutinosa*, *S. austriaca*, *S. tomentosa* and *S. verticillata* roots. Phytochemistry 52, 1105–1109.
- Nantasenamat, C., Isarankura-Na-Ayudhya, C., Naenna, T., Prachayasittikul, V., 2009. A practical overview of quantitative structure-activity relationships. EXCLI J. 8, 74–88.
- Orhan, I., Aslan, S., Kartal, M., Sener, B., Baser, K.H.C., 2008. Inhibitory effect of Turkish *Rosmarinus officinalis* L. on acetylcholinesterase and butyrylcholinesterase enzymes. Food Chem. 108, 663–668.
- Orhan, I.E., Orhan, G., Gurkas, E., 2011. An overview on natural cholinesterase inhibitors - a multi-targeted drug class - and their mass production. Mini Rev. Med. Chem. 11, 836–842.
- Park, J.H., Park, O.K., Yan, B.C., Ahn, J.H., Kim, I.H., Lee, J.C., Kwon, S.H., Yoo, K.Y.,



- Lee, C.H., Hwang, I.K., et al., 2014. Neuroprotection via maintenance or increase of antioxidants and neurotrophic factors in ischemic gerbil hippocampus treated with tanshinone I. *Chin. Med. J.* 127, 3396–3405.
- Ren, Y., Houghton, P.J., Hider, R.C., Howes, M.J., 2004. Novel diterpenoid acetylcholinesterase inhibitors from *Salvia miltiorrhiza*. *Planta Med.* 70, 201–204.
- Rowinska-Zyrek, M., Salerno, M., Kozłowski, H., 2015. Neurodegenerative diseases - understanding their molecular bases and progress in the development of potential treatments. *Coord. Chem. Rev.* 284, 298–312.
- Roy, K., Das, R.N., 2014. A review on principles, theory and practices of 2D-QSAR. *Curr. Drug Metab.* 15, 346–379.
- Sairafianpour, M., Christensen, J., Steerk, D., Budnik, B.A., Kharazmi, A., Bagherzadeh, K., Jaroszewski, J.W., 2001. Leishmanicidal, antiplasmodial, and cytotoxic activity of novel diterpenoid 1,2-quinones from *Perovskia abrotanoides*: source of tanshinones. *J. Nat. Prod.* 64, 1398–1403.
- Salt, D.W., Maccari, L., Botta, M., Ford, M.G., 2004. Variable selection and specification of robust QSAR models from multicollinear data: arylpiperazinyli derivatives with affinity and selectivity for alpha2-adrenoceptors. *J. Comp. Aided Mol. Des.* 18, 495–509.
- Shang, Q., Wang, H., Li, S., Xu, H., 2013. The effect of sodium tanshinone IIA sulfate and simvastatin on elevated serum levels of inflammatory markers in patients with coronary heart disease: a study protocol for a randomized controlled trial. *Evid.-Based Complement. Altern. Med.* 2013, Article number 756519.
- Singh, U.C., Kollman, P.A., 1984. An approach to computing electrostatic charges for molecules. *J. Comp. Chem.* 5, 129–145.
- Ślusarczyka, S., Topolski, J., Domaradzki, K., Adams, M., Hamburger, M., Matkowski, A., 2015. Isolation and fast selective determination of nor-abietanoid diterpenoids from *Perovskia atriplicifolia* roots using LC-ESIMS/MS with multiple reaction monitoring. *Nat. Prod. Commun.* 10, 1149–1152.
- Todeschini, R., Ballabio, D., Consonni, V., Mauri, A., Pavan, M., 2004. Mobydigs Computer Software, Milano.
- Trott, O., Olson, A.J., 2010. AutoDock Vina: improving the speed and accuracy of docking with a scoring function, efficient optimization, and multithreading. *J. Comp. Chem.* 31, 455–461.
- Wang, X., Yeung, J.H.K., 2011. Inhibitory effect of tanshinones on rat CYP3A2 and CYP2C11 activity and its structure-activity relationship. *Fitoterapia* 82, 539–545.
- Weber, A., Bohm, M., Supuran, C.T., Scozzafava, A., Sotriffer, C.A., Klebe, G., 2006. 3D QSAR selectivity analyses of carbonic anhydrase inhibitors: insights for the design of isozyme selective inhibitors. *J. Chem. Inf. Model.* 46, 2737–2760.
- Wu, Z., Song, L., Liu, S.Q., Huang, D., 2014. Tanshinones extend chronological lifespan in budding yeast *Saccharomyces cerevisiae*. *Appl. Microbiol. Biotechnol.* 98, 8617–8628.
- Yin, Y., Huang, L., Liu, Y., Huang, S., Zhuang, J., Chen, X., Zhang, L., Wu, H., Shao, F., Zhao, Z., 2008. Effect of tanshinone on the levels of nitric oxide synthase and acetylcholinesterase in the brain of Alzheimer's disease rat model. *Clin. Investig. Med.* 31, 248–257.
- Zhou, Y., Li, W., Xu, L., Chen, L., 2011. In *Salvia miltiorrhiza*, phenolic acids possess protective properties against amyloid  $\beta$ -induced cytotoxicity and tanshinones act as acetylcholinesterase inhibitors. *Environ. Toxicol. Pharmacol.* 31, 443–452.

## 2.4 Acetylcholinesterase inhibitory assessment of isolated constituents from *Salsola grandis* Freitag, Vural & Adıgüzel and molecular modeling studies on N-acetyltryptophan

<b>Title</b>	<i>Acetylcholinesterase inhibitory assessment of isolated constituents from Salsola grandis Freitag, Vural &amp; Adıgüzel and molecular modeling studies on N-acetyltryptophan</i>
<b>Authors</b>	Ilkay Erdogan Orhan and Nurgun Kucukboyaci and Ihsan Calis and José P. Cerón-Carrasco and Helena den-Haan and Jorge Peña-García and Horacio Pérez-Sánchez.
<b>Journal</b>	<i>Phytochemistry Letters</i>
<b>Year</b>	2016
<b>State</b>	Published

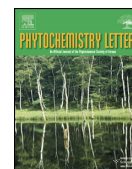
### PhD candidate contribution

Helena den Haan Alonso, declares to be the co-author and contributor of the article *Acetylcholinesterase inhibitory assessment of isolated constituents from Salsola grandis Freitag, Vural & Adıgüzel and molecular modeling studies on N-acetyltryptophan* in the section on computational chemistry.



Contents lists available at ScienceDirect

Phytochemistry Letters

journal homepage: [www.elsevier.com/locate/phytol](http://www.elsevier.com/locate/phytol)

## Acetylcholinesterase inhibitory assessment of isolated constituents from *Salsola grandis* Freitag, Vural & Adıgüzel and molecular modeling studies on *N*-acetyltryptophan



Ilkay Erdogan Orhan<sup>a,\*</sup>, Nurgun Kucukboyaci<sup>a</sup>, Ihsan Calis<sup>b</sup>, José P. Cerón-Carrasco<sup>c</sup>, Helena den-Haan<sup>c</sup>, Jorge Peña-García<sup>c</sup>, Horacio Pérez-Sánchez<sup>c,1</sup>

<sup>a</sup> Department of Pharmacognosy, Faculty of Pharmacy, Gazi University, 06330 Ankara, Turkey

<sup>b</sup> Department of Pharmacognosy, Faculty of Pharmacy, Near East University, Cyprus

<sup>c</sup> Bioinformatics and High Performance Computing Research Group (BIO-HPC), Universidad Católica San Antonio de Murcia (UCAM), 30107 Murcia, Spain

### ARTICLE INFO

#### Article history:

Received 20 August 2016

Received in revised form 1 October 2016

Accepted 17 October 2016

Available online 27 October 2016

#### Keywords:

*Salsola grandis*

Chenopodiaceae

Acetylcholinesterase

*N*-acetyltryptophan

*In silico*

Molecular docking

### ABSTRACT

*S. grandis* Freitag, Vural & N. Adıgüzel is an endemic plant species to Turkey. Since some other *Salsola* species have been reported to exert cholinesterase inhibitory effect, we aimed to investigate its inhibitory potential against AChE. The EtOH extract and thirteen constituents [ten flavonol derivatives; e.g. isorhamnetin-3-*O*-rutinoside (**1**), quercetin-3-*O*-rutinoside (**2**), quercetin-3-*O*-methyl ether (**3**), tilirosin (**4**), isorhamnetin-3-*O*-glucuronide (**5**), isorhamnetin-3-*O*-glucoside (**6**), quercetin-3-*O*-galactoside (**7**), quercetin-3-*O*-rhamnoside (**8**), quercetin (**9**), and manghaslin (**10**), two oleanane-type saponosides; e.g. momordin II b (**11**) and II c (**12**) as well as one amino acid derivative, *N*-acetyltryptophan (**13**)] isolated from the aerial parts of *Salsola grandis* (Chenopodiaceae) were tested for their possible inhibitory activity against acetylcholinesterase (AChE), related to pathogenesis of Alzheimer's disease. Although the EtOH extract was inactive, among the isolated compounds, only compound **13** exerted a notable inhibition of  $64.90 \pm 1.61\%$  at  $50 \mu\text{g mL}^{-1}$ , while compound **12** displayed a low inhibition ( $21.72 \pm 0.99\%$ ). Then, compound **13** was further subjected to molecular modeling experiments in order to give insights about its interactions at atomic level with AChE. The data indicated that *N*-acetyltryptophan (**13**) could be a promising model molecule for AD treatment.

© 2016 Phytochemical Society of Europe. Published by Elsevier Ltd. All rights reserved.

### 1. Introduction

The genus *Salsola* L. (Chenopodiaceae) is represented by sixteen species in the flora of Turkey, among which *S. grandis* Freitag, Vural & N. Adıgüzel is an endemic species (Freitag, 2000). The phytochemical studies on *Salsola* species have pointed out to rich presence of alkaloids in particular such as salsolin and salsolidin, besides flavonoids and isoflavonoids (Dauletmuratov and Komarova, 1980; Mnatsakanyan et al., 1981; Berhanu and Yordanos, 1990),

lignans, saponosides, and coumarins (Narantuyaa et al., 1986; Syrchina et al., 1992; Han et al., 2003). *Salsola* species have been reported to contain various constituents that have shown several biological activities such as anti-inflammatory, analgesic, anti-hypertensive, antioxidant, hepatoprotective, and tyrosinase inhibitory activity (Nofal et al., 2002; Han et al., 2003). In a previous study, the alkaloid extracts from *S. oppositifolia* Desf., *S. soda* L., and *S. tragus* L. growing in Italy were reported to have a varying degree of inhibition against acetylcholinesterase (AChE, EC 3.1.1.7) (Tundis et al., 2009).

AChE inhibitors are currently the most prescribed drug class for the treatment of Alzheimer's disease (AD), which is a progressive neurodegenerative disease encountered mainly in elderly population. According to the cholinergic hypothesis, deficit of acetylcholine (ACh) has been found in the brains of AD patients and, therefore, inhibition of AChE, the critical enzyme that hydrolyses ACh, is the most accepted treatment approach toward AD (Orhan et al., 2011). Several AChE inhibitors such as tacrine, rivastigmine, donepezil, and galanthamine are clinically available (Hogan, 2014).

**Abbreviations:** ACh, acetylcholine; AChE, acetylcholinesterase; AD, Alzheimer's disease; MPLC, medium pressure liquid chromatography; NMR, nuclear magnetic resonance; SCC, silica gel column chromatography; TLC, thin layer chromatography.

\* Corresponding author.

E-mail address: [iorhan@gazi.edu.tr](mailto:iorhan@gazi.edu.tr) (I.E. Orhan).

<sup>1</sup> To whom all molecular modeling correspondence should be addressed. Bioinformatics and High Performance Computing Research Group (BIO-HPC), Universidad Católica San Antonio de Murcia (UCAM), 30107 Murcia, Spain; Tel: +34 968278819, fax: +34 968278819; E-mail address: [hperez@ucam.edu](mailto:hperez@ucam.edu) (H. Pérez-Sánchez).

<http://dx.doi.org/10.1016/j.phytol.2016.10.017>

1874-3900/© 2016 Phytochemical Society of Europe. Published by Elsevier Ltd. All rights reserved.

However, due to their side effects and limited bioavailability, new AChE inhibitors of both natural and synthetic origins are under an extensive search.

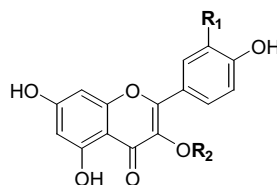
Up to date, we have investigated a large number of medicinal plants as well as natural compounds using *in vitro* and *in silico* (molecular docking) experiments, which led us to find different cholinesterase inhibitors such as *Salvia* L. species, *Angelica officinalis* L., *Hypericum perforatum* L., etc. (Senol et al., 2011a,b; Altun et al., 2013). As part of our ongoing efforts for this purpose, we have now aimed to investigate AChE inhibitory potential of the isolated constituents (1–13) and the main ethanol (EtOH) extract from *Salsola grandis* in the current study.

## 2. Results and discussion

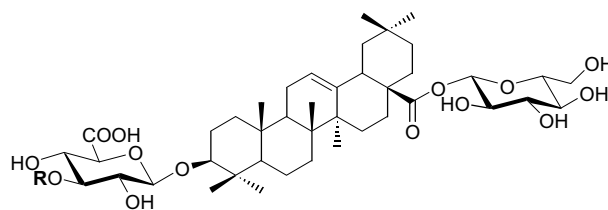
Our phytochemical studies on the main EtOH extract of the aerial parts of *S. grandis* resulted in isolation of thirteen known compounds (Fig. 1). The chemical structures of the isolated flavonoids and saponosides were identified as isorhamnetin-3-O-

rutinoside (**1**), quercetin-3-O-rutinoside (**2**), quercetin-3-O-methyl ether (**3**), tilioside (**4**), isorhamnetin-3-glucuronide (**5**), isorhamnetin-3-O-glucoside (**6**), quercetin-3-O-galactoside (**7**), quercetin-3-O-rhamnoside (**8**), quercetin (**9**), and manghaslin (**10**), momordin II b (**11**), and momordin II c (**12**) by comparing their spectroscopic data with the relevant literatures previously published (Mabry et al., 1970; Mnatsakanyan et al., 1981; Tomas et al., 1985; Vidal-Ollivier et al., 1989; Mizui et al., 1990; De Rosa et al., 2000; Kazuma et al., 2003; Tsukamoto et al., 2004; Guvenalp and Demirezer, 2005; Simon et al., 2006). Among them, compounds **3**, **4**, **5**, **7**, **8**, **10**, **11**, and **12** have been found to be isolated from the genus *Salsola* for the first time (Kucukboyaci et al., 2016). It should be also noted that presence of compounds **1**, **2**, **6**, **9**, and **13** were reported for the first time in *S. grandis* by our group. Compound **13** was earlier isolated from *S. collina* Pall., which is widely distributed in Northeastern and Southwestern of China (Jin et al., 2011).

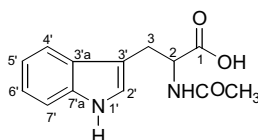
In spite of the large number of isolated compounds in the EtOH extract of *Salsola grandis*, only compound **13** displayed a marked



Flavonols	R <sub>1</sub>	R <sub>2</sub>
<b>1</b> Isorhamnetin-3-O-rutinoside	OCH <sub>3</sub>	6-O-α-L-Rhamnopyranosyl-β-D-glucopyranose
<b>2</b> Quercetin-3-O-rutinoside	OH	6-O-α-L-Rhamnopyranosyl-β-D-glucopyranose
<b>3</b> Quercetin-3-O-methylether	OH	CH <sub>3</sub>
<b>4</b> Tilioside	H	4-O-E-Coumaroyl-β-D-glucopyranose
<b>5</b> Isorhamnetin-3-glucuronide	OCH <sub>3</sub>	β-D-Glucuronopyranose
<b>6</b> Isorhamnetin-3-O-glucoside	OCH <sub>3</sub>	β-D-Glucopyranose
<b>7</b> Quercetin-3-O-galactoside	OH	β-D-Galactopyranose
<b>8</b> Quercetin-3-O-rhamnoside	OH	α-L-Rhamnopyranose
<b>9</b> Quercetin	OH	H
<b>10</b> Manghaslin	OH	2,6-Di-O-α-L-Rhamnopyranosyl-β-D-glucopyranose



Saponosides	R
<b>11</b> Momordin II b	H
<b>12</b> Momordin II c	β-D-Xylopyranose



**13** N-Acetyltryptophan

Fig. 1. Chemical structures of the isolated compounds **1**–**13**.

AChE inhibition ( $64.90 \pm 1.61\%$ ) at  $50 \mu\text{g mL}^{-1}$ , whilst a low level of inhibition was observed with compound **12** ( $21.72 \pm 0.99\%$ ) at the same concentration (Table 1).

Docking calculations for control compound acetylcholine (ACh) were carried out in order to test capability of the protocol to predict residues that are widely known to interact with ACh (Bajda et al., 2013). In Fig. 3, the results obtained for ACh in the cavity of AChE are illustrated. We can observe that ACh lies close to residues from the catalytic triad, totally in agreement with the enzymatic mechanisms. Therefore, we can continue forward and analyze the information that docking methods can yield for the new compound reported in this work. In Fig. 4, docking results for compound **13** against AChE are shown. Key interactions are due to hydrogen bonds with residues GLU199 and TYR121. This way, compound **13** blocks ACh access to the catalytic triad, and thus, inhibits the enzyme. In addition, crystallographic pose of the drug Aricept<sup>®</sup> (purple skeleton) is shown in Fig. 4 and both molecules are observed to share the same interaction area and, therefore, similar enzyme blocking mechanism.

The genus *Salsola* consists of well-known medicinal plants with folkloric use and various pharmacological activities desired for human health. At the best of our knowledge, this work is the first attempt aimed at rationalizing the cholinesterase inhibitory effect of *Salsola grandis*. Nevertheless, a few studies earlier demonstrated cholinesterase inhibitory effect of several other *Salsola* species up to date. For instance; in an earlier similar study by Tundis et al. (2009), the major components were identified by gas chromatography-mass spectrometry (GC-MS) as tetrahydroisoquinoline alkaloids; salsoline, *N*-methylisosalolidine, salsolidine, and carnegine in the alkaloid extracts of the aerial parts of *S. oppositifolia*, *S. soda*, and *S. tragus* of Italian origin having varying levels of inhibition against AChE and butyrylcholinesterase (BChE). Besides alkaloids, hydroxycinnamic acid, and flavonoid derivatives were also reported to be present in *Salsola* species (Oueslati et al., 2006; Rasheed et al., 2013), while the root extract prepared from *S. vermiculata* displayed a robust AChE-inhibiting property (Rasheed et al., 2013). Indeed, triterpene derivatives from *S. bryosma* were demonstrated with BChE inhibitory activity (Ahmed et al., 2007).

The compounds **1**, **5**, and **6**, the isorhamnetin-derivative flavonoids isolated from *S. grandis*, did not inhibit AChE. According to our literature survey, no study is available so far on cholinesterase inhibitory action of isorhamnetin derivatives. Nevertheless, a marked number of studies have been published

on anti-cholinesterase effect of quercetin (**9**) and its derivatives. Actually, we also previously demonstrated some level of inhibition by quercetin against both AChE and BChE using *in vitro* and *in silico* methods (Khan et al., 2009), where its inhibitory effect was mild ( $\text{IC}_{50} = 353.86 \mu\text{M}$ ) in comparison to that of the reference (galanthamine,  $\text{IC}_{50} = 0.75 \mu\text{M}$ ). Consequently, ineffectiveness of quercetin (**9**) against AChE in our study could be explained to be resulted from testing at a very low concentration herein due to scarcity of amount of the compound. On the other hand, 3-*O*-methylquercetin and 3,7-*O*-dimethylquercetin isolated from *Cistus laurifolius* L. were also not able to inhibit AChE (Akkol et al., 2012) as the quercetin derivatives isolated herein did not have any inhibition. Another report by Kim et al. (2014) indicated that quercetin-3-*O*-glucuronide and isorhamnetin-3-*O*-glucuronide strongly inhibited AChE with  $\text{IC}_{50}$  values of 8.2 and 23.2  $\mu\text{M}$ , respectively.

Momordin and its glycosides were firstly isolated from *Momordica charantia* L., and later on, *Panax bipinnatifidus* Seem. and *Kochia scoparia* (L.) Schrad. However, this compound does not possess cholinesterase inhibitory effect as we have shown herein for the first time.

Molecular docking analysis was used to simulate the binding conformation of compound **13** into the active gorge of AChE enzyme and provide information about which are the most important interactions between the compound and the enzyme, namely hydrogen bonds with residues GLU199 and TYR121. These results reveal structure of the active site allow us to complete the picture of the interaction pattern involved.

### 3. Experimental section

#### 3.1. Chemicals

In the extraction procedure, ethanol (EtOH), *n*-hexane, chloroform ( $\text{CHCl}_3$ ), ethyl acetate (EtOAc), and *n*-butanol (*n*-BuOH) were of analytical grade and purchased from Merck Co. Analytical thin layer chromatography (TLC) was performed on precoated Kieselgel 60 F<sub>254</sub> plates (Art. 5554, Merck). The plates sprayed with 1% vanillin- $\text{H}_2\text{SO}_4$  solution [vanillin (Boehringer Mannheim) and  $\text{H}_2\text{SO}_4$  (Merck Co.)].

#### 3.2. Plant material

The aerial parts of *S. grandis* were collected at flowering stage from Nallihan bird sanctuary (Ankara, Turkey) in July 2010 and identified by Prof. Dr. Mecit Vural from the Department of Botany, Faculty of Science, Gazi University (Ankara, Turkey). A voucher specimen (GUE 2641) is deposited at the Herbarium of Faculty of Pharmacy, Gazi University, Turkey.

#### 3.3. Extraction, fractionation and purification procedure

The aerial parts of the plant sample were dried in shade at room temperature and powdered to a fine grade using a laboratory scale mill. The powdered plant material (2270 g) was extracted with 96% EtOH (30 L) at room temperature and evaporated to dryness under reduced pressure below  $40^\circ\text{C}$  to yield "EtOH extract" (185.28 g). The EtOH extract (127.54 g) was firstly dissolved in 200 mL of EtOH and extracted with *n*-hexane ( $8 \times 300 \text{ mL}$ ) in a separatory funnel. Combined *n*-hexane extracts were evaporated under reduced pressure to yield "*n*-Hexane subextract" (21.71 g). After removal of EtOH from the remaining extract, it was diluted with distilled  $\text{H}_2\text{O}$  to 150 mL and further fractionated by successive solvent extractions with  $\text{CHCl}_3$  ( $5 \times 250 \text{ mL}$ ), EtOAc ( $10 \times 300 \text{ mL}$ ), and *n*-BuOH saturated with  $\text{H}_2\text{O}$  ( $13 \times 300 \text{ mL}$ ). Each extract as well as the remaining water phase after solvent extractions was evaporated to dryness under reduced pressure to yield " $\text{CHCl}_3$  subextract"

**Table 1**  
AChE inhibitory activity (%  $\pm$  S.E.M.) of the compounds **1-13**.

Samples	Inhibition against AChE (% $\pm$ S.E.M. <sup>a</sup> ) at $50 \mu\text{g mL}^{-1}$ <sup>b</sup>
EtOH extract	- <sup>c</sup>
1	-
2	-
3	-
4	-
5	-
6	-
7	-
8	-
9	-
10	-
11	-
12	$21.72 \pm 0.99$ <sup>****</sup>
13	$64.90 \pm 1.61$ <sup>***</sup>
Galanthamine <sup>d</sup>	$94.07 \pm 0.89$

<sup>a</sup> Standard error mean ( $n = 3$ ).

<sup>b</sup> Final concentration in microplate well is  $5 \mu\text{g mL}^{-1}$ .

<sup>c</sup> No inhibition.

<sup>d</sup> Reference for AChE and BChE inhibition tested at  $1000 \mu\text{g mL}^{-1}$ .

\* $p < 0.05$ . \*\* $p < 0.01$ . \*\*\* $p < 0.001$ . \*\*\*\* $p < 0.0001$ .

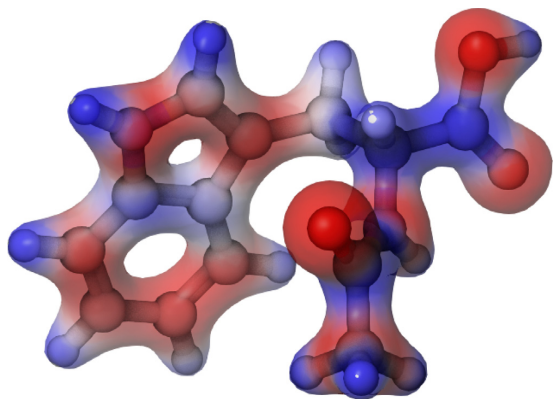


**Fig. 2.** Molecular electrostatic potential map computed for compound **13** (Red and blue colors stand for negative and positive regions, respectively). (For interpretation of the references to colour in this figure legend, the reader is referred to the web version of this article.)

(3.63 g), “EtOAc subextract” (3.74 g), “*n*-BuOH subextract” (17.76 g) and “R-H<sub>2</sub>O subextract” (52.84 g), respectively.

Chromatographic separation of the *n*-BuOH subextract using silica gel and Sephadex LH-20 column chromatography techniques led us to isolate thirteen compounds identified as ten known flavonol derivatives; *i.e.* isorhamnetin-3-*O*-rutinoside (**1**), quercetin-3-*O*-rutinoside (**2**), quercetin-3-*O*-methyl ether (**3**), tiliroside (**4**), isorhamnetin-3-*O*-glucuronide (**5**), isorhamnetin-3-*O*-glucoside (**6**), quercetin-3-*O*-galactoside (**7**), quercetin-3-*O*-rhamnoside (**8**), quercetin (**9**), and manghaslin (**10**), two oleanane-type

saponosides; momordin II b (**11**) and II c (**12**) as well as one amino acid derivative, *N*-acetyltryptophan (**13**). Details of the isolation procedure and chemical characterization were reported in our recently published paper (Kucukboyaci et al., 2016).

#### 3.4. Microtiter assay for determination of AChE inhibition

AChE inhibitory activity of the main EtOH extract of *S.grandis* and compounds **1-13** was measured by slightly modified spectrophotometric method of Ellman et al. (1961). Electric eel AChE (Type-VI-S; EC 3.1.1.7, Sigma, St. Louis, MO, USA) was used, while acetylthiocholine iodide (Sigma, St. Louis, MO, USA) was employed as the substrate of the reaction. 5,5'-Dithio-bis(2-nitrobenzoic)acid (DTNB; Sigma, St. Louis, MO, USA) was used for the measurement of the anti-AChE activity. Briefly, in this method, 140  $\mu$ L of sodium phosphate buffer (pH 8.0), 20  $\mu$ L of DTNB, 20  $\mu$ L of test solution and 20  $\mu$ L of AChE solution were added by multichannel automatic pipette (Gilson pipetman, Paris, France) in a 96-well microplate and incubated for 15 min at 25 °C. The reaction was then initiated with the addition of 10  $\mu$ L of acetylthiocholine iodide. Hydrolysis of acetylthiocholine iodide was monitored by the formation of the yellow 5-thio-2-nitrobenzoate anion as a result of the reaction of DTNB with thiocholines, catalyzed by enzymes at 412 nm utilizing a 96-well microplate reader (VersaMax Molecular Devices, Sunnyvale, CA, USA). The measurements and calculations were evaluated by using Softmax PRO 4.3.2.LS software (Sunnyvale, CA, USA). Percentage of AChE inhibition was determined by comparison of reaction rates of the samples relative to blank sample (ethanol in phosphate buffer pH = 8) using the formula  $(E-S)/E \times 100$ , where *E* is the activity of enzyme without test sample and *S* is the activity of enzyme with test sample. The experiments were done in triplicate.

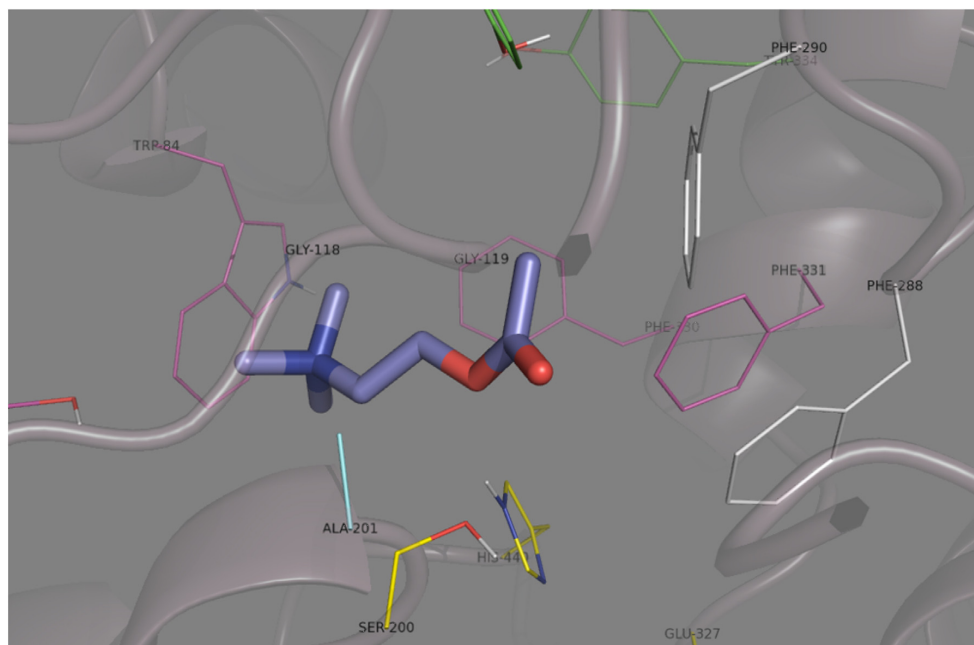


**Fig. 3.** Interactions of acetylcholine with residues within binding site of AChE [Crystal structure used was PDB:1EVE. Residues are colored according to their binding area as yellow (catalytic triad), pink (anionic site), grey (acyl pocket), blue (oxyanion hole) and green (peripheral anionic site)]. (For interpretation of the references to colour in this figure legend, the reader is referred to the web version of this article.)

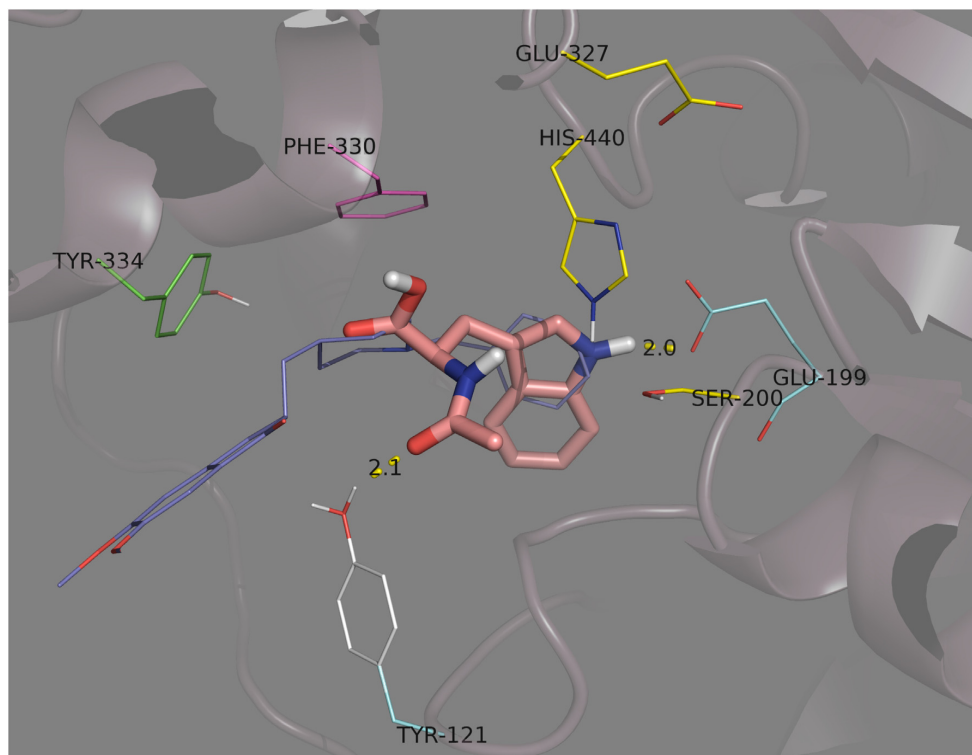


**Fig. 4.** Interactions of compound **13** (orange skeleton, representation in sticks) with residues within binding site of AChE [Crystal structure used was PDB:1EVE. Residues are colored according to their binding area as yellow (catalytic triad), pink (anionic site) and green (peripheral anionic site). Drug Aricept<sup>®</sup> is depicted with purple skeleton. Hydrogen bonds established between compound **13** and residues TYR121 and GLU199 (these two residues are cyan colored) are depicted with yellow dashed lines].(For interpretation of the references to colour in this figure legend, the reader is referred to the web version of this article.)

Galanthamine (Sigma, St. Louis, MO, USA), the anticholinesterase alkaloid-type of drug obtained from the bulbs of snowdrop (*Galanthus* sp.), was used as the reference.

### 3.5. Statistical analysis of *in vitro* data

Data obtained from *in vitro* enzyme inhibition assays were expressed as the mean standard error ( $\pm$ SEM). Statistical differences between the reference and the sample groups were evaluated by ANOVA (one way). Dunnett's multiple comparison tests were used as *post hoc* tests.  $p < 0.05$  was considered to be significant [ $*p < 0.05$ ;  $**p < 0.01$ ;  $***p < 0.001$ ,  $****p < 0.0001$ ].

### 3.6. Molecular modeling experiments

Molecular modeling experiments have been performed only on compound **13** as it was the only one having AChE inhibition over 50%. The geometry compound **13** was fully optimized within the density functional theory (DFT) framework at the B3LYP/6-31G(d) level (Lee et al., 1998; Becker, 1993). Frequency calculations were subsequently performed to ascertain the nature of every localized structure: a stable structure corresponds to a minimum in the potential energy surface and consequently all frequencies are real. Partial atomic charges were next computed by using the Merz-Singh-Kollman ESP protocol (Singh and Kollman, 1984; Besler et al., 1990) to be used during docking simulations. Quantum chemical

calculations were performed with the Gaussian 09 suite of programs (Gaussian, 2009), and distribution of partial charges for compound **13** can be seen in Fig. 2.

The structure for AChE was extracted from the crystal structures of Protein Data Bank (PDB) with code 1EVE and converted to PDBQT format using default parameters of AutoDock tools (Morris et al., 2009). Molecular docking calculations were carried out using default parameters in AutoDock Vina (Trott and Olson, 2010). Graphical representations of the docking results were rendered with PyMOL (Molecular Graphics System, version 1.3, Schrödinger, LLC).

## 4. Conclusions

In the present study, only *N*-acetyltryptophan (**13**) among thirteen compounds (**1-13**) isolated from *S. grandis* has been revealed to exert a prominent AChE inhibitory activity. In addition to the *in vitro* data for compound **13**, molecular modeling studies using the selected computational protocol provided an insight into interpreting these results at atomic level, which revealed that compound **13** shares a similar interaction pattern to the one of the known drug donepezil (Aricept<sup>®</sup>). In this study, we disclose the first *in vitro* and *in silico* study on cholinesterase inhibitory effect of *N*-acetyltryptophan, which might be a promising precursor model for AChE-inhibiting molecules with neuroprotective potential particularly for AD treatment.

## Acknowledgements

This study was financially supported by the Scientific Research Project Unit of Gazi University (Turkey), the Fundación Séneca del Centro de Coordinación de la Investigación de la Región de Murcia (Spain) and the European Regional Development Fund (ERDF) (Belgium). "Powered@NLHPC: This research was partially supported by the supercomputing infrastructure of the NLHPC (ECM-02)". This work was partially supported by the computing facilities of Extremadura Research Centre for Advanced Technologies (CETA–CIEMAT), funded by the European Regional Development Fund (ERDF). CETA–CIEMAT belongs to CIEMAT and the Government of Spain. The authors also thankfully acknowledge the computer resources and the technical support provided by the Plataforma Andaluza de Bioinformática of the University of Málaga. J.P.C.-C. acknowledges the support provided by the Centro de Alto Rendimiento de la Región de Murcia within its Research Program (CFE-CAR-23/15).

## References

- Ahmed, Z., Mehmood, S., Ifzal, R., Malik, A., Afza, N., Iqbal, L., 2007. Butyrylcholinesterase inhibitory triterpens from *Salsola bryosma*. Polish J. Chem. 81, 1427–1432.
- Akkol, E.K., Orhan, I.E., Yesilada, E., 2012. Anticholinesterase and antioxidant effects of the ethanol extract: ethanol fractions and isolated flavonoids from *Cistus laurifolius* L. leaves. Food Chem. 131, 626–631.
- Altun, M.L., Sever Yilmaz, B., Orhan, I.E., Saltan, G., 2013. Assessment of cholinesterase and tyrosinase inhibitory and antioxidant effects of *Hypericum perforatum* L. (St. John's wort). Ind. Crops Prod. 43, 87–92.
- Bajda, M., Więckowska, A., Hebda, M., Guziar, N., Sottriffer, C.A., Malawska, B., 2013. Structure-based search for new inhibitors of cholinesterases. Int. J. Mol. Sci. 14, 5608–5632.
- Becker, A.D., 1993. A new mixing of Hartree-Fock and local density-functional theories. J. Chem. Phys. 98, 1372–1377.
- Berhanu, M.A., Yordanos, W., 1990. Isoflavonoids from the roots of *Salsola somalensis*. Phytochemistry 30, 1281–1284.
- Besler, B.H., Merz, K.M., Kollman, P.A., 1990. Atomic charges derived from semiempirical methods. J. Comput. Chem. 11, 431–439.
- Dauletmuratov, S., Komarova, M.N., 1980. Alkaloid content in *Salsola richteri* (Moq.) Kar growing on the territory of the Karakalpak ASSR. Rast. Resursy 16, 86–88.
- De Rosa, S., Iodice, C., Mitova, M., Handjieva, N., Popov, S., Anchev, M., 2000. Triterpene saponins and iridoid glucosides from *Galium rivale*. Phytochemistry 54, 751–756.
- Ellman, G.L., Courtney, K.D., Andres, V., Featherstone, R.M., 1961. A new and rapid colorimetric determination of acetylcholinesterase activity. Biochem. Pharmacol. 7, 88–95.
- Freitag, H., 2000. *Salsola* L. In: Güner, A., Özhatay, N., Ekim, T., Başer, K.H.C. (Eds.), Flora of Turkey and the East Aegean Islands, vol. 11. Edinburgh University Press, Edinburgh, pp. 62.
- Gaussian 09 Revision D.01. In: Frisch, M.J., Trucks, G.W., Schlegel, H.B., Scuseria, G.E., Robb, M.A., Cheeseman, J.R., Scalmani, G., Barone, V., Mennucci, B., Petersson, G.A., Nakatsuji, H., Caricato, M., Li, X., Hratchian, H.P., Izmaylov, A.F., Bloino, J., Zheng, G., Sonnenberg, J.L., Hada, M., Ehara, M., Toyota, K., Fukuda, R., Hasegawa, J., Ishida, M., Nakajima, T., Honda, Y., Kitao, O., Nakai, H., Vreven, T., Montgomery, J.A.Jr, Peralta, J.E., Ogliaro, F., Bearpark, M., Heyd, J.J., Brothers, E., Kudin, K.N., Staroverov, V.N., Kobayashi, R., Normand, J., Raghavachari, K., Rendell, A., Burant, J.C., Iyengar, S.S., Tomasi, J., Cossi, M., Rega, N., Millam, J.M., Klene, M., Knox, J.E., Cross, J.B., Bakken, V., Adamo, C., Jaramillo, J., Gomperts, R., Stratmann, R.E., Yazyev, O., Austin, A.J., Cammi, R., Pomelli, C., Ochterski, J.W., Martin, R.L., Morokuma, K., Zakrzewski, V.G., Voth, G.A., Salvador, P., Dannenberg, J.J., Dapprich, S., Daniels, A.D., Farkas, Ö., Foresman, J.B., Ortiz, J.V., Cioslowski, J., Fox, D.J. (Eds.), Gaussian Inc., Wallingford CT.
- Guvenalp, Z., Demirezer, L.O., 2005. Flavonol glycosides from *Asperula arvensis* L. Turk. J. Chem. 29, 163–169.
- Han, K.M., Maharvi, G.M., Abbaskhan, A., Hayat, S., Khan, M.T.H., Makhmoor, T., Choudhary, M.I., Shaheen, F., Rahman, A., 2003. Three tyrosinase inhibitors and antioxidant compounds from *Salsola foetida*. Helv. Chim. Acta 86, 457–464.
- Hogan, D.B., 2014. Long-term efficacy and toxicity of cholinesterase inhibitors in the treatment of Alzheimer disease. Can. J. Psychiatry 59, 618–623.
- Jin, Y.S., Du, J.L., Yang, Y., Jin, L., Song, Y., Xiang, W., Chen, H.S., 2011. Chemical and biologically active constituents of *Salsola collina*. Chem. Nat. Compd. 47, 257–260.
- Kazuma, K., Noda, N., Suzuki, M., 2003. Malonylated flavonol glycosides from the petals of *Clitoria ternatea*. Phytochemistry 62, 229–237.
- Khan, M.T.H., Orhan, I., Senol, F.S., Kartal, M., Sener, B., Dvorská, M., Šmejkal, K., Šlapetová, T., 2009. Cholinesterase inhibitory activities of some flavonoid derivatives and chosen xanthone and their molecular docking studies. Chem. Biol. Interact. 181, 383–389.
- Kim, S.Y., Park, J.Y., Park, P.S., Bang, S.H., Lee, K.M., Lee, Y.R., Jang, Y.H., Kim, M.J., Chun, W., Heo, M.Y., Kwon, Y., 2014. Flavonoid glycosides as acetylcholinesterase inhibitors from the whole plants of *Persicaria thunbergii*. Nat. Prod. Sci. 20, 191–195.
- Kucukboyaci, N., Akkol, E.K., Sutar, I., Calis, I., 2016. *In vivo* anti-inflammatory and antinociceptive activities of the extracts and chemical constituents of an endemic Turkish plant, *Salsola grandis*. Rec. Nat. Prod. 10, 369–379.
- Lee, C., Yang, W., Parr, R.G., 1998. Development of the Colle-Salvetti correlation-energy formula into a functional of the electron density. Phys. Rev. B Condens. Matter 37, 785–789.
- Mabry, T.J., Markham, K.R., Thomas, M.B., 1970. The Systematic Identification of Flavonoids. Springer, Berlin.
- Mizui, F., Kasai, R., Ohtani, K., Tanaka, O., 1990. Saponins from bran of quinoa, *Chenopodium quinoa* Willd. II. Chem. Pharm. Bull. 38, 375–377.
- Mnatsakanyan, V.A., Agababyan, E.Y., Arutyunyan, L.S., 1986. Flavonoids of *Salsola glauca* and *Salsola macera*. Khim. Priir. Soedin 5, 660–661.
- Morris, G.M., Huey, R., Lindstrom, W., Sanner, M.F., Bewle, R.K., Goodsell, D.S., Olson, A.J., 2009. AutoDock4 and AutoDockTools4: automated docking with selective receptor flexibility. J. Comput. Chem. 30(16), 2785–2791.
- Narantuyaa, S., Batsuren, D., Batirov, E.K., Malikov, V.M., 1986. Chemical study of the Flora of Mongolia. Coumarins of *Salsola laricifolia*. Chem. Nat. Compd. 22, 228–229.
- Nofal, S.M., Nada, S.A., Hassan, N.S., Abdel-Alim, M.A., El-Sharabasy, F.S., 2002. Preventive effect of *Salsola villosa* and *Salsola volkensii* aqueous alcoholic extract on acute and chronic liver injury in albino rats. Some pharmacological, histological and histochemical studies. Egypt. Med. J. 1, 115–139.
- Orhan, I.E., Orhan, G., Gurkas, E., 2011. An overview on natural cholinesterase inhibitors – a multi-targeted drug class – and their mass production. Mini Rev. Med. Chem. 11, 836–842.
- Oueslati, M.H., Ben Jannet, H., Mighri, Z., Chriaa, J., Abreu, P.M., 2006. Phytochemical constituents from *Salsola tetrandra*. J. Nat. Prod. 69, 1366–1369.
- Rasheed, D.M., El Zalabani, S.M., Koheil, M.A., El-Hefnawy, H.M., Farag, M.A., 2013. Metabolite profiling driven analysis of *Salsola* species and their anti-acetylcholinesterase potential. Nat. Prod. Res. 27, 2320–2327.
- Senol, F.S., Orhan, I.E., Aslan Erdem, S., Kartal, M., Sener, B., Kan, Y., Celep, F., Kahraman, A., Dogan, M., 2011a. Comparative evaluation of cholinesterase inhibitory and antioxidant activities of wild and cultivated samples of sage (*Salvia fruticosa*) by activity-guided fractionation. J. Med. Food 14, 1476–1483.
- Senol, F.S., Skalicka-Wozniak, K., Khan, M.T.H., Orhan, I.E., Sener, B., Glowinski, K., 2011b. An *in vitro* and *in silico* approach to cholinesterase inhibitory and antioxidant effects of the methanol extract furanocoumarin fraction, and major coumarins of *Angelica officinalis* L. fruits. Phytochem. Lett. 4, 462–467.
- Simon, A., Toth, G., Duddeck, H., Soliman, H.S.M., Mahmoud, I.L., Samir, H., 2006. Glycosides from *Bougainvillea glabra*. Nat. Prod. Res. 20, 63–67.
- Singh, U.C., Kollman, P.A., 1984. An approach to computing electrostatic charges for molecules. J. Comput. Chem. 5, 129–145.
- Syrchina, A.I., Gorshkov, A.G., Shcherbakov, V.V., Zinchenko, S.V., Vereshchagin, A.L., Zaikov, K.L., Semenov, A.A., 1992. Flavonolignans of *Salsola collina*. Chem. Nat. Compd. 28, 155–158.
- Tomas, F., Morenilla, A., Barberan, F.A.T., 1985. Two flavonol glycosides from *Salsola kali*. Fitoterapia 56, 365–336.
- Trott, O., Olson, A.J., 2010. AutoDock Vina: improving the speed and accuracy of docking with a new scoring function, efficient optimization, and multithreading. J. Comput. Chem. 31(2), 455–461.
- Tsukamoto, S., Tomise, K., Aburatani, M., Loizzo, M.R., Bonesi, M., Statti, G., Menichini, F., 2004. Isolation of cytochrome P450 inhibitors from strawberry fruit, *Fragaria ananassa*. J. Nat. Prod. 67, 1839–1841.
- Tundis, R., Menichini, F., Conforti, F., Loizzo, M.R., Bonesi, M., Statti, G., Menichini, F., 2009. A potential role of alkaloid extracts from *Salsola* species (Chenopodiaceae) in the treatment of Alzheimer's disease. J. Enzyme Inhib. Med. Chem. 24, 818–824.
- Vidal-Ollivier, E., Balansard, G., Faure, R., Babadjamian, A., 1989. Revised structures of triterpenoid saponins from the flowers of *Calendula officinalis*. J. Nat. Prod. 52, 1156–1159.



## 2.5 Profiling Auspicious Butyrylcholinesterase Inhibitory Activity of Two Herbal Molecules: Hyperforin and Hyuganin C

<b>Title</b>	<i>Profiling Auspicious Butyrylcholinesterase Inhibitory Activity of Two Herbal Molecules: Hyperforin and Hyuganin C</i>
<b>Authors</b>	Ilkay Erdogan Orhan, F Sezer Senol Deniz, Steinar Trædal-Henden, José P Cerón-Carrasco, Helena den Haan, Jorge Peña-García, Horacio Pérez-Sánchez, Esra Emerce, Krystyna Skalicka-Wozniak
<b>Journal</b>	<i>Chemistry &amp; biodiversity</i>
<b>Year</b>	2019
<b>State</b>	Published

### PhD candidate contribution

Helena den Haan Alonso, declares to be the co-author and contributor of the article *Profiling Auspicious Butyrylcholinesterase Inhibitory Activity of Two Herbal Molecules: Hyperforin and Hyuganin C* in the section on computational chemistry.

## Profiling Auspicious Butyrylcholinesterase Inhibitory Activity of Two Herbal Molecules: Hyperforin and Hyuganin C

Ilkay Erdogan Orhan,<sup>a</sup> F. Sezer Senol Deniz,<sup>a</sup> Steinar Trædal-Henden,<sup>b</sup> José P. Cerón-Carrasco,<sup>c</sup> Helena den Haan,<sup>c</sup> Jorge Peña-García,<sup>c</sup> Horacio Pérez-Sánchez,<sup>\*c</sup> Esra Emerce,<sup>d</sup> and Krystyna Skalicka-Wozniak<sup>\*e</sup>

<sup>a</sup> Department of Pharmacognosy, Faculty of Pharmacy, Gazi University, 06330 Ankara, Turkey

<sup>b</sup> IT-Department, UiT – the Arctic University of Norway, 9037 Tromsø, Norway

<sup>c</sup> Bioinformatics and High Performance Computing Research Group, Universidad Católica San Antonio de Murcia (UCAM), 30107 Guadalupe, Spain, e-mail: hperez@ucam.edu

<sup>d</sup> Department of Pharmaceutical Toxicology, Faculty of Pharmacy, Gazi University, 06330 Ankara, Turkey

<sup>e</sup> Department of Pharmacognosy with Medicinal Plant Unit, Medical University of Lublin, 20-093 Lublin, Poland, e-mail: kskalicka@pharmacognosy.org

Cholinergic therapy based on cholinesterase (ChE) inhibitory drugs is the mainstay for the treatment of Alzheimer's disease. Therefore, an extensive research has been continuing for the discovery of drug candidates as inhibitors of acetyl- and butyrylcholinesterase. In this study, two natural molecules, e.g. hyperforin and hyuganin C were tested *in vitro* for their AChE and BChE inhibitory activity. Both of the compounds were ineffective against AChE, whereas hyperforin ( $IC_{50} = 141.60 \pm 3.39 \mu\text{M}$ ) and hyuganin C ( $IC_{50} = 38.86 \pm 1.69 \mu\text{M}$ ) were found to be the highly active inhibitors of BChE as compared to galantamine ( $IC_{50} = 46.58 \pm 0.91 \mu\text{M}$ ) which was used as the reference. Then, these molecules were further proceeded to molecular docking experiments in order to establish their interactions at the active site of BChE. The molecular docking results indicated that both of them are able to block the access to key residues in the catalytic triad of the enzyme, while they complement some of the hydrophobic residues of the cavity, what is consistent with our *in vitro* data. While both compounds were predicted as mutagenic, only hyuganin C showed hepatotoxicity in *in silico* analysis. According to whole outcomes that we *obtained*, particularly hyuganin C besides hyperforin are the promising BChE inhibitors, which can be the promising compounds for AD therapy.

**Keywords:** butyrylcholinesterase, enzyme inhibition, molecular docking, natural products, coumarin.

### Introduction

Alzheimer's disease (AD), is a progressive neurodegenerative disorder with a complex pathogenesis, which mainly affects the elderly population and currently it is the most common type of dementia. For instance; the number of AD patients only in US was assessed as 5.3 million people, which is estimated to increase up to 7.1 million by 2025.<sup>[1,2]</sup> Although the pathogenesis of AD is still under debate, yet, two major mechanisms have been proposed in order to elucidate the pathogenesis of the disease as 'amyloid hypothesis' and 'cholinergic hypothesis'.<sup>[3]</sup> In cholinergic hypothesis,

deficiency in cholinergic neurotransmission through acetylcholine (ACh) and butyrylcholine (BCh) has been proven in the brains of AD patients. ACh and BCh are hydrolyzed by two sister enzymes from cholinesterase (ChE) family available in the brains of mammals; e.g. acetylcholinesterase (AChE, EC 3.1.1.7) and butyrylcholinesterase (BChE, EC 3.1.1.8), respectively. Therefore, ChE inhibitors are the mostly prescribed drug class for the treatment of AD at the moment.<sup>[4]</sup>

Although BChE, also found in neurons and glia, possesses ability to hydrolyze ACh, it is known to be less specific to this substrate than AChE.<sup>[5]</sup> It has been reported that BChE activity is increased up to 120%

and excess amount of the enzyme was observed in AD patients.<sup>[6]</sup> However, despite inhibition of BChE is an important strategy, currently, almost all cholinesterase inhibitors used in clinic target AChE.<sup>[7]</sup>

Natural molecules have been highlighted as promising targets in drug discovery and development research since numerous clinically available drugs have been firstly derived from a natural compound. Up to date, many strong enzyme inhibitors of natural origin related to cholinesterases have been reported.<sup>[8–11]</sup> Among all possible candidates, hyperforin (a prenylated carbocyclic acylphloroglucinol derivative) and hyuganin C (coumarin derivative) are the natural molecules from *Hypericum perforatum* L. (St. John's wort, Hypericeae) and *Mutellina purpurea* (POIR.) REDURON, CHARPIN & PIMENOV (Apiaceae), respectively (Figure 1).<sup>[12]</sup>

The aim of the present contribution is to investigate ChE inhibitory potential of these two natural compounds through *in vitro* and *in silico* techniques. This particular choice of hyperforin as target compound was guided by data available on ChE inhibitory activity of *H. perforatum* extracts from findings by our and other research groups.<sup>[13–15]</sup> However, no data was available on type of compounds responsible for the ChE inhibitory effect of this plant. On the other hand, coumarin derivatives have shown a marked ChE inhibitory effect in many studies.<sup>[16,17]</sup> Therefore, we decided to test hyperforin and hyuganin C for their possible ChE inhibitory potential using ELISA microtiter assays. Later, their BChE inhibitory results were evaluated by molecular docking experiments and energy calculations. Additionally, *in silico* toxicological analysis were performed on these compounds.

## Results and Discussion

Natural products have been shown to exert strong enzyme inhibitory properties in many cases. Hyper-

forin, one of the well-known biomolecules found in *H. perforatum*, has been reported to contribute to antidepressant effect of the plant. As discussed elsewhere, the ethyl acetate extract exerted BChE inhibition ( $50.79 \pm 3.07\%$ ) at  $200 \mu\text{g mL}^{-1}$ , which was consistent with a similar study on the same plant growing in Poland.<sup>[18]</sup> Since hyperforin amount has been usually found to be higher than that of hypericin in this plant,<sup>[14,15]</sup> we have tested BChE inhibitory effect of hyperforin in particular. Actually, hyperforin as a lipophilic natural compound has been shown to possess neuroprotective effect by various mechanisms *via* reducing microglia-mediated neuroinflammation,<sup>[19]</sup> blocking degradation of calpain-mediated transient receptor potential canonical (subtype) 6 channels,<sup>[20]</sup> improving cognitive performance through decreasing astrogliosis and microglia activation as well as increasing spatial memory *in vivo*<sup>[21]</sup> and *N*-methyl-D-aspartate (NMDA)-antagonistic effect.<sup>[22]</sup> Depending on its neuroprotective effect, hyperforin has been suggested as a promising alternative for elderly patients with degenerative disorders most of who also develop depression as shown by the latest research.<sup>[23–25]</sup> Consequently, the current results on the moderate BChE inhibitory effect of hyperforin ( $\text{IC}_{50} = 141.60 \pm 3.39 \mu\text{M}$ ) may also donate to its neuroprotective effect (Table 1).

Many coumarin derivatives of both natural and synthetic origins have been shown to possess strong ChE inhibitory properties.<sup>[4,16,17]</sup> For instance; 7-hydroxycoumarin derivatives<sup>[26,27]</sup> as well as 4-methylcoumarins<sup>[28]</sup> were suggested to be promising synthetic lead molecules with coumarin skeleton. Besides, we have revealed three coumarins, *e.g.* imperatorin, xanthotoxin, and bergapten isolated from the fruits of *Angelica officinalis* L., with a potent BChE inhibition,<sup>[29]</sup> while mesuagenin B was reported from *Mesua elegans* (KING) KOSTERM. as a marked BChE-inhibiting coumarin derivative.<sup>[30]</sup> Taking these findings into account, hyuganin C was tested herein for its probable ChE-inhibiting effect. Actually, hyuganin C obtained from *Mutellina purpurea* is a rare coumarin

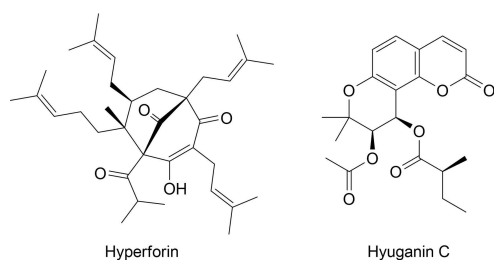


**Figure 1.** Chemical structures of hyperforin and hyuganin C.

**Table 1.**  $\text{IC}_{50}$  Values ( $\mu\text{M}$ ) of hyperforin and hyuganin C ( $n=3$ ;  $\pm$  SD)

Compounds tested	$\text{IC}_{50}$ [ $\mu\text{M}$ ]	
	AChE inhibition	BChE inhibition
Hyperforin	–	$141.60 \pm 3.39$
Hyuganin C	–	$38.86 \pm 1.69$
Galantamine hydrobromide (reference)	$2.52 \pm 0.15$	$46.58 \pm 0.91$

derivative, which was previously isolated only from *Peucedanum japonicum* THUNB.<sup>[31]</sup> and *Angelica furcijuga* KITAGAWA from Apiaceae family.<sup>[32]</sup> In our wide screening of natural molecules for their enzyme inhibitory potential, we have discovered potent BChE inhibitory activity of hyuganin C ( $IC_{50}=38.86 \pm 1.69 \mu\text{M}$ ), which was superior to that of galantamine ( $IC_{50}=46.58 \pm 0.91 \mu\text{M}$ ), the reference drug (Table 1). Since only a few BChE inhibitors are available, hyuganin C could be a new model compound for anti-Alzheimer drug leads acting through this mechanism.

Taking the marked *in vitro* BChE inhibitory data of these two natural molecules into consideration, they were subjected to molecular docking experiments in order to understand, at the molecular level, the rationale under their inhibitory activity. Having that information in hand is important, since it can help to discover new molecules in the same context. After analysis of docking results, energetic analysis of docking results for both hyperforin and hyuganin C is displayed in Figures 2 and 3.

On the other hand, Figures 4 and 5 show a representation of the active site of the enzyme with the two compounds docked and hydrogen bonds and hydrophobic interactions highlighted. Energetically, we can see that, in these two cases, the main stabilizing interactions are electrostatic complementarity between the ligands and the active site of the enzyme (as reflected by the high values of Gauss1 and Gauss2 terms), hydrophobic complementarity with

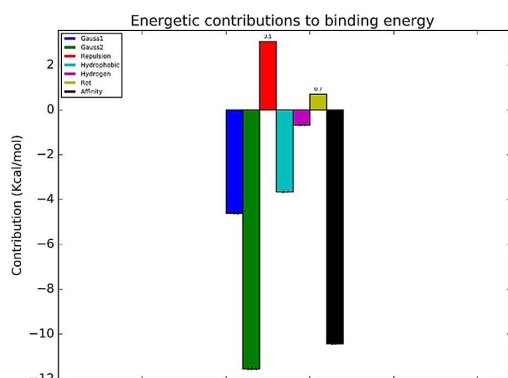


**Figure 2.** Energetic contributions (kcal/mol) to binding of hyperforin to BChE obtained from docking simulations. Depicted contributions are; van der electrostatic interactions type Gauss1 (dark blue) and Gauss2 (green), Repulsive term (red), Hydrophobic term (light blue), hydrogen bonds (pink), entropic losses associated with ligand's rotatable bonds (yellow) and total predicted binding energy (black).

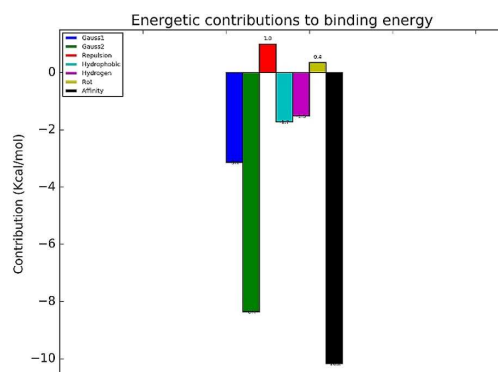


**Figure 3.** Energetic contributions (kcal/mol) to binding of hyuganin C to BChE obtained from docking simulations. Depicted contributions are; van der electrostatic interactions type Gauss1 (dark blue) and Gauss2 (green), Repulsive term (red), Hydrophobic term (light blue), hydrogen bonds (pink), entropic losses associated with ligand's rotatable bonds (yellow) and total predicted binding energy (black).

active site residues and established hydrogen bonds (Figures 2 and 3). When the detailed representation of docking poses (Figures 4 and 5) was investigated, we could observe the directionality of the network of hydrogens bond established and the complementarity of hydrophobic interactions. In the case of hyperforin, main hydrogen bonds are formed with residues SER79 and HIS438 (from catalytic triad), while the main hydrophobic interactions are created with residues TRP82, THR120, TRP231, VAL288, TYR332 (peripheral anionic site), PHE398, TRP430, and TYR440. For hyuganin C, a strong network of hydrogen bonds is formed with residues GLY115, GLY116, GLY117, SER198 and LEU286 (catalytic triad), while hydrophobic interactions are set with residues TRP82 (peripheral anionic site), PHE329 (anionic site) and PHE398. Therefore, both compounds block the access to key residues involved in the normal functioning of the enzyme such as parts of the catalytic triad and anionic and peripheral anionic sites and at the same time they complement some of the hydrophobic residues of the cavity. All these reasons can explain the inhibitory activity of the mentioned compounds.

Because of the lack of toxicology data in the literature for hyperforin and hyuganin C, computational toxicology assessments were performed for these compounds and possible toxic effects particularly mutagenicity and hepatotoxicity were estimated. The mutagenicity analysis was performed in agreement with current international guideline recom-

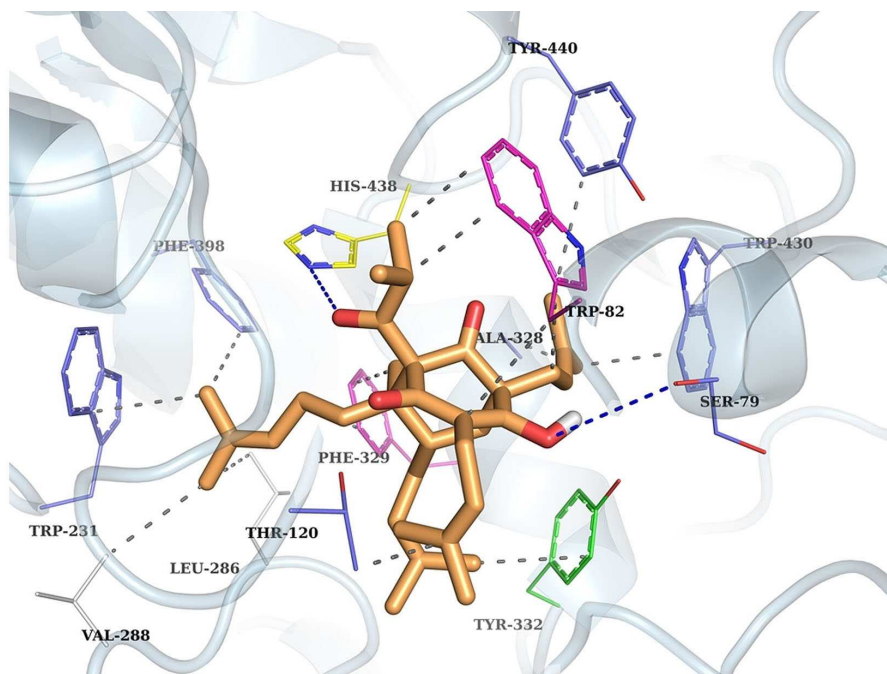


**Figure 4.** Interactions of hyperforin (orange skeleton, representation in sticks) with residues within binding site of BChE (Crystal structure used was PDB:1P0I). Residues are colored according to their binding area as yellow (catalytic triad), pink (anionic site), and green (peripheral anionic site). Hydrogen bonds established between hyperforin and residues HIS438 and SER79 are depicted with deep blue dashed lines. Grey dashed lines represent hydrophobic interactions.

mending the combined use of two complementary (Q) SARs<sup>[33]</sup> and outcomes obtained from two systems were assessed by combining<sup>[34]</sup> (Quantitative) structure-activity relationship ((Q)SAR) analysis have shown that hyperforin has most likely mutagenic effect due to carrying  $\alpha,\beta$ -unsaturated carbonyl as a toxicophore group. Hyuganin C has also shown mutagenicity. In terms of hepatotoxicity, although the system did not show potential hepatotoxicity for hyperforin, this compound could be out of the applicability domain of the model. However, hyuganin C was predicted as hepatotoxic compound with high reliability in the system. Considering the major predicted biological and toxicological activity profiles for the compounds, hyuganin C may cause dyspnea (Pa: 0.872) and sleep disturbance (Pa: 0.783) while hyperforin have become important for treatments of depression (Pa: 0.981), mood disorders (Pa: 0.978), Alzheimer's disease (Pa: 0.909), and neurodegenerative diseases (Pa: 0.906). Although *in silico* methods are not yet capable of fully replacing *in vitro*, *in vivo* toxicological testing or epidemiological methods, these are suitable tools for

the initial safety screening of compounds. Recently, regulatory authorities have increasingly supported the application of these techniques. In addition to the biological activity studies of hyperforin and hyuganin C, the further analysis of the possible toxicities, especially the toxic effects predicted in the study, will contribute to the process of developing new drugs.

## Conclusions

Screening of two natural molecules for their ChE inhibitory potential resulted in finding a potent inhibition by hyuganin C and moderate inhibition by hyperforin in comparison to that of galantamine as the reference drug, whereas none of them could inhibit AChE. According to obtained results it can be concluded that hyperforin is responsible for the marked BChE inhibitory effect of *Hypericum perforatum* extracts reported previously. We herein also provide with the molecular modeling results, which enlighten the main interactions involved between

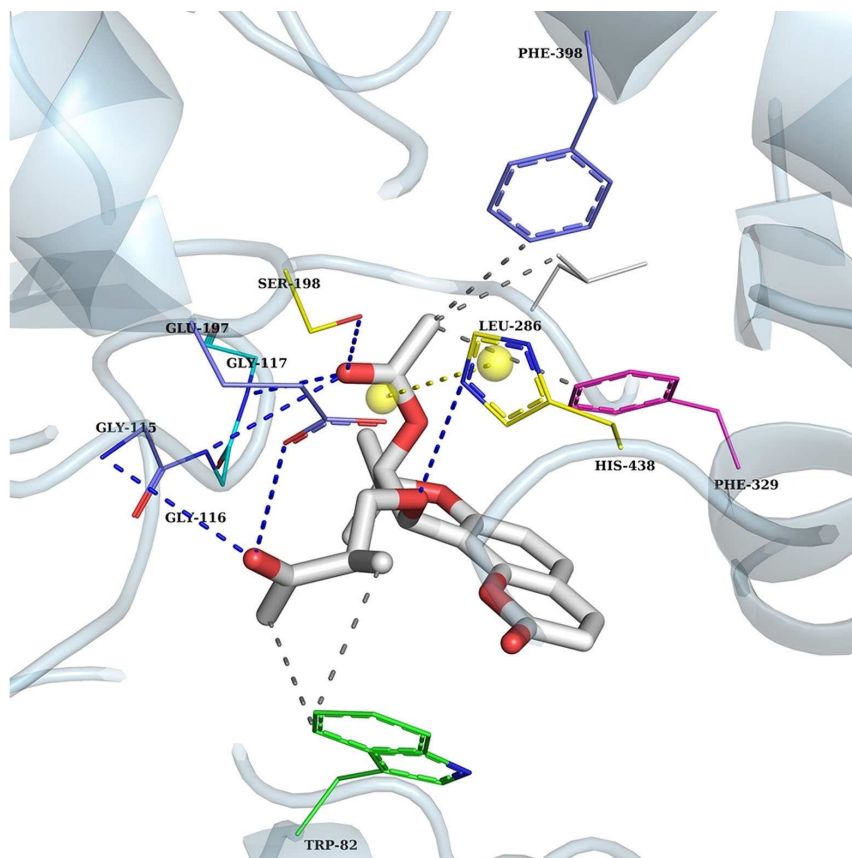


**Figure 5.** Interactions of hyuganin C (white skeleton, representation in sticks) with residues within binding site of BChE (Crystal structure used was PDB:1P0I). Residues are colored according to their binding area as yellow (catalytic triad), pink (anionic site) and green (peripheral anionic site). Hydrogen bonds established between hyperforin and residues GLY117, GLY115, GLY116, SER198 and HIS438 and SER79 are depicted with deep blue dashed lines. Grey dashed lines represent hydrophobic interactions.

the compounds and the enzyme. On the other hand, hyuganin C seems to be a quite promising natural compound which can serve as a lead for new drugs for the treatment of AD.

## Experimental Section

### Compounds

Hyperforin (Sigma-H1792, purity  $\geq 98\%$  by HPLC) was delivered by Sigma-Aldrich Co. (St. Louis, Missouri, USA), while hyuganin C was isolated according to previously described method.<sup>[8]</sup> Briefly, 50 g of the seeds of *Mutellina purpurea* was powdered and then extracted under the reflux with petroleum ether. 300 mg of the obtained crude dry extract was subjected to high-

performance counter current chromatography (HP-CCC) to further isolation. A mixture of *n*-heptane, ethyl acetate, methanol, and water 3:2:3:2 (v/v) was used. Finally, hyuganin C was obtained in pure form (7.94 mg) within 26 minutes, which identified using LC-DAD-ESI(Q)TOF-MS, and 1D- and 2D-NMR techniques.

### Microtiter Assays for ChE Inhibition

Slightly modified spectrophotometric Ellman method<sup>[35]</sup> was used for determination of AChE and BChE inhibitory activity. Electric eel AChE (Type-VI-S; EC 3.1.1.7) and horse serum BChE (EC 3.1.1.8,) were used. ACh iodide and BCh chloride were used as the substrates of the reaction. DTNB (=5,5'-dithiobis(2-nitrobenzoic acid)) was used for the measurement of

the anticholinesterase activity and galantamine was used as the reference drug. All substances were delivered by Sigma (St. Louis, Missouri, USA). Briefly, 140  $\mu\text{L}$  of sodium phosphate buffer (pH 8.0), 20  $\mu\text{L}$  of DTNB, 20  $\mu\text{L}$  of test solution and 20  $\mu\text{L}$  of AChE/BChE solution were added in a 96-well microplate and incubated for 15 min at 25  $^{\circ}\text{C}$ . The addition of 10  $\mu\text{L}$  of acetylthiocholine iodide/butrylthiocholine chloride initiated reaction. Hydrolysis of acetylthiocholine iodide/butrylthiocholine chloride was monitored by the formation of the yellow 5-thio-2-nitrobenzoate anion as a result of the reaction of DTNB with thiocholines, catalyzed by enzymes at 412 nm utilizing a 96-well microplate reader (VersaMax Molecular Devices, Sunnyvale, CA, USA). SoftMax PRO 4.3.2.LS software (Sunnyvale, CA, USA) was used for the measurements and calculations. Comparison of reaction rates of the samples relative to blank sample (ethanol in phosphate buffer pH=8) using the formula  $[(E-S)/E] \times 100$ , where  $E$  is the activity of enzyme without test sample and  $S$  is the activity of enzyme with test sample, let to calculate the percentage of inhibition of AChE/BChE. The experiments were performed in triplicate.

#### Molecular Docking Experiments

The geometry of each ligand was fully optimized within the density functional theory (DFT) framework at the B3LYP/6-31G(d) level.<sup>[36,37]</sup> Vibrational calculations were subsequently performed to ascertain the nature of every localized structure: a stable structure corresponds to a minimum in the potential energy surface and consequently all frequencies are real. Partial atomic charges were next computed by using the Merz–Singh–Kollman ESP protocol to be used during docking simulations.<sup>[38,39]</sup> All quantum chemical calculations were performed with the Gaussian 09 suite of programs,<sup>[40]</sup> and partial charges distribution for all compounds that can be seen from Figures 2 and 3.

The molecular structures used in this study were initially designed using AutoDock tools<sup>[41]</sup> or derived from experimental data. The structure for BChE was extracted from the crystal structure of Protein Data Bank (PDB) with code 1P0I. The receptor was prepared for docking in AutoDock by removing water molecules, adding hydrogen atoms and Gasteiger charges, merging non-polar hydrogens and assigning AD4 atom types. Molecular docking calculations were carried out using default parameters in AutoDock Vina.<sup>[42]</sup> Top pose of every compound was retained for

further analysis. Graphical representations of the docking results were prepared using PyMOL (Molecular Graphics System, version 1.6, Schrödinger, LLC).

#### In silico Toxicological Analysis

Mutagenic effects of the hyperforin and hyuganin C were assessed with statistical-based (VEGA QSAR model (v1.1.4) – mutagenicity (Ames test) consensus model (v1.0.2)) and knowledge-based (Toxtree SAR model (v3.1.0) – *in vitro* mutagenicity (Ames) alerts by ISS) *in silico* systems. Toxtree model conducts the Benigni/Bossa rulebase.<sup>[43]</sup> Mutagenicity consensus model performs a consensus assessment using applicability domain analysis based on the predictions of the CAESAR, SarPy, ISS and KNN mutagenicity models. QSAR model for hepatotoxicity was performed based on the VEGA hepatotoxicity model (IRFMN) 1.0.0. For prediction of the compounds' potential biological activities and possible adverse/toxic effects in humans, PASS (Prediction of Activity Spectra for Substances) software (v2.0) was used. The program output file represents a list of biological or toxicological effects with two probabilities as Pa (probability to be active) and Pi (probability to be inactive). In this study,  $P_a > 0.7$ , which indicates that the compound is very likely to show activity in experiments, was taken into consideration.

#### Acknowledgements

This work has been funded by the Fundación Séneca del Centro de Coordinación de la Investigación de la Región de Murcia under Projects 20524/PDC/18 and 20988/PI/18 and by a grant from the Spanish Ministry of Economy and Competitiveness (CTQ2017-87974). The research was partially supported by the supercomputing infrastructure of University of Tromsø (Norway). The authors also thankfully acknowledge the computer resources and the technical support provided by the Plataforma Andaluza de Bioinformática of the University of Málaga (Spain). Powered@NLHPC: This research was partially supported by the supercomputing infrastructure of the NLHPC (ECM-02). The work was partially financed from grant no POLTUR/PLANT-ALZH/5/2015 (Poland).

### Author Contribution Statement

I.E. O performed experiments with enzyme inhibition, analyzed obtained data, and wrote the article. F. S. S. D. performed experiments with enzyme inhibition. S. T.-H. conceived and designed *in silico* experiments. J. P. C.-C., H. den-H. and J. P.-G. performed *in silico* experiments. H. P.-S. conceived, designed, supervised and commented the results of *in silico* experiments. E. E. performed toxicological tasks. K. S.-W. isolated hyuganin C, analyzed obtained data, and wrote the article.

### References

- [1] A. L. Sosa-Ortiz, I. Acosta-Castillo, M. J. Prince, 'Epidemiology of dementias and Alzheimer's disease', *Arch. Med. Res.* **2012**, *43*, 600–608.
- [2] A. Kulshreshtha, P. Piplani, 'Current pharmacotherapy and putative disease-modifying therapy for Alzheimer's disease', *Neurol. Sci.* **2016**, *37*, 1403–1435.
- [3] C. Lane-Donovan, G. T. Philips, J. Herz, 'More than cholesterol transporters: lipoprotein receptors in CNS function and neurodegeneration', *Neuron* **2014**, *83*, 771–787.
- [4] I.E. Orhan, G. Orhan, E. Gurkas, 'An overview on natural cholinesterase inhibitors – a multi-targeted drug class – and their mass production', *Mini-Rev. Med. Chem.* **2011**, *11*, 836–842.
- [5] C. I. Wright, C. Geula, M. M. Mesulam, 'Neuroglial cholinesterases in the normal brain and in Alzheimer's disease: Relationship to plaques, tangles and patterns of selective vulnerability', *Ann. Neurol.* **1993**, *34*, 373–384.
- [6] E. Giacobini, 'Cholinesterases: New roles in brain function and in Alzheimer's disease', *Neurochem. Res.* **2003**, *28*, 515–522.
- [7] I.E. Orhan, 'Current concepts on selected plant secondary metabolites with promising inhibitory effects against enzymes linked to Alzheimer's disease', *Curr. Med. Chem.* **2012**, *19*, 2252–2261.
- [8] P. Kumar, V. K. Singh, D. K. Singh, 'Kinetics of enzyme inhibition by active molluscicidal agents ferulic acid, umbelliferone, eugenol and limonene in the nervous tissue of snail *Lymnaea acuminata*', *Phytother. Res.* **2009**, *23*, 172–177.
- [9] R. Mogana, A. Adhikari, S. Debnath, S. Hazra, B. Hazra, K. Teng-Jin, C. Wiart, 'The antiacetylcholinesterase and anti-leishmanial activities of *Canarium patentinervium* Miq.', *BioMed Res. Int.* **2014**, 903529. doi: 10.1155/2014/903529.
- [10] M. Y. Ali, S. Jannat, H. A. Jung, R. J. Choi, A. Roy, J. S. Choi, 'Anti-Alzheimer's disease potential of coumarins from *Angelica decursiva* and *Artemisia capillaris* and structure-activity analysis', *Asian Pac. J. Trop. Med.* **2016**, *9*, 103–111.
- [11] I.E. Orhan, F. S. Senol, S. Shekfeh, K. Skalicka-Wozniak, E. Banoglu, 'Pteryxin - A promising butyrylcholinesterase-inhibiting coumarin derivative from *Mutellina purpurea*', *Food Chem. Toxicol.* **2017**, *109*, 970–974.
- [12] K. Skalicka-Wozniak, T. Mroczek, M. Walasek, K. Glowinski, 'Efficient isolation of dihydropyranocoumarins and simple coumarins from *Mutellina purpurea* fruits', *Planta Med.* **2016**, *82*, 1105–1109.
- [13] M. L. Altun, B. S. Yilmaz, I.E. Orhan, G. S. Citoglu, 'Assessment of cholinesterase and tyrosinase inhibitory and antioxidant effects of *Hypericum perforatum* L. (St. John's wort)', *Ind. Crops Prod.* **2013**, *43*, 87–92.
- [14] B. Božin, N. Kladar, N. Grujić, G. Anačkov, I. Samojlik, N. Gavarić, B. S. Čonić, 'Impact of origin and biological source on chemical composition, anticholinesterase and antioxidant properties of some St. John's wort species (*Hypericum* spp., Hypericaceae) from the central Balkans', *Molecules* **2013**, *18*, 11733–11750.
- [15] I.E. Orhan, M. Kartal, 'LC-DAD-MS-Assisted quantification of marker compounds in *Hypericum perforatum* L. (St. John's Wort) and its antioxidant activity', *Turk. J. Pharm. Sci.* **2015**, *12*, 279–286.
- [16] L. G. de Souza, M. N. Rennã, J. D. Figueroa-Villar, 'Coumarins as cholinesterase inhibitors: A review', *Chem.-Biol. Interact.* **2016**, *254*, 11–23.
- [17] K. Skalicka-Wozniak, I.E. Orhan, G. A. Cordell, S. M. Nabavi, B. Budzyńska, 'Implication of coumarins towards central nervous system disorders', *Pharmacol. Res.* **2016**, *103*, 188–203.
- [18] N. Wszelaki, A. Kuciun, A. Kiss, 'Screening of traditional European herbal medicines for acetylcholinesterase and butyrylcholinesterase inhibitory activity', *Acta Pharmaceut.* **2010**, *60*, 119–128.
- [19] S.-K. Lee, J.-E. Kim, Y.-J. Kim, M.-J. Kim, T.-C. Kang, 'Hyperforin attenuates microglia activation and inhibits p65-Ser276 NF-κB phosphorylation in the rat piriform cortex following status epilepticus', *Neurosci. Res.* **2014**, *85*, 39–50.
- [20] Y. Lin, J. Zhang, J. Fu, F. Chen, J. Wang, Z.-L. Wu, S.-Y. Yuan, 'Hyperforin attenuates brain damage induced by transient middle cerebral artery occlusion (MCAO) in rats via inhibition of TRPC6 channels degradation', *J. Cereb. Blood Flow Metab.* **2013**, *33*, 253–262.
- [21] T. N. Griffith, L. Varela-Nallar, M. C. Dinamarca, N. C. Inestrosa, 'Neurobiological effects of hyperforin and its potential in Alzheimer's disease therapy', *Curr. Med. Chem.* **2010**, *17*, 391–406.
- [22] V. Kumar, A. Mdžinarishvili, C. Kiewert, T. Abbruscato, U. Bickel, C. J. Van Der Schyf, J. Klein, 'NMDA receptor-antagonistic properties of hyperforin, a constituent of St. John's wort', *J. Pharmacol. Sci.* **2006**, *102*, 47–54.
- [23] F. Yang, M. Ran, W. Luo, 'Depression of persons with dementia and family caregiver burden: Finding positives in caregiving as a moderator', *Geriatr. Gerontol. Int.* **2019**, doi: 10.1111/ggi.13632.
- [24] A. Ezzati, M. J. Katz, C. A. Derby, M. E. Zimmerman, R. B. Lipton, 'Depressive symptoms predict incident dementia in a community sample of older adults: results from the Einstein aging study', *J. Geriatr. Psychiatry Neurol.* **2019**, doi: 10.1177/0891988718824036.
- [25] K. Javaherian, B. M. Newman, H. Weng, J. Hassenstab, C. Xiong, D. Coble, A. M. Fagan, T. Benzinger, J. C. Morris, 'Examining the Complicated Relationship Between Depressive Symptoms and Cognitive Impairment in Preclinical



- Alzheimer Disease', *Alzheimer Dis. Assoc. Disord.* **2019**, *33*, 15–20.
- [26] J. P. Cerón-Carrasco, M. Fanuel, A. Charaf-Edding, D. Jacquemin, 'Interplay between solvent models and predicted optical spectra: A TD-DFT study of 7-OH-coumarin', *Chem. Phys. Lett.* **2013**, *556*, 122–126.
- [27] M. Alipour, M. Khoobi, A. Moradi, H. Nadri, F. Homayouni Moghadam, S. Emami, Z. Hasanpour, A. Foroumadi, A. Shafiee, 'Synthesis and anti-cholinesterase activity of new 7-hydroxycoumarin derivatives', *Eur. J. Med. Chem.* **2014**, *82*, 536–544.
- [28] S. C. Zeljković, Z. Czarnocki, A. Zawadzka, M. Panasiewicz, F. Kovač, 'Cholinesterase inhibition of selected 4-methylcoumarins in comparison to their antioxidant activity', *Curr. Bioact. Compds.* **2014**, *10*, 254–259.
- [29] F. S. Senol, K. Skalicka-Woźniak, M. T. H. Khan, I. E. Orhan, B. Sener, K. Główniak, 'An *In Vitro* and *in silico* approach to cholinesterase inhibitory and antioxidant effects of the methanol extract, furanocoumarin fraction, and major coumarins of *Angelica officinalis* L. fruits', *Phytochem. Lett.* **2011**, *4*, 462–467.
- [30] K. Awang, G. Chan, M. Litaudon, N. H. Ismail, M. T. Martin, F. Gueritte, '4-Phenylcoumarins from *Mesua elegans* with acetylcholinesterase inhibitory activity', *Bioorg. Med. Chem.* **2010**, *18*, 7873–7877.
- [31] K.-C. Jang, S.-C. Kim, E.-Y. Song, Y.-C. Um, S. C. Kim, Y.-J. Lee, 'Isolation and identification of anticancer and anti-inflammatory substances in *Peucedanum japonicum* Thunb', *Acta Hort.* **2008**, *765*, 49–53.
- [32] M. Yoshikawa, N. Nishida, K. Ninomiya, T. Ohgushi, M. Kubo, T. Morikawa, H. Matsuda, 'Inhibitory effects of coumarin and acetylene constituents from the roots of *Angelica furcijuga* on D-galactosamine/lipopolysaccharide-induced liver injury in mice and on nitric oxide production in lipopolysaccharide-activated mouse peritoneal macrophages', *Bioorg. Med. Chem.* **2006**, *14*, 456–463.
- [33] 'Assessment and control of DNA reactive (mutagenic) impurities in pharmaceuticals to limit potential carcinogenic risk, M7(R1)', ICH, 2017.
- [34] J. D. Wichard, 'In silico prediction of genotoxicity', *Food Chem. Toxicol.* **2017**, *106*, 595–599.
- [35] G. L. Ellman, K. D. Courtney, V. Andres, R. M. Featherstone, 'A new and rapid colorimetric determination of acetylcholinesterase activity', *Biochem. Pharmacol.* **1961**, *7*, 88–95.
- [36] C. Lee, W. Yang, R. G. Parr, 'Development of the Colle-Salvetti correlation-energy formula into a functional of the electron density', *Phys. Rev. B* **1988**, *37*, 785–789.
- [37] A. D. Becke, 'Density-functional thermochemistry III. The role of exact exchange', *J. Chem. Phys.* **1993**, *98*, 5648–5652.
- [38] U. C. Singh, P. A. Kollman, 'An approach to computing electrostatic charges for molecules', *J. Comput. Chem.* **1984**, *5*, 129–145.
- [39] B. H. Besler, K. M. Merz, P. A. Kollman, 'Atomic charges derived from semiempirical methods', *J. Comput. Chem.* **1990**, *11*, 431–439.
- [40] M. J. Frisch, G. W. Trucks, H. B. Schlegel, G. E. Scuseria, M. A. Robb, J. R. Cheeseman, G. Scalmani, V. Barone, G. A. Petersson, H. Nakatsuji, X. Li, M. Caricato, A. Marenich, J. Bloino, B. G. Janesko, R. Gomperts, B. Mennucci, H. P. Hratchian, J. V. Ortiz, A. F. Izmaylov, J. L. Sonnenberg, D. Williams-Young, F. Ding, F. Lipparini, F. Egidi, J. Goings, B. Peng, A. Petrone, T. Henderson, D. Ranasinghe, V. G. Zakrzewski, J. Gao, N. Rega, G. Zheng, W. Liang, M. Hada, M. Ehara, K. Toyota, R. Fukuda, J. Hasegawa, M. Ishida, T. Nakajima, Y. Honda, O. Kitao, H. Nakai, T. Vreven, K. Throssell, J. A. Montgomery, Jr., J. E. Peralta, F. Ogliaro, M. Bearpark, J. J. Heyd, E. Brothers, K. N. Kudin, V. N. Staroverov, T. Keith, R. Kobayashi, J. Normand, K. Raghavachari, A. Rendell, J. C. Burant, S. S. Iyengar, J. Tomasi, M. Cossi, J. M. Millam, M. Klene, C. Adamo, R. Cammi, J. W. Ochterski, R. L. Martin, K. Morokuma, O. Farkas, J. B. Foresman, D. J. Fox, Gaussian, Gaussian 09, Revision A.02, Inc., Wallingford CT, **2016**.
- [41] G. M. Morris, R. Huey, W. Lindstrom, M. F. Sanner, R. K. Belew, D. S. Goodsell, A. J. Olson, 'AutoDock4 and AutoDockTools4: automated docking with selective receptor flexibility', *J. Comput. Chem.* **2009**, *30*, 2785–2791.
- [42] O. Trott, A. J. Olson, 'AutoDock Vina: Improving the speed and accuracy of docking with a new scoring function, efficient optimization, and multithreading', *J. Comput. Chem.* **2010**, *31*, 455–461.
- [43] R. Benigni, C. Bossa, N. Jeliakova, T. Netzeva, A. Worth, 'The Benigni/Bossa rulebase for mutagenicity and carcinogenicity - a module of Toxtree', European Commission report EUR 23241, OPOCE, 2008.

Received January 10, 2019

Accepted March 19, 2019

## 2.6 Selective *in vitro* and *in silico* cholinesterase inhibitory activity of isoflavones and stilbenes from *Belamcandae chinensis rhizoma*

<b>Title</b>	<i>Selective in vitro and in silico cholinesterase inhibitory activity of isoflavones and stilbenes from Belamcandae chinensis rhizoma</i>
<b>Authors</b>	Sylwester Ślusarczyk, F. Sezer Senol Deniz, Dorota Woźniak, Łukasz Pecio, Horacio Pérez-Sánchez, José P. Cerón-Carrasco, Anna Stochmal, Helena den-Haan Alonso, Adam Matkowski, Ilkay Erdogan Orhan.
<b>Journal</b>	<i>Phytochemistry Letters</i>
<b>Year</b>	2019
<b>State</b>	Published

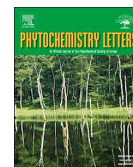
### PhD candidate contribution

Helena den Haan Alonso, declares to be the co-author and contributor of the article *Selective in vitro and in silico cholinesterase inhibitory activity of isoflavones and stilbenes from Belamcandae chinensis rhizoma* in the section on computational chemistry.



Contents lists available at ScienceDirect

Phytochemistry Letters

journal homepage: [www.elsevier.com/locate/phytol](http://www.elsevier.com/locate/phytol)

## Selective *in vitro* and *in silico* cholinesterase inhibitory activity of isoflavones and stilbenes from *Belamcandae chinensis rhizoma*



Sylwester Ślusarczyk<sup>a</sup>, F. Sezer Senol Deniz<sup>b</sup>, Dorota Woźniak<sup>a</sup>, Łukasz Pecio<sup>c</sup>,  
Horacio Pérez-Sánchez<sup>d</sup>, José P. Cerón-Carrasco<sup>d</sup>, Anna Stochmal<sup>c</sup>, Helena den-Haan Alonso<sup>d</sup>,  
Adam Matkowski<sup>a,e,\*</sup>, Ilkay Erdogan Orhan<sup>b</sup>

<sup>a</sup> Department of Pharmaceutical Biology and Botany, Wrocław Medical University, Wrocław, Poland

<sup>b</sup> Department of Pharmacognosy, Faculty of Pharmacy, Gazi University, 06330, Ankara, Turkey

<sup>c</sup> Department of Biochemistry and Crop Quality, IUNG-Institute of Soil Science and Plant Cultivation, Pulawy, Poland

<sup>d</sup> Bioinformatics and High Performance Computing Research Group, Universidad Católica San Antonio de Murcia (UCAM), Spain

<sup>e</sup> Botanical Garden of Medicinal Plants, Laboratory for Experimental Herbs Cultivation, Wrocław Medical University, Poland

### ARTICLE INFO

#### Keywords:

Piceatannol

Cholinesterases

*Iris domestica*

Irilin D

Resveratrol

### ABSTRACT

Isoflavonoids and stilbenes were suggested as potential lead structures for inhibition of cholinesterases and in management of dementia. The Traditional Chinese (TCM) herb *Belamcandae chinensis rhizoma* (the rhizome of *Iris domestica* (L.) Goldblatt & Mabb) contains both classes of natural products. Here, we isolated eight isoflavonoids: irisflorethin (1), tectorigenin(2), iristectorigenin B(3), irigenin (4), irilin D (5), iridin (6), tectoridin (7), iristectorin B (8), two stilbenes; piceatannol (9) and resveratrol (10) as well as the xanthone glucoside – mangiferin (11). The compounds were tested against acetyl- (AChE) and butyrylcholinesterase (BChE) using ELISA microtiter assay. Molecular docking studies were also performed on the active compounds.

Among the tested polyphenols, piceatannol inhibited both cholinesterases (up to 67% and 91% of AChE and BChE, respectively) whereas irilin D and resveratrol were only active against BChE. Irisflorethin was selective but weak inhibitor against AChE (36% inhibition at 100 µg/mL). The remaining isoflavones were moderately active against BChE (below 40% inhibition).

In conclusion, the TCM and pharmacopoeial drug – *Belamcandae chinensis rhizoma* is rich in potential cholinesterase inhibitors that can provide lead structures for further development of selective drugs. Moreover, the *in vitro* results would suggest a novel indication of this traditional anti-inflammatory, phytoestrogenic and anti-allergic herb.

### 1. Introduction

Search for inhibitors of cholinesterases has been driven by their pivotal role as a drug category that helps to slow down the debilitating symptoms of neurodegenerative conditions, such as Alzheimer's disease (AD). The cognitive impairment, developing towards severe dementia can be temporarily managed by one of the few available Acetylcholinesterase (AChE) inhibitors based on natural structures – galanthamine and physostigmine. However, many other natural compounds exert such action *in vitro* and *in vivo* but clinical evidence is missing and their activity is usually rather moderate (Perry and Howes, 2011). Natural compounds usually differ in their selectivity to one of the two forms, i.e. AChE and butyrylcholinesterase (BChE), while the typically preferred is rather AChE targeting. BChE, which is also

considered as promising target for drug discovery since its enzymatic activity upsurges in the late stages of AD. In fact, it has been reported that BChE inhibitors can also act in a similar way to those of AChE inhibitors and slow down cognitive decline (Li et al., 2008).

Among a huge number of natural products that have been shown to be inhibitors of *in vitro* activity of cholinesterases (Orhan et al., 2017, 2018), several classes of polyphenols are usually considered promising (Pinho et al., 2013; Politeo et al., 2018). On the other hand, polyphenols showing such activity could also contribute to the dementia prevention *via* their well-established anti-inflammatory properties (Sawikr et al., 2017). Thereof, stilbenoids, such as resveratrol, and isoflavonoids, such as genistein are mentioned as markedly active and as potential lead structures. However, among these two structural classes, there are many more compounds that have not been studied.

\* Corresponding author at: Department of Pharmaceutical Biology and Botany, Wrocław Medical University, Wrocław, Poland.

E-mail address: [pharmaceutical.biology@wp.eu](mailto:pharmaceutical.biology@wp.eu) (A. Matkowski).

<https://doi.org/10.1016/j.phytol.2019.02.006>

Received 30 October 2018; Received in revised form 22 January 2019; Accepted 4 February 2019

Available online 14 February 2019

1874-3900/ © 2019 Phytochemical Society of Europe. Published by Elsevier Ltd. All rights reserved.

This drew our attention to the traditional medicinal plant that contains both isoflavonoids and stilbenoids, among others.

*Iris domestica* (L.) Goldblatt & Mabb. (syn. *Belamcanda chinensis* L.) DC. (Iridaceae) occurs naturally in South and East Asia. Despite the fact that former monotypic genus *Belamcanda* has been included in the extended genus *Iris*, this classification has been questioned (Wilson, 2011; Mavrodiev et al., 2014) and the final systematic position of this plant is possible to be changed. To avoid the nomenclature ambiguity, we use the commonly acknowledged pharmacognostic name of the drug *Belamcandae chinensis rhizoma* instead of full binomial name (*I. domestica*).

Rhizomes are a pharmacopoeial raw material of East and South-East Asian traditional phytotherapies under the pharmacognostic name *Belamcandae chinensis rhizoma*, also known under the TCM name *she-gan*. Pharmacological properties that have been confirmed by now, include: antiinflammatory, antidiabetic, antiosteoporotic, estrogenic, anti-allergic, anti-asthmatic, cytotoxic, and antimicrobial (Woźniak and Matkowski, 2015; Szandruk et al., 2018). Apart from the Chinese, Korean and a couple of other Asian Pharmacopoeias, also the European Pharmacopoeia has been monographing the raw material of this plant for several years, which proves its increasing popularity and usefulness around the world. The main class of compounds responsible for this broad spectrum of activity are polyphenols, among them isoflavones, xanthenes, stilbenes, and phenolic acids. Several cytotoxic iridal triterpenes are also contributing to the overall phytochemical profile of the plant (Woźniak and Matkowski, 2015). In the literature, various methods of isolation and identification of main constituents from this raw material can be found. On the other hand, there is still some degree of inconsistency and ambiguity in the composition assessment. Despite previous reports showing no anti-AChE activity of methanol extract from *she-gan* (Kaufmann, 2016), we hypothesize that individual polyphenols due to their structural characteristics may demonstrate such activity, also against BChE. Tectorigenin has been shown to have anti-neuroinflammatory activity (Lim et al., 2018), and related *Iris* species were active against cholinesterases (Conforti et al., 2009). The aim of this work was to develop and optimize the method of isolation and identification of polyphenolic compounds from *Belamcandae chinensis rhizoma* for further bioactivity testing towards *in vitro* inhibition of two cholinesterases - BChE and AChE. The most active compounds were also assessed for their affinity to these enzymes by the molecular docking study.

## 2. Results and discussion

### 2.1. Identification of compounds 1-10

All isolated compounds from *Iris domestica* extract (a representative HPLC profile shown in Fig. 1) were identified based on MS/MS and NMR spectra and have been characterized as given below. Their structures and the annotation of NMR shift data are presented in Fig. 2.

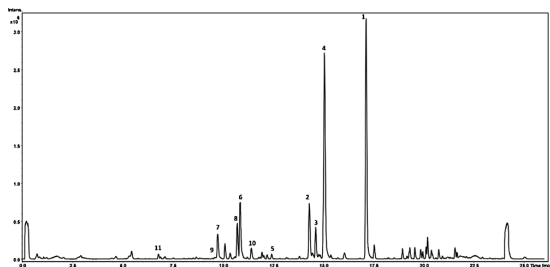


Fig. 1. A representative HPLC-MS BPC (Base Peak Chromatogram) of the primary extract from dried *Belamcandae chinensis rhizoma* (extracting solvent 80% MeOH). Identification of particular compounds based on High Resolution Mass Spectrometry, supported with electronic database.

The identification was based on the spectra analysis and available literature (Monthakantirat et al., 2005; Gómez-Zaleta et al., 2006; Lee et al., 2011; Jun et al., 2012; Tisserant et al., 2016)

From this species, we obtained:

**Compound 1 Irisfloreutin** white needle fluff ( $c = 0.13$ , MeOH:H<sub>2</sub>O (1:1, v/v)). UV  $\lambda_{\max}$  (nm):220,265,323, HR-Q-TOF-MS (pos.)  $m/z$  387.1082 [M+H]<sup>+</sup>, (calc.for C<sub>20</sub>H<sub>19</sub>O<sub>8</sub><sup>+</sup> = 387.1074), diagnostic fragment ions in positive at  $m/z$  372.0831 [M+H-15]<sup>+</sup>, 357.0600 [M+H-30]<sup>+</sup>, lost one and two -CH<sub>3</sub> group respectively, 326.0782 lost another two methyl groups. Lack of a clear and unambiguous signal in negative mode.

**Compound 2 5,7,4'-trihydroxy-6-methoxyisoflavone, Tectorigenin**, white amorphous powder ( $c = 0.13$ , MeOH:H<sub>2</sub>O (1:1, v/v)). UV  $\lambda_{\max}$  (nm):220,265, HR-Q-TOF-MS (pos.)  $m/z$  301.0704 [M+H]<sup>+</sup>, (calc.for C<sub>16</sub>H<sub>13</sub>O<sub>6</sub><sup>+</sup> = 301.0707), diagnostic fragment ions in positive at  $m/z$  286.0466 [M+H-15]<sup>+</sup>, 268.0361 [M+H-18]<sup>+</sup>, lost methyl and hydroxyl groups, HR-Q-TOF-MS (neg.) 299.0555[M-H]<sup>-</sup>, 621.0995[2M-H+Na]<sup>-</sup>, 284.0320[M-H-15]<sup>-</sup>, 256.0370[M-H-28]<sup>-</sup>.

**Compound 3 5,7,4'-Trihydroxy-6,3'-dimethoxyisoflavone, Iristectorigenin B**, white amorphous powder ( $c = 0.13$ , MeOH:H<sub>2</sub>O (1:1, v/v)). UV  $\lambda_{\max}$  (nm):210,265, HR-Q-TOF-MS (pos.)  $m/z$  331.0809[M+H]<sup>+</sup>, (calc.for C<sub>17</sub>H<sub>15</sub>O<sub>7</sub><sup>+</sup> = 331.0812), diagnostic fragment ions in positive at  $m/z$  316.0574 [M+H-15]<sup>+</sup>, 301.0342 [M+H-30]<sup>+</sup> lost two methyl groups, 2,730,391[M+H-28]<sup>+</sup>, HRQ-TOF-MS (neg.) 329.0658[M-H]<sup>-</sup>, 314.0426[M-H-15]<sup>-</sup> 299.0193[M-H-30]<sup>-</sup>, 271.0243[M-H-30-28]<sup>-</sup>, 255.0296[M-H-15-28]<sup>-</sup>.

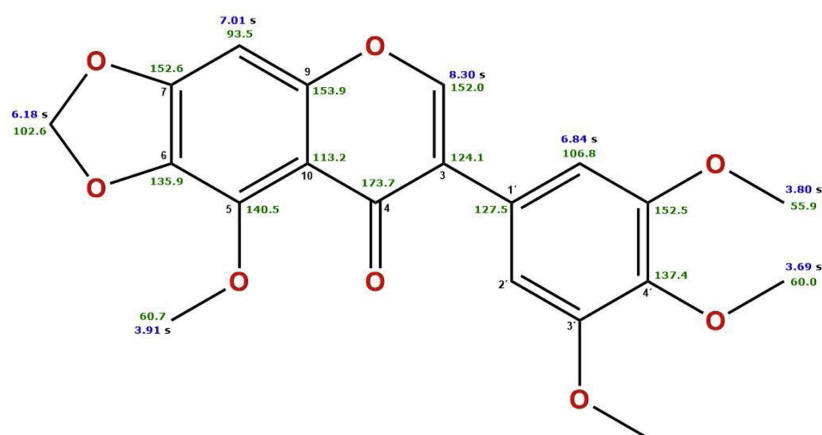
**Compound 4 5,7,3'-trihydroxy-6,4',5'-trimethoxyisoflavone, Irirogenin**, white amorphous powder ( $c = 0.13$ , MeOH:H<sub>2</sub>O (1:1, v/v)). UV  $\lambda_{\max}$  (nm):215,265, HR-Q-TOF-MS (pos.)  $m/z$  361.0917 [M+H]<sup>+</sup>, (calc.for C<sub>18</sub>H<sub>17</sub>O<sub>8</sub><sup>+</sup> = 361.0918), diagnostic fragment ions in positive at  $m/z$  345.0602 [M+H-15]<sup>+</sup>, 331.0444 [M+H-30]<sup>+</sup>, 303.0494[M+H-60]<sup>+</sup>. 285.0390[M+H-60-18]<sup>+</sup>, lost one,two and three -CH<sub>3</sub> group and H<sub>2</sub>O respectively, HR-Q-TOF-MS (neg.) 359.0765[M-H]<sup>-</sup>, 344.0529[M-H-15]<sup>-</sup>, 329.0296[M-H-30]<sup>-</sup>, 314.0062[M-H-45]<sup>-</sup>.

**Compound 5 5,7,3',4'-tetrahydroxy-6-methoxyisoflavone, Iridin D** white needle fluff ( $c = 0.13$ , MeOH:H<sub>2</sub>O (1:1, v/v)). UV  $\lambda_{\max}$  (nm):220,265, HR-Q-TOF-MS (pos.)  $m/z$  315.0852 [M+H]<sup>+</sup>, (calc.for C<sub>17</sub>H<sub>15</sub>O<sub>6</sub><sup>+</sup> = 315.0863), diagnostic fragment ions in positive at  $m/z$  300.0625 [M+H-15]<sup>+</sup>, 285.0388 [M+H-30]<sup>+</sup>, lost one and two -CH<sub>3</sub> group respectively, 299.0914 [M+H-18]<sup>+</sup>. Lack of a clear and unambiguous signal in negative mode.

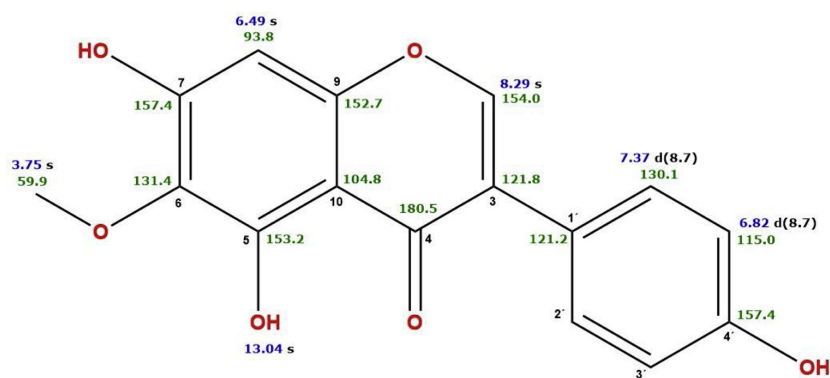
**Compound 6 5,3'-Dihydroxy-6,4',5'-trimethoxyisoflavone-7-O-glucoside, Iridin** white amorphous powder ( $c = 0.13$ , MeOH:H<sub>2</sub>O (1:1, v/v)). UV  $\lambda_{\max}$  (nm):215,265, HR-Q-TOF-MS (pos.)  $m/z$  523.1442 [M+H]<sup>+</sup>, (calc.for C<sub>24</sub>H<sub>27</sub>O<sub>13</sub><sup>+</sup> = 523.1446), diagnostic fragment ions in positive at  $m/z$  1045.2808 [2M+H]<sup>+</sup>, 361.0917 [M+H-162]<sup>+</sup>, lost glucose moiety, 346.0680[M+H-15]<sup>+</sup>, 331.0449[M+H-30]<sup>+</sup>, lost one and two -CH<sub>3</sub> group, 301.0705 [M+H-60]<sup>+</sup>,286.0469. HRQ-TOF-MS (neg.) 521.1294[M-H]<sup>-</sup>, 1043.2649[2M-H]<sup>-</sup>, 359.0769[M-H-162]<sup>-</sup>, 343.0457[M-H-15]<sup>-</sup>, 328.0224[M-H-30]<sup>-</sup>.

**Compound 7 5,4'-dihydroxy-6-methoxyisoflavone-7-O-glucoside, Tectoridin**, white amorphous powder ( $c = 0.13$ , MeOH:H<sub>2</sub>O (1:1, v/v)). UV  $\lambda_{\max}$  (nm):220,265, HR-Q-TOF-MS (pos.)  $m/z$  463.1241 [M+H]<sup>+</sup>, (calc.for C<sub>22</sub>H<sub>23</sub>O<sub>11</sub><sup>+</sup> = 463.1235), diagnostic fragment ions in positive at  $m/z$  485.1058 [M+H+Na]<sup>+</sup>, 301.0708 [M+H-162]<sup>+</sup> lost glucosyl, HR-Q-TOF-MS (neg.) 461.1086[M-H]<sup>-</sup>, 299.0556[M-H-162]<sup>-</sup>, 283.0248[M-H-162-15]<sup>-</sup>.

**Compound 8 5,7,4'-trihydroxy-6,3'-methoxyisoflavone, Iristectorin B**, white amorphous powder ( $c = 0.13$ , MeOH:H<sub>2</sub>O (1:1, v/v)). UV  $\lambda_{\max}$  (nm):210,265, HR-Q-TOF-MS (pos.)  $m/z$  493.1348[M+H]<sup>+</sup>, (calc.for C<sub>23</sub>H<sub>25</sub>O<sub>12</sub><sup>+</sup> = 493.1341), diagnostic fragment ions in positive at  $m/z$  331.0815 [M+H-162]<sup>+</sup>, 316.0580 [M+H-162-15]<sup>+</sup>, lost glucosyl and methyl groups, 301.0343 [M+H-162-30]<sup>+</sup>, 273.0394, HRQ-TOF-MS (neg.) 491.1188[M-H]<sup>-</sup>, 329.0670[M-H-162]<sup>-</sup>, 313.0358[M-H-18]<sup>-</sup>,

**BCr-LH-Fr36-49-1****KNOWN**Chemical Formula: C<sub>20</sub>H<sub>18</sub>O<sub>8</sub>  
Exact Mass: 386,1002

Quat	CH
173.7	152.0
153.9	106.8
152.6	93.5
152.5	
140.5	CH <sub>3</sub>
137.4	60.7
135.9	60.0
127.5	55.9
124.1	
113.2	
CH <sub>2</sub>	
102.6	

DMSO-*d*<sub>6</sub>+TFA, 30°C**Irisflorentin****Bel\_4-7****KNOWN**Chemical Formula: C<sub>16</sub>H<sub>12</sub>O<sub>6</sub>  
Exact Mass: 300,0634

Quat	CH
180.5	154.0
157.4	130.1
153.2	115.0
152.7	93.8
152.7	131.4
131.4	
121.8	CH <sub>3</sub>
121.2	59.9
104.8	
CH <sub>2</sub>	
-	

DMSO-*d*<sub>6</sub>, 30°C**Tectorigenin**

Fig. 2. Structures and <sup>1</sup>H-NMR (blue) and <sup>13</sup>C-NMR (green) signals of the compounds (1-11) isolated from *Belamcandae chinensis* rhizome (Based on <sup>1</sup>H and <sup>13</sup>C-NMR data and direct comparison of spectral data from the literature).

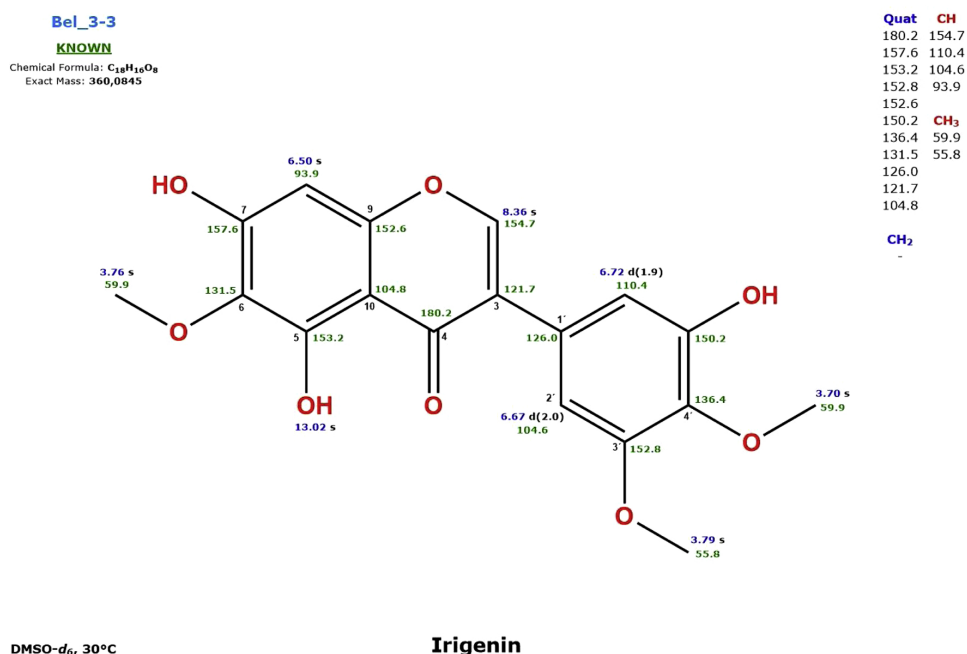
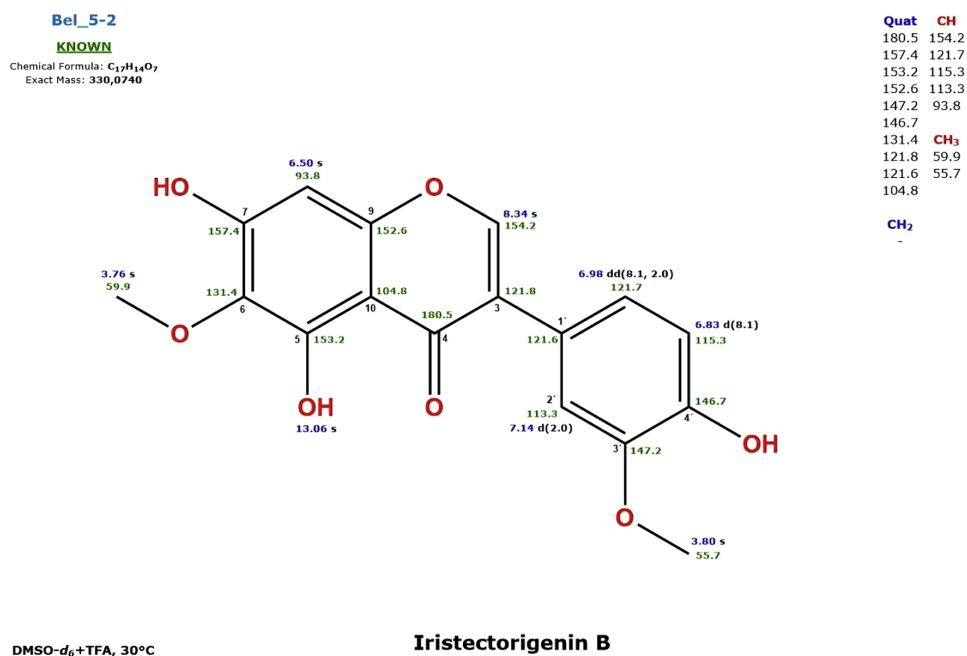


Fig. 2. (continued)

256.0370[M-H-28]<sup>-</sup>.

Compound 9 3,3',4',5-tetrahydroxystilbene, piceatannol, brownish amorphous powder (c = 0.13, MeOH:H<sub>2</sub>O (1:1, v/v)). UV λ<sub>max</sub>

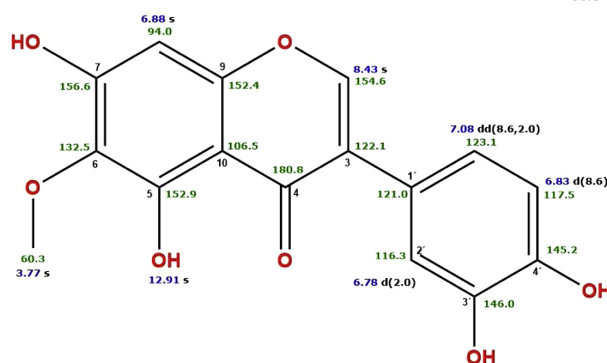
(nm):220,305, HR-Q-TOF-MS (pos.) *m/z* 245.0805[M+H]<sup>+</sup>, (calc.for C<sub>14</sub>H<sub>13</sub>O<sub>4</sub><sup>+</sup> =245.0808), diagnostic fragment ions in positive at *m/z* [M+H-15]<sup>+</sup>, [M+H-30]<sup>+</sup>, HRQ-TOF-MS (neg.) 243.0659[M-H]<sup>-</sup>,

## Bel\_2\_3

KNOWN

Chemical Formula: C<sub>16</sub>H<sub>12</sub>O<sub>7</sub>  
Exact Mass: 316,0583

CH	Quat
154.6	180.8
123.1	156.6
117.5	152.9
116.3	152.4
146.0	146.0
94.0	145.2
	132.5
	121.0
	122.1
	106.5
CH <sub>3</sub>	106.5
60.3	

DMSO-d<sub>6</sub>+TFA, 30°C

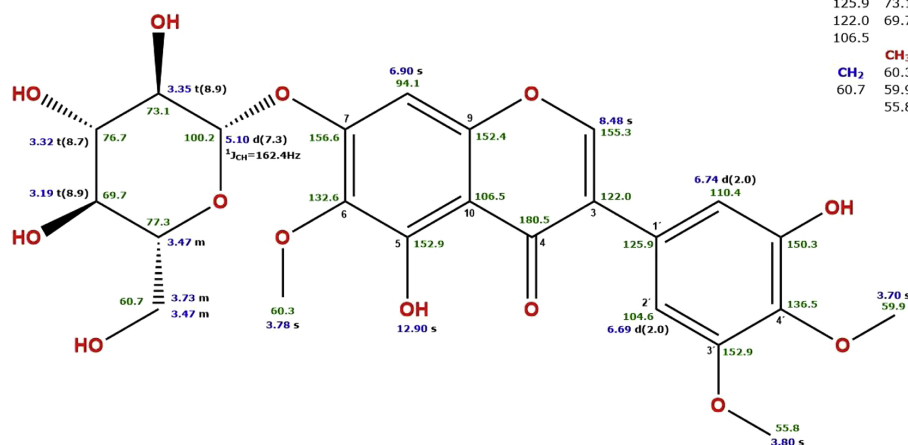
## Irilin D

## Bel\_2\_4

KNOWN

Chemical Formula: C<sub>24</sub>H<sub>26</sub>O<sub>13</sub>  
Exact Mass: 522,1373

Quat	CH
180.5	155.3
156.6	110.4
152.9	104.6
152.4	100.2
150.3	94.1
136.5	77.3
132.6	76.7
125.9	73.1
122.0	69.7
106.5	69.7
	60.3
	59.9
	55.8
CH <sub>2</sub>	60.3
60.7	59.9
	55.8

DMSO-d<sub>6</sub>+TFA, 30°C

## Iridin (irigenin 7-O-β-glucopyranoside)

Fig. 2. (continued)

201.0548[M-H-15]<sup>-</sup>159.0441 [M-H-30]<sup>-</sup>,Compound 10 3,4',5-trihydroxystilbene, resveratrol, brownish  
amorphous powder (c = 0.13, MeOH:H<sub>2</sub>O (1:1, v/v)). UV λ<sub>max</sub>(nm):220,305, HR-Q-TOF-MS (pos.) m/z 229.0861[M+H]<sup>+</sup>, (calc. for  
C<sub>14</sub>H<sub>13</sub>O<sub>3</sub><sup>+</sup> = 229.0859), diagnostic fragment ions in positive at m/z  
165.0702 [M+H-64]<sup>+</sup>, 181.0650[M+H-48]<sup>+</sup>, 153.0699, 107.0492,

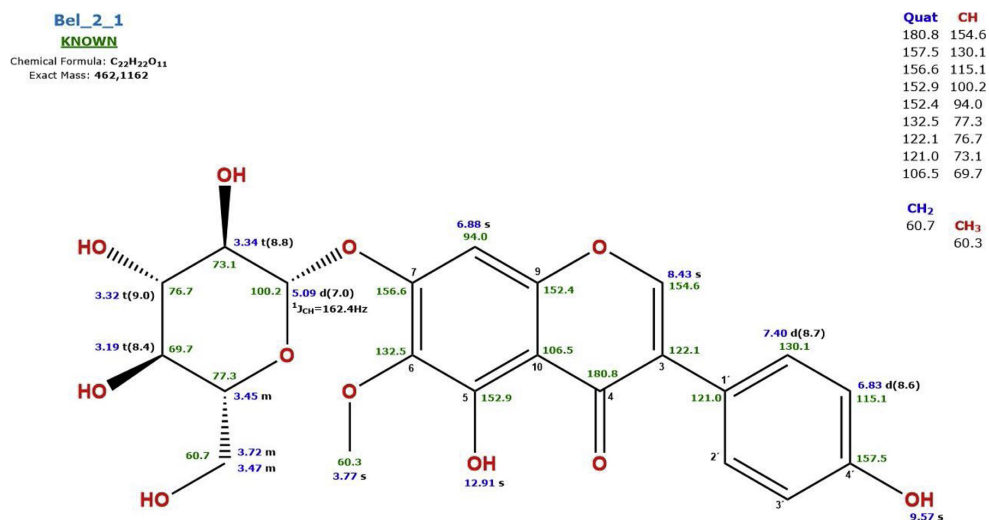
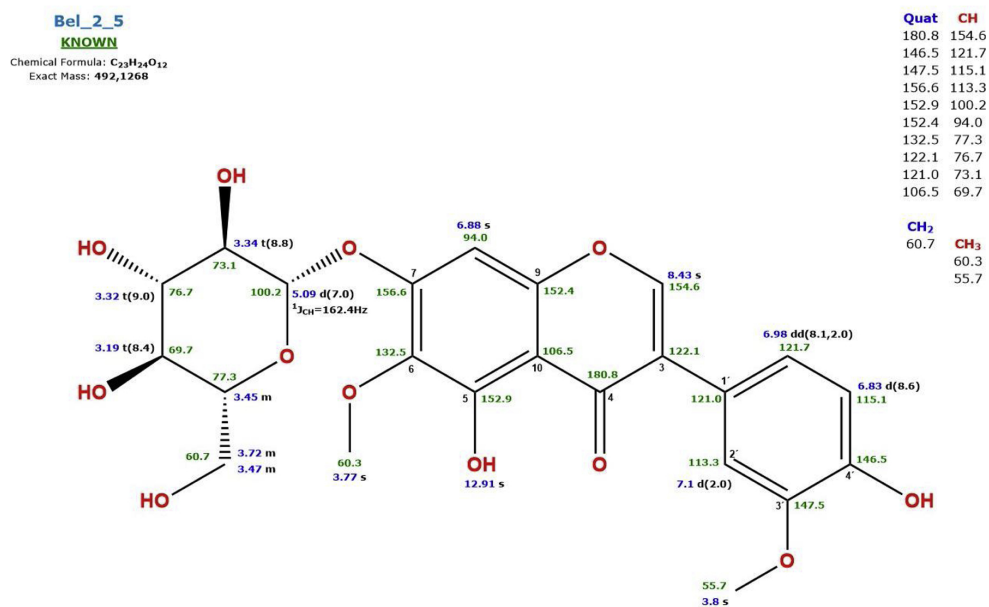
DMSO-d<sub>6</sub>+TFA, 30°C**Tectoridin (tectorigenin 7-O-β-glucopyranoside)**DMSO-d<sub>6</sub>+TFA, 30°C**Iristectorin B (Iristectorigenin-7-O-β-glucopyranoside)**

Fig. 2. (continued)

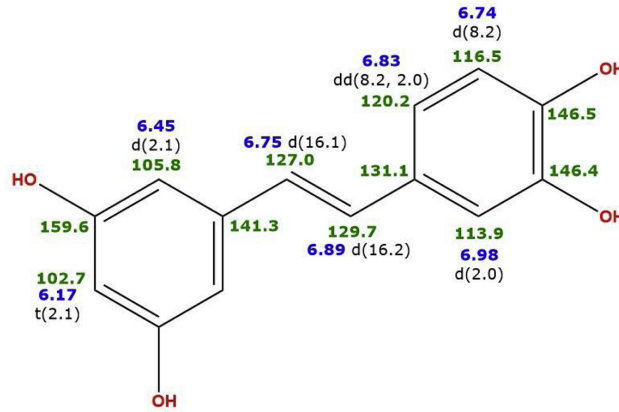


S. Ślusarczyk, et al.

Phytochemistry Letters 30 (2019) 261–272

Bel\_6-1

KNOWN

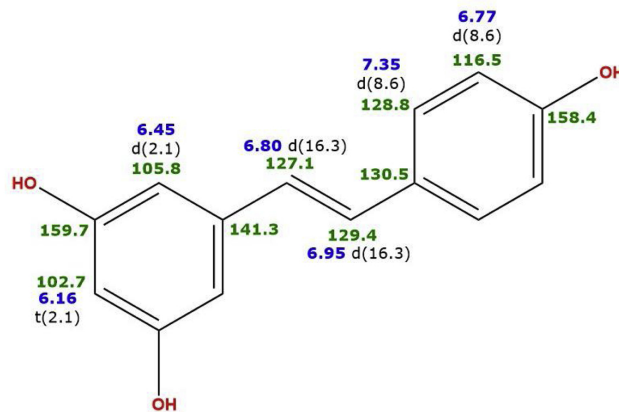
Chemical Formula: C<sub>14</sub>H<sub>12</sub>O<sub>4</sub>  
Exact Mass: 244,0736

Quat	CH
159.6	129.7
146.5	127.0
146.4	120.2
141.3	116.4
131.1	113.9
	105.8
CH <sub>2</sub>	102.7
-	CH <sub>3</sub>
	-

CD<sub>3</sub>OD, 30°C**(E)-Piceatannol**  
3,3',4,5'-tetrahydroxystilbene

Bel\_6-2

KNOWN

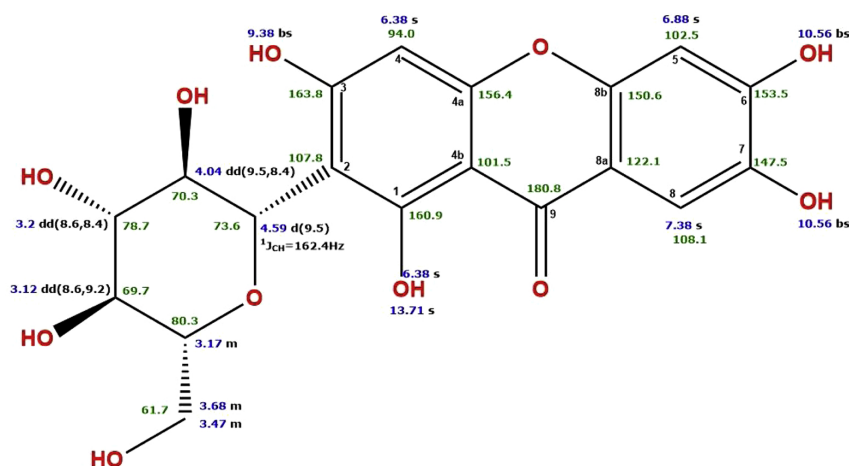
Chemical Formula: C<sub>14</sub>H<sub>12</sub>O<sub>3</sub>  
Exact Mass: 228,0786

Quat	CH
159.7	129.4
158.4	128.8
141.3	127.1
130.5	116.5
	113.9
CH <sub>2</sub>	105.8
-	102.7
	CH <sub>3</sub>
	-

CD<sub>3</sub>OD, 30°C**Resveratrol**  
3,4',5-trihydroxystilbene

Fig. 2. (continued)

**KNOWN**  
Chemical Formula: C<sub>19</sub>H<sub>18</sub>O<sub>11</sub>  
Exact Mass: 422,0849



Quat	CH
180.8	108.1
163.8	102.5
160.9	94.0
156.4	80.3
153.5	78.7
150.6	73.6
147.5	70.3
122.1	69.7
107.8	
101.5	CH <sub>3</sub>
	CH <sub>2</sub>
61.7	

DMSO-*d*<sub>6</sub> 30°C

### Mangiferin

Fig. 2. (continued)

HR-Q-TOF-MS (neg.) 227.0711[M-H]<sup>-</sup>, 185.0608[M-H-42]<sup>-</sup>, 143.0504 [M-H-42-42]<sup>-</sup>, 159.0817, 119.0505

#### 2.2. Inhibition of cholinesterase isoforms

None of the tested compounds had significant (above 50% inhibition at 100 µg/mL) activity against AChE. The standard drug selective for AChE, the alkaloid galanthamine had IC<sub>50</sub> value in the lower micromolar range (2.02 µM), whereas for the polyhydroxylated stilbene - piceatannol - the only compound for which we were able to calculate this value, IC<sub>50</sub> was over 100 times higher (218.93 µM). Quite opposite, piceatannol was highly and dose-dependently active against BChE (over 90% inhibition with IC<sub>50</sub> at 18 µg/mL (74 µM), that is stronger than galanthamine (IC<sub>50</sub> = 98.16 µM). The second stilbenoid - resveratrol, well-known for its broad spectrum of bioactivities, was only moderately active against BChE and completely inactive against AChE. Other resveratrol analogues can also exhibit AChE inhibitory activity. For example several oligomeric highly hydroxylated compounds isolated from *Hopea chinensis* with IC<sub>50</sub> values lower (ca. 5–11 µM) than in our study, but the experimental details were different and could account for the discrepancy (Yan et al., 2012). Also, anti-BChE activity was not considered in the cited paper. On the other hand, Csuk et al (2013) reported selective anti-BChE properties of several semisynthetic resveratrol derivatives, with a fluorinated derivative being both the strongest and the most selective. It suggests that modifications of structure can further improve the enzyme-inhibitory properties. Also, natural stilbenes from *Ficus sp.* (Seramboonpaisarn and Sawasdee, 2012, Badgular et al., 2014), showed selectivity to BChE, but resveratrol and gnetol (a positional piceatannol isomer) were the most potent and their IC<sub>50</sub> lower than in our study. However, the experimental differences could result in the different absolute values. Another positional isomer of piceatannol - oxyresveratrol administered in an improved-

bioavailability drug delivery system, demonstrated significant neuroprotective *in vivo* in a β-amyloid-based murine model of neurodegeneration (Sangsen et al., 2018). The superior activity of piceatannol over resveratrol in our study suggests that it can be even more promising compound for further studies.

All isoflavonoids were generally weaker than both isolated stilbenes, disregarding the enzyme isoform. However, the most methoxylated isoflavone aglycone - iriflorentin had clear selectivity towards AChE (36% inhibition compared to 9% of BChE activity). This compound is also a pharmacopoeial quality marker but the research on its pharmacological properties lags behind the more studied tectorigenin and irigenin (Woźniak and Matkowski, 2015). Due to its relatively low polarity (XLogP3 is 2.9 - compared to tectorigenin's 2.6 - source PubChem) its pharmacokinetic and pharmacodynamic properties are likely to differ from other isoflavonoids. Therefore, this structure might be considered for further studies to elucidate the mechanisms of its selectivity.

Other isoflavonoid aglycones were moderately but specifically active against BChE only (20–40% inhibition at 100 µg/mL).

Isoflavonoids have been previously reported as a class that could be considered as moderate cholinesterase inhibitors. For example, pomiferin was inhibiting AChE at IC<sub>50</sub> of 96 µM but did not act against BChE (Orhan et al., 2009). However, Iridaceae-type isoflavonoids were rather weakly inhibiting both cholinesterases in the study by Conforti et al. (2009) using *Iris pumila* as source of the isolated compounds.

Also, like in stilbenoids, semisynthetic derivatives were designed as dual-target cholinesterase inhibitors and a decoration of the isoflavonoid skeleton with piperidine was shown to be most promising (Feng et al., 2017). It would be thus recommended to try similar approach using Iridaceae-isoflavones as a scaffold for such amendment.

Some evidence exists for *in vivo* action of isoflavonoids in the improvement of brain function in dementia. For example, a mixture of

soybean isoflavones improved cognitive function in mice model of senescent dementia, with concurrently observed decrease in AChE activity in brain cortex. It clearly suggests that cholinesterase inhibition can be one also a mechanism of action *in vivo* (Yang et al., 2011)

Methoxylated isoflavonoids have also an additional advantage over non-methoxylated counterparts in having higher bioavailability (Walle, 2009; Chen et al., 2018) Unfortunately, piceatannol exhibited rather poor bioavailability, albeit not lower than other stilbenoids (Kershaw and Kim, 2017).

The activity of all glycosides (both isoflavonoids and a xanthonoid mangiferin) was either negligible or none at all. This is in agreement with the well established general rule that most of glycosides have weaker activity than the respective aglycons. However, *in vivo* studies are necessary to account for the potential biotransformation of the glycosides that would facilitate aglycone release resulting in higher activity than observed *in vitro*. Mangiferin, a strong antioxidant and antiinflammatory polyphenol has been frequently mentioned as a potential preventive and complementary remedy in neurodegenerative disorders (Matkowski et al., 2013). However, in our study it had no activity against any of the two isoforms. Hence, other mechanisms should be explored to elucidate its contribution to the postulated neuroprotective potential of *Belamcandae chinensis rhizoma*.

The low activity of glycosides, which predominate in the crude drug and in some solvent extracts may explain the lack of *Belamcandae chinensis rhizoma* extract in a comprehensive screening published by Kaufmann et al. (2016) where 80 TCM herbs were compared against AChE and only a couple of isoquinoline alkaloid-containing drugs were shown to be active. However, we cannot exclude a composition diversity between herbs of different origin to play a role and *Iris domestica*, a source of this herb has been repeatedly shown to be quite variable (Woźniak and Matkowski, 2015).

Other species of *Iris* were also studied in similar experiments with various results. For example *I. schachtii*, in which the main constituents were kaempferol and catechin (Mocan et al., 2018) had negligible activity against both cholinesterases. Conversely, *I. germanica* total flavonoid aglycones (hydrolyzed ethyl acetate fraction) exhibited high activity against AChE and BChE [(Ullah et al., 2016). However, in no previous studies, any of the isolated here isoflavonoids or stilbenoids were suggested as anti-cholinesterase active principle of *Iris* sp.

Taking the marked *in vitro* AChE and BChE inhibitory data of the studied compounds into consideration (Table 1), irilin B, piceatannol

and resveratrol were subjected to molecular docking experiments in order to understand, at the molecular level, the rationale under their inhibitory activity. Having that information in hand is important since it can help to discover new molecules in the same context. After analysis of docking results, structural analysis of docking results for selected compounds from Table 1 for which IC<sub>50</sub> was calculated, is displayed in Figs. 3 and 4. On these figures one can appreciate a representation of the active site of the enzyme with the different compounds docked and hydrogen bonds highlighted. When the detailed representation of docking poses was investigated, we could observe the directionality of the network of hydrogens bond established. Main hydrogen bonds are formed with residues from catalytic triad (yellow color) and peripheral anionic site (green color). Therefore, studied compounds block the access to key residues involved in the normal functioning of the enzyme such as parts of the catalytic triad and peripheral anionic sites. These reasons can explain the inhibitory activity of the mentioned compounds.

Although the *in vitro* screening gives only approximate picture into the therapeutic potential of the bioactive compounds, the lack of a perfect animal model and the still disputed etiopathology of many neurodegeneration - based dementias - including AD (Makin, 2018), the *in vitro* and *in silico* results can provide some input to the rational drug design as well as to more evidence-based implementation of herbal drugs into the management of these globally increasing maladies, at least before a specific targeted drug will have been discovered. The postulated contribution of inflammatory response to progression of neurodegeneration renders natural polyphenols interesting candidate structures to be involved in search for antidementive therapeutics.

In summary, we conclude that several polyphenols from *Belamcandae chinensis rhizoma* have been enough active in the *in vitro* and *in silico* screening to warrant future studies aimed at their anti-cholinesterase properties and potential further development as complementary therapeutics in cognitive impairment of various backgrounds in which inhibition of BuChE isoform would be beneficial. Piceatannol and irilin B, although minor constituents in the phytochemical profile, demonstrate the high selectivity combined with high (piceatannol) or moderate (irilin B) inhibition strength. The mechanisms of the inhibition need to be verified experimentally, though. This is a novel area of indication for this traditional antiinflammatory medicinal plant.

**Table 1**

Inhibition of Acetylcholinesterase (AChE) and Butyrylcholinesterase (BChE) by isoflavonoids and stilbenoids isolated from *Belamcandae chinensis rhizoma* as well as reference drug - galanthamine. Inhibition % given at 100 µg/mL (± S.D. n = 6) compound concentration and IC<sub>50</sub> in µg/mL and µM (in brackets). Statistically insignificant ( $p \geq 0.05$ ) differences between means are indicated by the same superscript letters.

Compound	AChE Inhibition [% ± S.D.] 100 µg/mL	IC <sub>50</sub> AChE [µg/mL (µM)]	BuChE Inhibition [% ± S.D.] 100 µg/mL	IC <sub>50</sub> BuChE [µg/mL (µM)]
(1) Irisfloreantin	36.25 ± 1.22	–	9.34 ± 2.21 <sup>a</sup>	–
(2) Tectorigenin	–	–	18.08 ± 2.93 <sup>b</sup>	–
(3) Iristectorigenin A	–	–	37.07 ± 0.47	–
(4) Irirogenin	–	–	20.12 ± 2.47 <sup>b</sup>	–
(5) Iriilin B	3.67 ± 1.44	–	49.72 ± 2.83	109.53 ± 6.02/ (348.82 ± 19.17)
(6) Iridin	–	–	4.29 ± 2.04	–
(7) Tectoridin	–	–	–	–
(8) Iristectorin A	–	–	9.44 ± 0.09 <sup>a</sup>	–
(9) Piceatannol	67.07 ± 1.52	53.42 ± 2.22/ (218.93 ± 9.10)	91.10 ± 1.26	18.20 ± 0.89/ (74.55 ± 3.65)
(10) Resveratrol	14.43 ± 1.46	–	56.30 ± 2.33	78.07 ± 4.24/ (342.41 ± 18.60)
(11) Mangiferin	–	–	8.99 ± 2.26 <sup>a</sup>	–
Galanthamine	97.17 ± 2.89	0.58 ± 0.02/ (2.02 ± 0.07)	86.77 ± 2.86	28.16 ± 1.51/ (98.12 ± 5.26)

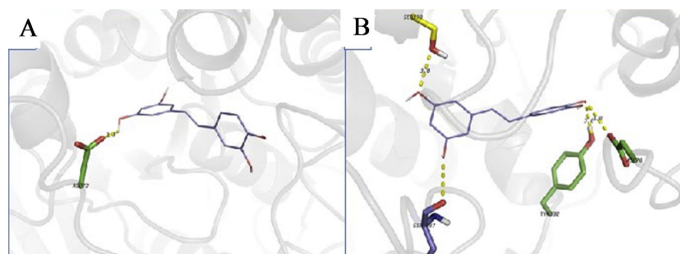


Fig. 3. Interactions of piceatannol (purple skeleton) that interact with both AChE (A) and BChE (B), in transparent grey cartoon fashion. Residues are colored according to their binding area as yellow (catalytic triad), and green (peripheral anionic site). Hydrogen bonds established between compounds and depicted residues are shown with deep yellow dashed lines.

### 3. Materials and methods

#### 3.1. Chemicals

All solvents: methanol, acetonitrile n-hexan used for this work were of analytical grade and purchased from Merck (Darmstadt, Germany), deuterated solvents : water-d<sub>2</sub>, methanol-d<sub>4</sub>, 3-(Trimethylsilyl)-1-propanesulfonic acid sodium salt (TSP) from Armar AG (Döttingen Switzerland), Ultrapure water was obtained from (Milli-Q® Simplicity 185, Millipore Corp., Billerica MA) system. Formic acid (FA), MS-grade was purchased from Sigma-Aldrich (St. Louis, USA). The chromatographic stationary phases were purchased: Cosmosil 140C18-PREP from Nacalai Tesque Inc. (Kyoto, Japan), Sephadex LH-20 and Silica gel 60 (60–200 mesh) from Sigma-Aldrich, (Steinheim, Germany). Mangiferin analytical standard was from ChromaDex (Irvine, CA, USA).

#### 3.2. Plant material

The underground parts of cultivated *Iris domestica* (third year of cultivation) were harvested from the certified collection (under the approval of Ministry of Environment, Republic of Poland, Decision No. DOPogiz-4210-26-6024-/05/kl) of the Botanical Garden of Medicinal Plants in Wrocław, Poland (17°04'27"E, 51°07'03"N, 117 m asl) in the fall of 2017. The voucher specimen have been preserved in the herbarium of the Botanical Garden under the accession no. Iridaceae-Belamcandachinensis-2017-1\*. The rhizomes were washed under tap water to remove soil and debris, cut into approximately 1 cm pieces and dried in the herbal dryer at 30 °C. Then, the dried material was ground in the herbal mill for further processing.

#### 3.3. Instrumentation and chromatographic conditions

##### 3.3.1. Liquid chromatography-mass spectrometry and high-resolution mass spectrometry

The primary aqueous methanol extract of *Belamcandae chinensis rhizoma* was profiled by LC-MS using a Dionex UltiMate 3000RS (Thermo Scientific, Darmstadt, Germany) system with a charged aerosol detector for preliminary peak detection, interfaced with a high-resolution quadrupole time-of-flight mass spectrometer (HR/Q-TOF/MS, Impact II, Bruker Daltonik GmbH, Bremen, Germany). Separation was achieved on an Acquity UPLC BEH C18 column (100 × 2.1 mm,

1.7 μm, Waters, Manchester, UK) maintained at 30 °C. The mobile phase consisted of: A (0.1% formic acid in Milli-Q water, v/v) and B (0.1% formic acid in acetonitrile, v/v). The gradient elution at a flow rate of 0.4 ml/min was: 2% B from 0 to 1 min with a short 0.3 min calibration segment, and the concentration of B was then increased to 60% from 1 to 20 min. The column was eluted with this concentration of solvent B for 4 min and was then re-equilibrated for 0.3 min. The samples were kept at 15 °C in the autosampler. The injection volume was 5.0 μl. Operating parameters of the ESI ion source in positive and negative modes were as follows: capillary voltage 3 kV (negative) or 4.5 kV (positive), drying gas flow 6 L/min, temperature 200 °C, nebulizer pressure 0.7 bar, collision radio frequency 700.0 V, transfer time 100.0 μs, and pre pulse storage 7.0 μs. Ultrapure nitrogen was used as drying and nebulizer gas, and argon was used as collision gas. Collision energy was set automatically from 15 to 75 eV depending on the *m/z* of fragmented ion. Acquired data were calibrated internally with sodium formate introduced to the ion source at the beginning of each separation via a 20 μL loop. Processing of spectra was performed with Bruker DataAnalysis 4.3 software. (Bruker Daltonik GmbH, Bremen, Germany). All analyses were performed in triplicate and repeated twice.

##### 3.3.2. NMR spectroscopy

NMR data (compound 1–10) were acquired at room temperature on a Bruker Avance III™ 500 MHz spectrometer (Bruker, BioSpin, Rheinstetten, Germany) equipped with 5 mm 1H{109Ag-31P} broadband inverse (BBI) probe operating at 500.13 MHz for <sup>1</sup>H, and 125.77 MHz for <sup>13</sup>C experiments. NMR data for compound 11 (mangiferin) were acquired at room temperature on a Bruker Avance 300 MHz spectrometer. Topspin 2.0 software was used for data processing.

##### 3.3.3. Preparative chromatography

Semi-preparative HPLC was performed on a chromatographic system equipped with a Gilson 321 pump, a Gilson GX-271 liquid handler with a 2 mL sample loop, a Gilson Prep ELS™ II detector, and either a semi-preparative reversed phase columns Atlantis Prep T3 250 mm × 10 mm i.d., 5 μm (Waters, Milford, MA). All fractions were lyophilized using Gamma 2–16 LSC freeze dryer (Martin Christ Gefriertrocknungsanlagen GmbH, Germany).

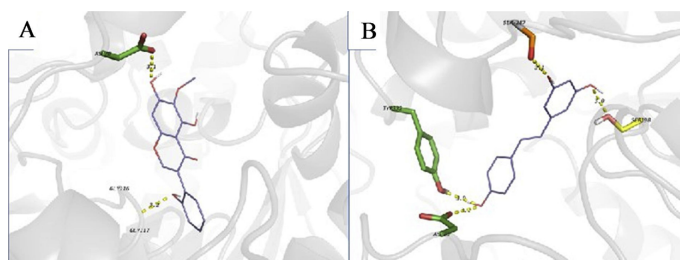


Fig. 4. Interactions of isolated compounds from extracts (purple skeleton) that only interact with BChE, in transparent grey cartoon fashion. Shown compounds are irilin B (A) and resveratrol (B). Residues are colored according to their binding area as yellow (catalytic triad), and green (peripheral anionic site). Hydrogen bonds established between compounds and depicted residues are shown with deep yellow dashed lines.

### 3.4. Procedure of compounds isolation

500 g of powdered rhizomes were extracted three times with 1.5 L ethyl acetate in ultrasonic bath at 40 °C for 40 min each repetition. Combined filtered extracts were concentrated under reduced pressure, dissolved in 80% aq. MeOH solution (v/v) and defatted in the separating funnel with n-hexane. Subsequently the obtained extract was lyophilized to obtain 19.8 g.

Afterwards, the extract (4 g x 5) was applied onto 95 cm x 3.2 cm i.d. glass column (Millipore Corp., Bedford, MA) packed with Sephadex LH-20 (40–120 μm) and eluted with methanol (acidified with 0.1% formic acid) at a flow rate of 5 mL min<sup>-1</sup>. As a result, 6 fractions were obtained according to the ELS<sup>TM</sup> II detector and checked by UPLC-PDA-MS. Fraction I (FI) 6.8 g consisting of nonpolar fatty acids was discarded.

Fractions FII through FV enriched in isoflavones was subjected to semipreparative HPLC, on Atlantis Prep T3 at 25 °C, using isocratic elution with MeCN:H<sub>2</sub>O:FA in various proportions (see below) at 4 mL min<sup>-1</sup>.

FII (1.76 g) – MeCN:H<sub>2</sub>O:FA (5:5:0.1, v/v), gave irisfloreantin (1) (12.4 mg).

Fraction FIII (2.94 g) eluted with MeCN:H<sub>2</sub>O:FA (4:6:0.1, v/v), yielded tectorigenin (2) 60 mg, iristectorigenin (3) 26 mg, and irigenin (4) 220 mg.

Fraction FIV (0.59 g) was separated with MeCN:H<sub>2</sub>O:FA (3:7:0.1, v/v) to obtain: irilin B (5) 5.2 mg, iridin (6) 45 mg.

FV (0.59 g) was separated with MeCN:H<sub>2</sub>O:FA (2:8:0.1, v/v) and tectoridin(7) 6.1 mg, iristectorin (8) 3.1 mg were obtained.

FVI (0.15 g) was separated with MeCN:H<sub>2</sub>O:FA (1:9:0.1, v/v) to obtain both stilbenes - picetannol (9) 70.6 mg, and resveratrol (10) 6 mg.

Isolation of mangiferin (11) was performed using the same procedure as published previously (Matkowski et al., 2009; Nowak et al., 2018). The dried primary extract was suspended in 10% MeOH, and subjected to sequential liquid-liquid extraction with diethyl ether and butanol (in a 300 mL separatory funnel, aqueous:organic fractions in 1:1 ratio, fractionation repeated 6 times). The butanol fraction was further purified using SPE with C-18 silica gel (Fluka, Switzerland) eluted sequentially with water, 40% MeOH, and pure MeOH. The fraction obtained with 40% MeOH contained mangiferin. Mangiferin was purified using reversed-phase Flash Chromatography in an isocratic system eluted with 25% ACN in 1% acetic acid. Mangiferin was eluted within the first four of 12 fractions and recrystallized three times from dioxane:water mixture (1:1). The yield of pure mangiferin was 396 mg from 150 g of crude extract. The identity and purity of the obtained compounds were confirmed by liquid chromatography-mass spectrometry (LC-HRMS) and NMR spectroscopy (<sup>1</sup>H, <sup>13</sup>C). Purity of the isolated compound was at least 95%, and none of the detected impurities exceeded 1% of the peak area.

### 3.5. Microtiter assays for AChE and BChE enzyme inhibition

AChE and BChE inhibitory activity of the extracts was determined by modified spectrophotometric method of Ellman et al. (1961). Electric eel acetylcholinesterase (Type-VI-S, EC 3.1.1.7, Sigma) and horse serum butyrylcholinesterase (EC 3.1.1.8, Sigma) were used as the enzyme sources, while acetylthiocholine iodide and butyrylthiocholine chloride (Sigma, St. Louis, MO, USA) were employed as substrates of the reaction. 5,5'-Dithio-bis(2-nitrobenzoic)acid (DTNB, Sigma, St. Louis, MO, USA) was used for the measurement of the cholinesterase activity. All the other reagents and conditions were the same as described in our previous publication<sup>10</sup>. In brief, 140 μL of 0.1 mM sodium phosphate buffer (pH 8.0), 20 μL of 0.2 M DTNB, 20 μL of sample solutions (in a dilution series of 1–100 μg/mL) and 20 μL of 0.2 M acetylcholinesterase/butyrylcholinesterase solution were added by multi-channel automatic pipette (Gilson Pipetman, France) in a 96-well microplate and incubated for 15 min at 25 °C. The reaction was then initiated with the addition of 10 μL of 0.2 M acetylthiocholine iodide/

butyrylthiocholine chloride. The hydrolysis of acetylthiocholine iodide/butyrylthiocholine chloride was monitored by the formation of the yellow 5-thio-2-nitrobenzoate anion as a result of the reaction of DTNB with thiocholines, catalyzed by enzymes at a wavelength of 412 nm utilizing a 96-well microplate reader (VersaMax, Molecular Devices, USA). Galanthamine, the reference anticholinesterase alkaloid-type of drug isolated from the bulbs of snowdrop (*Galanthus* sp.), was purchased from Sigma (St. Louis, MO, USA).

### 3.6. Data processing for enzyme inhibition assays

The measurements and calculations were evaluated by using Softmax PRO 4.3.2.LS software. Percentage of inhibition of AChE/BChE was determined by comparison of rates of reaction of test samples relative to blank sample (ethanol in phosphate buffer pH = 8). IC<sub>50</sub> was calculated from the dose-response curve as a concentration at which half of the maximum extrapolated inhibition occurred. Extent of the enzymatic reaction was calculated based on the following equation:  $E = (C - T) / C \times 100$ , where  $E$  is the activity of the enzyme.  $E$  value expresses the effect of the test sample or the positive control on acetylcholinesterase and butyrylcholinesterase enzyme activity articulated as the percentage of the remaining activity in the presence of test sample or positive control.  $C$  value is the absorbance of the control solvent (blank) in the presence of enzyme, where  $T$  is the absorbance of the tested sample (plant extract or positive control in the solvent) in the presence of enzyme.

### 3.7. Statistical analysis of data

Data obtained from *in vitro* enzyme inhibition experiments were expressed as means (± S.D.) from at least three independent experiments performed in triplicate. Statistical differences between the reference and the sample groups were evaluated by ANOVA (one way). Dunnett's multiple comparison tests was used as post hoc tests.  $p < 0.05$  was considered to be significant.

### 3.8. Molecular modeling

The initial geometries of the studied compounds were built up with GaussView by using the standard parameters, which were next fully optimized at the B3LYP/6–31 G(d) level (Becke, 1993), within the density functional theory (DFT) framework. The stability of all localized structures were confirmed by performing additional vibrational calculations, e.g., all minima in the potential energy surface present real frequencies only. The DFT study was eventually completed by computing all partial atomic charges as described in the Merz-Singh-Kollman ESP protocol (Singh and Kollman, 1984; Besler et al., 1990). All DFT calculations were performed with the Gaussian 16 suite of program. (Gaussian 16).

The molecular structures for the enzymes AChE and BChE were extracted from the crystal structures of Protein Data Bank (PDB) files with codes 1EVE and 1POI. Their molecular files were prepared with Autodock Tools (Morris et al., 2009) for docking by removing water molecules, adding hydrogen atoms and Gasteiger charges, merging non-polar hydrogens and assigning AD4 atom types. Molecular docking calculations were carried out in the active site of both enzymes using default parameters in AutoDock Vina (Trott and Olson, 2009). Top pose of each compound was retained for further analysis. Graphical representations of the docking results were prepared using PyMOL (Molecular Graphics System, version 1.6, Schrödinger, LLC).

### Acknowledgements

S. Ślusarczyk received support from Polish National Center of Science postdoctoral grant FUGA (2014/12/S/NZ9/00715) under the appreciated mentoring of Prof. Dr. Anna Stochmal from IUNG Institute of Cultivation and Soil Science at Puławy, Poland. The valuable help in obtaining mass

spectra from Dr. Mariusz Kowalczyk from the same Institute is kindly acknowledged. The cultivation and analysis of experimental plants is supported by the grant for special research facility funded by the Polish Ministry of Science and Higher Education (MNiSW grant decision No. 215259/E-394/SPUB/2016/1) and Medical University grant No. ST-D.030.17.028.01. This work has been funded by a grant from the Spanish Ministry of Economy and Competitiveness (CTQ2017-87974-R). This research was partially supported by the supercomputing infrastructure of University of Tromsø (Norway), by the Plataforma Andaluza de Bioinformática of the University of Málaga (Spain). Powered@NLHPC, and the NLHPC (ECM-02). The work was partially financed from grant no POLTUR/PLANT-ALZH/5/2015 (Poland).

#### Appendix A. Supplementary data

Supplementary material related to this article can be found, in the online version, at doi:<https://doi.org/10.1016/j.phytol.2019.02.006>.

#### References

- Becke, A.D., 1993. Density-functional thermochemistry III. The role of exact exchange. *J. Chem. Phys.* 98, 5648–5652. <https://doi.org/10.1063/1.464913>.
- Besler, B.H., Merz, K.M., Kollman, P.A., 1990. Atomic charges derived from semiempirical methods. *J. Comput. Chem.* 11, 431–439. <https://doi.org/10.1002/jcc.540110404>.
- Chen, L., Teng, H., Xie, Z., Cao, H., Cheang, W.S., Skalicka-Woźniak, K., Georgiev, M.I., Xiao, J., 2018. Modifications of dietary flavonoids towards improved bioactivity: an update on structure–activity relationship. *Crit. Rev. Food Sci. Nutr.* 58, 513–527. <https://doi.org/10.1080/10408398.2016.1196334>.
- Conforti, F., Rigano, D., Menichini, F., Loizzo, M.R., Senatore, F., 2009. Protection against neurodegenerative diseases of *Iris pseudopumila* extracts and their constituents. *Fitoterapia* 80, 62–67. <https://doi.org/10.1016/j.fitote.2008.10.005>.
- Csuk, R., Albert, S., Kluge, R., Strohl, D., 2013. Resveratrol derived butyrylcholinesterase inhibitors. *Arch. Pharm. Chem. Life Sci.* 346, 499–503. <https://doi.org/10.1002/ardp.201300051>.
- Ellman, G.L., Courtney, K.D., Andres, V., Featherstone, R.M., 1961. A new and rapid colorimetric determination of acetylcholinesterase activity. *Biochem. Pharmacol.* 7, 88–95. [https://doi.org/10.1016/0006-2952\(61\)90145-9](https://doi.org/10.1016/0006-2952(61)90145-9).
- Feng, B., Li, X., Xia, J., Wu, S.J., 2017. Discovery of novel isoflavone derivatives as AChE/BuChE dual-targeted inhibitors: synthesis, biological evaluation and molecular modelling. *J. Enzyme Inhib. Med. Chem.* 32, 968–977. <https://doi.org/10.1080/14756366.2017.1347163>.
- Gómez-Zaleta, B., Ramírez-Silva, M.-T., Gutiérrez, A., González-Vergara, E., Güzado-Rodríguez, M., Rojas-Hernández, A., 2006. UV/vis, IR, and <sup>13</sup>C NMR spectroscopic studies to determine mangiferin pKa values spectrochim. *Acta A Mol. Biomol. Spectrosc.* 64 (4), 1002–1009. <https://doi.org/10.1016/j.saa.2005.09.009>.
- Jun, H., Hoang, M.H., Lee, J.W.J., Yaoyao, J.H., Lee, D.H., Lee, H.J., Lee, W.D., Seo, B.Y., Hwang, S.J., 2012. Iristectorigenin B isolated from *Belamcanda chinensis* is a liver X receptor modulator that increases ABCA1 and ABCG1 expression in macrophage RAW 264.7 cells. *Biotechnol. Lett.* 34, 2213. <https://doi.org/10.1007/s10529-012-1036-y>.
- Kaufmann, D., Dogra, A.K., Tahrani, A., Herrmann, F., Wink, M., 2016. Extracts from traditional Chinese medicinal plants inhibit acetylcholinesterase, a known Alzheimer's disease target. *Molecules* 21, 1161. <https://doi.org/10.3390/molecules21091161>.
- Kershaw, J., Kim, K.-H., 2017. The therapeutic potential of piceatannol, a natural stilbene, in metabolic diseases: a review. *J. Med. Food* 20, 427–438. <https://doi.org/10.1089/jmf.2017.3916>.
- Lee, Y.S., Kim, S.H., Kim, J.K., Lee, S., Jung, S.H., Lim, S.S., 2011. Preparative isolation and purification of seven isoflavones from *Belamcanda chinensis*. *Phytochem. Anal.* 22, 468–473. <https://doi.org/10.1002/pea.1306>.
- Li, B., Duysen, E.G., Carlson, M., Lockridge, O., 2008. The butyrylcholinesterase knockout mouse as a model for human butyrylcholinesterase deficiency. *J. Pharmacol. Exp. Ther.* 324, 1146–1154. <https://doi.org/10.1124/jpet.107.133330>.
- Lim, H.S., Kim, Y.J., Kim, B.Y., Park, G., Jeong, S.J., 2018. The anti-neuroinflammatory activity of tectorigenin pretreatment via downregulated NF-κB and ERK/JNK pathways in BV-2 microglial and microglia inactivation in mice with lipopolysaccharide. *Front. Pharmacol.* 9, 462. <https://doi.org/10.3389/fphar.2018.00462>.
- Makin, S., 2018. The amyloid hypothesis on trial. *Nature* 559, S4–S7. <https://doi.org/10.1038/d41586-018-05719-4>.
- Matkowski, A., Kuś, P., Janda, B., Oleszek, W., Woźniak, D., 2009. Isolation and antioxidant activity evaluation of mangiferin from *Belamcanda rhizoma*. *Acta Biochem. Pol.* 56 (suppl.2), 14–15 2009.
- Matkowski, A., Kus, P., Goralska, E., Woźniak, D., 2013. Mangiferin – a bioactive xanthoid, not only from Mango and not just antioxidant. *Mini Rev. Med. Chem.* 13, 439–455. <https://doi.org/10.2174/138955713804999838>.
- Mavrodiev, E.V., Martínez-Azorín, M., Dranishnikov, P., Crespo, M.B., 2014. At least 23 genera instead of one: the case of *Iris* l. s.l. (Iridaceae). *PLoS One* 9 (8), e106459. <https://doi.org/10.1371/journal.pone.0106459>.
- Mocan, A., Zengin, G., Mollica, A., Uysal, A., Gunes, E., Crişan, G., Aktumsek, A., 2018. Biological effects and chemical characterization of *Iris schachtii* markgr. Extracts: a new source of bioactive constituents. *Food Chem. Toxicol.* 112, 448–457. <https://doi.org/10.1016/j.fct.2017.08.004>.
- Monthakantirat, O., De-Eknankul, W., Umehara, K., Yoshinaga, Y., Miyase, T., Warashina, T., Noguchi, H., 2005. Phenolic constituents of the rhizomes of the Thai medicinal plant *Belamcanda chinensis* with proliferative activity for two breast cancer cell lines. *J. Nat. Prod.* 68 (3), 361–364. <https://doi.org/10.1021/np040175c>.
- Morris, G.M., Huey, R., Lindstrom, W., Sanner, M.F., Belew, R.K., Goodsell, D.S., Olson, A.J., 2009. AutoDock4 and AutoDockTools4: automated docking with selective receptor flexibility. *J. Comput. Chem.* 30, 2785–2791. <https://doi.org/10.1002/jcc.21256>.
- Nowak, B., Matuszewska, A., Szandruk, M., Matkowski, A., Woźniak, D., Zduniak, K., Rzeszutko, M., Landwójtowicz, M., Jędrzejuk, D., Piasecki, T., Kwiatkowska, J., Bolanowski, M., Szeląg, A., 2018. Effect of long-term administration of mangiferin from *Belamcanda chinensis* on bone metabolism in ovariectomized rats. *J. Funct. Food.* 46, 12–18. <https://doi.org/10.1016/j.jff.2018.04.048>.
- Orhan, I., Senol, F.S., Kartal, M., Dvorská, M., Zemlicka, M., Smejkal, K., Mokry, P., 2009. Cholinesterase inhibitory effects of the extracts and compounds of *Maclura pomifera* (Rafin.) Schneider. *Food. Chem. Toxicol.* 47, 1747–1751. <https://doi.org/10.1016/j.fct.2009.04.023>.
- Orhan, I.E., Kucukboyaci, N., Calis, I., Cerón-Carrasco, J.P., den-Haan, H., Peña-García, J., Pérez-Sánchez, H., 2017. Acetylcholinesterase inhibitory assessment of isolated constituents from *Salsola grandis* Freitag, Vural & Adıgüzel and molecular modeling studies on N-acetyltryptophan. *Phytochem. Lett.* 20, 373–378. <https://doi.org/10.1016/j.phytol.2016.10.017>.
- Orhan, I.E., Jedrejek, D., Senol, F.S., Salmas, R.E., Durdagi, S., Kowalska, I., Pecio, L., Oleszek, W., 2018. Molecular modeling and in vitro approaches towards cholinesterase inhibitory effect of some natural xanthohumol, naringenin, and acyl phloroglucinol derivatives. *Phytomedicine* 42, 25–33. <https://doi.org/10.1016/j.phymed.2018.03.009>.
- Perry, E., Howes, M.J., 2011. Medicinal plants and dementia therapy: herbal hopes for brain aging? *CNS Neurosci. Ther.* 17, 683–698. <https://doi.org/10.1111/j.1755-5949.2010.00202.x>.
- Pinho, B.R., Ferreresb, F., Valentão, P., Andrade, P.B., 2013. Nature as a source of metabolites with cholinesterase-inhibitory activity: an approach to Alzheimer's disease treatment. *J. Pharm. Pharmacol.* 65, 1681–1700. <https://doi.org/10.1111/jph.12081>.
- Politeo, O., Bektašević, M., Carev, I., Jurin, M., Roje, M., 2018. Phytochemical composition, antioxidant potential and cholinesterase inhibition potential of extracts from *Mentha pulegium* L. *Chem. Biodivers.* 15, e1800374. <https://doi.org/10.1002/cbdv.201800374>.
- Sangsen, Y., Sookawate, T., Likhitwitayawuid, K., Sritularak, B., Wiwattanapatapee, R., 2018. A self-microemulsifying formulation of oxysresveratrol prevents amyloid Beta protein-induced neurodegeneration in mice. *Planta Med.* 84, 820–828. <https://doi.org/10.1055/s-0043-125337>.
- Sawikr, Y., Yarla, N.S., Peluso, I., Kamal, M.A., Aliev, G., Bishayee, A., 2017. Neuroinflammation in Alzheimer's disease: the preventive and therapeutic potential of polyphenolic nutraceuticals. *Adv. Protein. Chem. Struct. Biol.* 108, 33–57. <https://doi.org/10.1016/bs.apcsb.2017.02.001>.
- Sermboonpaisarn, T., Sawasdee, P., 2012. Potent and selective butyrylcholinesterase inhibitors from *Ficus foveolata*. *Fitoterapia* 83, 780–784. <https://doi.org/10.1016/j.fitote.2012.03.009>.
- Singh, U.C., Kollman, P.A., 1984. An approach to computing electrostatic charges for molecules. *J. Comput. Chem.* 5, 129–145. <https://doi.org/10.1002/jcc.540050204>.
- Szandruk, M., Merwid-Łąd, A., Szeląg, A., 2018. The impact of mangiferin from *Belamcanda chinensis* on experimental colitis in rats. *Inflammopharmacology* 26, 571–581. <https://doi.org/10.1007/s10787-017-0337-0>.
- Tisserant, L.-P., Hubert, J., Lequart, M., Borie, N., Maurin, N., Pilard, S., Jeandet, P., Aziz, A., Renault, J.-H., Nuzillard, J.-M., Clément, C., Boitel-Conti, M., Courrot, E., 2016. <sup>13</sup>C NMR and LC-MS profiling of stilbenes from elicited grapevine hairy root cultures. *J. Nat. Prod.* 79 (11), 2846–2855. <https://doi.org/10.1021/acs.jnatprod.6b00608>.
- Ullah, F., Ayaz, M., Sadiq, A., Hussain, A., Ahmad, S., Imran, M., Zeb, A., 2016. Phenolic flavonoid contents, anticholinesterase and antioxidant evaluation of *Iris germanica* var. *florentina*. *Nat. Prod. Res.* 30, 1440–1444. <https://doi.org/10.1080/14786419.2015.1057585>.
- Walle, T., 2009. Methylation of dietary flavones increases their metabolic stability and chemopreventive effects. *Int. J. Mol. Sci.* 10, 5002–5019. <https://doi.org/10.3390/ijms10115002>.
- Wilson, C.A., 2011. Subgeneric classification in *Iris* re-examined using chloroplast sequence data. *Taxon* 60 (1), 27–35. <https://doi.org/10.1002/tax.601004>.
- Woźniak, D., Matkowski, A., 2015. *Belamcanda chinensis rhizoma* - a review of phytochemistry and bioactivity. *Fitoterapia* 107, 1–14. <https://doi.org/10.1016/j.fitote.2015.08.015>.
- Yan, T., Wang, T., Wei, W., Jiang, N., Qin, Y.H., Tan, R.X., Ge, H.M., 2012. Polyphenolic acetylcholinesterase inhibitors from *Hopea chinensis*. *Planta Med.* 78, 1015–1019. <https://doi.org/10.1055/s-0031-1298623>.
- Yang, H., Jin, G., Ren, D., Luo, S., Zhou, T., 2011. Mechanism of isoflavone aglycone's effect on cognitive performance of senescence-accelerated mice. *Brain Cogn.* 76, 206–210. <https://doi.org/10.1016/j.bandc.2010.10.008>.

## 2.7 Structure-based discovery of clinically approved drugs as Zika virus NS2B-NS3 protease inhibitors that potently inhibit Zika virus infection *in vitro* and *in vivo*

<b>Title</b>	<i>Structure-based discovery of clinically approved drugs as Zika virus NS2B-NS3 protease inhibitors that potently inhibit Zika virus infection in vitro and in vivo</i>
<b>Authors</b>	Shuofeng Yuan, Jasper Fuk-Woo Chan, Helena den-Haan, Kenn Ka-Heng Chik, Anna Jinxia Zhang, Chris Chung-Sing Chan, Vincent Kwok-Man Poon, Cyril Chik-Yan Yip, Winger Wing-Nga Mak, Zheng Zhu, Zijiao Zou, Kah-Meng Tee, Jian-Piao, Kwok-Hung Chan, Jorge de la Peña, Horacio Pérez-Sánchez, José Pedro Cerón-Carrasco, Kwok-Yung Yuen.
<b>Journal</b>	<i>Antiviral Research</i>
<b>Year</b>	2017
<b>State</b>	Published

### PhD candidate contribution

Helena den Haan Alonso, declares that she is the main co-author and main contributor of the bioinformatic work of the article *Structure-based discovery of clinically approved drugs as Zika virus NS2B-NS3 protease inhibitors that potently inhibit Zika virus infection in vitro and in vivo*.



Contents lists available at ScienceDirect

## Antiviral Research

journal homepage: [www.elsevier.com/locate/antiviral](http://www.elsevier.com/locate/antiviral)

## Structure-based discovery of clinically approved drugs as Zika virus NS2B-NS3 protease inhibitors that potently inhibit Zika virus infection *in vitro* and *in vivo*



Shuofeng Yuan<sup>a,1</sup>, Jasper Fuk-Woo Chan<sup>a,b,c,d,\*\*,1,2</sup>, Helena den-Haan<sup>e,f,1</sup>,  
 Kenn Ka-Heng Chik<sup>a</sup>, Anna Jinxia Zhang<sup>a</sup>, Chris Chung-Sing Chan<sup>a</sup>,  
 Vincent Kwok-Man Poon<sup>a</sup>, Cyril Chik-Yan Yip<sup>a</sup>, Winger Wing-Nga Mak<sup>a</sup>, Zheng Zhu<sup>a</sup>,  
 Zijiao Zou<sup>a</sup>, Kah-Meng Tee<sup>a</sup>, Jian-Piao Cai<sup>a</sup>, Kwok-Hung Chan<sup>a</sup>, Jorge de la Peña<sup>e</sup>,  
 Horacio Pérez-Sánchez<sup>e,\*\*\*,2</sup>, José Pedro Cerón-Carrasco<sup>e,\*\*\*\*,2</sup>,  
 Kwok-Yung Yuen<sup>a,b,c,d,g,\*,2</sup>

<sup>a</sup> Department of Microbiology, Li Ka Shing Faculty of Medicine, The University of Hong Kong, Pokfulam, Hong Kong Special Administrative Region

<sup>b</sup> State Key Laboratory of Emerging Infectious Diseases, The University of Hong Kong, Pokfulam, Hong Kong Special Administrative Region

<sup>c</sup> Research Centre of Infection and Immunology, The University of Hong Kong, Pokfulam, Hong Kong Special Administrative Region

<sup>d</sup> Carol Yu Centre for Infection, The University of Hong Kong, Pokfulam, Hong Kong Special Administrative Region

<sup>e</sup> Bioinformatics and High Performance Computing Research Group (BIO-HPC), Computer Engineering Department, Universidad Católica San Antonio de Murcia (UCAM), Spain

<sup>f</sup> Villapharma Research S.L., Parque Tecnológico de Fuente Álamo, Ctra. El Estrecho-Lobosillo, Km. 2.5, Av. Azul, Fuente Álamo de Murcia, Murcia, Spain

<sup>g</sup> The Collaborative Innovation Center for Diagnosis and Treatment of Infectious Diseases, The University of Hong Kong, Pokfulam, Hong Kong Special Administrative Region

## ARTICLE INFO

## Article history:

Received 12 March 2017

Received in revised form

1 June 2017

Accepted 11 July 2017

Available online 14 July 2017

## Keywords:

Zika

Flavivirus

Novobiocin

Protease

Treatment

Molecular modelling

## ABSTRACT

Zika virus (ZIKV) infection may be associated with severe complications in fetuses and adults, but treatment options are limited. We performed an *in silico* structure-based screening of a large chemical library to identify potential ZIKV NS2B-NS3 protease inhibitors. Clinically approved drugs belonging to different drug classes were selected among the 100 primary hit compounds with the highest predicted binding affinities to ZIKV NS2B-NS3-protease for validation studies. ZIKV NS2B-NS3 protease inhibitory activity was validated in most of the selected drugs and *in vitro* anti-ZIKV activity was identified in two of them (novobiocin and lopinavir-ritonavir). Molecular docking and molecular dynamics simulations predicted that novobiocin bound to ZIKV NS2B-NS3-protease with high stability. Dexamethasone-immunosuppressed mice with disseminated ZIKV infection and novobiocin treatment had significantly ( $P < 0.05$ ) higher survival rate (100% vs 0%), lower mean blood and tissue viral loads, and less severe histopathological changes than untreated controls. This structure-based drug discovery platform should facilitate the identification of additional enzyme inhibitors of ZIKV.

© 2017 Elsevier B.V. All rights reserved.

\* Corresponding author. State Key Laboratory of Emerging Infectious Diseases, Carol Yu Centre for Infection, Department of Microbiology, Li Ka Shing Faculty of Medicine, The University of Hong Kong, Queen Mary Hospital, 102 Pokfulam Road, Pokfulam, Hong Kong Special Administrative Region.

\*\* Corresponding author. State Key Laboratory of Emerging Infectious Diseases, Carol Yu Centre for Infection, Department of Microbiology, Li Ka Shing Faculty of Medicine, The University of Hong Kong, Queen Mary Hospital, 102 Pokfulam Road, Pokfulam, Hong Kong Special Administrative Region.

\*\*\* Corresponding author. Bioinformatics and High Performance Computing Research Group (BIO-HPC), Computer Engineering Department, Universidad Católica San Antonio de Murcia (UCAM), Spain.

\*\*\*\* Corresponding author. Bioinformatics and High Performance Computing Research Group (BIO-HPC), Computer Engineering Department, Universidad Católica San Antonio de Murcia (UCAM), Spain.

E-mail addresses: [jfwchan@hku.hk](mailto:jfwchan@hku.hk) (J.F.-W. Chan), [hperez@ucam.edu](mailto:hperez@ucam.edu) (H. Pérez-Sánchez), [jpceron@ucam.edu](mailto:jpceron@ucam.edu) (J.P. Cerón-Carrasco), [kyyuen@hku.hk](mailto:kyyuen@hku.hk) (K.-Y. Yuen).

<sup>1</sup> These authors contributed equally to the study as co-first authors.

<sup>2</sup> These authors contributed equally to the study as co-corresponding authors.

<http://dx.doi.org/10.1016/j.antiviral.2017.07.007>

0166-3542/© 2017 Elsevier B.V. All rights reserved.



## 1. Introduction

Zika virus is an emerging human-pathogenic flavivirus that has caused an unprecedented large-scale epidemic of congenital microcephaly and malformations in the Americas (Chan et al., 2017a; Zhu et al., 2016). Initially thought to be a completely self-limiting illness in infected adults, an increasing number of serious complications were recently reported among adult patients as the epidemic expanded in the Americas and other regions (Duffy et al., 2009; Musso and Gubler, 2016). These included severe neurological complications, such as Guillain-Barré syndrome, meningoencephalitis, and myelitis, thrombocytopenia and disseminated intravascular coagulation with hemorrhagic complications, hepatic dysfunction, acute respiratory distress syndrome, shock, multi-organ dysfunction syndrome, and death (Arzuza-Ortega et al., 2016; Azevedo et al., 2016; Cao-Lormeau et al., 2016; Carteaux et al., 2016; Chraïbi et al., 2016; Mecharles et al., 2016; Sarmiento-Ospina et al., 2016; Soares et al., 2016). Alarming, human cases of hematospermia and mouse models of orchitis with possible long-term effects on male fertility were also described (Chan et al., 2016c; Foy et al., 2011; Govero et al., 2016; Ma et al., 2016; Musso et al., 2015). Currently, treatment options for ZIKV infection in pregnant patients and severe ZIKV-associated complications remain limited.

To identify immediately available anti-ZIKV treatment options, a number of drug repurposing programmes have been conducted by screening drug libraries using cell culture-based antiviral assays (Barrows et al., 2016; Retallack et al., 2016; Xu et al., 2016). However, most of these clinically approved drugs found to have *in vitro* anti-ZIKV activity are anti-cancer or immunomodulating agents which are immunosuppressive or contraindicated in pregnancy (FDA pregnancy category D). Moreover, such screening approach does not elucidate the anti-ZIKV mechanisms of these drugs which are important for further development of safer and more effective drug analogues than the lead drug compound. An alternative approach to discover other potential anti-ZIKV treatment options is by repurposing clinically approved drugs which inhibit the key enzymes of ZIKV, including protease, helicase, and/or polymerase. In this study, we performed an *in silico* structure-based virtual screening of a large chemical library consisting >8000 drug compounds to identify potential ZIKV NS2B-NS3 protease inhibitors. Among the validated ZIKV NS2B-NS3 protease inhibitors, novobiocin and lopinavir-ritonavir were verified to inhibit virus replication *in vitro*. Importantly, treatment with novobiocin significantly improved the clinical outcome of mice with disseminated ZIKV infection. These results illustrated the capability of our systematic *in silico*, *in vitro*, and *in vivo* approach to expand the treatment options for ZIKV infection. Our findings provided a new avenue for the development of novel anti-ZIKV agents.

## 2. Materials and methods

### 2.1. *In silico* structure-based virtual screening of chemical library and molecular docking

All compounds deposited in the DrugBank v5.0.1 were set up for docking simulations by using AmberTools (AMBER 2017; University of California, San Francisco) (Case et al., 2017). The crystal structure of ZIKV NS2B-NS3 protease (Protein Data Bank (PDB) code 5LCO) was used to build up the protein model system (Lei et al., 2016). Other details of virtual screening calculations are specified in the Supplementary Methods.

### 2.2. Molecular dynamics simulations

Molecular dynamics simulations were conducted to predict the stability of the novobiocin-ZIKV NS2B-NS3 complex. Protocols are fully outlined in the Supplementary Methods.

### 2.3. Virus strain and titration

A clinical isolate of ZIKV (Puerto Rico strain PRVABC59) obtained from a patient in the recent South American epidemic was kindly provided by Brandy Russell and Barbara Johnson, Centers for Disease Control and Prevention, USA. The virus was cultured and titrated as we previously described with slight modifications (Chan et al., 2016b; Zhou et al., 2014) (Supplementary methods).

### 2.4. Cell lines and drug compounds

Vero and Huh-7 cell lines were obtained from American Type Culture Collection and JCRB cell bank of Okayama University, Japan, respectively, as we previously described (Chan et al., 2013a, 2016b). Aprotinin (Sigma-Aldrich, Missouri, USA), desmopressin acetate (Ferring Pharmaceuticals, Saint Prex, Switzerland), lopinavir-ritonavir (Abbott Laboratories, Illinois, USA), montelukast (Merck & Co., Inc., New Jersey, USA), novobiocin sodium (Sigma-Aldrich Chemie GmbH, Steinheim, Germany), octreotide acetate (Novartis, Basel, Switzerland), rifampicin (Gruppo Lepetit Srl, Milan, Italy), sirolimus (Pfizer, New York city, USA), tacrolimus (Astellas Pharma, Tokyo, Japan) were used for the *in vitro* and/or *in vivo* studies.

### 2.5. Cell viability assay and CPE inhibition assay

The 50% effective cytotoxic concentration (CC<sub>50</sub>) of the selected drugs in Vero and Huh-7 cells were determined by thiazolyl blue tetrazolium bromide (MTT) assay as we previously described with modifications (Chan et al., 2017a; Yuan et al., 2016). To confirm the antiviral activity of novobiocin, the MTT-based CPE inhibition assay was also performed as previously described with slight modifications (Chan et al., 2017a). The half maximal inhibitory concentration (IC<sub>50</sub>) and CC<sub>50</sub> were calculated using Sigma plot (SPSS) in an Excel add-in ED50V10. Other details are described in the Supplementary Methods.

### 2.6. Viral load reduction and plaque reduction assays

Viral load reduction assay and plaque reduction assay was performed for the evaluation of antiviral activity. Experimental protocols are specified in supplementary methods as previously described with modifications (Chan et al., 2013b, 2016b, 2017a, 2017b). Both assays were performed in triplicate and repeated twice for confirmation.

### 2.7. Time-of-drug-addition assay

Time-of-drug-addition assay was performed for novobiocin to determine which phase(s) of virus cycle the drug interfered with (Chan et al., 2017a; Kato et al., 2016). Details are described in the Supplementary Methods.

### 2.8. Fluorescence-based protease inhibition assay

The recombinant ZIKV NS2B-NS3 protease was produced as previously described with some modifications (Lei et al., 2016). Experimental conditions are described in supplementary methods. To detect ZIKV NS2B-NS3 protease activity, a fluorescence-based enzymatic assay was conducted in 96-well black micro-plates

(Greiner Bio-One, Kremsmünster, Germany). A 7-amino-4-methylcoumarine substrate, Bz-Nle-Lys-Lys-Arg-AMC, was used (Lei et al., 2016). To detect if each drug inhibited ZIKV NS2B-NS3 protease activity, 5 nM ZIKV NS2B-NS3 protease and 10  $\mu$ M substrate was fixed in the assay. The assay protocol was optimized according our recent report (Chan et al., 2017a). Other details are outlined in the Supplementary Methods.

### 2.9. Mouse model and in vivo evaluation of novobiocin treatment

The *in vivo* treatment effect of novobiocin was evaluated in our recently established animal model for ZIKV infection using dexamethasone-immunosuppressed mice with disseminated ZIKV infection (Chan et al., 2016c). Approval was obtained from the Committee on the Use of Live Animals in Teaching and Research of The University of Hong Kong. Experimental design and other details are described in Table S1 and Supplementary Methods, respectively.

### 2.10. Statistical analyses

All statistical analyses were performed with GraphPad Prism software (GraphPad Software, Inc). Kaplan-Meier survival curves were analyzed by the log-rank test. Student's t-test was used to determine significant differences in weight losses and virus titers among individual treatment groups as previously reported (Chan et al., 2016c). *P*-values <0.05 were considered statistically significant.

## 3. Results

### 3.1. Identification of primary hit compounds in *in silico* structure-based virtual screening

To identify potential inhibitors of ZIKV NS2B-NS3 protease, a total of 8227 entries from the DrugBank database were screened using Lead Finder software (Stroganov et al., 2008), in which the ZIKV NS2B-NS3 protease crystal structure was utilized as inputs to the program (Lei et al., 2016) (Fig. 1). The top 100 primary hit compounds were ranked by their predicted binding affinities to the ZIKV NS2B-NS3 protease (Table S2).

### 3.2. Validation of ZIKV NS2B-NS3 protease inhibition by primary hit compounds belonging to different drug classes

To verify whether the primary hit compounds inhibited ZIKV NS2B-NS3 protease activity, we selected 8 clinically approved drugs that belonged to different drug classes (i.e. desmopressin acetate, lopinavir-ritonavir, montelukast, novobiocin, octreotide acetate, rifampicin, sirolimus, and tacrolimus) for further evaluation. Lopinavir-ritonavir instead of ritonavir was used for further evaluation because lopinavir-ritonavir is the commercially available preparation that is more commonly used clinically. Other drug compounds were not selected because most of them were not clinically approved drugs, did not have well-known pharmacokinetic and pharmacodynamic properties, and/or belonged to the same drug classes as these 8 drugs. We performed a fluorescence-based protease inhibition assay that recorded fluorescence signals in the presence or absence of the drugs. To detect the enzymatic activity of the purified ZIKV NS2B-NS3 protein, we first used four concentrations of the protease substrate (0.1  $\mu$ M, 1  $\mu$ M, 10  $\mu$ M, and 100  $\mu$ M) for comparison and observed a dose-dependent increase of fluorescence intensity upon protein addition to the substrate (Fig. 2A). Cleavage of the peptide substrate released fluorescence signals, which reached a plateau when 50 nM protein was added.

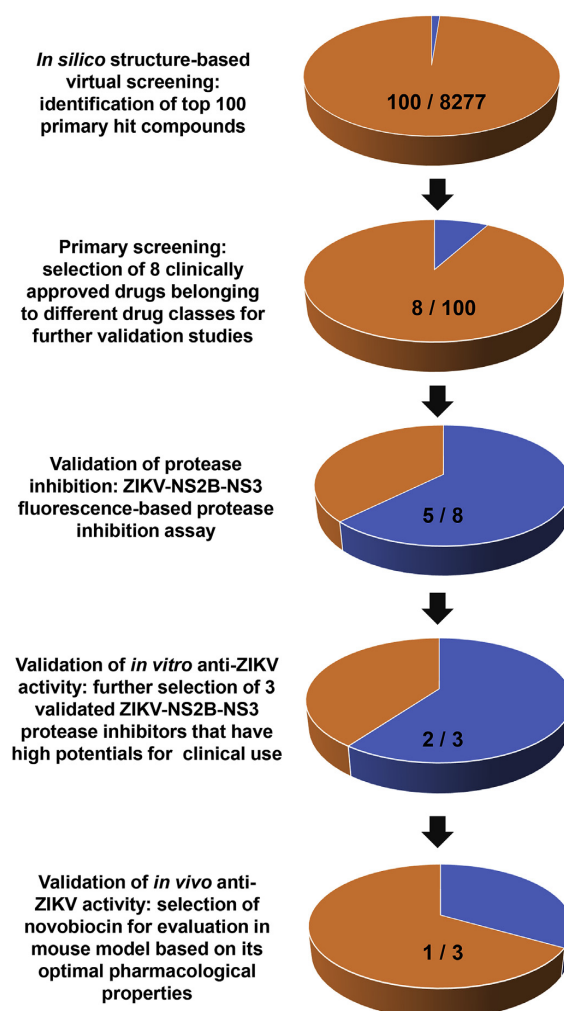


**Fig. 1.** Screening pipeline. *In silico* virtual screening of a chemical library with 8277 drug compounds was performed. Among the top 100 primary hit compounds with the highest predicted binding affinities with ZIKV NS2B-NS3 protease, 8 clinically approved drugs belonging to different drug classes were selected for validation of anti-ZIKV NS2B-NS3 protease activity. Other drug compounds were not selected because most of them were not clinically approved drugs, did not have well-known pharmacokinetic and pharmacodynamic properties, and/or belonged to the same drug classes as these 8 drugs (see also Table S2). Among them, 5 (62.5%) were demonstrated to have anti-ZIKV NS2B-NS3 protease activity in a fluorescence-based enzymatic assay. Three of these 5 drugs which have high potentials for clinical use in pregnancy and/or patients with severe ZIKV-associated complications were then selected for further evaluation. The anti-ZIKV activity of these 3 drugs (novobiocin, lopinavir-ritonavir, and rifampicin) were then evaluated by viral load reduction, cytopathic effect inhibition, and/or plaque reduction assays. Novobiocin and lopinavir-ritonavir demonstrated anti-ZIKV activity in viral load reduction assay. Based on its higher selectivity index than lopinavir-ritonavir, novobiocin was then selected for further evaluation in a mouse model.

Compared to the baseline control, as much as 25-fold increase in fluorescence intensity was detected with input of 10  $\mu$ M and 100  $\mu$ M substrate. These results suggested that the purified ZIKV NS2B-NS3 protein maintained protease activity. To detect the inhibitory effect of the drugs on ZIKV NS2B-NS3 protease activity,

36

S. Yuan et al. / Antiviral Research 145 (2017) 33–43

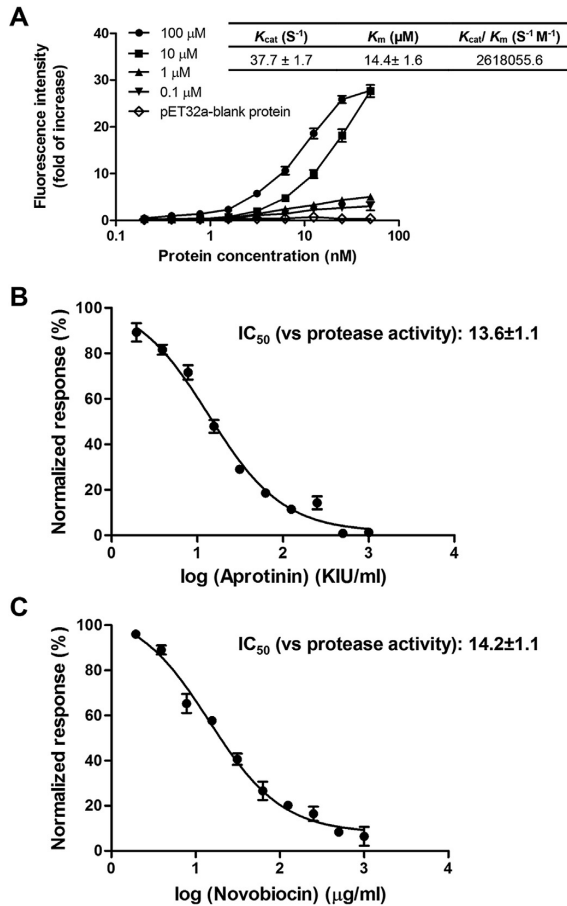


**Fig. 2.** Novobiocin inhibited protease activity of ZIKV NS2B-NS3. (A) ZIKV NS2B-NS3 protein dose-dependent of fluorescence intensity are shown, indicating the cleavage of the fluorescent substrate (Bz-Nle-Lys-Lys-Arg-AMC) by the protein. Four concentrations of the substrate (100  $\mu M$ , 10  $\mu M$ , 1  $\mu M$ , and 0.1  $\mu M$ ) were tested for the purpose of assay optimization. A pET32a (+)-blank protein (Fig. S5), incubated with 100  $\mu M$  substrate, was included as a mock-purified enzyme control. Results are shown as the number of fold changes of fluorescence intensity after ZIKV NS2B-NS3 protein was added as compared to baseline level. Kinetic parameters were analyzed and plotted using Michaelis-Menten equation with GraphPad Prism version 6 (GraphPad Software, San Diego California USA). (B) and (C) Increasing concentrations of aprotinin (positive control) and novobiocin blocked the protease cleavage activity as measured by the decrease in fluorescence intensity values. The concentrations of substrate and ZIKV NS2B-NS3 protease were fixed as 10  $\mu M$  and 5 nM, respectively. The experiments were carried out in triplicate and repeated twice for confirmation. Data are presented as mean values  $\pm$  standard error of the mean (error bars). IC<sub>50</sub>, half maximal inhibitory concentration (concentration of the drug at which there was 50% reduction in protease activity).

we measured fluorescence signals in the presence of a range of different concentrations of the drugs, using aprotinin as a positive control (Phoo et al., 2016). As shown in Fig. 2B, aprotinin inhibited ZIKV NS2B-NS3 protease activity in a dose-dependent manner, with an apparent IC<sub>50</sub> of 13.6  $\pm$  1.1 KIU/ml. This result validated the specificity of our protease inhibition assay. At the fixed concentration of 10  $\mu M$  substrate and 5 nM ZIKV NS2B-NS3 protease, we observed a dose-dependent reduction in protease activity with increasing concentrations of 5 of the 8 (62.5%) drugs, including novobiocin (Fig. 2C), desmopressin acetate, octreotide acetate,

lopinavir-ritonavir, and rifampicin (Figs. S1A–H). Our results confirmed that these drugs inhibited ZIKV NS2B-NS3 protease activity and that the *in silico* virtual screening was useful in predicting potential ZIKV NS2B-NS3 protease inhibitors.

### 3.3. Validation of the *in vitro* anti-ZIKV activity of selected ZIKV NS2B-NS3 protease inhibitors

Among the validated ZIKV NS2B-NS3 protease inhibitors, we further selected 3 clinically approved drugs with good side effect profiles that could potentially be used in pregnant patients and/or patients with severe ZIKV-associated complications (novobiocin, lopinavir-ritonavir, and rifampicin) for *in vitro* anti-ZIKV activity testing. Cytotoxicity and antiviral potency of the drugs were evaluated in two different cell lines (Vero and Huh-7 cells) that could robustly support ZIKV replication (Chan et al., 2016b). The 50% effective cytotoxic concentrations (CC<sub>50</sub>) of novobiocin, lopinavir-ritonavir, and rifampicin in Vero cells were 850.50  $\mu g/ml$  (1388.02  $\mu M$ ), 30.00  $\mu g/ml$ , and 400.00  $\mu g/ml$  (486.00  $\mu M$ ), respectively, while in Huh-7 cells, 1103.18  $\mu g/ml$  (1800.39  $\mu M$ ), 32.12  $\mu g/ml$ , and 400.00  $\mu g/ml$  (486.00  $\mu M$ ), respectively. In the viral load reduction assay, dose-dependent reduction in virus titer was observed in novobiocin-treated (half maximal inhibitory concentration (IC<sub>50</sub>) = 26.12  $\pm$  0.33  $\mu g/ml$  or 42.63  $\mu M$  in Vero cells and 38.14  $\pm$  4.53  $\mu g/ml$  or 62.24  $\mu M$  in Huh-7 cells) and lopinavir-ritonavir-treated (IC<sub>50</sub> = 4.78  $\pm$  0.41  $\mu g/ml$  in Vero cells and 3.31  $\pm$  0.36  $\mu g/ml$  in Huh-7 cells) (Figs. 3A, B, S2A, and S2B), but not rifampicin-treated culture supernatants (data not shown). The mean virus titer was significantly reduced ( $P < 0.05$ ) at  $\geq 25.00$   $\mu g/ml$  (40.80  $\mu M$ ) of novobiocin and at  $\geq 50.00$   $\mu g/ml$  of lopinavir-ritonavir. The apparent lack of potent antiviral activity of lopinavir-ritonavir against ZIKV in our previous study was likely related to the lower drug concentrations used (Chan et al., 2017a). Given the higher selectivity index (CC<sub>50</sub>/IC<sub>50</sub>) of novobiocin (28.92–32.56) than lopinavir-ritonavir (6.28–9.70), we further validated the anti-ZIKV activity of novobiocin in cytopathic effect (CPE) inhibition and plaque reduction assays. In the CPE inhibition assay, novobiocin protected Vero cells from developing ZIKV-induced CPE (IC<sub>50</sub> = 53.26  $\pm$  2.48  $\mu g/ml$  or 86.92  $\mu M$ ). In the plaque reduction assay, novobiocin achieved 100% plaque reduction at concentrations  $\geq 50.00$   $\mu g/ml$  (81.60  $\mu M$ ) (IC<sub>50</sub> = 15.21  $\pm$  0.14  $\mu g/ml$  or 24.82  $\mu M$ ) (Fig. 3C).

### 3.4. Novobiocin was predicted to interact with the key enzymatic sites of ZIKV NS2B-NS3 protease

To better characterize the structural interactions between novobiocin and ZIKV NS2B-NS3 protease, molecular docking was performed to predict the binding site of novobiocin within the ZIKV NS2B-NS3 protein (Fig. 4A–C). As shown in Fig. 4B, three hydrogen bonds were formed between the ligand and the protein through residues MET51\* (\*denotes ZIKV NS2B residues), SER81\*, and LYS54, and broad areas of hydrophobic stabilization were formed between the compound and residues HIS51 and VAL155 (Fig. 4B and C). Interestingly, two of these predicted interacting residues (SER81\* and HIS51) were also identified as contacting residues between the boronate inhibitor cn-716 and the ZIKV NS2B-NS3 protease in another report (Lei et al., 2016). These results suggested that novobiocin, like the protease inhibitor cn-716, might also impair the ZIKV NS2B-NS3 catalytic efficiency. To explore the mode of protease inhibition, enzyme kinetic experiments were performed in the presence or absence of the drug. As shown in Fig. 4D, novobiocin appeared as a competitive ZIKV NS2B-NS3 protease inhibitor (global  $R^2 = 0.99$ ). Molecular dynamics simulations provided additional insights into the stability of the

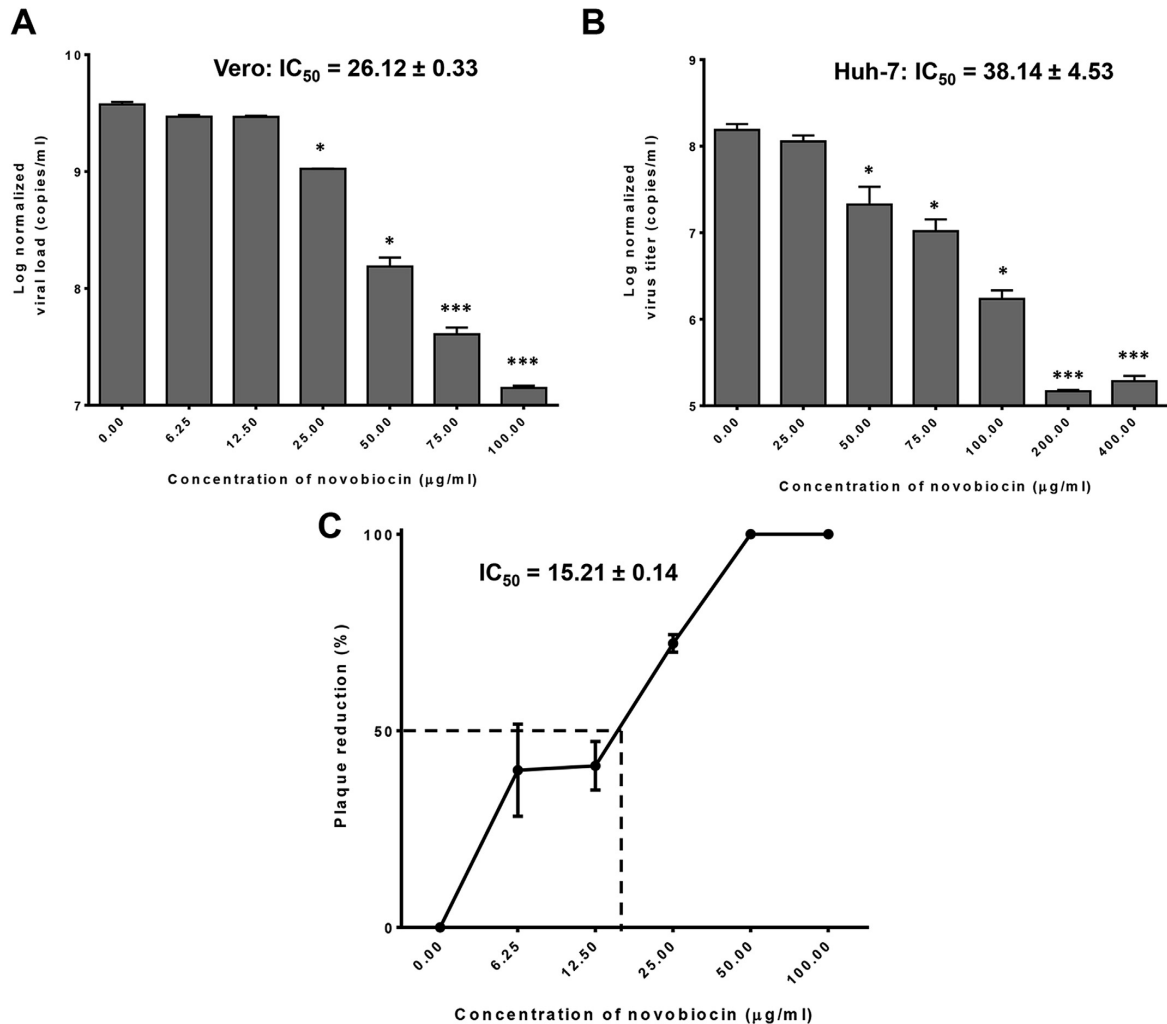


**Fig. 3.** Evaluation of the *in vitro* anti-ZIKV activity of novobiocin. (A) ZIKV viral load reduction quantified by quantitative reverse transcription-polymerase chain reaction (qRT-PCR) in Vero cells at 48 h after ZIKV inoculation (0.05 MOI) with novobiocin. (B) ZIKV viral load reduction quantified by qRT-PCR in Huh-7 cells at 48 h after ZIKV inoculation (0.05 MOI) with novobiocin. (C) Half maximal inhibitory concentration ( $IC_{50}$ ) of novobiocin as determined by plaque reduction assay. All experiments were performed in triplicates and repeated twice for confirmation. \* denotes  $P < 0.05$  and \*\*\* denotes  $P < 0.0001$  (compared to the DMSO control group by Student's *t*-test). Data are presented as mean values  $\pm$  standard error of the mean (error bars).

novobiocin-ZIKV NS2B-NS3 complex and showed that the geometrical fluctuations associated with the drug-protein binding were quickly stabilized (Figs. S3A and S3B). Overall, these findings suggested that the binding of novobiocin to its binding pocket at ZIKV NS2B-NS3 was highly stable and that the drug potentially inhibited ZIKV NS2B-NS3 protease activity by diminishing its catalytic efficiency.

### 3.5. Novobiocin inhibited the post-entry events of ZIKV replication cycle

To investigate the phase of ZIKV replication cycle interrupted by novobiocin, we performed a time-of-drug-addition assay by exposing ZIKV-infected cells to novobiocin at different timepoints during the virus replication cycle, followed by measurement of

virus titers at 18 h post-inoculation (hpi). Vero cells were infected by 2 multiplicity of infection (MOI) of ZIKV, when novobiocin was added during the virus replication stage (0,3,6,9, or 12hpi), viral loads were significantly reduced ( $P < 0.05$ ) within 12 h (Fig. S4). No significant inhibitory activity was observed when novobiocin was added at the virus adsorption stage (0-1hpi) or at the release stage (14hpi). ZIKV attachment was also not affected when the Vero cells were pretreated by novobiocin (-1 to 0hpi). As the duration of a single ZIKV life cycle has been previously determined to be around 12–14 h, in which the onset of intracellular viral RNA production occurs at ~10-12hpi, and progeny virions are assembled and released after 12hpi (Zmurko et al., 2016; Chan et al., 2017a), our time-of-drug-addition results indicated that novobiocin interfered with post-entry events during the ZIKV replication cycle within stages after virus internalization and prior to budding, which was

38

S. Yuan et al. / Antiviral Research 145 (2017) 33–43

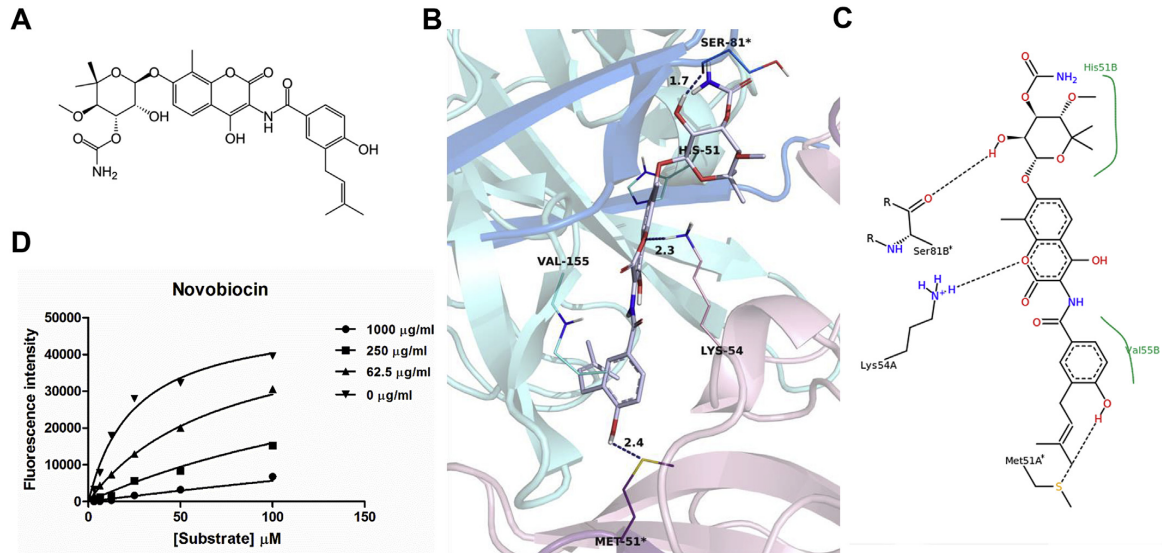


**Fig. 4.** Molecular model of novobiocin docked with ZIKV NS2B-NS3. (A) Chemical structure of novobiocin. (B) Ribbon-and-stick representation showing the predicted interacting amino acid residues between novobiocin and ZIKV NS2B-NS3 using the crystal structure of ZIKV NS2B-NS3 protease (PDB ID:5LCO). Novobiocin is represented by sticks where the carbon skeleton is displayed with light grey color, oxygen atoms in red color, nitrogen atoms in blue color, and polar hydrogen atoms in white color. ZIKV NS2B-NS3 is represented by ribbons, with blue ribbons for monomer A and purple ribbons for monomer B. Established hydrogen bonds between the ligand and the protein are depicted with deep blue dashed lines with bond length shown in Å. Main interacting residues are represented by lines and labeled. Interacting residues from NS2B are marked by \*. (C) Two-dimensional representation of the protein-ligand interactions between novobiocin and ZIKV NS2B-NS3. Hydrogen bonds and hydrophobic contact areas are represented by black dashed lines and green lines, respectively. The main interacting residues are labeled. The dashed lines represent bonds between hydrogen and acceptor atoms that are involved. The 3D and 2D figures were generated in PyMol (The PyMOL Molecular Graphics Syst, Version 1.8 Schrödinger, LLC) and PoseView (Stierand and Rarey, 2010), respectively. (D) Novobiocin exhibited a competitive mode of protease inhibition. In the assay, concentration of ZIKV NS2B-NS3 protease was fixed as 5 nM, while different concentrations of substrate (100, 50, 25, 12.5, 6.25, 3.125 and 0  $\mu$ M) were added to plot the enzyme kinetic curves. Four concentrations of the drug (1000, 250, 62.5 and 0  $\mu$ g/ml) were tested individually against the different concentrations of substrate. The experiments were repeated twice for confirmation. The data were analyzed for mode of inhibition by GraphPad Prism 6 in the module of enzyme kinetics.  $R^2 > 0.95$  was considered as statistically significant. (For interpretation of the references to colour in this figure legend, the reader is referred to the web version of this article.)

compatible with its hypothesized role as a ZIKV NS2B-NS3 protease inhibitor.

### 3.6. Treatment with novobiocin improved clinical outcome of dexamethasone-immunosuppressed mice with disseminated ZIKV infection

Extending from the *in silico* and *in vitro* findings, we further evaluated the *in vivo* therapeutic effects of novobiocin in our recently established animal model of dexamethasone-immunosuppressed mice with disseminated ZIKV infection (Chan et al., 2016c). We treated the dexamethasone-immunosuppressed mice with subcutaneous novobiocin 100 mg/kg q12h from 1 to 13 day-post-infection (dpi) as they tolerated this dosage well without developing clinical symptoms and had weight loss of <5% (Fig. 5A). Higher dosages (150 mg/kg q12h or 200 mg/kg q12h) of novobiocin led to the development of lethargy, poor feeding, and body weight loss of >10% among the mice after 6–8 days of treatment and were therefore not used in our *in vivo* treatment study. Consistent with our previous findings, the control mice with dexamethasone-immunosuppression and ZIKV inoculation developed  $\geq 10\%$  body weight loss with high clinical scores soon after dexamethasone withdrawal (10dpi), which warranted euthanasia of all the mice at 12dpi (Fig. 5A–C). Immunohistochemical (5dpi) and hematoxylin and eosin (H&E) (12dpi) staining of the major organ tissues of these mice showed abundant ZIKV NS1 antigen expression (Fig. 6A, D and G) and marked inflammatory infiltrates (Fig. 7A, D and G), respectively. In contrast, all the novobiocin-treated, dexamethasone-

immunosuppressed mice with ZIKV inoculation survived and developed  $\leq 8\%$  weight loss with minimal clinical symptoms after dexamethasone withdrawal which gradually recovered at 13–14dpi (survival, 100% novobiocin-treated mice vs 0% untreated control mice,  $P < 0.05$ ). Corroborating with the clinical parameters, ZIKV NS1 antigen expression was rarely detected by immunohistochemical staining in the organs (5dpi) (Fig. 6B, E and H) and minimal inflammatory infiltrates were seen in H&E-stained tissues (12dpi) (Fig. 7B, E and H) of these novobiocin-treated mice. The absence of ZIKV NS1 antigen expression in immunohistochemical staining (Fig. 6C, F and I) and inflammatory infiltrates in H&E staining (Fig. 7C, F and I) in the organ tissues of the mock-infected control mice with dexamethasone immunosuppression and novobiocin treatment indicated that these changes were not due to drug-induced effects. The mean viral loads of the blood and most major organ tissues of the novobiocin-treated mice were significantly lower than those of the untreated control mice (with  $\geq 2$ -log reduction) at both 5dpi and 14dpi (Fig. 8A and B).

## 4. Discussion

Our recent report on the identification of bromocriptine as an anti-ZIKV inhibitor validated ZIKV NS2B-NS3 protease as a drug-gable target for the development of Zika therapeutics (Chan et al., 2017a). In this study, we adopted an *in silico* structure-based approach to rapidly screen a large chemical library and successfully identified numerous other clinically approved drugs with inhibitory activity on the ZIKV NS2B-NS3 protease. We further

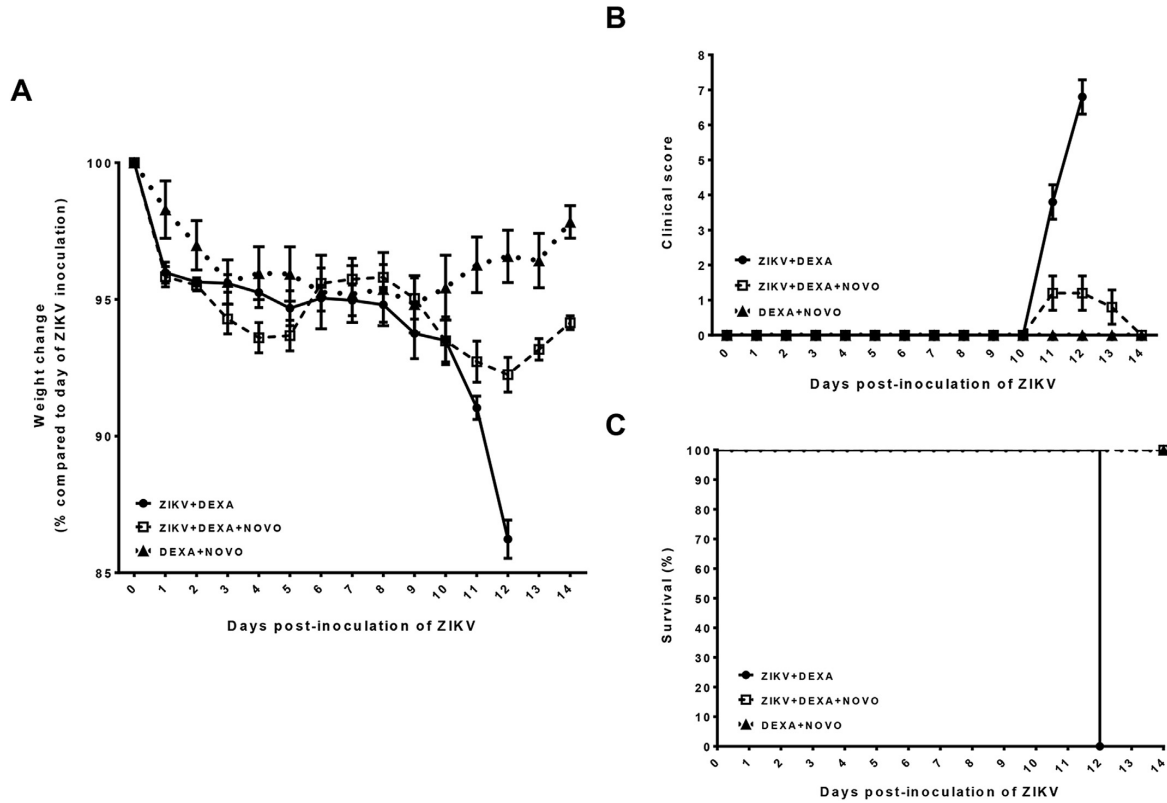


**Fig. 5.** Comparison of the clinical findings of the dexamethasone-immunosuppressed and ZIKV-infected BALB/c mice with and without novobiocin treatment. (A) Body weights, (B) clinical scores, and (C) survival times and rates. Body weights of the mice were monitored for 14 days (survival mice) or until euthanasia. The mice were treated with novobiocin 100 mg/kg every 12 h subcutaneously at 1dpi to 13dpi inclusively (see also Table S1).  $n = 8$  for each group. Results were combined from two independent experiments. Clinical scores: normal = 0; ruffled fur = 2; lethargy, pinched, hunched, wasp waisted = 3; labored breathing, rapid breathing, inactive, neurological = 5; and immobile = 10. Abbreviations: DEXA, dexamethasone; NOVO, novobiocin; ZIKV, Zika virus.

validated the anti-ZIKV activity of novobiocin in multiple *in vitro* antiviral assays and in an immunodeficient mouse model. Novobiocin, also known as albamycin or cathomycin, is an aminocoumarin antibiotic that exerts its antibacterial effects (mainly against *Staphylococcus* sp.) by targeting the GyrB subunit of bacterial DNA gyrase to competitively inhibit the adenosine triphosphatase reaction catalyzed by GyrB (Kirby et al., 1956; Flatman et al., 2006). The inhibitory activity of novobiocin on the replication of various DNA viruses, including herpesviruses (herpes simplex virus, cytomegalovirus, Epstein-Barr virus, Kaposi sarcoma-associated herpes virus, and vaccinia virus), simian virus 40, and duck hepatitis B virus, have been previously described (Civitico et al., 1990; Droge et al., 1985; Furlini et al., 1983; Gonzalez-Molleda et al., 2012; Pessina et al., 1992; Sekiguchi and Shuman, 1997; Wu et al., 2014). The proposed antiviral mechanism of novobiocin against these DNA viruses is via blockade of host topoisomerases to inhibit viral replication and assembly (Sekiguchi and Shuman, 1997; Wu et al., 2014). Our findings described a novel mechanism by which novobiocin inhibited the replication of an RNA virus belonging to *Flaviviridae*.

Molecular docking and molecular dynamics simulations indicated that the binding between novobiocin and ZIKV NS2B-NS3 was highly stable. We employed the deposited structure with

PDB code 5LC0, which is the ZIKV protease dimer, in our *in silico* analysis. The dimerization is mediated by a set of polar contacts from both NS2B cofactor and NS3 and may be further driven by the membrane association of the polyprotein in the *in vivo* membrane-rich environment where the effective local concentration of the replicative enzyme is very high (Lei et al., 2016; Phoo et al., 2016). The HIS51 residue predicted to be interacting with novobiocin is a conserved catalysis residue of ZIKV NS2B-NS3 protease activity (Phoo et al., 2016). These results suggested that novobiocin may provide cross-protection against different ZIKV subtypes/strains. The functional fluorescence-based protease inhibition assay confirmed that novobiocin inhibited ZIKV NS2B-NS3 protease activity. The ZIKV NS2B-NS3 protease is an attractive antiviral target because it plays a pivotal role in processing the viral polyprotein to generate structural and non-structural viral proteins during viral replication (Lei et al., 2016).

The treatment efficacy of novobiocin for ZIKV infection was also evaluated in our recently established mouse model (Chan et al., 2016c). In contrast to the untreated control mice which developed disseminated ZIKV infection with abundant ZIKV NS1 antigen expression in organ tissues collected at 5dpi and clinical deterioration with multiorgan inflammation soon after dexamethasone withdrawal at 10dpi warranting euthanasia at 12dpi, novobiocin-

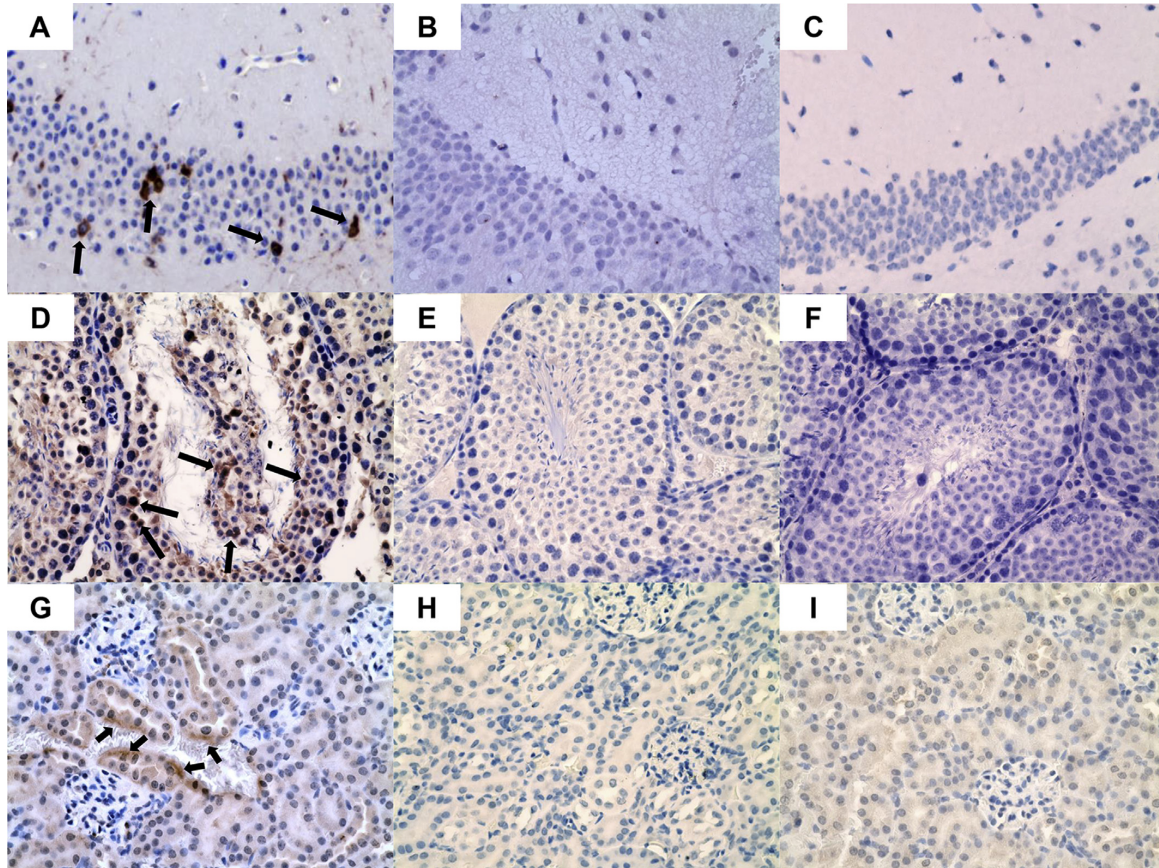


**Fig. 6.** Representative immunohistochemistry findings in different groups of mice in this study. Representative immunohistochemistry findings at 5 days post-ZIKV inoculation in the brain (top row: A, B, C), testis (middle row: D, E, F), and kidney (bottom row: G, H, I) (original magnification  $\times 400$ ) of dexamethasone-immunosuppressed BALB/c mice with ZIKV inoculation but without novobiocin treatment (left column: A, D, G), dexamethasone-immunosuppressed BALB/c mice with ZIKV inoculation and novobiocin treatment (middle column: B, E, H), and dexamethasone-immunosuppressed BALB/c mice with mock infection and novobiocin treatment (right column: C, F, I). Arrows indicate cells with ZIKV NS1 protein expression stained in brown by 3,3'-diaminobenzidine (DAB) in the organ tissue sections. (For interpretation of the references to colour in this figure legend, the reader is referred to the web version of this article.)

treated mice had minimal ZIKV NS1 antigen expression in their organ tissues collected at 5dpi and little inflammatory infiltrate upon dexamethasone withdrawal at 12dpi. There were significantly reduced mean viral loads in the blood and the major organ tissues, including the testis and kidney which are important in the transmission of ZIKV, during both early (5dpi) and late (14dpi) stages of infection. Although novobiocin's penetration into the central nervous system through non-inflamed meninges may be limited, the early control of viremia and penetration of the drug through possibly inflamed meninges likely contributed to the improved clinical outcome of the novobiocin-treated mice.

Novobiocin was withdrawn from sale in the United States in 2011 because it was no longer considered an effective antibacterial agent, as numerous other newer anti-staphylococcal antibiotics became available. Nevertheless, treatment with novobiocin is generally well tolerated clinically and may be considered in pregnant women if the potential benefits outweigh the side effects (FDA pregnancy category C) (Kirby et al., 1956). A few other clinically approved drugs that are non-immunosuppressive and belong to

FDA pregnancy categories B or C have also recently been reported to have *in vitro* anti-ZIKV effects. These included azithromycin, chloroquine, daptomycin, ivermectin, mefloquine, niclosamide, and sofosbuvir (Barrows et al., 2016; Bullard-Feibelman et al., 2016; Delvecchio et al., 2016; Retallack et al., 2016; Xu et al., 2016). However, except for sofosbuvir, none of these has been proven to be effective in animal models (Bullard-Feibelman et al., 2016). Importantly, most of these drugs have  $IC_{50}$  values that are not achievable by routine oral therapeutic dosages. The  $C_{max}:IC_{50}$  ratio achievable with routine therapeutic dosage of oral novobiocin (1.17–4.11) is markedly higher than those of oral mefloquine (0.58), oral ivermectin (0.30), oral azithromycin (0.26), and oral chloroquine (0.12) (Barrows et al., 2016; Drusano et al., 1986; Retallack et al., 2016; Xu et al., 2016). Oral and parenteral niclosamide are insoluble (Zhang et al., 2015). Daptomycin is only available for intravenous administration. Sofosbuvir is expensive ( $\geq 1000$  USD/tablet). Moreover, the mechanisms of anti-ZIKV activity of most of these drugs have not been elucidated. The limitations of these drugs make our findings especially important for further

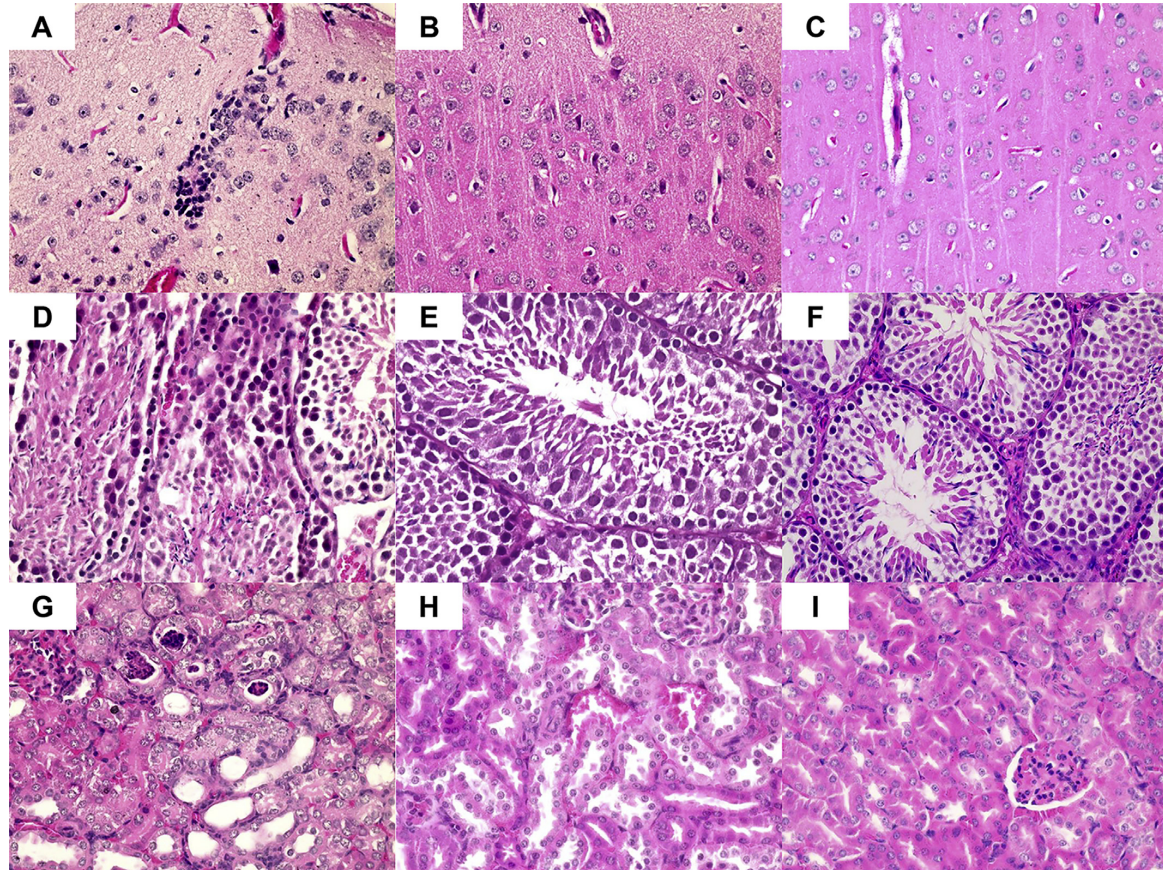


**Fig. 7.** Representative histological findings in different groups of mice in this study. Representative histological findings at 12–14 days post-ZIKV inoculation in the brain (top row: A, B, C), testis (middle row: D, E, F), and kidney (bottom row: G, H, I) (H&E, original magnification  $\times 400$ ) of dexamethasone-immunosuppressed BALB/c mice with ZIKV inoculation but without novobiocin treatment (left column: A, D, G), dexamethasone-immunosuppressed BALB/c mice with ZIKV inoculation and novobiocin treatment (middle column: B, E, H), and dexamethasone-immunosuppressed BALB/c mice with mock infection and novobiocin treatment (right column: C, F, I). Each organ was entirely embedded in one paraffin block, and one full-face paraffin section at the maximum diameter of each organ was examined per block. Marked inflammatory infiltration with distorted tissue architecture could be seen in the brain (A), testis (D), and kidney (G) of the dexamethasone-immunosuppressed mice with ZIKV inoculation without novobiocin treatment. The mice with ZIKV-inoculation with novobiocin treatment and the control mice with mock infection and novobiocin treatment had no or mild inflammatory infiltrate, and preserved tissue architecture.

development of novobiocin into a clinically useful anti-ZIKV treatment option. Nevertheless, these drugs may still be useful for treating different groups of ZIKV-infected patients when used under special circumstances (e.g.: Cmax:IC<sub>50</sub> ratio of a 500 mg intravenous dose of azithromycin against ZIKV can be as high as 2.31). Further evaluation of their *in vivo* effects, alone or in combination, in animal models and clinical trials should be considered.

The successful identification of numerous ZIKV NS2B-NS3 protease inhibitors among primary hit compounds and validation of novobiocin as a potent anti-ZIKV drug has demonstrated the capability of our combined *in silico*, *in vitro*, and *in vivo* platform to discover enzyme inhibitors of ZIKV among immediately available clinically approved drugs. The same approach should be considered for screening other large chemical libraries for potential ZIKV helicase or polymerase inhibitors to expand the treatment options for ZIKV infection.

#### Author contributions

S.Y., J.F.-W.C., H.d.-H., H.P.-S., J.P.C.-C., and K.-Y.Y. designed the study. H.d.-H., J.d.I.P., H.P.-S., and J.P.C.-C. performed the *in silico* experiments. S.Y., J.F.-W.C., K.K.-H.C., A.J.Z., C.C.-S.C., V.K.-M.P., C.C.-Y.Y., W.W.-N.M., Z.Z., Z.Z. K.-M.T., J.-P.C., and K.-H.C. performed the *in vitro* and *in vivo* experiments. S.Y., J.F.-W.C., H.d.-H., H.P.-S., J.P.C.-C., and K.-Y.Y. performed data analysis and interpretation. S.Y., J.F.-W.C., H.d.-H., H.P.-S., J.P.C.-C., and K.-Y.Y. wrote the manuscript.

#### Conflict of interest statement

J.F.-W.C. has received travel grants from Pfizer Corporation Hong Kong and Astellas Pharma Hong Kong Corporation Limited, and was an invited speaker for Gilead Sciences Hong Kong Limited. The other authors declared no conflict of interests. The funding sources had no role in study design, data collection, analysis or



42

S. Yuan et al. / Antiviral Research 145 (2017) 33–43

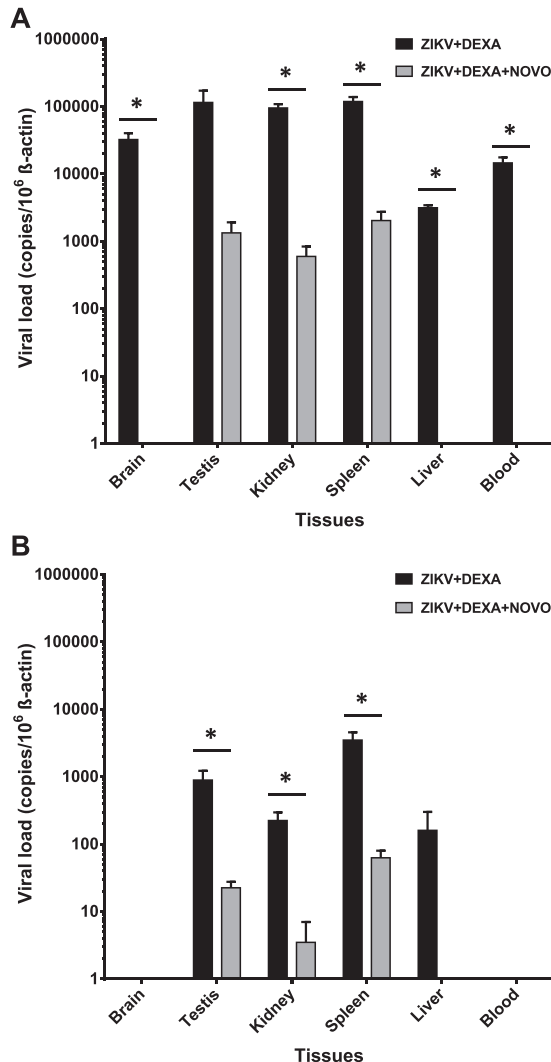


**Fig. 8.** Viral loads in the blood and major organs of dexamethasone-immunosuppressed BALB/c mice with ZIKV inoculation with or without novobiocin treatment. Mice with novobiocin treatment had reduced ZIKV blood and tissue viral loads as compared to untreated mice at (A) 5 days post-ZIKV inoculation ( $n = 3$  per group from two independent experiments) and (B) 14 days post-ZIKV inoculation ( $n = 5$  per group from two independent experiments). ZIKV RNA copies in the blood and tissues of the mice were determined by qRT-PCR and normalized by  $\beta$ -actin. \* denotes  $P$ -values of  $<0.05$ . Data are presented as mean values  $\pm$  standard error of the mean (error bars). Abbreviations: DEXA, dexamethasone; NOVO, novobiocin; ZIKV, Zika virus.

interpretation or writing of the report. The corresponding authors had full access to all the data in the study and had final responsibility for the decision to submit for publication.

#### Acknowledgements

The authors are grateful to the technical support provided by the staff at Department of Microbiology, The University of Hong Kong, and the computer resources and the technical support provided by

Centro de Alto Rendimiento de la Región de Murcia within its Research Program (CFE-CAR-23/15), the Plataforma Andaluza de Bioinformática of the University of Málaga, the supercomputing infrastructure of the NLHPC (ECM-02), the e-infrastructure program of the Research Council of Norway, and the supercomputer center of UiT - the Arctic University of Norway, and the supercomputing infrastructure of Poznan Supercomputing Center. This work was partly supported by the donations of Hui Hoy and Chow Sin Lan Charity Fund Limited; and funding from the Consultancy Service for Enhancing Laboratory Surveillance of Emerging Infectious Diseases of the Department of Health, Hong Kong Special Administrative Region; the Collaborative Innovation Center for Diagnosis and Treatment of Infectious Diseases, the Ministry of Education of China; and the Fundación Séneca del Centro de Coordinación de la Investigación de la Región de Murcia under Projects 18946/JLI/13 and 19419/PI/14-1.

#### Appendix A. Supplementary data

Supplementary data related to this article can be found at <http://dx.doi.org/10.1016/j.antiviral.2017.07.007>.

#### References

- Arzuza-Ortega, L., Polo, A., Perez-Tatis, G., López-García, H., Parra, E., Pardo-Herrera, L.C., Rico-Turca, A.M., Villamil-Gómez, W., Rodríguez-Morales, A.J., et al., 2016. Fatal sickle cell disease and Zika virus infection in girl from Colombia. *Emerg. Infect. Dis.* 22, 925–927.
- Azevedo, R.S., Araujo, M.T., Martins Filho, A.J., Oliveira, C.S., Nunes, B.T., Cruz, A.C., Nascimento, A.G., Medeiros, R.C., Caldas, C.A., Araujo, F.C., et al., 2016. Zika virus epidemic in Brazil. I. Fatal disease in adults: clinical and laboratorial aspects. *J. Clin. Virol.* 85, 56–64.
- Barrows, N.J., Campos, R.K., Powell, S.T., Prasanth, K.R., Schott-Lerner, G., Soto-Acosta, R., Galarza-Muñoz, G., McGrath, E.L., Urrabaz-Garza, R., Gao, J., et al., 2016. A screen of FDA-approved drugs for inhibitors of Zika virus infection. *Cell Host Microbe* 20, 259–270.
- Bullard-Feibelman, K.M., Govero, J., Zhu, Z., Salazar, V., Veselinovic, M., Diamond, M.S., Geiss, B.J., 2016. The FDA-approved drug sofosbuvir inhibits Zika virus infection. *Antivir. Res.* 137, 134–140.
- Cao-Lormeau, V.M., Blake, A., Mons, S., Lastère, S., Roche, C., Vanhomwegen, J., Dub, T., Baudouin, L., Teissier, A., Larre, P., et al., 2016. Guillain-Barre Syndrome outbreak associated with Zika virus infection in French Polynesia: a case-control study. *Lancet* 387, 1531–1539.
- Carteaux, G., Maquart, M., Bedet, A., Contou, D., Brugières, P., Fourati, S., Cleret de Langavant, L., de Broucker, T., Brun-Buisson, C., Leparco-Goffart, I., et al., 2016. Zika virus associated with meningoencephalitis. *N. Engl. J. Med.* 374, 1595–1596.
- Case, D.A., Cerutti, D.S., Cheatham III, T.E., Darden, T.A., Duke, R.E., Giese, T.J., Gohlke, H., Goetz, A.W., Greene, D., Homeyer, N., et al., 2017. AMBER 2017. University of California, San Francisco. <http://ambermd.org/doc12/Amber17.pdf>.
- Chan, J.F., Chan, K.H., Choi, G.K., To, K.K., Tse, H., Cai, J.P., Yeung, M.L., Cheng, V.C., Chen, H., Che, X.Y., Lau, S.K., Woo, P.C., Yuen, K.Y., 2013a. Differential cell line susceptibility to the emerging novel human betacoronavirus 2c EMC/2012: implications for disease pathogenesis and clinical manifestation. *J. Infect. Dis.* 207, 1743–1752.
- Chan, J.F., Chan, K.H., Kao, R.Y., To, K.K., Zheng, B.J., Li, C.P., Li, P.T., Dai, J., Mok, F.K., Chen, H., et al., 2013b. Broad-spectrum antivirals for the emerging Middle East respiratory syndrome coronavirus. *J. Infect.* 67, 606–616.
- Chan, J.F., Choi, G.K., Yip, C.C., Cheng, V.C., Yuen, K.Y., 2016a. Zika fever and congenital Zika syndrome: an unexpected emerging arboviral disease. *J. Infect.* 72, 507–524.
- Chan, J.F., Yip, C.C., Tsang, J.O., Tee, K.M., Cai, J.P., Chik, K.K., Zhu, Z., Chan, C.C., Choi, G.K., Sridhar, S., et al., 2016b. Differential cell line susceptibility to the emerging Zika virus: implications for disease pathogenesis, non-vector-borne human transmission and animal reservoirs. *Emerg. Microbes Infect.* 5, e93.
- Chan, J.F., Zhang, A.J., Chan, C.C., Yip, C.C., Mak, W.W., Zhu, H., Poon, V.K., Tee, K.M., Zhu, Z., Cai, J.P., et al., 2016c. Zika virus infection in dexamethasone-immunosuppressed mice demonstrating disseminated infection with multi-organ involvement including orchitis effectively treated by recombinant type I interferons. *EBioMedicine* 14, 112–122.
- Chan, J.F., Chik, K.K., Yuan, S., Yip, C.C., Zhu, Z., Tee, K.M., Tsang, J.O., Chan, C.C., Poon, V.K., Lu, G., et al., 2017a. Novel antiviral activity and mechanism of bromocriptine as a Zika virus NS2B-NS3 protease inhibitor. *Antivir. Res.* 141, 29–37.
- Chan, J.F., Yip, C.C., Tee, K.M., Zhu, Z., Tsang, J.O., Chik, K.K., Tsang, T.G., Chan, C.C., Poon, V.K., Sridhar, S., et al., 2017b. Improved detection of Zika virus RNA in human and animal specimens by a novel, highly sensitive and specific real-time

- RT-PCR assay targeting the 5'-untranslated region of Zika virus. *Trop. Med. Int. Health*. <http://dx.doi.org/10.1111/tmi.12857> [Epub ahead of print].
- Chraïbi, S., Najioullah, F., Bourdin, C., Pegliasco, J., Deligny, C., Résière, D., Meniane, J.C., 2016. Two cases of thrombocytopenic purpura on onset of Zika virus infection. *J. Clin. Virol.* 83, 61–62.
- Civitico, G., Wang, Y.Y., Luscombe, C., Bishop, N., Tachedjian, G., Gust, I., Locarnini, S., 1990. Antiviral strategies in chronic hepatitis B virus infection: II. Inhibition of duck hepatitis B virus in vitro using conventional antiviral agents and supercoiled-DNA active compounds. *J. Med. Virol.* 31, 90–97.
- Delvecchio, R., Higa, L.M., Pezzuto, P., Valadao, A.L., Garcez, P.P., Monteiro, F.L., Loiola, E.C., Dias, A.A., Silva, F.J., Aliota, M.T., et al., 2016. Chloroquine, an endocytosis blocking agent, inhibits Zika virus infection in different cell models. *Viruses* 8.
- Droge, P., Sogo, J.M., Stahl, H., 1985. Inhibition of DNA synthesis by aphidicolin induces supercoiling in simian virus 40 replicative intermediates. *EMBO J.* 4, 3241–3246.
- Drusano, G.L., Townsend, R.J., Walsh, T.J., Forrest, A., Antal, E.J., Standiford, H.C., 1986. Steady-state serum pharmacokinetics of novobiocin and rifampin alone and in combination. *Antimicrob. Agents Chemother.* 30, 42–45.
- Duffy, M.R., Chen, T.H., Hancock, W.T., Powers, A.M., Kool, J.L., Lanciotti, R.S., Pretrick, M., Marfel, M., Holzbauer, S., Dubray, C., et al., 2009. Zika virus outbreak on Yap Island, Federated States of Micronesia. *N. Engl. J. Med.* 360, 2536–2543.
- Flatman, R.H., Eustaquio, A., Li, S.M., Heide, L., Maxwell, A., 2006. Structure-activity relationships of aminocoumarin-type gyrase and topoisomerase IV inhibitors obtained by combinatorial biosynthesis. *Antimicrob. Agents Chemother.* 50, 1136–1142.
- Foy, B.D., Kobylinski, K.C., Chilson Foy, J.L., Blitvich, B.J., Travassos da Rosa, A., Haddow, A.D., Lanciotti, R.S., Tesh, R.B., 2011. Probable non-vector-borne transmission of Zika virus, Colorado, USA. *Emerg. Infect. Dis.* 17, 880–882.
- Furlini, G., Coppolecchia, P., Re, M.C., Baldassarri, B., Ripalti, A., Landini, M.P., 1983. In-vivo effect of novobiocin on primary cytomegalovirus infection. *J. Antimicrob. Chemother.* 12, 503–506.
- Gonzalez-Molleda, L., Wang, Y., Yuan, Y., 2012. Potent antiviral activity of topoisomerase I and II inhibitors against Kaposi's sarcoma-associated herpesvirus. *Antimicrob. Agents Chemother.* 56, 893–902.
- Govero, J., Esakky, P., Scheaffer, S.M., Fernandez, E., Drury, A., Platt, D.J., Gorman, M.J., Richner, J.M., Caine, E.A., Salazar, V., et al., 2016. Zika virus infection damages the testes in mice. *Nature* 540, 438–442.
- Kato, F., Ishida, Y., Oishi, S., Fujii, N., Watanabe, S., Vasudevan, S.G., Tajima, S., Takasaki, T., Suzuki, Y., Ichiyama, K., et al., 2016. Novel antiviral activity of bromocriptine against dengue virus replication. *Antivir. Res.* 131, 141–147.
- Kirby, W.M., Hudson, D.G., Noyes, W.D., 1956. Clinical and laboratory studies of novobiocin, a new antibiotic. *AMA Arch. Intern. Med.* 98, 1–7.
- Lei, J., Hansen, G., Nitsche, C., Klein, C.D., Zhang, L., Hilgenfeld, R., 2016. Crystal structure of Zika virus NS2B-NS3 protease in complex with a boronate inhibitor. *Science* 353, 503–505.
- Ma, W., Li, S., Ma, S., Jia, L., Zhang, F., Zhang, Y., Zhang, J., Wong, G., Zhang, S., Lu, X., et al., 2016. Zika virus causes testis damage and leads to male infertility in mice. *Cell* 167, 1511–1524, e10.
- Mecharles, S., Herrmann, C., Poullain, P., Tran, T.H., Deschamps, N., Mathon, G., Landais, A., Breurec, S., Lannuzel, A., 2016. Acute myelitis due to Zika virus infection. *Lancet* 387, 1481.
- Musso, D., Gubler, D.J., 2016. Zika virus. *Clin. Microbiol. Rev.* 29, 487–524.
- Musso, D., Roche, C., Robin, E., Nhan, T., Teissier, A., Cao-Lormeau, V.M., 2015. Potential sexual transmission of Zika virus. *Emerg. Infect. Dis.* 21, 359–361.
- Pessina, A., Mineo, E., Gribaldo, L., Neri, M.G., 1992. Lack of in vitro antiviral activity of fluoroquinolones against herpes simplex virus type 2. *Arch. Virol.* 122, 263–269.
- Phoo, W.W., Li, Y., Zhang, Z., Lee, M.Y., Loh, Y.R., Tan, Y.B., Ng, E.Y., Lescar, J., Kang, C., Luo, D., 2016. Structure of the NS2B-NS3 protease from Zika virus after self-cleavage. *Nat. Commun.* 7, 13410.
- Retalack, H., Di Lullo, E., Arias, C., Knopp, K.A., Laurie, M.T., Sandoval-Espinosa, C., Mancía Leon, W.R., Krencik, R., Ullian, E.M., Spatazza, J., et al., 2016. Zika virus cell tropism in the developing human brain and inhibition by azithromycin. *Proc. Natl. Acad. Sci. U. S. A.* 113, 14408–14413.
- Sarmiento-Ospina, A., Vasquez-Serna, H., Jimenez-Canizales, C.E., Villamil-Gomez, W.E., Rodriguez-Morales, A.J., 2016. Zika virus associated deaths in Colombia. *Lancet Infect. Dis.* 16, 523–524.
- Sekiguchi, J., Shuman, S., 1997. Novobiocin inhibits vaccinia virus replication by blocking virus assembly. *Virology* 235, 129–137.
- Stierand, K., Rarey, M., 2010. Drawing the PDB: protein-ligand complexes in two dimensions. *ACS Med. Chem. Lett.* 1, 540–545.
- Soares, C.N., Brasil, P., Carrera, R.M., Sequeira, P., de Filippis, A.B., Borges, V.A., Theophilo, F., Ellul, M.A., Solomon, T., 2016. Fatal encephalitis associated with Zika virus infection in an adult. *J. Clin. Virol.* 83, 63–65.
- Stroganov, O.V., Novikov, F.N., Stroylov, V.S., Kulkov, V., Chilov, G.G., 2008. Lead finder: an approach to improve accuracy of protein-ligand docking, binding energy estimation, and virtual screening. *J. Chem. Inf. Model.* 48, 2371–2385.
- Wu, T., Wang, Y., Yuan, Y., 2014. Antiviral activity of topoisomerase II catalytic inhibitors against Epstein-Barr virus. *Antivir. Res.* 107, 95–101.
- Xu, M., Lee, E.M., Wen, Z., Cheng, Y., Huang, W.K., Qian, X., Tcw, J., Kouznetsova, J., Ogden, S.C., Hammack, C., et al., 2016. Identification of small-molecule inhibitors of Zika virus infection and induced neural cell death via a drug repurposing screen. *Nat. Med.* 22, 1101–1107.
- Yuan, S., Chu, H., Zhang, K., Ye, J., Singh, K., Kao, R.Y., Chow, B.K., Zhou, J., Zheng, B.J., 2016. A novel small-molecule compound disrupts influenza A virus PB2 cap-binding and inhibits viral replication. *J. Antimicrob. Chemother.* 71, 2489–2497.
- Zhang, X., Zhang, Y., Zhang, T., Zhang, J., Wu, B., 2015. Significantly enhanced bioavailability of niclosamide through submicron lipid emulsions with or without PEG-lipid: a comparative study. *J. Microencapsul.* 32, 496–502.
- Zhou, J., Chu, H., Li, C., Wong, B.H., Cheng, Z.S., Poon, V.K., Sun, T., Lau, C.C., Wong, K.K., Chan, J.Y., et al., 2014. Active replication of Middle East respiratory syndrome coronavirus and aberrant induction of inflammatory cytokines and chemokines in human macrophages: implications for pathogenesis. *J. Infect. Dis.* 209, 1331–13342.
- Zhu, Z., Chan, J.F., Tee, K.M., Choi, G.K., Lau, S.K., Woo, P.C., Tse, H., Yuen, K.Y., 2016. Comparative genomic analysis of pre-epidemic and epidemic Zika virus strains for virological factors potentially associated with the rapidly expanding epidemic. *Emerg. Microbes Infect.* 5, e22.
- Zmurko, J., Marques, R.E., Schols, D., Verbeken, E., Kaptein, S.J., Neyts, J., 2016. The viral polymerase inhibitor 7-deaza-2'-C-methyladenosine is a potent inhibitor of in vitro Zika virus replication and delays disease progression in a robust mouse infection model. *PLoS Negl. Trop. Dis.* 10, e0004695.

## 2.8 Exploring African Medicinal Plants for Potential Anti-Diabetic Compounds with the DIA-DB Inverse Virtual Screening Web Server


<b>Title</b>	<i>Exploring African Medicinal Plants for Potential Anti-Diabetic Compounds with the DIA-DB Inverse Virtual Screening Web Server</i>
<b>Author</b>	Andreia S.P. Pereira, Helena den Haan, Jorge Peña-García, Marién M Moreno, Horacio Pérez-Sánchez, Zeno Apostolides.
<b>Journal</b>	<i>Molecules (MDPI)</i>
<b>Year</b>	2019
<b>State</b>	Published

### PhD candidate contribution

Helena den Haan Alonso, declares to be the co-author and contributor of the article *Exploring African Medicinal Plants for Potential Anti-Diabetic Compounds with the DIA-DB Inverse Virtual Screening Web Server* in the section on computational chemistry.

Article

# Exploring African Medicinal Plants for Potential Anti-Diabetic Compounds with the DIA-DB Inverse Virtual Screening Web Server

Andreia S.P. Pereira <sup>1</sup>, Helena den Haan <sup>2</sup>, Jorge Peña-García <sup>2</sup>, Marién M. Moreno <sup>2</sup>,  
Horacio Pérez-Sánchez <sup>2,\*</sup>  and Zeno Apostolides <sup>1,\*</sup>

<sup>1</sup> Department of Biochemistry, Genetics and Microbiology, University of Pretoria, Pretoria, Hillcrest 0083, South Africa; asdpereira@gmail.com

<sup>2</sup> Structural Bioinformatics and High Performance Computing Research Group (BIO-HPC), Universidad Católica de Murcia, 30107 Murcia, Spain; hden@alu.ucam.edu (H.d.H.); Jorge.dlpg@gmail.com (J.P.-G.); memoreno@ucam.edu (M.M.M.)

\* Correspondence: hperez@ucam.edu (H.P.-S.); zeno.apostolides@up.ac.za (Z.A.); Tel.: +34-968278819 (H.P.-S.); +27-12-420-2486 (Z.A.)

Received: 17 April 2019; Accepted: 4 May 2019; Published: 24 May 2019



**Abstract:** Medicinal plants containing complex mixtures of several compounds with various potential beneficial biological effects are attractive treatment interventions for a complex multi-faceted disease like diabetes. In this study, compounds identified from African medicinal plants were evaluated for their potential anti-diabetic activity. A total of 867 compounds identified from over 300 medicinal plants were screened *in silico* with the DIA-DB web server (<http://bio-hpc.eu/software/dia-db/>) against 17 known anti-diabetic drug targets. Four hundred and thirty compounds were identified as potential inhibitors, with 184 plants being identified as the sources of these compounds. The plants *Argemone ochroleuca*, *Clivia miniata*, *Crinum bulbispermum*, *Danais fragans*, *Dioscorea dregeana*, *Dodonaea angustifolia*, *Eucomis autumnalis*, *Gnidia kraussiana*, *Melianthus comosus*, *Mondia whitei*, *Pelargonium sidoides*, *Typha capensis*, *Vinca minor*, *Voacanga africana*, and *Xysmalobium undulatum* were identified as new sources rich in compounds with a potential anti-diabetic activity. The major targets identified for the natural compounds were aldose reductase, hydroxysteroid 11-beta dehydrogenase 1, dipeptidyl peptidase 4, and peroxisome proliferator-activated receptor delta. More than 30% of the compounds had five or more potential targets. A hierarchical clustering analysis coupled with a maximum common substructure analysis revealed the importance of the flavonoid backbone for predicting potential activity against aldose reductase and hydroxysteroid 11-beta dehydrogenase 1. Filtering with physiochemical and the absorption, distribution, metabolism, excretion and toxicity (ADMET) descriptors identified 28 compounds with favorable ADMET properties. The six compounds—crotofoline A, erythraline, henningsiine, nauclefidine, vinburnine, and voaphylline—were identified as novel potential multi-targeted anti-diabetic compounds, with favorable ADMET properties for further drug development.

**Keywords:** diabetes; anti-diabetic; DIA-DB; medicinal plants; *in silico*; virtual screening

## 1. Introduction

According to the World Health Organization, in 2016, diabetes was the seventh leading cause of death, with an estimated 1.6 million people having died from the disease [1]. Diabetes is a chronic disease arising from impaired insulin secretion and insulin resistance, leading to its defining feature of hyperglycemia [2]. It is a multi-organ disease affecting the pancreas, liver, muscles, kidney, and central nervous system, and several complications such as hypertension, stroke, blindness, and kidney

disease are associated with diabetes [2,3]. The main type of treatment for diabetes and controlling the associated hyperglycemia is in the form of insulin that primarily focuses on lowering and maintaining blood glucose levels [2]. However, in more recent years, as diabetes is a multifaceted disease, there has been an increase in the development of specific enzyme-targeted drugs, and specific inhibitors for targets like alpha-glucosidase, dipeptidyl peptidase-4 (DPP4), glucagon-like peptide-1 (GLP-1) receptor, and sodium-glucose co-transporter-2 (SGLT2) have been approved [3]. Unfortunately, some of these approved drugs have been met with some adverse effects [3]. As a better understanding of the pathogenesis and complexity in treating the disease arises, so too does the need for the development of more effective and safer drugs to treat the disease.

Throughout history, plants have played an important role in medicinal drug discovery as rich sources of unique and novel compounds for drug development. In several cultures, there is widespread traditional use of decoctions prepared from medicinal plants in the treatment of diabetes [4–8]. The use of decoctions prepared from medicinal plants in the treatment of a complex multi-faceted disease like diabetes is attractive, as they often contain more than one compound with various beneficial biological effects, thus potentially creating an effective and affordable multi-targeted treatment strategy [9,10]. In some cases, extensive scientific evaluations have been conducted on some of these traditional medicinal plants to validate their use in the treatment of diabetes, however, for the majority, there is a lack of scientific knowledge.

*In silico* virtual screening methodologies are ideal for initial exploratory evaluations of the potential anti-diabetic activity of traditional medicinal plants. As plants are complex mixtures of several different compounds, with *in silico* virtual screening methods, hundreds of compounds can be screened against multiple diabetes targets rapidly and cost effectively. This strategy has been employed to identify anti-cancer, anti-stroke, and anti-Alzheimer's compounds from traditional Chinese medicines, as well as their potential mechanisms of action [11–13]. In this study, we have implemented similar *in silico* methodologies to identify novel African medicinal plants as rich sources of compounds with potential anti-diabetic activity.

## 2. Results and Discussion

### 2.1. Inverse Virtual Screening and Identification of Compounds with Potential Anti-Diabetic Activity

In this study, the anti-diabetic potential of natural compounds from African medicinal plants was explored with the DIA-DB web server (<http://bio-hpc.eu/software/dia-db/>) [14]. A total of 867 compounds were screened *in silico* against 17 diabetes targets. The ligands found crystallized with each protein target were also screened to decide a cutoff docking score, so as to distinguish between potential active and inactive compounds. The docking scores of the crystallized ligands ranged from  $-11.3$  to  $-5.7$  kcal/mol, and in some cases, the test compounds had better docking scores than the docking scores for the crystallized ligands (Table 1). A docking cutoff score of  $-9$  kcal/mol was set, as it was deemed a reasonable average docking score that covered the top 10%–20% of the test compounds for each protein target [11–13].

Of the 867 test compounds, a total of 430 were predicted as potentially active compounds, and the majority of these compounds were not limited to a single protein target only, with 30% of the predicted active compounds having five or more protein targets (Figure 1 and Table S2). Hydroxysteroid 11-beta dehydrogenase 1 (HSD11B1), peroxisome proliferator-activated receptor delta (PPARD), and DPP4 had the most predicted active compounds, with 208, 190, and 149, respectively, while protein targets peroxisome proliferator-activated receptor alpha (PPARA), insulin receptor (INSR), and intestinal maltase-glucoamylase (MGAM) had the least, with 6, 18, and 18, respectively (Figure S1). The difference in the number of predicted active compounds likely reflects the differences in the nature of the binding pockets of the target proteins, with some having large binding cavities that can accommodate different types and sizes of scaffolds.

**Table 1.** The docking scores obtained for the ligands crystallised with protein targets versus the lowest energy obtained for a test compound.

Mode of Action	Protein Target	Function	PDB Code	Crystallized Ligand–Docking Score (kcal/mol)	Test Compounds–Lowest Energy (kcal/mol)	Test Compound Name
Regulation of insulin secretion and sensitivity	DPP4	Degrades and inactivates glucagon-like peptide-1 that stimulates insulin secretion from the pancreas [15]	4A5S	−10.5	−11.8	Cryptospirolepine
	FFAR1	Binding of free fatty acids to the receptor results in increased glucose-stimulated insulin secretion [16]	4PHU	−9.8	−11.6	Procyanidin C1
	HSD11B1	Converts inactive glucocorticoid precursors to active glucocorticoids; glucocorticoids counteract the effects of insulin [17]	4K1L	−8.3	−12.8	Cryptomisine
	INSR	Regulates glucose uptake, as well as glycogen, lipid, and protein synthesis [15]	3EKN	−8.7	−10.9	Typharin
	PTPN9	Dephosphorylates the insulin receptor, thereby reducing insulin sensitivity [18]	4GE6	−7.7	−10.2	Cryptospirolepine
	RBP4	Secreted as an adipokine that reduces insulin signaling and promotes gluconeogenesis [19]	2WR6	−7.9	−11	Benzo[c]phenanthridine
Regulation of glucose metabolism	AKR1B1	Catalyses the reduction of glucose to sorbitol in the polyol pathway, and plays a role in diabetic complications [20]	3G5E	−11.3	−11.9	Pterygospermin
	AMY2A	Hydrolyses alpha-1,4-glycosidic bonds to starch during digestion of starch to glucose [21]	4GQR	−7.9	−11.5	Clivimine
	GCK	Phosphorylates glucose to glucose-6-phosphate for glycolysis or glycogen synthesis [18]	3IMX	−10.6	−13	Cryptomisine
	MGAM	Hydrolyzes 1,4-alpha bonds, the last step in the digestion of starch to glucose [21]	3L4Y	−5.7	−10	Cryptospirolepine
	PDK2	Responsible for inactivating the pyruvate dehydrogenase complex that is involved during glucose oxidation [22]	4MPC	−7.8	−11.5	Clivimine
	PYGL	Catalyses the first step of glycogenolysis by the phosphorylation of glycogen to glucose-1-phosphate [23]	3DDS	−9.6	−10.8	Cryptomisine

Table 1. Cont.

Mode of Action	Protein Target	Function	PDB Code	Crystallized Ligand-Docking Score (kcal/mol)	Test Compounds—Lowest Energy (kcal/mol)	Test Compound Name
Regulation of lipid metabolism	NR5A2	Regulates the expression of the genes involved in bile acid synthesis, cholesterol synthesis, and steroidogenesis [24]	4DOR	−6.5	−12.2	Clivimine
	PPARA	Regulates the expression of the genes involved in lipid metabolism, in particular, the oxidation of fatty acids, as well as lipoprotein assembly and lipid transport [25]	3FEI	−8.3	−11.4	Biscryptolepine
	PPARD	Regulates the expression of the genes involved in fatty acid catabolism [25]	3PEQ	−11.3	−14.3	Cryptomisine
	PPARG	Regulates the expression of the genes involved in adipogenesis and lipid metabolism, particularly fatty acid transport, lipid droplet formation, triacylglycerol metabolism, and lipolysis of triglycerides [25]	2FVJ	−10	−11.9	Cryptoquindoline
	RXRA	Heterodimerizes with PPARs, thereby initiating gene transcription [25]	1FM9	−10.6	−10.9	Crinasiatine

Aldose reductase (AKR1B1); dipeptidyl peptidase-4 (DPP4); free fatty acid receptor 1 (FFAR1); glucokinase (GCK); hydroxysteroid 11-beta dehydrogenase 1 (HSD11B1); insulin receptor (INSR); intestinal maltase-glucoamylase (MGAM); liver glycogen phosphorylase (PYGL); liver receptor homolog-1 (NR5A2); pancreatic alpha-amylase (AMY2A); peroxisome proliferator-activated receptor alpha (PPARA); peroxisome proliferator-activated receptor delta (PPARD); peroxisome proliferator-activated receptor gamma (PPARG); protein tyrosine phosphatase non-receptor type 9 (PTPN9); pyruvate dehydrogenase kinase isoform 2 (PDK2); retinoid X receptor alpha (RXRA); retinol binding protein 4 (RBP4).

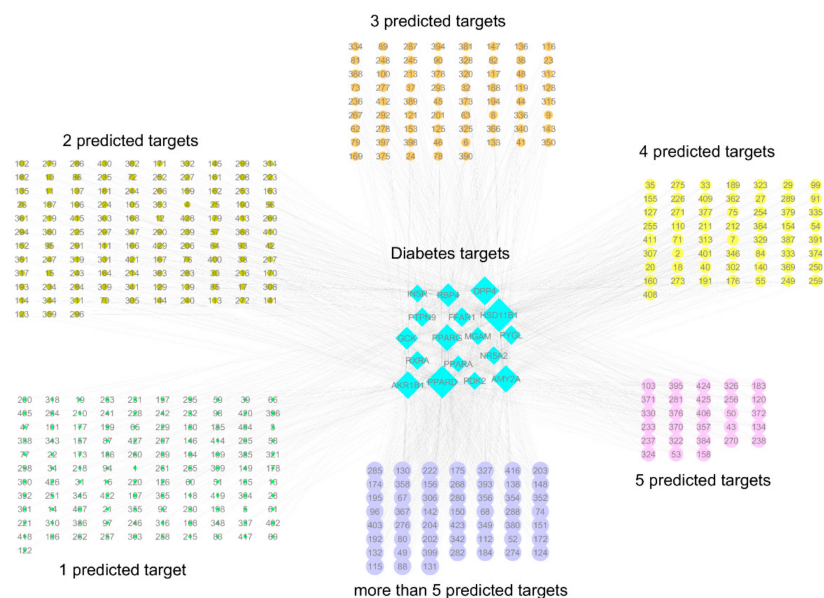


**Figure 1.** The network of compounds identified by virtual screening with the DIA-DB web server and their predicted targets. All of the predicted active compounds are represented by a number that corresponds to those given to the compounds in Table S2. The size of the target node depicts the number of predicted compounds, while the size of the compound node depicts the number of predicted targets. For the individual compound–target networks, please refer to Figure S1.

The significance of the potential for multi-targeted compounds becomes apparent when one looks at the complexity of the diabetes disease pathogenesis. Diabetes is not the result of the dysregulation of a single target and/or pathway, but rather the dysregulation of multiple processes such as glucose and lipid metabolism, as well as insulin signaling in several organ systems, such as the pancreas, liver, muscles, and adipose tissue, leading to the hallmark of hyperglycemia [2,26] (Figure 2). Compounds capable of regulating one or more of the protein targets associated with these dysregulated processes across the different organ systems may be more effective in managing the disease than a “single target single drug” approach [27–29]. Not surprising, several manuscripts can be found in the literature on the potential use of combination drug therapy for the treatment of diabetes, including the combination of drugs with medicinal plants or herbs [9,10,30].

A total of 184 plants were identified as sources for the predicted active compounds (Table 2 and Table S3). Some plants were found to contain several predicted active compounds, while with others only one compound was identified. A limitation to this study was that one could not look at plants specifically enriched for anti-diabetic compounds, as not all of the compounds for all of the plants were listed in the books, and in several cases, only one major compound was listed for a plant. Following extensive literature searches for previous literature on the anti-diabetic potential of the plants and the compounds, it was found that of the 430 predicted active compounds, 125 had previous literature on their anti-diabetic potential, leaving a total of 305 newly identified potential anti-diabetic compounds.



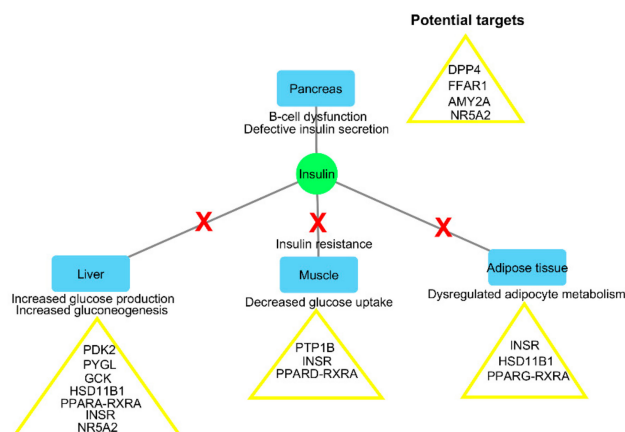


**Figure 2.** A simplified overview of some of the organ systems and their dysregulation involved in diabetes pathogenesis (adapted from Moller, 2001 [26]; DeFronzo et al., 2014 [2]). Potential targets identified in each organ system relate to some of the virtual screening targets of the DIA-DB web server. Dipeptidyl peptidase-4 (DPP4); free fatty acid receptor 1 (FFAR1); glucokinase (GCK); hydroxysteroid 11-beta dehydrogenase 1 (HSD11B1); insulin receptor (INSR); liver glycogen phosphorylase (PYGL); liver receptor homolog-1 (NR5A2); pancreatic alpha-amylase (AMY2A); peroxisome proliferator-activated receptor alpha (PPARA); peroxisome proliferator-activated receptor delta (PPARD); peroxisome proliferator-activated receptor gamma (PPARG); protein tyrosine phosphatase (PTP); pyruvate dehydrogenase kinase isoform 2 (PDK2); retinoid X receptor alpha (RXRA).

From the plants, 82 plants were found with previous literature (namely traditional and experimental evidence) (Table S3); 12 plants were identified with traditional use for diabetes (Table S3), but no experimental evidence to date; and 90 plants were identified as new potential sources of anti-diabetic compounds (Table 2). Of particular interest was that the majority of these 90 plants were sourced from *Poisonous Plants of South Africa* [31], indicating the potential for toxicity of the compounds.

More than 60% of the plants with previous experimental literature on their anti-diabetic activity were found to contain one or more compound/s that were also found to have previous literature on their anti-diabetic potential. This suggests that these compounds are likely responsible for the observed experimental activity of the medicinal plant. This is true in the case of several plants, such as *Aspalathus linearis* and compounds aspalathin, isoorientin, orientin, and quercetin [32–34]; *Cryptolepis sanguinolenta* and compound cryptolepine [35]; *Garcinia kola* and compounds garcinia biflavonoid 1 and 2 and kolaflavanone [36,37]; *Glycyrrhiza glabra* and compound glycyrrhizin [38]; *Hoodia gordonii* and compound P57 [39]; *Ligustrum lucidum* and compound oleanolic acid [40]; *Moringa oleifera* and compounds kaempferol and quercetin [41]; *Olea europaea* and compounds oleuropein and oleanolic acid [42]; *Punica granatum* and compounds punicalin and punicalagin [43]; *Ruta graveolens* and compound rutin [44]; *Styphnolobium japonicum* and compound sophoricoside [45]; *Syzygium cordatum* and compound oleanolic acid [46]; *Vernonia amygdalina* and compounds 1,5-dicaffeoylquinic acid, chlorogenic acid and luteolin-7-rutinoside [47]; and *Withania somnifera* and compound withaferin A [48]. The identification of both plants and compounds with previous literature on their potential anti-diabetic activity provides some validation for the methodology used in this study.

**Table 2.** Plants with no previous anti-diabetic evidence, identified by virtual screening and their predicted bioactive compounds.

Plant Name	Family	Compounds
<i>Acokanthera oppositifolia</i>	Apocynaceae	Acolongifloroside K <sup>31</sup> , acovenoside A <sup>32</sup> , ouabain <sup>304</sup>
<i>Adenium multiflorum</i>	Apocynaceae	Obebioside <sup>294</sup>
<i>Agapanthus africanus</i>	Amaryllidaceae	Agapanthagenin <sup>36</sup>
<i>Amaryllis belladonna</i>	Amaryllidaceae	Acetylcaranine <sup>30</sup> , caranine <sup>97</sup> , lycorine <sup>277</sup>
<i>Anagallis arvensis</i>	Primulaceae	Arvenin I <sup>60</sup> , arvenin II <sup>61</sup>
<i>Asclepias fruticosa</i>	Apocynaceae	Afroside <sup>35</sup> , 19-deoxyuscharin <sup>20</sup> , gomphoside <sup>195</sup>
<i>Aster bakeranus</i>	Asteraceae	ent-16-Kauren-18-oic-acid <sup>162</sup> , ent-16-Kauren-19-oic-acid <sup>163</sup> , friedelin <sup>174</sup>
<i>Balanites maughamii</i>	Zygophyllaceae	Cryptogenin <sup>127</sup> , diosgenin <sup>153</sup>
<i>Bersama lucens</i>	Meliantaceae	Melianthugenin <sup>282</sup>
<i>Boophae disticha</i>	Amaryllidaceae	3-Acetylnerbowdine <sup>16</sup> , buphanisin <sup>93</sup>
<i>Bowiea volubilis</i>	Asparagaceae	Bovogenin A <sup>89</sup> , bovoside A <sup>90</sup>
<i>Brabejum stellatifolium</i>	Proteaceae	Amygdalin <sup>51</sup>
<i>Cestrum laevigatum</i>	Solanaceae	Parquin <sup>310</sup>
<i>Chrysanthemum cinerariifolium</i>	Asteraceae	Pyrethrin I <sup>330</sup>
<i>Clivia miniata</i>	Amaryllidaceae	Cliviamartine <sup>112</sup> , cliviasine <sup>113</sup> , clividine <sup>114</sup> , clivimine <sup>115</sup> , clivonine <sup>116</sup> , hippeastrine <sup>217</sup> , lycorine <sup>277</sup>
<i>Cotyledon orbiculata</i>	Crassulaceae	Orbicuside A <sup>302</sup> , tyledoside C <sup>397</sup>
<i>Crinum bulbispermum</i>	Amaryllidaceae	Acetylcaranine <sup>30</sup> , bulbispermine <sup>92</sup> , crinamine <sup>122</sup> , crinasiadine <sup>123</sup> , crinasiatine <sup>124</sup> , galanthamine <sup>180</sup> , hippeastrine <sup>217</sup> , lycorine <sup>277</sup> , pratorimine <sup>319</sup>
<i>Crinum macowanii</i>	Amaryllidaceae	Crinamine <sup>122</sup> , lycorine <sup>277</sup> , pratorimine <sup>319</sup>
<i>Crotalaria spartioides</i>	Fabaceae	Retrorsine <sup>343</sup>
<i>Croton gratissimus</i>	Euphorbiaceae	Crotofolin A <sup>125</sup> , crotonin <sup>126</sup>
<i>Cucumis africanus</i>	Cucurbitaceae	Cucurbitacin B <sup>133</sup>
<i>Cyclamen persicum</i>	Primulaceae	Cyclamin <sup>137</sup>
<i>Cynanchum africanum</i>	Apocynaceae	Cynafoside B <sup>139</sup>
<i>Danais fragans</i>	Rubiaceae	1-Hydroxydimethylanthraquinone <sup>8</sup> , kaempferol-3-O-rhamnoglucoside <sup>250</sup> , quercitrin <sup>335</sup> , rubiadin <sup>348</sup> , rubiadin xyloglucoside <sup>349</sup>
<i>Datura stramonium</i>	Solanaceae	Hyoscyamine <sup>220</sup>
<i>Delphinium grandiflorum</i>	Ranunculaceae	Nudicauline <sup>293</sup>
<i>Digitalis purpurea</i>	Plantaginaceae	Digitoxin <sup>150</sup>
<i>Dioscorea dregeana</i>	Dioscoreaceae	Deltonin <sup>145</sup> , deltoside <sup>146</sup> , dioscin <sup>152</sup> , diosgenin <sup>153</sup> , hircinol <sup>218</sup>
<i>Dodonaea angustifolia</i>	Sapindaceae	Beta-sitosterol <sup>70</sup> , hautriwaic acid <sup>205</sup> , stigmasterol <sup>375</sup>
<i>Drimia robusta</i>	Hycinthaceae	12-Beta-hydroxyscillirosidin <sup>4</sup> , proscillaridin A <sup>324</sup>
<i>Eriocephalus africanus</i>	Asteraceae	Ivangustine <sup>246</sup>
<i>Erythrina caffra</i>	Fabaceae	Erythraline <sup>169</sup>
<i>Erythrina lysistemon</i>	Fabaceae	Erythraline <sup>169</sup>
<i>Erythrophleum lasianthum</i>	Fabaceae	Erythrophleine <sup>170</sup>
<i>Eschscholzia californica</i>	Papaveraceae	Dihydrosanguinarine <sup>151</sup>
<i>Eucomis autumnalis</i>	Asparagaceae	Autumnariniol <sup>65</sup> , autumnariol <sup>66</sup> , 3,9-dihydroeucomnalin <sup>19</sup> , eucosterol <sup>171</sup>
<i>Euphorbia ingens</i>	Euphorbiaceae	Ingenol <sup>231</sup>
<i>Ficus salicifolia</i>	Moraceae	Aviprin <sup>69</sup>
<i>Geigeria ornativa</i>	Asteraceae	Vermeerin <sup>407</sup>
<i>Geranium incanum</i>	Geraniaceae	Geraniin <sup>189</sup>
<i>Gnidia kraussiana</i>	Thymelaeaceae	Gnidicin <sup>192</sup> , gnidilatin <sup>193</sup> , gniditrin <sup>194</sup> , 12-hydroxydaphnetoxin <sup>5</sup>
<i>Griffonia simplicifolia</i>	Fabaceae	Indole-3-acetyl aspartic acid <sup>230</sup>
<i>Homeria pallida</i>	Iridaceae	1,2-Epoxy-scillirosidin <sup>1</sup>
<i>Hyaenanche globosa</i>	Picrodendraceae	Urushiol III <sup>402</sup>
<i>Hypericum aethiopicum</i>	Hypericaceae	Hypericin <sup>222</sup>
<i>Ipomoea purpurea</i>	Convolvulaceae	Ergine <sup>167</sup>

Table 2. Cont.

Plant Name	Family	Compounds
<i>Kalanchoe lanceolata</i>	Crassulaceae	Lanceotoxin A <sup>258</sup> , hellebrigenin <sup>210</sup>
<i>Lippia rehmannii</i>	Verbenaceae	Icterogenin <sup>229</sup> , lantadene A <sup>259</sup>
<i>Lotononis laxa</i>	Fabaceae	Integerrimine <sup>234</sup> , senecionine <sup>359</sup>
<i>Melianthus comosus</i>	Francoaceae	3-Epioleanolic acid <sup>*17</sup> , hellebrigenin-3-acetate <sup>211</sup> , melianthugenin <sup>282</sup> , oleanolic acid <sup>*299</sup>
<i>Melilotus alba</i>	Fabaceae	Dicoumarol <sup>148</sup>
<i>Moraea polystachya</i>	Iridaceae	16-Beta-formyloxybovogenin A <sup>7</sup>
<i>Mundulea sericea</i>	Fabaceae	Deguelin <sup>142</sup> , rotenone <sup>347</sup> , tephrosin <sup>384</sup>
<i>Ocotea bullata</i>	Lauraceae	Ocubullenone <sup>295</sup>
<i>Peddiea africana</i>	Thymelaeaceae	Peddiea factor A1 <sup>311</sup>
<i>Pelargonium sidoides</i>	Geraniaceae	Catechin <sup>*100</sup> , gallic acid <sup>*181</sup> , quercetin <sup>*331</sup> , sitosterol-3- $\beta$ -glucoside <sup>*364</sup>
<i>Phytolacca dodecandra</i>	Phytolaccaceae	Lemmatoxin <sup>262</sup> , oleanoglycotxin <sup>298</sup>
<i>Plumbago auriculata</i>	Plumbaginaceae	Plumbagin <sup>*318</sup>
<i>Polygala fruticosa</i>	Polygalaceae	Frutinone A <sup>175</sup> , presenegenin <sup>321</sup>
<i>Ptaeroxylon obliquum</i>	Rutaceae	Umtatin <sup>22</sup>
<i>Quercus robur</i>	Fagaceae	Catalagin <sup>*99</sup> , digallic acid <sup>149</sup>
<i>Rapanea melanophloeos</i>	Primulaceae	3-Oxo-20,24-dammaradien-26-ol <sup>18</sup> , sakurasosaponin <sup>353</sup>
<i>Rhododendron indicum</i>	Ericaceae	Grayanotoxin I <sup>197</sup>
<i>Rhus undulata</i>	Anacardiaceae	Apigenin dimethylether <sup>56</sup>
<i>Sansevieria hyacinthoides</i>	Asparagaceae	Ruscogenin-(25S)-form <sup>350</sup>
<i>Sarcostemma viminale</i>	Apocynaceae	Sarcovimisine B <sup>356</sup>
<i>Scabiosa columbaria</i>	Caprifoliaceae	Chlorogenic acid <sup>*106</sup>
<i>Scadoxus puniceus</i>	Amaryllidaceae	Haemanthamine <sup>206</sup> , haemanthidine <sup>207</sup>
<i>Schotia brachypetala</i>	Fabaceae	3,3,4,5,5-Pentahydroxystilbene <sup>*14</sup>
<i>Scilla natalensis</i>	Asparagaceae	Proscillaridin A <sup>324</sup>
<i>Senecio retrorsus</i>	Asteraceae	Retrorsine <sup>343</sup>
<i>Senecio serratuloides</i>	Asteraceae	Platyphylline <sup>317</sup> , senecionine <sup>359</sup>
<i>Smodingium argutum</i>	Anacardiaceae	3,8,11-Heptadecadienylcatechol <sup>15</sup>
<i>Solanum pseudocapsicum</i>	Solanaceae	Solanocapsine <sup>367</sup>
<i>Spirostachys africana</i>	Euphorbiaceae	Stachenol <sup>372</sup> , stachenone <sup>373</sup>
<i>Strophanthus speciosus</i>	Apocynaceae	Christyoside <sup>107</sup>
<i>Synadenium grantii</i>	Euphorbiaceae	4-Deoxy-13-O-phenylacetyl-12-O-tigloylphorbol <sup>21</sup>
<i>Synaptolepis kirkii</i>	Thymelaeaceae	Synaptolepis factor K1 <sup>381</sup> , synaptolepis factor K7 <sup>382</sup>
<i>Tetradenia riparia</i>	Lamiaceae	Ibozol <sup>228</sup> , 8-(14)-15-isopimaradiene-7,18-diol <sup>26</sup>
<i>Thesium minkwitzianum</i>	Santalaceae	Thesinine <sup>389</sup>
<i>Thesium hystrix</i>	Santalaceae	Quercetin <sup>*331</sup>
<i>Thevetia peruviana</i>	Apocynaceae	Thevetin A <sup>390</sup> , thevetin B <sup>391</sup>
<i>Tylecodon wallichii</i>	Crassulaceae	Cotyledoside <sup>121</sup>
<i>Typha capensis</i>	Typhaceae	Catechin <sup>*100</sup> , typhaphtalide <sup>398</sup> , typharin <sup>399</sup> , thyphasterol <sup>400</sup>
<i>Urginea maritima</i>	Asparagaceae	Scillaren A <sup>357</sup> , scillarenin <sup>358</sup>
<i>Urginea sanguinea</i>	Asparagaceae	Scillaren A <sup>357</sup>
<i>Valeriana capensis</i>	Valerianaceae	Valerenic acid <sup>405</sup>
<i>Vinca minor</i>	Apocynaceae	Eburnamonine <sup>*160</sup> , vincamine <sup>*417</sup>
<i>Xerophyta retinervis</i>	Velloziaceae	Amentoflavone <sup>*49</sup>
<i>Zanthoxylum capense</i>	Rutaceae	Sanguinarine <sup>*354</sup>

The numbers 1–430 serves as the identification of each compound in Figure 1. \* All of the compounds identified with some previous literature on their potential anti-diabetic activity.

Of interest were the plants found containing compounds with previous literature on the compound's potential anti-diabetic activity, but to date, the medicinal plant itself has not been evaluated for its potential antidiabetic activity. These plants were *Argemone ochroleuca* with compounds berberine [49], protopine [50] and sanguinarine [51]; *Dioscorea dregeana* with compounds dioscin [52,53], diosgenin [18,54] and hircinol [55]; *Dodonaea angustifolia* with compounds beta-sitosterol [56] and

stigmasterol [57,58]; *Melianthus comosus* with compounds 3-epioleanolic acid [59] and oleanolic acid [60]; *Pelargonium sidoides* with compounds catechin [61], gallicocatechin [62,63], quercetin [64] and sitosterol-3-glucoside [65,66]; and *Vinca minor* with compounds eburnamonine and vincamine [67]. These plants represent a good initial point for exploratory *in vitro* anti-diabetic studies. These plants with their bioactive compounds and predicted targets are depicted in Figure 3.

Other plants of interest were those that had no previous literature, but contained several compounds (also with no previous literature) that were identified in this study as having a potential anti-diabetic activity. These plants were *Mondia whitei* and compounds 5-chloropropacin, 7-hydroxy-4,6-dimethoxypropacin and propacin; *Voacanga Africana* and its compounds ibogaine, ibogamine, iboxygaine, vinburnine, voacamine, voacangine, voacorine, voaphylline and vobtusine; and *Xysmalobium undulatum* and compounds allouzarin, alloxysmalorin, uzarigenin, uzarin (Figure 3). Of note, these three plants have been used traditionally to treat diabetes, but lack the accompanying scientific evidence [68–70]. The identification of the compounds found in these plants with a potential anti-diabetic activity provide some rationale for the traditional use of these plants in the treatment of diabetes. The plants *Clivia miniata*, *Crinum bulbispermum*, *Danais fragans*, *Eucomis autumnalis*, *Gnidia kraussiana*, and *Typha capensis* were also of interest, as these plants were found to contain four or more compounds that had been previously identified as having potential anti-diabetic activity (Figure 3).

## 2.2. Identification of Potentially Important Scaffolds for Enzyme Activity

A hierarchical clustering analysis of the compounds identified in each protein target group was performed using Tanimoto similarities to identify whether any compounds showed some similar molecular features [11–13] (Figure S2). From these clustering results, the maximum common substructure (MCS) analysis was performed in an attempt to identify any potential scaffolds important for predicting the potential activity within the largest cluster group identified (Table 3). No clustering of compounds was found for six of the protein target-compound groups, namely INSR, liver receptor homolog-1 (NR5A2), pyruvate dehydrogenase kinase isoform 2 (PDK2), PPARA, protein tyrosine phosphatase non-receptor type 9 (PTPN9), liver glycogen phosphorylase (PYGL), and retinoid X receptor alpha (RXRA). This is not surprising, as these protein target-compound groups were relatively small groups, with the number of predicted active compounds below 50—the two exceptions being the free fatty acid receptor 1 (FFAR1) and the MGAM protein-compound groups, which had only 37 and 18 predicted active compounds, respectively. Within the FFAR1 and MGAM groups, two clusters of similar compounds were evident that encompassed the majority of the compounds within the groups, namely 26 of 37 for FFAR1 and 12 of 18 for MGAM. Interestingly though, the MCS analysis produced only relatively small scaffold structures for the similar compounds within these groups, namely, a phenol group for FFAR1 and a methoxyphenol for MGAM. The importance of the benzene ring with a substituent group was also evident in the protein-compound groups of glucokinase (GCK), PPARD, peroxisome proliferator-activated receptor gamma (PPARG), and retinol binding protein 4 (RBP4).

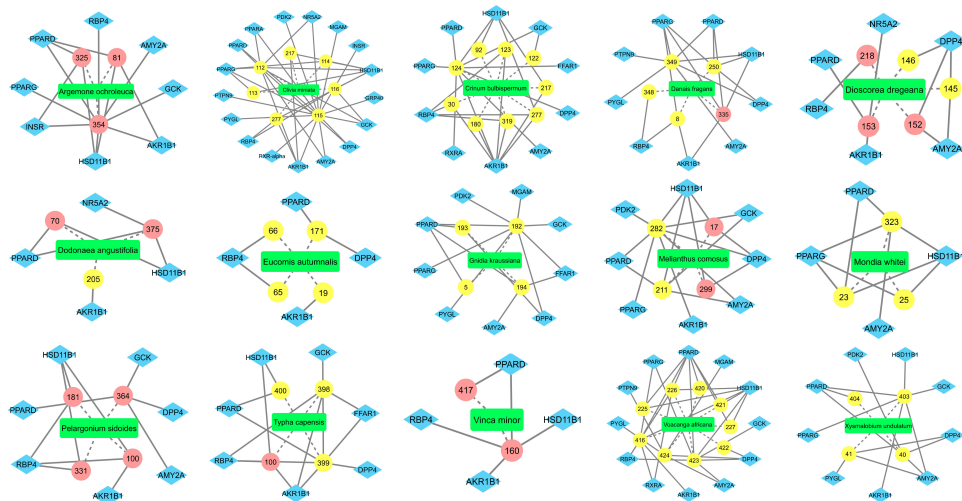


**Figure 3.** Fifteen plants identified as new sources rich in compounds with potential anti-diabetic activity for exploratory *in vitro* anti-diabetic studies. Compounds represented by their assigned numerical identity (Table S2); compounds represented by pink ellipses are compounds with previous literature on their anti-diabetic potential; compounds represented by yellow ellipses are novel compounds. Dashed edges represent the edges connecting the plant with its predicted bioactive compounds; solid edges represent the edges connecting the compounds with their predicted protein targets.

**Table 3.** Summary of hierarchical clustering and maximum common substructure found in the largest cluster for each protein target group.

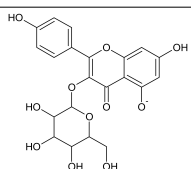
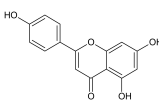
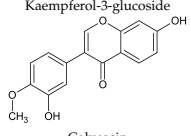
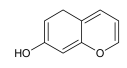
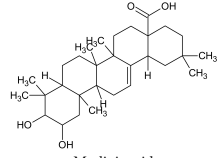
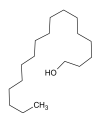
Target Enzyme	Total Number of Compounds	Largest Cluster	Cluster Centroid	Maximum Common Substructure
11HSDB1	208	40	 Kaempferol-3-glucoside	
AKR1B1	135	71	 Calycosin	
AMY2A	129	38	 Maslinic acid	

Table 3. Cont.

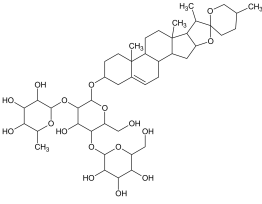
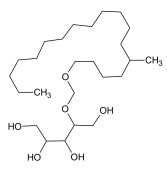
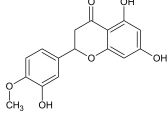
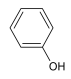
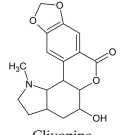
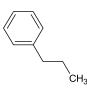
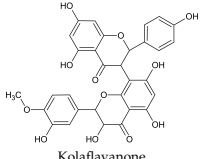
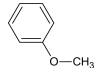
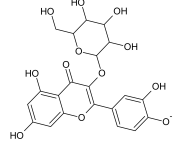
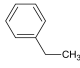
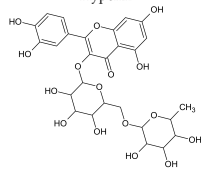
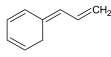
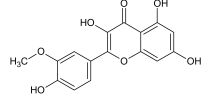
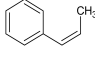
Target Enzyme	Total Number of Compounds	Largest Cluster	Cluster Centroid	Maximum Common Substructure
DPP4	149	23	 <p>Balanitin-6</p>	
FFAR1	37	26	 <p>Hesperitin</p>	
GCK	77	33	 <p>Clivonine</p>	

Table 3. Cont.

Target Enzyme	Total Number of Compounds	Largest Cluster	Cluster Centroid	Maximum Common Substructure
MGAM	18	12	 <p>Kolafavanone</p>	
PPARD	190	57	 <p>Hyperin</p>	
PPARG	124	89	 <p>Rutin</p>	
RBP4	85	48	 <p>Isorhamnetin</p>	



The hierarchical clustering analysis of the HSD11B1 group revealed a total of 37 different clusters (Figure S2), with the largest cluster containing 40 similar compounds, and based on an MCS analysis, an important scaffold for HSD11B1 activity would be a flavonoid type of backbone. Interestingly, three compounds found in this group, namely apigenin, quercetin, and genistein, were recently shown to inhibit HSD11B1 [71]. Similarly, in the aldose reductase (AKR1B1) group, the centroid of the largest cluster found was calycosin, an isoflavone, and the MCS was a benzopyranol scaffold that can be found in the backbone of flavonoids. As with HSD11B1, there is literature on the inhibitory activity of AKR1B1 by flavonoids and their glycosides [72,73]. For the DPP4 and pancreatic alpha-amylase (AMY2A) groups, a more hydrophobic core scaffold with a hydrophilic head/tail was observed as the MCS for these two protein targets. The compounds found in the largest cluster of these groups had predominately triterpenoid or steroidal backbones with/without a glycosidic group attached, such as shown in the two centroid compounds maslinic acid and balanitin-6. The compounds corosolic acid, betulinic acid, glycyrrhizin, and sitosterol-3-glucoside with this type of backbone found in the AMY2A group, have been shown in previous literature to inhibit the enzyme [52,66,74].

### 2.3. Molecular Similarity Evaluation of Predicted Active Compounds and Known/Experimental Anti-Diabetic Drugs

A Tanimoto similarity analysis was performed to determine whether any similar molecular features occurred between the natural compounds and known/experimental anti-diabetic drugs [11–13]. As seen in Figure 4, only a small portion (approximately 10%) of the predicted active compounds showed some similarity with the known anti-diabetic drugs. Thus, for the most part, natural compounds from African medicinal plants present rather novel and unique scaffolds for anti-diabetic drug design. The majority of these compounds showed similar molecular features to fasiglifam (TAK-875), an experimental FFAR1 agonist [2].

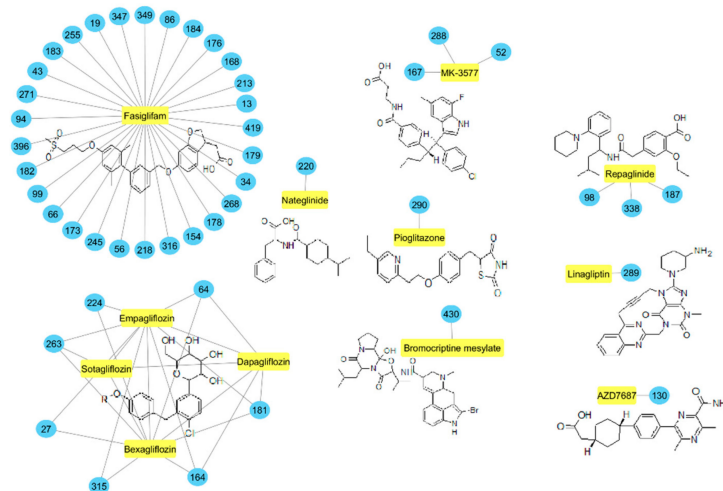


**Figure 4.** Molecular similarity analysis of predicted active compounds and some known/experimental anti-diabetic drugs. The similarity was performed on the extended connectivity fingerprint 4 (ECFP4) molecular fingerprints of compounds with a Tanimoto similarity cut-off score of 0.7.

Three of these compounds, namely, biochanin A (86), fujikinetin (176), and hesperitin (213), were also found by the DIA-DB web server as potential FFAR1 agonists; thus, these similarity studies with known drugs may further support their potential activity. Of interest was that seven of the predicted active compounds, namely, 8-hydroxy-pinonesin (27), aspalathin (64), epicatechin (164), gallicocatechin (181), hypoxoside (224), leucocyanidin (263), and pinonesin (315), showed some structural similarity

with the gliflozins bexagliflozin, dapagliflozin, empagliflozin, and sotagliflozin. The gliflozins are SGLT2 inhibitors [3]. Although SGLT2 was not included in the DIA-DB target screening panel, the similarity of these compounds with the known drugs may present SGLT2 as a novel anti-diabetic target for these seven compounds, and, of note, aspalathin has been found to be an inhibitor of SGLT2 [75]. Similarly, compounds carpanaquine (98), gelsemicine (187), and rauvoxinin (338), as well as hyoscyamine (220), showed some molecular similarity with repaglinide and nateglinide, respectively. Repaglinide and nateglinide are ATP-dependent potassium ( $K^+$ ) channel binders that stimulate the release of insulin from the pancreatic  $\beta$ -cells [76].

#### 2.4. Prediction of Oral Bioavailability and Favourable Absorption, Distribution, Metabolism, Excretion and Toxicity (ADMET) Properties of the Predicted Active Compounds

The oral bioavailability, as well as some ADMET parameters, were evaluated for each of the compounds. These are not only important parameters to evaluate for further drug development [11–13], but considering that in some areas where easy access to anti-diabetic medication is not always a possibility, an important way for patients to receive some form of anti-diabetic treatment would be through the use of a decoction from a medicinal plant having anti-diabetic properties. Therefore, factors such as the aqueous solubility and oral bioavailability of the bioactive compounds would be of great importance. Also, as several of the compounds investigated in this study were found in *Poisonous Plants of South Africa* [31], it is important to study the potential toxicity of these compounds.

The ADMET parameters for the predicted active compounds were compared to a group of 48 approved and experimental anti-diabetic drugs [2,3]. Also, a comparison of the ADMET parameters for the predicted active compounds with no previous literature (novel compounds) was compared to that of the predicted active compounds that had some previous literature on their potential anti-diabetic activity (known compounds). These known compounds would serve as another “positive control”.

A summary of the Lipinski’s rule of five is depicted in Figure 5. As can be seen from Figure 5, a major violation of Lipinski’s rule of five was the molecular weight of the compounds, with 30% of the predicted active compounds violating this rule, namely, that the molecular weight must not exceed 500 g/mol (Figure 5a) [77]. This was also the major violation for the anti-diabetic drug control group. The number of hydrogen bond donors and acceptors for the majority of predicted active compounds was within the limitations (Figure 5b,c). No compound was found to violate all four rules, and 16% had three violations—only acarbose in the anti-diabetic drug control group had three violations. Nearly 50% of the predicted active compounds violated one or more of Lipinski’s rule of five, versus only 25% of the anti-diabetic drug control group. This is not surprising, as often such target-specific anti-diabetic drugs are designed taking these factors into consideration. It was also observed that the compounds predicted as having poor oral absorption were also predicted to have poor Caco-2 cell permeability and vice versa (Figure 5d).

A complete summary of all of the ADMET parameters evaluated for the compounds can be found in Table 4. The two major toxicity failures and points of concern for the predicted active compounds were immunotoxicity and blockage of the hERG  $K^+$  channels, with 75% of the compounds being predicted as potential immunotoxins, and 45% predicted as potential inhibitors of the hERG  $K^+$  channels. Interestingly, these two toxicity parameters were also the two major failures for the anti-diabetic drug control group. The model for the prediction of immunotoxicity is built on a training set of T- and B-cell growth inhibition data from the National Cancer Institute [78]. In some cases, it is likely that the predicted immunotoxicity may rather be a function of the compound concentration than a specific effect, and also, the model cannot distinguish immunosuppressive effects from immunomodulatory or immunostimulant effects. The predictive model for the human ether-a-go-go-related gene potassium (hERG  $K^+$ ) channel blockage is often used to predict the potential cardiac toxicity of the compounds [79]. It was expected that some of the compounds would be predicted as potential cardiac toxins, as some of the predicted active compounds are known cardiac glycosides, such as digitoxin, tyledoside C, bovoside, oleandrin, proscillaridin A, scillaren A, uzarin, and gomphoside [31,80].

Molecules 2019, 24, 2002

16 of 30

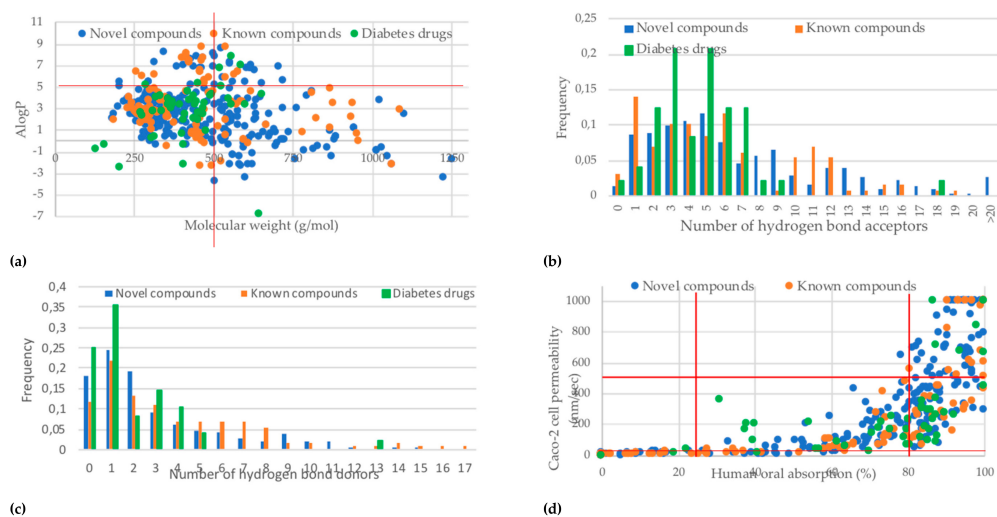


**Figure 5.** Prediction of druglikeness and bioavailability of hit compounds (novel and known) versus diabetic drugs (a) molecular weight versus AlogP, Lipinski's rule of five, namely: compounds need to have a molecular weight of 500 g/mol or less and AlogP must be below 5; (b) frequency of hydrogen bond acceptors, Lipinski's rule of five—not more than 10 hydrogen bond acceptors; (c) frequency of hydrogen bond donors, Lipinski's rule of five—not more than 5 hydrogen bond donors; (d) QikProp prediction of percent human oral absorption versus Caco-2 cell permeability, percentage oral bioavailability below 25% is poor and above 80% is high, predicted cell permeability for non-active transport below 25 nm<sup>2</sup>/s is poor, while above 500 nm<sup>2</sup>/s is very good.

**Table 4.** Summary of the Absorption, Distribution, Metabolism, Excretion and Toxicity (ADMET) parameters predicted *in silico* for predicted active compounds versus diabetes drugs.

ADMET Property	Unknown Compounds	Known Compounds	Diabetes Drugs
Lipinski violations (1–4)	136/305 (45%)	75/125 (60%)	12/48 (25%)
Veber violations (1–2)	89/305 (29%)	42/125 (36%)	9/48 (19%)
Aqueous solubility QPlogS	34/305 (11%)	33/125 (26%)	6/48 (13%)
Caco-2 cell permeability (<25 nm/s)	66/305 (22%)	40/125 (32%)	3/48 (6%)
Binding to human serum albumin	37/305 (12%)	23/125 (18%)	6/48 (13%)
Human oral absorption (<25%)	55/305 (18%)	32/125 (26%)	3/48 (6%)
Rat oral LD <sub>50</sub> (1–50 mg/kg)	53/305 (17%)	4/125 (3%)	1/48 (2%)
Hepatotoxicity	4/305 (1%)	4/125 (3%)	8/48 (17%)
Carcinogenicity	70/305 (23%)	31/125 (25%)	6/48 (13%)
Immunotoxicity	233/305 (76%)	89/125 (71%)	16/48 (33%)
Mutagenicity	49/305 (16%)	17/125 (14%)	1/48 (2%)
Cytotoxicity	58/305 (19%)	11/125 (9%)	1/48 (2%)
Blockage of hERG K <sup>+</sup> channels	132/305 (43%)	58/125 (46%)	20/48 (42%)

\* Recommended values: QPlogS: predicted aqueous solubility should be between  $-6.5$  and  $0.5 \text{ mol dm}^{-3}$ ; Caco-2 cell permeability:  $<25 \text{ nm/s}$  poor and  $>500 \text{ nm/s}$  great; Binding to human serum albumin: QPlogK<sub>h</sub> should be between  $-1.5$  and  $1.5$ ; Human oral absorption:  $<25\%$  poor and  $>80\%$  great; Rat oral LD<sub>50</sub>:  $<50 \text{ mg/kg}$  is fatal if swallowed; Blockage of hERG K<sup>+</sup> channels: concern if predicted QPlogHERG is  $<-5$ .

After taking all of the ADMET parameters into account, only 28 of the predicted active compounds were found to have favorable ADMET properties, and these are shown in Table 5. These compounds present novel scaffolds with potential anti-diabetic activity and favorable ADMET properties for further drug design and development. Of these 28 compounds, eight have shown anti-diabetic properties in previous studies, and these were 2-hydroxygenistein [81], apigenin [82], catechin [61], cyanidin [83], eburnamonine [67], epicatechin [84], eriodictyol [85], and lapachol [86].

Ten of the compounds, namely, apigenin, catechin, crotofoline A, cyanidin, eburnamonine, erythraline, henningsiine, nauclefidine, vinburnine, and voaphylline were predicted as potential inhibitors of three or more anti-diabetic targets. AKR1B1, HSD11B1, PPAR $\delta$ , and RBP4 were the major targets identified for the 28 compounds. Also, of particular note, was that the plant *Voacanga africana* was found to contain three of these compounds with favorable ADMET properties, namely vinburnine, voaphylline, and withasomnine, and two of these compounds, vinburnine and voaphylline, were identified as potential multi-targeted compounds. These observations provide some evidence for the traditional use of *Voacanga africana* in the treatment of diabetes and further *in vitro* and *in vivo* studies are now needed to validate its use for diabetes.

Table 5. Predicted active compounds with favorable ADMET properties.

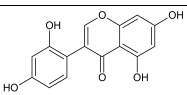
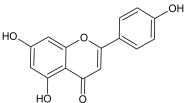
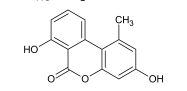
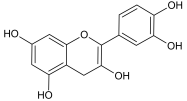
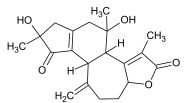
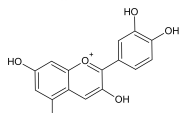
Compound	Structure	Predicted Targets (Docking Score in kcal/mol)	Potential Anti-Diabetic Effect	Plant
2-Hydroxygenistein		AKR1B1 (−9.1)	Regulation of glucose metabolism	<i>Cajanus cajan</i>
Apigenin		AKR1B1 (−9.1), HSD11B1 (−9.0), RBP4 (−9.9), and RXRA (−9.1)	Regulation of insulin secretion, glucose metabolism, and lipid metabolism	<i>Cajanus cajan</i>
Autumnarinol		RBP4 (−9.0)	Regulation of insulin secretion	<i>Eucomis autumnalis</i>
Catechin		AKR1B1 (−9.0), HSD11B1 (−9.5), and RBP4 (−9.3)	Regulation of insulin secretion and glucose metabolism	<i>Adansonia digitate</i> , <i>Combretum micranthum</i> , <i>Prunus africana</i> , <i>Sclerocarya birrea</i> , <i>Pelargonium sidoides</i> , and <i>Typha capensis</i>
Crotofoline A		AMY2A (−9.2), HSD11B1 (−9.9), and PPARD (−9.3)	Regulation of insulin secretion, glucose metabolism, and lipid metabolism	<i>Croton gratissimus</i>
Cyanidin		AKR1B1 (−9.1), HSD11B1 (−9.5), and RBP4 (−9.2)	Regulation of insulin secretion and glucose metabolism	<i>Rhoicissus tridentate</i>

Table 5. Cont.

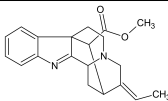
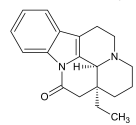
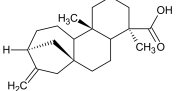
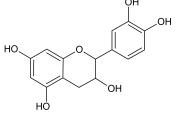
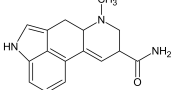
Compound	Structure	Predicted Targets (Docking Score in kcal/mol)	Potential Anti-Diabetic Effect	Plant
Desacetylformonoakammiline		HSD11B1 (-9.1), PPARD (-9.0)	Regulation of insulin secretion and lipid metabolism	<i>Rauwolfia vomitoria</i>
Eburnamonine		AKR1B1 (-9.4), HSD11B1 (-9.2), PPARD (-9.3), and RBP4 (-9.4)	Regulation of insulin secretion, glucose metabolism, and lipid metabolism	<i>Vinca minor</i>
Ent-16-kauran-19-oic acid		HSD11B1 (-9.4) and PPARD (-9.4)	Regulation of insulin secretion and lipid metabolism	<i>Aster bakeranus</i>
Epicatechin		AKR1B1 (-9.2) and RBP4 (-9.3)	Regulation of insulin secretion and glucose metabolism	<i>Acacia karroo</i> , <i>Harungana madagascariensis</i> , and <i>Prunus Africana</i>
Ergine		HSD11B1 (-9.5) and RBP4 (-9.4)	Regulation of insulin secretion	<i>Ipomoea purpurea</i>

Table 5. Cont.

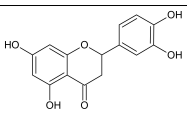
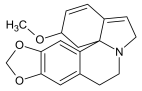
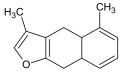
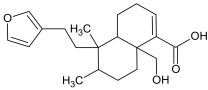
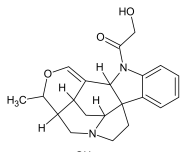
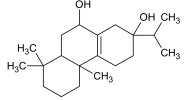
Compound	Structure	Predicted Targets (Docking Score in kcal/mol)	Potential Anti-Diabetic Effect	Plant
Eriodictyol		HSD11B1 (−9.2) and RBP4 (−9.5)	Regulation of insulin secretion	<i>Cyclopia intermedia</i>
Erythraline		AKR1B1 (−9.0), GCK (−9.8), and RBP4 (−9.0)	Regulation of insulin secretion and glucose metabolism	<i>Erythrina caffra</i> and <i>Erythrina lysistemon</i>
Furanoedesma-1,3-diene		RBP4 (−9.0)	Regulation of insulin secretion	<i>Commiphora myrrha</i>
Hautriwaic acid		AKR1B1 (−9.3)	Regulation of glucose metabolism	<i>Dodonaea angustifolia</i>
Henningsiine		AMY2A (−9.1), HSD11B1 (−9.6), PPARD (−10.0), and PPARG (−9.0)	Regulation of insulin secretion, glucose metabolism, and lipid metabolism	<i>Strychnos henningsii</i>
Ibozol		GCK (−9.7)	Regulation of glucose metabolism	<i>Tetradenia riparia</i>

Table 5. Cont.

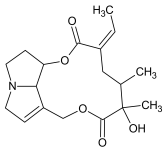
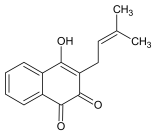
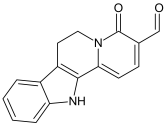
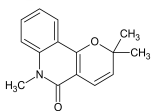
Compound	Structure	Predicted Targets (Docking Score in kcal/mol)	Potential Anti-Diabetic Effect	Plant
Integerrimine		HSD11B1 (−9.1) and PPAR $\delta$ (−9.3)	Regulation of insulin secretion and lipid metabolism	<i>Lotononis laxa</i>
Lapachol		AKR1B1 (−9.2)	Regulation of glucose metabolism	<i>Kigelia africana</i>
Nauclefidine		AKR1B1 (−10.1), HSD11B1 (−9.0), and RBP4 (−10.0)	Regulation of insulin secretion and glucose metabolism	<i>Nauclea latifolia</i>
N-methylflindersine		AKR1B1 (−9.2) and RBP4 (−9.5)	Regulation of insulin secretion and glucose metabolism	<i>Toddalia asiatica</i>



Table 5. Cont.

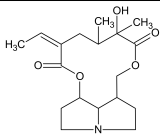
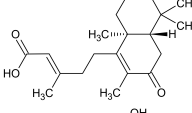
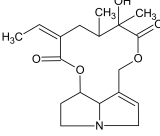
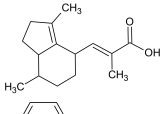
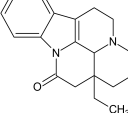
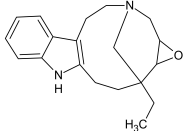
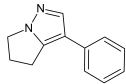
Compound	Structure	Predicted Targets (Docking Score in kcal/mol)	Potential Anti-Diabetic Effect	Plant
Platyphylline		HSD11B1 (−9.4) and PPAR $\delta$ (−9.3)	Regulation of insulin secretion and lipid metabolism	<i>Senecio serratuloides</i>
Rhinocerotoic acid		HSD11B1 (−9.2) and RBP4 (−9.9)	Regulation of insulin secretion	<i>Elytropappus rhinocerotis</i>
Senecionine		HSD11B1 (−10.3) and PPAR $\delta$ (−9.4)	Regulation of insulin secretion and lipid metabolism	<i>Senecio serratuloides</i>
Valerenic acid		AKR1B1 (−9.0)	Regulation of glucose metabolism	<i>Valeriana capensis</i>
Vinburnine		AKR1B1 (−9.6), HSD11B1 (−9.1), PPAR $\delta$ (−9.3), PPAR $\gamma$ (−9.4), RBP4 (−10.7), and RXRA (−9.3)	Regulation of insulin secretion, glucose metabolism and lipid metabolism	<i>Voacanga africana</i>

Table 5. Cont.

Compound	Structure	Predicted Targets (Docking Score in kcal/mol)	Potential Anti-Diabetic Effect	Plant
Voaphylline		AMY2A (−9.0), DPP4 (−9.6), GCK (−9.1), HSD11B1 (−9.3), PPARD (−9.1), PPARG (−9.8), and RBP4 (−9.2)	Regulation of insulin secretion, glucose metabolism, and lipid metabolism	<i>Voacanga africana</i>
Withasomnine		FFAR1 (−9.1)	Regulation of insulin secretion	<i>Voacanga africana</i>

### 3. Materials and Methods

#### 3.1. Preparation of Compound Structures and Inverse Virtual Screening of Potential Anti-Diabetic Activity

The natural compounds were sourced from three books that catalogue the different medicinal plants found in Africa, as well as their medicinal uses and chemical constituents. These three books were *African Herbal Pharmacopoeia* [87], *Medicinal Plants of South Africa* [80], and *Poisonous Plants of South Africa* [31]. Where a graphical representation of the compound was given in the books, the two-dimensional structure of the compounds was created with Advanced Chemistry Development (ACD)/ChemSketch freeware version 12.02, 2010 [88], and then converted to its representative simplified molecular-input line-entry system (SMILES) notation. Where only the name of the compound was given, the two-dimensional structure and SMILES notation was obtained from PubChem [89]. The SMILES notations for the compounds analyzed in this study can be found in Table S1.

The SMILES notation of each compound was subsequently submitted to the DIA-DB web server that employs inverse virtual screening of compounds with Autodock Vina against a given set of 17 protein targets associated with diabetes [14]. These targets were AKR1B1, DPP4, FFAR1, GCK, HSD11B1, INSR, MGAM, PYGL, NR5A2, AMY2A, PPARA, PPAR, PPARG, PTPN9, PDK2, RXRA, and RBP4.

A cutoff docking score of  $-9$  kcal/mol was set to distinguish between potential active and inactive compounds. The predicted compound–target network was generated by Cytoscape version 3.4.0 [90], and the NetworkAnalyzer Application version 2.7 [91] was used to evaluate some of the basic network features.

#### 3.2. Clustering and Maximum Common Substructure Analysis of Predicted Active Compounds

A hierarchical clustering analysis was performed for each compound–target group using Schrödinger Canvas Suite version 3.2.013 [92]. The molecular fingerprint was calculated from the two-dimensional structure of the compounds in the form of extended connectivity fingerprint 4 (ECFP4). From these fingerprints, a hierarchical clustering analysis was performed using the metric of the Tanimoto similarity and the average cluster linkage method, which clusters according to the average distance between all of the inter-cluster pairs. An MCS analysis was then performed on the largest cluster identified within each compound–target group using the criteria of atomic number, aromaticity, and bond order.

#### 3.3. Similarity Studies with Known/Experimental Anti-Diabetic Drugs

The known/experimental anti-diabetic drugs were sourced from Defronzo et al., 2014 [2], and Gougari et al., 2017 [3], and their SMILES representations were obtained from PubChem. The molecular similarity network was generated with Cytoscape and the ChemViz2 Application version 1.1.0 [93]. The molecular similarity was performed using the metric of the Tanimoto similarity on the calculated ECFP4 molecular fingerprints of the compounds. A Tanimoto score of 0.7 or greater indicated molecular similarity.

#### 3.4. Studies on Oral Bioavailability and ADMET Properties of the Predicted Active Compounds

The physiochemical descriptors of molecular weight, AlogP, hydrogen bond acceptors, hydrogen bond donors, number of rotatable bonds, and polar surface area were calculated from the two-dimensional structures of the compounds using the Schrödinger Canvas Suite [92]. For the calculation of the QikProp descriptors, three-dimensional structures of the compounds were generated and optimized with LigPrep from Schrödinger Maestro version 11.2.013 [94]. The QikProp descriptors of aqueous solubility (QPlogS), Caco-2 cell permeability, binding to human serum albumin, percent human oral absorption, and blockage of the hERG K<sup>+</sup> channels, were subsequently calculated from the three-dimensional structures with the Schrödinger Canvas Suite. The ProTox-II web server was used to predict the potential toxicity of the compounds from their SMILES notation representations [95].

The rat oral lethal dose 50 (LD50), hepatotoxicity, carcinogenicity, cytotoxicity, mutagenicity, and immunotoxicity were evaluated with the ProTox-II web server.

#### 4. Conclusions

African medicinal plants were identified as rich sources of compounds with potential anti-diabetic activity through the use of inverse virtual screening with the DIA-DB web server (Figure 6). The observation that some of the compounds identified with the DIA-DB web server had some previous literature on their potential anti-diabetic activity provided validation for the use of the DIA-DB web server for the identification of compounds with potential anti-diabetic activity. Also, the identification of compounds with previous literature on their potential anti-diabetic activity provided some clues as to the bioactive constituents of medicinal plants with known anti-diabetic activity, as well as the rationale for the traditional use of some medicinal plants.

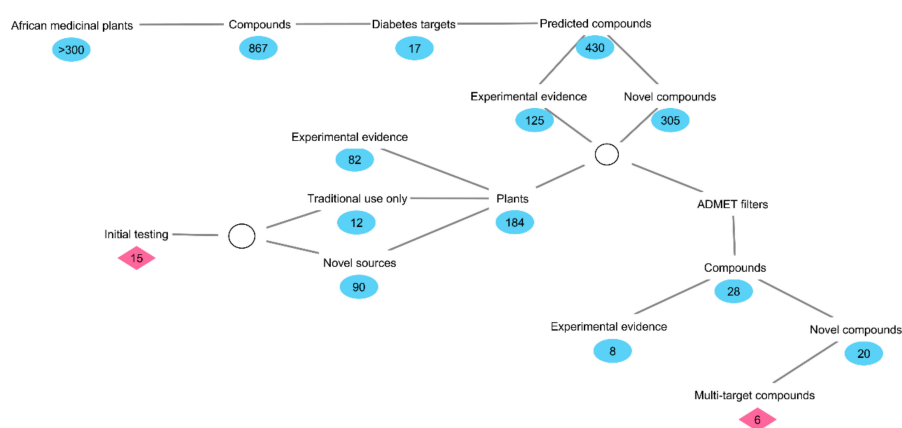


**Figure 6.** A brief summary of the methodology and results obtained for the *in silico* exploration of African medicinal plants for potential anti-diabetic compounds.

Several plants were identified as new sources rich in compounds with potential anti-diabetic activity, and included *Argemone ochroleuca*, *Clivia miniata*, *Crinum bulbispermum*, *Danais fragans*, *Dioscorea dregeana*, *Dodonaea angustifolia*, *Eucomis autumnalis*, *Gnidia kraussiana*, *Melianthus comosus*, *Mondia whitei*, *Pelargonium sidoides*, *Typha capensis*, *Vinca minor*, *Voacanga Africana*, and *Xysmalobium undulatum*. These plants represent a good initial point for exploratory *in vitro* anti-diabetic studies. As for the compounds, a total of 28 compounds were identified as having favorable ADMET properties, and importantly, several of these were identified as novel potential multi-targeted anti-diabetic compounds, such as crotofoline A, erythraline, henningsiine, nauclefidine, vinburnine, and voaphylline. These compounds present as novel scaffolds for further drug design and development. There is now the need for further *in vitro* and *in vivo* studies to confirm the potential bioactivity of these compounds identified by the DIA-DB web server.

**Supplementary Materials:** The following are available online at <http://www.mdpi.com/1420-3049/24/10/2002/s1>: Table S1—SMILES notations of all compounds evaluated in the study. Table S2—Assigned numerical identity of predicted active compounds, their plant sources and predicted targets. Figure S1—Individual predicted active compound–protein target networks. Table S3—Plants having scientific anti-diabetic evidence and evidence of traditional use only identified by virtual screening and their predicted bioactive compounds. Figure S2—Dendrograms of hierarchical clustering analysis.

**Author Contributions:** The roles of the authors in this manuscript were as follows: conceptualization, A.S.P.P., H.P.-S., and Z.A.; methodology, A.S.P.P., H.d.D., J.P.-G., and M.M.M.; software, A.S.P.P., H.d.D., J.P.-G., and M.M.M.; validation, A.S.P.P., H.d.D., J.P.-G., and M.M.M.; formal analysis, H.P.-S. and Z.A.; investigation, A.S.P.P., H.P.-S., and Z.A.; resources, H.P.-S. and Z.A.; data curation, A.S.P.P.; writing (original draft preparation), A.S.P.P.;

writing (review and editing), H.P.-S. and Z.A.; visualization, A.S.P.P. and Z.A.; supervision, H.P.-S. and Z.A.; project administration, H.P.-S. and Z.A.; funding acquisition, H.P.-S. and Z.A.

**Funding:** The National Research Foundation of South Africa provided support for the postdoctoral fellowship of ASP Pereira. This work has been partly funded by a grant from the Spanish Ministry of Economy and Competitiveness (CTQ2017-87974-R) and by the Fundación Séneca del Centro de Coordinación de la Investigación de la Región de Murcia under Projects 20988/PI/18 and 20524/PDC/18. This research was partially supported by the supercomputing infrastructure of Poznan Supercomputing Center, by the e-infrastructure program of the Research Council of Norway, and the supercomputer center of UiT—the Arctic University of Norway. The authors also thankfully acknowledge the computer resources and the technical support provided by the Plataforma Andaluza de Bioinformática of the University of Málaga. Powered@NLHPC: This research was partially supported by the supercomputing infrastructure of the NLHPC (ECM-02).

**Conflicts of Interest:** The authors declare no conflict of interest.

## References

1. World Health Organization. Fact Sheet. 15 November 2017. Available online: <http://www.who.int/news-room/fact-sheet/detail/diabetes> (accessed on 10 April 2019).
2. DeFronzo, R.A.; Triplitt, C.L.; Abdul-Ghani, M.; Cersosimo, E. Novel agents for the treatment of type 2 diabetes. *Diabetes Spectr.* **2014**, *27*, 100–112. [[CrossRef](#)] [[PubMed](#)]
3. Gourgari, E.; Wilhelm, E.E.; Hassanzadeh, H.; Aroda, V.R.; Shoulson, I. A comprehensive review of the FDA-approved labels of diabetes drugs: Indications, safety, and emerging cardiovascular safety data. *J. Diabetes Complicat.* **2017**, *31*, 1719–1727. [[CrossRef](#)]
4. Abo, K.; Fred-Jaiyesimi, A.; Jaiyesimi, A. Ethnobotanical studies of medicinal plants used in the management of diabetes mellitus in South Western Nigeria. *J. Ethnopharmacol.* **2008**, *115*, 67–71. [[CrossRef](#)]
5. Bahmani, M.; Zargarani, A.; Rafieian-Kopaei, M.; Saki, K. Ethnobotanical study of medicinal plants used in the management of diabetes mellitus in the Urmia, Northwest Iran. *Asian Pac. J. Trop. Med.* **2014**, *7*, S348–S354. [[CrossRef](#)]
6. Deutschländer, M.; Lall, N.; Van De Venter, M. Plant species used in the treatment of diabetes by South African traditional healers: An inventory. *Pharm. Biol.* **2009**, *47*, 348–365. [[CrossRef](#)]
7. Grover, J.; Yadav, S.; Vats, V. Medicinal plants of India with anti-diabetic potential. *J. Ethnopharmacol.* **2002**, *81*, 81–100. [[CrossRef](#)]
8. Li, W.; Zheng, H.; Bukuru, J.; De Kimpe, N. Natural medicines used in the traditional Chinese medical system for therapy of diabetes mellitus. *J. Ethnopharmacol.* **2004**, *92*, 1–21. [[CrossRef](#)] [[PubMed](#)]
9. Ghadge, A.A.; Kuvalekar, A.A. Controversy of oral hypoglycemic agents in type 2 diabetes mellitus: Novel move towards combination therapies. *Diabetes Metab. Syndr. Clin. Res. Rev.* **2017**, *11*, S5–S13. [[CrossRef](#)]
10. Prabhakar, P.; Kumar, A.; Doble, M. Combination therapy: A new strategy to manage diabetes and its complications. *Phytomedicine* **2014**, *21*, 123–130. [[CrossRef](#)]
11. Chen, B.-W.; Li, W.-X.; Wang, G.-H.; Li, G.-H.; Liu, J.-Q.; Zheng, J.-J.; Wang, Q.; Li, H.-J.; Dai, S.-X.; Huang, J.-F. A strategy to find novel candidate anti-Alzheimer's disease drugs by constructing interaction networks between drug targets and natural compounds in medical plants. *PeerJ* **2018**, *6*, e4756. [[CrossRef](#)]
12. Dai, S.-X.; Li, W.-X.; Han, F.-F.; Guo, Y.-C.; Zheng, J.-J.; Liu, J.-Q.; Wang, Q.; Gao, Y.-D.; Li, G.-H.; Huang, J.-F. *In silico* identification of anti-cancer compounds and plants from traditional Chinese medicine database. *Sci. Rep.* **2016**, *6*, 25462. [[CrossRef](#)]
13. Liu, J.-Q.; Dai, S.-X.; Zheng, J.-J.; Guo, Y.-C.; Li, W.-X.; Li, G.-H.; Huang, J.-F. The identification and molecular mechanism of anti-stroke traditional Chinese medicinal compounds. *Sci. Rep.* **2017**, *7*, 41406. [[CrossRef](#)]
14. Sánchez-Pérez, A.; Muñoz, A.; Peña-García, J.; den-Haan, H.; Bekas, N.; Katsikoudi, A.; Tzakos, A.G.; Pérez-Sánchez, H. DIA-DB: A Web-Accessible Database for the Prediction of Diabetes Drugs. In *International Conference on Bioinformatics and Biomedical Engineering, 2015*; Springer: New York, NY, USA, 2015; pp. 655–663.
15. Aronoff, S.L.; Berkowitz, K.; Shreiner, B.; Want, L. Glucose metabolism and regulation: Beyond insulin and glucagon. *Diabetes Spectr.* **2004**, *17*, 183–190. [[CrossRef](#)]
16. Wagner, R.; Kaiser, G.; Gerst, F.; Christiansen, E.; Due-Hansen, M.E.; Grundmann, M.; Machicao, F.; Peter, A.; Kostenis, E.; Ulven, T. Reevaluation of fatty acid receptor 1 (FFAR1/GPR40) as drug target for the stimulation of insulin secretion in humans. *Diabetes* **2013**, *62*, 2106–2111. [[CrossRef](#)]

17. Stulnig, T.; Waldhäusl, W.  $11\beta$ -hydroxysteroid dehydrogenase type 1 in obesity and type 2 diabetes. *Diabetologia* **2004**, *47*, 1–11. [[CrossRef](#)] [[PubMed](#)]
18. Saltiel, A.R.; Kahn, C.R. Insulin signalling and the regulation of glucose and lipid metabolism. *Nature* **2001**, *414*, 799–806. [[CrossRef](#)]
19. Herman, M.A.; Kahn, B.B. Glucose transport and sensing in the maintenance of glucose homeostasis and metabolic harmony. *J. Clin. Invest.* **2006**, *116*, 1767–1775. [[CrossRef](#)] [[PubMed](#)]
20. Yabe-Nishimura, C. Aldose reductase in glucose toxicity: A potential target for the prevention of diabetic complications. *Pharmacol. Rev.* **1998**, *50*, 21–34.
21. Etxeberria, U.; de la Garza, A.L.; Campión, J.; Martínez, J.A.; Milagro, F.I. Antidiabetic effects of natural plant extracts via inhibition of carbohydrate hydrolysis enzymes with emphasis on pancreatic alpha amylase. *Expert Opin. Ther. Targets* **2012**, *16*, 269–297. [[CrossRef](#)]
22. Jeoung, N.H. Pyruvate dehydrogenase kinases: Therapeutic targets for diabetes and cancers. *Diabetes Metab. J.* **2015**, *39*, 188–197. [[CrossRef](#)]
23. Martin, J.; Veluraja, K.; Ross, K.; Johnson, L.; Fleet, G.; Ramsden, N.; Bruce, I.; Orchard, M.; Oikonomakos, N. Glucose analog inhibitors of glycogen phosphorylase: The design of potential drugs for diabetes. *Biochemistry* **1991**, *30*, 10101–10116. [[CrossRef](#)]
24. Mellado-Gil, J.M.; Cobo-Vuilleumier, N.; Gauthier, B.R. Islet  $\beta$ -cell mass preservation and regeneration in diabetes mellitus: Four factors with potential therapeutic interest. *J. Transplant.* **2012**, *2012*, 230870. [[CrossRef](#)]
25. Monsalve, F.A.; Pyarasani, R.D.; Delgado-Lopez, F.; Moore-Carrasco, R. Peroxisome proliferator-activated receptor targets for the treatment of metabolic diseases. *Mediat. Inflamm.* **2013**, *2013*, 549627. [[CrossRef](#)]
26. Moller, D.E. New drug targets for type 2 diabetes and the metabolic syndrome. *Nature* **2001**, *414*, 821–827. [[CrossRef](#)]
27. Csermely, P.; Agoston, V.; Pongor, S. The efficiency of multi-target drugs: The network approach might help drug design. *Trends Pharmacol. Sci.* **2005**, *26*, 178–182. [[CrossRef](#)]
28. Peters, J.-U. Polypharmacology—foe or friend? *J. Med. Chem.* **2013**, *56*, 8955–8971. [[CrossRef](#)]
29. Reddy, A.S.; Zhang, S. Polypharmacology: Drug discovery for the future. *Expert Rev. Clin. Pharmacol.* **2013**, *6*, 41–47. [[CrossRef](#)]
30. Cho, Y.; Kang, Y.; Lee, S.; Lee, J.; Park, J.-Y.; Lee, W.; Kim, Y.-J.; Jung, C. Efficacy and safety of combination therapy with SGLT2 and DPP4 inhibitors in the treatment of type 2 diabetes: A systematic review and meta-analysis. *Diabetes Metab.* **2018**, *44*, 393–401. [[CrossRef](#)]
31. Van Wyk, B.-E.; Heerden, F.v.; Oudtshoorn, B.v. *Poisonous Plants of South Africa*; Briza Publications: Pretoria, South Africa, 2002.
32. Beltrán-Debón, R.; Rull, A.; Rodríguez-Sanabria, F.; Iswaldi, I.; Herranz-López, M.; Aragonès, G.; Camps, J.; Alonso-Villaverde, C.; Menéndez, J.; Micol, V. Continuous administration of polyphenols from aqueous rooibos (*Aspalathus linearis*) extract ameliorates dietary-induced metabolic disturbances in hyperlipidemic mice. *Phytomedicine* **2011**, *18*, 414–424. [[CrossRef](#)]
33. Kamakura, R.; Son, M.J.; de Beer, D.; Joubert, E.; Miura, Y.; Yagasaki, K. Antidiabetic effect of green rooibos (*Aspalathus linearis*) extract in cultured cells and type 2 diabetic model KK-A y mice. *Cytotechnology* **2015**, *67*, 699–710. [[CrossRef](#)]
34. Muller, C.; Joubert, E.; De Beer, D.; Sanderson, M.; Malherbe, C.; Fey, S.; Louw, J. Acute assessment of an aspalathin-enriched green rooibos (*Aspalathus linearis*) extract with hypoglycemic potential. *Phytomedicine* **2012**, *20*, 32–39. [[CrossRef](#)]
35. Bierer, D.E.; Fort, D.M.; Mendez, C.D.; Luo, J.; Imbach, P.A.; Dubenko, L.G.; Jolad, S.D.; Gerber, R.E.; Litvak, J.; Lu, Q. Ethnobotanical-directed discovery of the antihyperglycemic properties of cryptolepine: Its isolation from *Cryptolepis sanguinolenta*, synthesis, and *in vitro* and *in vivo* activities. *J. Med. Chem.* **1998**, *41*, 894–901. [[CrossRef](#)]
36. Adaramoye, O. Antidiabetic effect of kolaviron, a biflavonoid complex isolated from *Garcinia kola* seeds, in Wistar rats. *African Health Sci.* **2012**, *12*, 498–506. [[CrossRef](#)]
37. Adaramoye, O.; Adeyemi, E. Hypoglycaemic and hypolipidaemic effects of fractions from kolaviron, a biflavonoid complex from *Garcinia kola* in streptozotocin-induced diabetes mellitus rats. *J. Pharm. Pharmacol.* **2006**, *58*, 121–128. [[CrossRef](#)]
38. Saxena, S. *Glycyrrhiza glabra*: Medicine over the millennium. *Nat. Prod. Radianc* **2005**, *4*, 358–367.

39. Vermaak, I.; Hamman, J.H.; Viljoen, A.M. *Hoodia gordonii*: An up-to-date review of a commercially important anti-obesity plant. *Planta Med.* **2011**, *77*, 1149–1160. [[CrossRef](#)]
40. Gao, D.; Li, Q.; Li, Y.; Liu, Z.; Fan, Y.; Liu, Z.; Zhao, H.; Li, J.; Han, Z. Antidiabetic and antioxidant effects of oleanolic acid from *Ligustrum lucidum* Ait in alloxan-induced diabetic rats. *Phytother. Res.* **2009**, *23*, 1257–1262. [[CrossRef](#)]
41. Muhammad, H.I.; Asmawi, M.Z.; Khan, N.A.K. A review on promising phytochemical, nutritional and glycemic control studies on *Moringa oleifera* Lam. in tropical and sub-tropical regions. *Asian Pac. J. Trop. Biomed.* **2016**, *6*, 896–902. [[CrossRef](#)]
42. Sato, H.; Genet, C.; Strehle, A.; Thomas, C.; Lobstein, A.; Wagner, A.; Mioskowski, C.; Auwerx, J.; Saladin, R. Anti-hyperglycemic activity of a TGR5 agonist isolated from *Olea europaea*. *Biochem. Biophys. Res. Commun.* **2007**, *362*, 793–798. [[CrossRef](#)]
43. Bellesia, A.; Verzelloni, E.; Tagliazucchi, D. Pomegranate ellagitannins inhibit  $\alpha$ -glucosidase activity *in vitro* and reduce starch digestibility under simulated gastro-intestinal conditions. *Int. J. Food Sci. Nutr.* **2015**, *66*, 85–92. [[CrossRef](#)]
44. Ahmed, O.M.; Moneim, A.A.; Yazid, I.A.; Mahmoud, A.M. Antihyperglycemic, antihyperlipidemic and antioxidant effects and the probable mechanisms of action of *Ruta graveolens* infusion and rutin in nicotinamide-streptozotocin-induced diabetic rats. *Diabetol. Croat.* **2010**, *39*, 15–35.
45. Wu, C.; Luan, H.; Wang, S.; Zhang, X.; Wang, R.; Jin, L.; Guo, P.; Chen, X. Modulation of lipogenesis and glucose consumption in HepG2 cells and C2C12 myotubes by sophoricoside. *Molecules* **2013**, *18*, 15624–15635. [[CrossRef](#)]
46. Musabayane, C.; Tufts, M.; Mapanga, R. Synergistic antihyperglycemic effects between plant-derived oleanolic acid and insulin in streptozotocin-induced diabetic rats. *Ren. Fail.* **2010**, *32*, 832–839. [[CrossRef](#)]
47. Ong, K.W.; Hsu, A.; Song, L.; Huang, D.; Tan, B.K.H. Polyphenols-rich *Vernonia amygdalina* shows anti-diabetic effects in streptozotocin-induced diabetic rats. *J. Ethnopharmacol.* **2011**, *133*, 598–607. [[CrossRef](#)]
48. Gorelick, J.; Rosenberg, R.; Smotrich, A.; Hanuš, L.; Bernstein, N. Hypoglycemic activity of withanolides and elicited *Withania somnifera*. *Phytochemistry* **2015**, *116*, 283–289. [[CrossRef](#)]
49. Yin, J.; Ye, J.; Jia, W. Effects and mechanisms of berberine in diabetes treatment. *Acta Pharm. Sinica B* **2012**, *2*, 327–334. [[CrossRef](#)]
50. Moser, C.; Vickers, S.P.; Brammer, R.; Cheetham, S.C.; Drewe, J. Antidiabetic effects of the *Cimicifuga racemosa* extract Ze 450 *in vitro* and *in vivo* in ob/ob mice. *Phytomedicine* **2014**, *21*, 1382–1389. [[CrossRef](#)]
51. Choi, J.; He, N.; Sung, M.K.; Yang, Y.; Yoon, S. Sanguinarine is an allosteric activator of AMP-activated protein kinase. *Biochem. Biophys. Res. Commun.* **2011**, *413*, 259–263. [[CrossRef](#)]
52. Ye, X.-P.; Song, C.-Q.; Yuan, P.; Mao, R.-G.  $\alpha$ -Glucosidase and  $\alpha$ -Amylase Inhibitory Activity of Common Constituents from Traditional Chinese Medicine Used for Diabetes Mellitus. *Chin. J. Nat. Med.* **2010**, *8*, 349–352. [[CrossRef](#)]
53. Yu, H.; Zheng, L.; Xu, L.; Yin, L.; Lin, Y.; Li, H.; Liu, K.; Peng, J. Potent effects of the total saponins from *Dioscorea nipponica* Makino against streptozotocin-induced type 2 diabetes mellitus in rats. *Phytother. Res.* **2015**, *29*, 228–240. [[CrossRef](#)]
54. Ghosh, S.; More, P.; Derle, A.; Patil, A.B.; Markad, P.; Asok, A.; Kumbhar, N.; Shaikh, M.L.; Ramanamurthy, B.; Shinde, V.S.; et al. Diosgenin from *Dioscorea bulbifera*: Novel hit for treatment of type II diabetes mellitus with inhibitory activity against alpha-amylase and alpha-glucosidase. *PLoS ONE* **2014**, *9*, e106039. [[CrossRef](#)] [[PubMed](#)]
55. Inthongkaew, P.; Chatsumpun, N.; Supasuteekul, C.; Kitisripanya, T.; Putalun, W.; Likhitwitayawuid, K.; Sritularak, B.  $\alpha$ -Glucosidase and pancreatic lipase inhibitory activities and glucose uptake stimulatory effect of phenolic compounds from *Dendrobium formosum*. *Revista Brasileira de Farmacogn* **2017**, *27*, 480–487. [[CrossRef](#)]
56. Saeidnia, S.; Manayi, A.; Gohari, A.R.; Abdollahi, M. The story of B-sitosterol—A review. *Eur. J. Med. Plants* **2014**, *4*, 590–610. [[CrossRef](#)]
57. Somsak, N.; Peerawit, P.; Chusri, T. Hypoglycemic activity in diabetic rats of stigmaterol and sitosterol-3-O- $\beta$ -D-glucopyranoside isolated from *Pseuderanthemum palatiferum* (Nees) Radlk. leaf extract. *J. Med. Plants Res.* **2015**, *9*, 629–635. [[CrossRef](#)]
58. Panda, S.; Jafri, M.; Kar, A.; Meheta, B.K. Thyroid inhibitory, antiperoxidative and hypoglycemic effects of stigmaterol isolated from *Butea monosperma*. *Fitoterapia* **2009**, *80*, 123–126. [[CrossRef](#)] [[PubMed](#)]

59. Wen, X.; Sun, H.; Liu, J.; Cheng, K.; Zhang, P.; Zhang, L.; Hao, J.; Zhang, L.; Ni, P.; Zographos, S.E. Naturally Occurring Pentacyclic Triterpenes as Inhibitors of Glycogen Phosphorylase: Synthesis, Structure-Activity Relationships, and X-ray Crystallographic Studies. *J. Med. Chem.* **2008**, *51*, 3540–3554. [[CrossRef](#)]
60. Castellano, J.M.; Guinda, A.; Delgado, T.; Rada, M.; Cayuela, J.A. Biochemical basis of the antidiabetic activity of oleanolic acid and related pentacyclic triterpenes. *Diabetes* **2013**, *62*, 1791–1799. [[CrossRef](#)] [[PubMed](#)]
61. Daisy, P.; Balasubramanian, K.; Rajalakshmi, M.; Eliza, J.; Selvaraj, J. Insulin mimetic impact of Catechin isolated from *Cassia fistula* on the glucose oxidation and molecular mechanisms of glucose uptake on Streptozotocin-induced diabetic Wistar rats. *Phytomedicine* **2010**, *17*, 28–36. [[CrossRef](#)]
62. Kamiyama, O.; Sanae, F.; Ikeda, K.; Higashi, Y.; Minami, Y.; Asano, N.; Adachi, I.; Kato, A. *In vitro* inhibition of  $\alpha$ -glucosidases and glycogen phosphorylase by catechin gallates in green tea. *Food Chem.* **2010**, *122*, 1061–1066. [[CrossRef](#)]
63. Murase, T.; Misawa, K.; Haramizu, S.; Hase, T. Catechin-induced activation of the LKB1/AMP-activated protein kinase pathway. *Biochem. Pharmacol.* **2009**, *78*, 78–84. [[CrossRef](#)] [[PubMed](#)]
64. Aguirre, L.; Arias, N.; Macarulla, M.T.; Gracia, A.; Portillo, M.P. Beneficial Effects of Quercetin on Obesity and Diabetes. *Open Nutraceuticals* **2011**, *4*, 189–199.
65. Bedekar, A.; Shah, K.; Koffas, M. Natural Products for Type II Diabetes Treatment. In *Natural Products for Type II Diabetes Treatment: Advances in Applied Microbiology*; Laskin, A.I., Gadd, G.M., Sariaslani, S., Eds.; Elsevier Science: San Diego, CA, USA, 2010; Volume 17, pp. 21–73.
66. Pullbutr, P.; Nualkaew, S.; Rattanakit, S.; Cushnie, B.; Jaruchotikamol, A. Inhibitory actions of *Pseuderanthemum palatiferum* (Nees) Radlk. leaf ethanolic extract and its phytochemicals against carbohydrate-digesting enzymes. *Asian Pac. J. Trop. Biomed.* **2016**, *6*, 93–99. [[CrossRef](#)]
67. Marles, R.J.; Farnsworth, N.R. Antidiabetic plants and their active constituents. *Phytomedicine* **1995**, *2*, 137–189. [[CrossRef](#)]
68. Kpodar, M.S.; Lawson-Evi, P.; Bakoma, B.; Eklu-Gadegbeku, K.; Agbonon, A.; Aklirikou, K.; Gbeassor, M. Ethnopharmacological survey of plants used in the treatment of diabetes mellitus in south of Togo (Maritime Region). *J. Herb. Med.* **2015**, *5*, 147–152. [[CrossRef](#)]
69. Bading Taika, B.; Bouckandou, M.; Souza, A.; Bourobou Bourobou, H.P.; MacKenzie, L.S.; Lione, L. An overview of anti-diabetic plants used in Gabon: Pharmacology and toxicology. *J. Ethnopharmacol.* **2018**, *216*, 203–228. [[CrossRef](#)]
70. Balogun, F.O.; Tshabalala, N.T.; Ashafa, A.O. Antidiabetic Medicinal Plants Used by the Basotho Tribe of Eastern Free State: A Review. *J. Diabetes Res.* **2016**, *2016*, 4602820. [[CrossRef](#)]
71. Zhu, Q.; Ge, F.; Dong, Y.; Sun, W.; Wang, Z.; Shan, Y.; Chen, R.; Sun, J.; Ge, R.S. Comparison of flavonoids and isoflavonoids to inhibit rat and human 11 $\beta$ -hydroxysteroid dehydrogenase 1 and 2. *Steroids* **2018**, *132*, 25–32. [[CrossRef](#)] [[PubMed](#)]
72. Mok, S.Y.; Lee, S. Identification of flavonoids and flavonoid rhamnosides from *Rhododendron mucronulatum* for *albiflorum* and their inhibitory activities against aldose reductase. *Food Chem.* **2013**, *136*, 969–974. [[CrossRef](#)] [[PubMed](#)]
73. Patil, K.K.; Cacche, R.N. Inhibition of glycation and aldose reductase activity using dietary flavonoids: A lens organ culture studies. *Int. J. Biol. Macromol.* **2017**, *98*, 730–738. [[CrossRef](#)]
74. Zhang, B.W.; Xing, Y.; Wen, C.; Yu, X.X.; Sun, W.L.; Xiu, Z.L.; Dong, Y.S. Pentacyclic triterpenes as  $\alpha$ -glucosidase and  $\alpha$ -amylase inhibitors: Structure-activity relationships and the synergism with acarbose. *Bioorg. Med. Chem. Lett.* **2017**, *27*, 5065–5070. [[CrossRef](#)]
75. Jesus, A.R.; Vila-Vicosa, D.; Machuqueiro, M.; Marques, A.P.; Dore, T.M.; Rauter, A.P. Targeting Type 2 Diabetes with C-Glucosyl Dihydrochalcones as Selective Sodium Glucose Co-Transporter 2 (SGLT2) Inhibitors: Synthesis and Biological Evaluation. *J. Med. Chem.* **2017**, *60*, 568–579. [[CrossRef](#)]
76. Hu, S.; Wang, S.; Fanelli, B.; Bell, P.A.; Dunning, B.E.; Geisse, S.; Schmitz, R.; Boettcher, B.R. Pancreatic b-Cell KATP Channel Activity and Membrane-Binding Studies with Nateglinide: A Comparison with Sulfonylureas and Repaglinide. *J. Pharmacol. Exp. Ther.* **2000**, *293*, 444–452.
77. Lipinski, C.A. Lead- and drug-like compounds: The rule-of-five revolution. *Drug Discov. Today Technol.* **2004**, *1*, 337–341. [[CrossRef](#)] [[PubMed](#)]
78. Schrey, A.K.; Nickel-Seeber, J.; Drwal, M.N.; Zwicker, P.; Schultze, N.; Haertel, B.; Preissner, R. Computational prediction of immune cell cytotoxicity. *Food Chem. Toxicol.* **2017**, *107*, 150–166. [[CrossRef](#)]



79. Ntie-Kang, F. An *in silico* evaluation of the ADMET profile of the StreptomeDB database. *Springerplus* **2013**, *2*, 353. [[CrossRef](#)]
80. Van Wyk, B.; Oudtshoorn, B.v.; Gericke, N. *Medicinal Plants of South Africa*; Briza Publications: Pretoria, South Africa, 1997.
81. Kaneta, H.; Koda, M.; Saito, S.; Imoto, M.; Kawada, M.; Yamazaki, Y.; Momose, I.; Shindo, K. Biological activities of unique isoflavones prepared from *Apios americana* Medik. *Biosci. Biotechnol. Biochem.* **2016**, *80*, 774–778. [[CrossRef](#)] [[PubMed](#)]
82. Panda, S.; Kar, A. Apigenin (4',5,7-trihydroxyflavone) regulates hyperglycaemia, thyroid dysfunction and lipid peroxidation in alloxan-induced diabetic mice. *J. Pharm. Pharmacol.* **2007**, *59*, 1543–1548. [[CrossRef](#)]
83. Gowd, V.; Jia, Z.; Chen, W. Anthocyanins as promising molecules and dietary bioactive components against diabetes – A review of recent advances. *Trends Food Sci. Technol.* **2017**, *68*, 1–13. [[CrossRef](#)]
84. Shay, J.; Elbaz, H.A.; Lee, I.; Zielske, S.P.; Malek, M.H.; Huttemann, M. Molecular Mechanisms and Therapeutic Effects of (-)-Epicatechin and Other Polyphenols in Cancer, Inflammation, Diabetes, and Neurodegeneration. *Oxid. Med. Cell. Longev.* **2015**, *2015*, 181260. [[CrossRef](#)] [[PubMed](#)]
85. Zhang, W.Y.; Lee, J.J.; Kim, Y.; Kim, I.S.; Han, J.H.; Lee, S.G.; Ahn, M.J.; Jung, S.H.; Myung, C.S. Effect of eriodictyol on glucose uptake and insulin resistance *in vitro*. *J. Agric. Food Chem.* **2012**, *60*, 7652–7658. [[CrossRef](#)] [[PubMed](#)]
86. Rani, M.P.; Raghu, K.G.; Nair, M.S.; Padmakumari, K.P. Isolation and identification of alpha-glucosidase and protein glycation inhibitors from *Stereospermum colais*. *Appl. Biochem. Biotechnol.* **2014**, *173*, 946–956. [[CrossRef](#)] [[PubMed](#)]
87. Brendler, T.; Eloff, J.N.; Gurib-Fakim, A.; Philips, L. *African Herbal Pharmacopoeia*; Association for African Medicinal Plants Standards: Port Louis, Mauritius, 2010.
88. *ACD/Chemsketch*, version 12.02; Advanced Chemistry Development, Inc.: Toronto, ON, Canada, 2015.
89. Kim, S.; Thiessen, P.A.; Bolton, E.E.; Chen, J.; Fu, G.; Gindulyte, A.; Han, L.; He, J.; He, S.; Shoemaker, B.A.; et al. PubChem Substance and Compound databases. *Nucleic Acids Res.* **2016**, *44*, D1202–D1213. [[CrossRef](#)]
90. *Cytoscape*, version 3.4.0; Cytoscape Consortium: San Diego, CA, USA, 2016.
91. *NetworkAnalyzer Application*, version 2.7; Max-Planck-Institut für Informatik: Saarbrücken, Germany, 2016.
92. *Schrödinger Canvas Suite*, version 3.2.013; Schrödinger, LLC: New York, NY, USA, 2017.
93. *UCSF ChemViz2 Cheminformatics Application*, version 1.1.0 for Cytoscape; Resource for Biocomputing, Visualization and Informatics: San Francisco, CA, USA, 2016.
94. *Schrödinger Maestro*, version 11.2.013; Schrödinger, LLC: New York, NY, USA, 2017.
95. Banerjee, P.; Eckert, A.O.; Schrey, A.K.; Preissner, R. ProTox-II: A webserver for the prediction of toxicity of chemicals. *Nucleic Acids Res.* **2018**, *46*, W257–W263. [[CrossRef](#)] [[PubMed](#)]

**Sample Availability:** Samples of the compounds are not available from the authors.



© 2019 by the authors. Licensee MDPI, Basel, Switzerland. This article is an open access article distributed under the terms and conditions of the Creative Commons Attribution (CC BY) license (<http://creativecommons.org/licenses/by/4.0/>).



## Chapter 3

# Industrial part of the thesis

### 3.1 Introduction

The Industrial PhD Programme is a strategy from the Catholic University of Murcia (UCAM) to promote applied research within several companies. The technology transfer from the university to the industrial sector seeks, through innovation, to provide a competitive advantage and promote the internationalization of our industry. Within the project, one of the main goals is to understand the needs of companies and what technology and knowledge can be provided from the university environment.

Eurofins Villapharma (<https://www.eurofinsdiscoveryservices.com/cms/cms-content/services/chemistry>) is a company focused on the design and synthesis of high value chemical compounds, with an original chemical structure, and potential to become new medicines in the future. This company has forged partnerships with several research entities and groups, allowing them to further diversify the collection of molecules it offers to its customers within the biopharmaceutical industry.

The drug discovery process has become very complex over the last few decades. Strategies in the industry have been changing to adapt to today's requirements, which demand greater efficiency in the developing process, both in terms of costs and time, and the discovery of innovative drugs. Following the guidelines of

the current market, Eurofins Villapharma tries to position itself as a company that plays a key role in its sector by expanding its technology. In this context, Eurofins Villapharma's collaboration with the research group *Bioinformatics and High Performance Computing Group* (BIO-HPC) arose. BIO-HPC research group is located at UCAM (<http://bio-hpc.eu>). Its main research area of interest is the exploitation of high-performance computing resources for the development and application of different chemoinformatics programs mainly oriented to drug discovery.

The industrial projects in which participated are mentioned below. Given that all these works have been carried out in collaboration with third parties and that the intellectual property of the results obtained has not yet been properly protected, and consequently with the confidentiality agreement that binds me to the company, I cannot reveal the results of these works.

### **3.2 Discovery and optimization of bioactive compounds in the context of Cancer**

The industrial part of this PhD has been developed mainly within two projects in which Eurofins Villapharma is a collaborating partner, FRIDASTEM (funded by the H2020 programme in the Eurostars call) and STEMHIT (funded by MINECO in the Retos-Colaboration industrial call), both aimed at the discovery of new chemical compounds for inhibiting the development of cancer stem cells.

Phosphorylation is one of the most often occurring post-transcriptional modifications in proteins (Khoury et al., 2011). This process is regulated by specific enzymes known as kinases (they add phosphate) and phosphatases (they remove it). 518 kinases have been described in the human proteome (Manning et al., 2002), which regulate critical vital functions in cells. These include those involved in mobility, proliferation and metabolism as well as survival, cell cycle control points (DNA damage control), antitumour immunity evasion and angiogenesis (Gross et al., 2015). Given the processes that regulate, frequently, an aberrant expression of

these enzymes is involved in the development of various diseases, including cancer. This revelation was confirmed by the text Cancer Gene Census in a report in 2004 where it revealed that the protein domain most commonly encoded by oncogenes is the quinoma (Futreal et al., 2004). Subsequent studies conducted by The Cancer Genome Atlas (TCGA) and the International Cancer Genome Consortium. (ICGC) showed that most protein kinases have mutation frequencies from low (less than 10%) to intermediate and others, to a lesser extent, frequencies greater than 10% in one or more types of cancer (Fleuren et al., 2016).

Considering the above-mentioned data, kinases have become a very attractive therapeutic target for the treatment of different types of cancer, being the discovery of small kinase-inhibiting compounds the goal for which more effort and resources are being invested both among research groups and by the pharmaceutical industry (Wu et al., 2015). However, finding these compounds is not a trivial affair, as evidenced by the fact that the first FDA-approved drug that acted as a kinase inhibitor (kinase STI-571, belonging to the Abl group of protein-tyrosine kinases) dates from 2001 (Müller et al., 2015) more than 20 years after the first oncogene of protein kinases (Cohen, 2002) was identified. However since then, 37 kinase inhibitors have been approved worldwide and more than 250 candidate drug compounds are at some stage of clinical trials (Klaeger et al., 2017).

In kinases the ATP binding site is found forming a cavity in an area arranged between the two catalytic lobes of the enzyme. This cavity has structural and morphological characteristics that make it druggable. This region of the enzyme is highly conserved throughout the kinome, which makes the task of finding selective inhibitors for a specific type of kinase especially complicated. Therefore, a fundamental objective of these projects was to optimize the compounds for which initial inhibition was obtained, considering as a *hit* those compounds with a LE (Ligand efficiency) lower than 0.3, in order to obtain new molecular entities with greater inhibition potential. For this purpose, different cheminformatic techniques were used, such as QSAR modeling (Gramatica, 2007; Pérez-Garrido et al., 2009) or the simulation of molecular coupling (Imbernón et al., 2017; Sánchez-Linares et al., 2012) and

molecular dynamics (Shivakumar et al., 2010; Tapia-Abellán et al., 2019).

The virtual screening techniques employed have played a fundamental role in the discovery of new molecules potentially active in the different contexts mentioned above. The simulation of the molecular docking used for the discovery of kinase-inhibiting molecules had a success rate of more than 60%. We have also observed that this technique is very dependent on the quality of the protein model being used.

### **3.3 Discovery of bioactive compounds enhancers of the cystic fibrosis transmembrane regulating protein (CFTR)**

Cystic fibrosis transmembrane regulating protein (CFTR) acts as a chlorine channel. Certain mutations in the gene encoding for the protein cause the expression of the transporter, as well as its activity, to be impaired in epithelial cells of respiratory organs. More than 2000 different mutations are known, being the PHE508 residue deletion the most common of all (W Loo et al., 2002), occurring in approximately 70% of patients. The consequence of these mutations is that the transcribed protein cannot acquire the correct quaternary structure and either degrades before reaching the membrane of the epithelial cells or manifests itself in the epithelials but is only partly functional (Lukacs and Verkman, 2011). Therefore, the objective of this project is to find bioactive compounds that act as pharmacological chaperones and allow the normal folding of the protein recovering its transport activity and normal distribution in the cell membranes more effectively than the two drugs currently approved for the treatment of the disease.

Within the framework of this industrial PhD we have collaborated to search for compounds that could be used in the treatment of cystic fibrosis. In this context, a virtual screening of different libraries of commercial compounds (including those of Eurofins Villapharma) was carried out. A total of twenty-eight three-dimensional pharmacophoric models were created based on the physical-chemical properties of the compounds, both activators and modulators of the activity of the CFTR, located

in the patents available in the databases to which the company has access.

The screening of approximately one million of compounds was carried out in three stages:

- In a first stage the compounds were clustered according to their structural similarity and filtered based on their molecular structure finally selecting approximately 500000 compounds of diverse structure and chemical nature.
- In the second stage the compounds were filtered considering certain minimum criteria that drugs must comply such as eliminating PAINS (Pan-Assay Interference), compounds with a molecular weight lower than 160 Da and higher than 650 Da and compounds with long aliphatic chains or containing more than 5 aromatic rings. This stage is performed on two-dimensional models of the compounds to accelerate the process using a textworkbench in KNIME (Berthold et al., 2009).
- In a third stage, up to 100 conformations of each of the molecules of the remaining chemical library were generated and the pharmacoforic models created before were used to filter the database.

When the three-dimensional structure of the therapeutic target is not available, virtual screening techniques based on ligands are a very good alternative. Of the different techniques available, pharmacoforic modeling is a very attractive method due to the reduced computational requirements and it has shown very promising results in the specific case of the discovery of drugs that enhance the CFTR transporter. Of the 611 compounds selected, 5 hits were obtained whose activity is much more potent and 3 compounds moderately more potent than the reference drug (VX-661).





## Chapter 4

# Conclusions and outlook

This doctoral thesis presented as a compilation of publications, has its starting-point in the drug discovery assisted by computer and the common denominator are the different computational techniques used for the search and optimization of bioactive compounds against different therapeutic targets: kinases proteins, CFTR transporter, cholinesterases,  $\alpha$ -galactosidase, Zika virus protease NS2B-NS3 and various proteins involved in diabetes.

In this chapter we synthesize the conclusions derived from the results that have been gradually obtained and that we can gather from all the thesis development and that perfectly can become premises to continue the research line.

### 4.1 Conclusions

The most relevant contributions derived from the different articles that make up this doctoral thesis are described below:

#### 4.1.1 Discovery of a novel pharmacological chaperone for the treatment of Fabry disease

- Virtual screening based on the three-dimensional shape of chemical compounds is a fast strategy that can reduce the molecular spectrum in large collections of molecules when looking for bioactive compounds that must fit to-

gether with a specific topology where compounds of a higher volume than the pocket where these compounds must interact cannot be accommodated.

- The simulation of the molecular docking carried out with the same pool of compounds in two different regions of the protein, the active site and an allosteric site, made it possible to identify compounds for which the method predicted a maximum affinity energy difference between the active site and the allosteric site. That is, compounds for which the computational method estimated an affinity at least twice lower at the active site than at the allosteric site comprising the enzyme residues A37, R38, T39, P40, T41, M42, E87, Y88, none of which overlap with the enzyme's active site.
- The experimental techniques carried out by our collaborators of the University of Naples demonstrated that the compound selected by this computational technique, 2,6-ditiopurine (DTP), is able not only to stabilize the enzyme  $\alpha$ -galactosidase, but also it is able to promote, both individually and in synergy with other chaperones, the maturation of the  $\alpha$ -galactosidase, as well as the mutant variety (A230T) that does not respond to treatment with 1-deoxygalacto-nojirimycin (DGJ), the only pharmacological chaperone on the market. In addition, DTP does not inhibit enzyme activity at concentrations of 6 mM at which DGJ does inhibit it completely.
- Experimental trials on variants of the enzyme  $\alpha$ -galactosidase with mutations that alter the conformation of the allosteric binding site proposed for DTP by the use of textititn silico methods show that the compound loses the ability to promote maturation and rescue enzyme activity. This implies that there is strong evidence to support the predictive model used.

#### **4.1.2 Description of the mode of action of cholinesterase-inhibiting bioactive compounds**

- By simulating the molecular docking the binding mode between the compound N-acetyl-tryptophan and acetylcholinesterase at its active site was

modelled. According to this simulation the compound is bound by hydrogen bonds to the residues GLU199 and TYR121 which would prevent acetylcholine access to the catalytic triad. The predicted three-dimensional conformation of the compound N-acetyl-tryptophan also overlaps with the crystallographic conformation of donepezil, from which it can be deduced that the mechanism of action of N-Acetyl-tryptophan must be similar to that of this drug.

- The first study *in silico* on the inhibitory effect of different kinds of tanshinones and rosmarinic acid on cholinesterase enzymes is shown in the scientific production that makes up this thesis. This study, by simulating the molecular docking, reveals how these compounds bind in the pocket of the catalytic site of the enzyme where hydrophobic and pi-pi stacking interactions with the enzyme acetylcholinesterase are most predicted and hydrogen bonds with residues of the catalytic triad in the case of butyrylcholinesterase. Additionally, a QSAR model was created to evaluate the selectivity of the compounds for the different cholinesterases according to their chemical structure. Thus, it was determined that the compounds with more aliphatic substituents had a greater affinity for butyrylcholinesterase, while those with more aromatic radicals had more selectivity for acetylcholinesterase than for butyrylcholinesterase.
- The simulation of the molecular docking of the compounds hyperforin and hyuganin C shows the potential interactions of both compounds at the active site of butyrylcholinesterase. In the case of hyuganin C a strong web of hydrogen bonds formed with the catalytic triad residues GLY115, GLY116, GLY117, SER198 and LEU286 and hydrophobic interactions with the residues TRP82 (peripheral anionic site), PHE329 (anionic site) and PHE398 were predicted. According to the same model, the stabilization of hyperforin in the active site is mainly due to hydrophobic interactions established with residues of the peripheral anionic site (TRP82, THR120, TRP231, VAL288, TYR332) and other

residues (PHE398, TRP430, TYR440) and to the hydrogen bonds that would be formed with SER79 and HIS438 residues of the catalytic triad. These interactions would explain how they inhibit butyrylcholinesterase by occupying the active site and by preventing access to its substrates up to the catalytic triad.

#### **4.1.3 Repositioning of an antibiotic as a NS2B-NS3 protease inhibitor for the treatment of Zika virus infection.**

- By modelling the molecular docking, the molecular pool of the Drugbank database (Law et al., 2013) were ranked according to the predicted energy affinity value of each compound for the protease NS2B-NS3 at the active site of a boronate inhibitor using as the structural model for the simulation the crystal 5LC0 (Lei et al., 2016). 8 compounds out of the 100 best molecules were selected for characterization *in vitro* as these drugs were already approved for therapeutical use and therefore had already passed clinical safety trials. 5 of the 8 selected drugs showed ability to inhibit viral protease in fluorescence-based inhibition assays conducted by our collaborators at the University of Hong Kong. In other words, more than 60% of the compounds tested that were selected by virtual screening techniques were active.
- A molecular dynamics simulation using the structural model of the protease bound to novobiocin, taking as a starting point the spatial conformation of the drug obtained by means of docking, made it possible to analyse in more detail the possible interactions between novobiocin and the protein that are responsible for the drug's inhibition potential. This simulation suggested that the bond between the drug and the catalytic site of the enzyme was highly stable. Our model predicted interactions by hydrogen bonds between novobiocin and residues MET51, SER81 and LYS54, as well as hydrophobic stabilization areas with residues HIS51 and VAL155. It should be noted that residues HIS51 and SER81 of protease also interact with boronate inhibitor as can be read in the work of Lei et al. (2016) and therefore perhaps these residues

play a key role in the catalytic activity of the enzyme. The HIS51 residue is also highly conserved in NS3B-NS2 proteases of different ZIKA virus strains, so novobiocin could be active against infection by different Zika virus subtypes.

- The efficacy of novobiocin treatment against Zika virus infection was evaluated using animal models (mice). It was found that viral load in organ tissues such as kidneys or testicles in novobiocin-treated mice was significantly lower than in untreated mice and the survival rate reached 100% in mice that were administered the drug versus 0% in untreated mice.

#### **4.1.4 Development of a virtual screening platform for the identification of new anti-diabetic compounds**

results

- The DIA-DB web server in which the doctoral candidate has participated in its development (see section 5.1.4) has been used to carry out a reverse virtual screening which aims to identify the potential therapeutic target of several natural compounds in the field of diabetes. Of the 867 natural compounds identified, through bibliographic references, in approximately 200 African plant species, potential anti-diabetic activity was predicted for a total of 430 compounds. For the vast majority of these compounds more than one possible therapeutic target was predicted, with proteins with larger active sites (Hydroxysteroid 11-beta dehydrogenase 1 (HSD11B1), peroxisome-proliferator-activated delta receptor, and dipeptidyl peptidase 4) being those for which higher affinity energies are predicted (above the threshold established in the study to consider a bioactive compound). More than 60% of the plants containing the compounds for which affinity for proteins involved in diabetes was predicted had already been linked by other scientists with anti-diabetic activity, which implies a validation of the relative efficacy of the predictive method used.
- The hierarchical classification of each group of compounds with affinity to

a protein obtained by means of the Tanimoto similarity index (Bajusz et al., 2015) made it possible to identify some molecular scaffolds common to several of the compounds identified as bioactive in the context of diabetes, such as the flavonoids inhibitors of HSD11B1.

- This same Tanimoto index was used to identify the degree of similarity of the compounds for which bioactivity was predicted with approved drugs and other experimentally evaluated bioactive molecules, observing that only 10% of the molecules modeled have a chemical structure similar to these compounds. This evaluation determines that most of the chemical compounds evaluated have original molecular scaffolds with respect to anti-diabetic drugs.
- Bioactive compounds that are candidates for drugs must comply with certain Absorption, Distribution, Metabolism, Excretion and Toxicity (ADMET) parameters, in addition to the ability to be soluble in water since most of these compounds are usually administered orally as plant extracts. Of the compounds evaluated, the computational method used for predicting ADMET properties predicts that only 28 compounds are favorable, of which 8 compounds have already been evaluated experimentally and 20 are presented as novel chemical structures with potential antidiabetic activity for four therapeutic targets.

## 4.2 Outlook

- The DTP pharmacological chaperone discovered in this research work is effective at high concentrations. Although the compound can accumulate in body cells at millimolar concentrations (Powell et al., 2010) without causing damage to the cells (Boulware et al., 2012; Qing et al., 1995) there is a risk of DTP interacting with other proteins in the cells, causing undesirable side effects. In addition, the compound has been shown to be ineffective in stabilizing some of the  $\alpha$ -galactosidase mutations that negatively impact its catalytic activity.

Therefore, it is necessary to carry out optimization techniques modifying the chemical structure of the compound to achieve greater specificity and affinity for the enzyme at the allosteric site.

- Through a QSAR study, hyuganin C was determined to be a potentially hepatotoxic compound. It would therefore be important to conduct studies *in vitro* of its biological activity, to assess its possible adverse effects, which would be helpful in the process of developing new drugs.
- Novobiocin is an antimicrobial agent that was withdrawn from sale because bacteria developed resistance to the drug being less effective compared to other available drugs. Despite excellent laboratory results, the compound has difficulty crossing the blood-brain barrier when the meninges are not inflamed. In addition, although it is not a contraindicated drug for pregnant women, it falls within the category C of the Food and Drug Administration (FDA), which means that its administration has not been shown to be completely safe for the fetus. Considering that one of the most serious sequelae of the disease is neurological damage in neonates, these two limitations could be an impediment for the use of the drug, so it would be advisable to optimize the compound by *in silico* techniques taking into account these two limiting factors.
- To check the computational method carried out in the section 2.8 of this thesis it is necessary to conduct the relevant experimental trials to corroborate whether the *in silico* characterized molecules actually exhibit the predicted anti-diabetic activity. If the experimental characterization is successful, the same computational method could be applied to other natural compounds present in extracts, both from plant sources and algae, in order to identify new bioactive molecules.





## Chapter 5

# Publications, collaborations and quality of journals

### 5.1 Collaborations and other publications

The ultimate goal of an industrial doctoral thesis is to establish cooperative ties between the university and the company so as to ensure a steady flow of knowledge, innovation and production between the two entities. During the course of the research work, which outcome is the thesis presented, collaborations have been established both with other companies (as detailed in the Chapter 3) and with other research groups. Below are the scientific publications and research projects in which the PhD student has been involved as a result of these collaborations that have not been included as results of the thesis:

#### 5.1.1 Publications in journals indexed in ISI

1. Budryn, G., Zaczyńska, D., Pałecz, B., Rachwał-Rosiak, D., Belica, S., den Haan, H., Peña-García, J., and Pérez-Sánchez, H. (2016). Interactions of free and encapsulated hydroxycinnamic acids from green coffee with egg ovalbumin, whey and soy protein hydrolysates. *LWT - Food Science and Technology*, 65:823–831

2. Cerón-Carrasco, J. P., den Haan, H., Peña-García, J., Contreras-García, J., and Pérez-Sánchez, H. (2016). Exploiting the cyclodextrins ability for antioxidants encapsulation: A computational approach to carnosol and carnosic acid embedding. *Computational and Theoretical Chemistry*, 1077:65–73
3. Pérez-Sánchez, H., Rezaei, V., Mezhuyev, V., Man, D., Peña-García, J., den Haan, H., and Gesing, S. (2016). Developing science gateways for drug discovery in a grid environment. *SpringerPlus*, 5(1):1300
4. Yar, M., Shahzadi, L., Farooq, A., Jalil Imran, S., Cerón-Carrasco, J. P., den Haan, H., Kumar, S., Peña-García, J., Pérez-Sánchez, H., Grycova, A., Dvorak, Z., and Vrzal, R. (2017). In vitro modulatory effects of functionalized pyrimidines and piperidine derivatives on Aryl hydrocarbon receptor (AhR) and glucocorticoid receptor (GR) activities. *Bioorganic Chemistry*, 71:285–293
5. Rauf, A., Farooq, U., Khan, A., Hadda, T. B., Naz, S., Ibrar, A., Jehan, N., Cerón-Carrasco, J. P., Haan, H. d., Peña-García, J., Pérez-Sánchez, H., Khan, H., Ramadan, M. F., Abu-Izneid, T., Bawazeer, S., Rauf, A., Farooq, U., Khan, A., Hadda, T. B., Naz, S., Ibrar, A., Jehan, N., Cerón-Carrasco, J. P., Haan, H. d., Peña-García, J., Pérez-Sánchez, H., Khan, H., Ramadan, M. F., Abu-Izneid, T., and Bawazeer, S. (2017). Sedative and muscle relaxant activities of diterpenoids from *Phlomidioschema parviflorum*. *Revista Brasileira de Farmacognosia*, 27(5):636–640
6. Jerbi, J., Springborg, M., den Haan, H., and Cerón-Carrasco, J. P. (2017). S-adenosyl-l-methionine analogs as enhanced methyl donors: Towards novel epigenetic regulators. *Chemical Physics Letters*, 690:74 – 81
7. Khan, H., Zafar, M., Den-Haan, H., Perez-Sanchez, H., and Kamal, M. A. (2018). In-silico Studies of Isolated Phytoalkaloid Against Lipoxygenase: Study Based on Possible Correlation. *Combinatorial Chemistry & High Throughput Screening*, 21(3):215–221

### 5.1.2 Editorials

1. den-Haan, H., Fassihi, A., Bueno-Crespo, A., Soto, J., Vegara-Meseguer, J., Montoro, S. and Pérez-Sánchez, H. (2015). Application of Modern Drug Discovery Techniques in the Context of Diabetes Mellitus and Atherosclerosis. *Drug Designing: Open Access*, 04(01)

### 5.1.3 Preprints

1. den Haan, H., José Hernández Morante, J., and Pérez-Sánchez, H. (2016). Computational evidence of a compound with nicotinic  $\alpha 4\beta 2$ -ach receptor partial agonist properties as possible coadjuvant for the treatment of obesity. *The preprint server for biology (bioRxiv)*

### 5.1.4 Congresses

1. Fahimeh Ghasemi, Alireza Mehri, Jorge Peña-García, Helena den-Haan, Alfonso Pérez-Garrido, Afshin Fassihi, and Horacio Pérez-Sánchez (2015). Improving activity prediction of Adenosine A2b receptor antagonists by machine learning methods. In *International Work-Conference on Bioinformatics and Biomedical Engineering*, pages 635–644, IWBBIO
2. Sánchez-Pérez, A., Muñoz, A., Peña-García, J., den Haan, H., Bekas, N., Katsikoudi, A., Tzakos, A. G., and Sánchez, H. P. (2015). DIA-DB: A Web-Accessible Database for the Prediction of Diabetes Drugs. In *Bioinformatics and Biomedical Engineering - Third International Conference, IWBBIO 2015, Granada, Spain, April 15-17, 2015. Proceedings, Part II*, pages 655–663
3. Peña-García, J., den Haan, H., Caballero, A., Imbernón, B., Cerón-Carrasco, J. P., Vicente-Contreras, A., and Pérez-Sánchez, H. (2016). GrantFinder, a web based tool for the search of research grant calls. In *4th International Work-Conference on Bioinformatics and Biomedical Engineering*, pages 326–333, IWBBIO
4. Jorge Peña-García, Alfonso Pérez-Garrido, Andrés Muñoz, Helena den-Haan,

- Baldomero Imbernón, José Pedro Cerón-Carrasco, Antonio Banegas-Luna, Jesús Soto, and Darius Mrozek (2016). ZincFetcher: a tool for easy compound filtering from ZINC database. In *4th International Work-Conference on Bioinformatics and Biomedical Engineering*, pages 343–351, IWBBIO
5. Ricardo Rodríguez-Schmidt, Jorge Peña-García, Alfonso Pérez-Garrido, Helena den-Haan, Andrés Bueno-Crespo, José Pedro Cerón-Carrasco, Jesús Soto, Anil Thapa, and Jon Atli-Benediktsson (2016). A hybrid machine learning and molecular modeling methodology for the prediction of novel blood anticoagulants. pages 334–342, IWBBIO
  6. Pérez-Sánchez, H., Peña-García, J., den Haan, H., Rodríguez-Schmidt, R., Cerón-Carrasco, J. P., Raposo, A. N., Bouarkat, M., Sabeur, S. A., and Díaz-Baños, F. G. (2016). HYDROWEB, an Online Tool for the Calculation of Hydrodynamic Properties of Macromolecules. In Ortuño, F. and Rojas, I., editors, *Bioinformatics and Biomedical Engineering*, Lecture Notes in Computer Science, pages 82–90, IWBBIO. Springer International Publishing

### 5.1.5 Patents

1. Yuan, S. Chan, J. Y. K. d.-H. H. P.-G. J. C.-C. J. and Pérez-Sánchez, H. (PCT/CN2017/088420, US 62491007 (2017). Patent pending). Zika virus protease inhibitors and methods of use thereof

## 5.2 Data on quality of publications

The articles that compose this PhD thesis have been published in journals indexed in the *Journal Citation Reports*, a platform used to assess the relative importance of each journal within its thematic area based on a series of standard indicators that measure the quality of each journal. The following subsections show a series of indicators associated with each journal in which the work has been published. In summary, two articles belong to the first quartile of at least one of their categories, two to the second quartile, one to the third quartile and two to the fourth quartile.

### 5.2.1 Identification of an allosteric binding site on human lysosomal alpha-galactosidase opens the way to new pharmacological chaperones for Fabry disease - *PLOS ONE*

In this section we present the data related to the journal where the first article that forms part of this thesis *Identification of an allosteric binding site on human lysosomal alpha-galactosidase opens the way to new pharmacological chaperones for Fabry disease* has been published. In the figures 5.1, 5.2 and 5.3 we present the quality indicators and the impact factor of the journal *PLOS ONE*.

**PLoS One**  
 ISSN: 1932-6203  
 PUBLIC LIBRARY SCIENCE  
 1160 BATTERY STREET, STE 100, SAN FRANCISCO, CA 94111  
 USA  
[Go to Journal Table of Contents](#) [Go to Ulrich's](#)

**Titles**  
 ISO: PLoS One  
 JCR Abbrev: PLOS ONE

**Categories**  
 MULTIDISCIPLINARY SCIENCES - SCIE

**Languages**  
 English

0 Issues/Year;  
 Open Access from 2006

Figure 5.1: Title and data of the journal publishing the article *Identification of an allosteric binding site on human lysosomal alpha-galactosidase opens the way to new pharmacological chaperones for Fabry disease*.

Key Indicators													
Year	Total Cites	Journal Impact Factor	Impact Factor Without Journal Self Cites	5 Year Impact Factor	Immediacy Index	Citable Items	Cited Half-Life	Citing Half-Life	Eigenfactor Score	Article Influence Score	% Articles in Citable Items	Normalized Eigenfactor	Average JIF Percentile
2017	582,878	2.766	2.599	3.352	0.405	20,328	4.3	8.2	1.86157	1.000	97.99	217.4...	77.344
2016	508,248	2.806	2.614	3.394	0.429	22,077	3.7	8.1	1.92176	1.053	98.24	220.5...	77.344
2015	425,015	3.057	2.775	3.535	0.396	28,114	3.1	7.9	1.81369	1.137	99.13	206.7...	83.333
2014	332,716	3.234	2.885	3.702	0.489	30,040	2.7	7.7	1.53341	1.209	99.12	171.7...	85.088
2013	226,708	3.534	3.053	4.015	0.416	31,496	2.5	7.4	1.16582	1.370	99.15	128.4...	86.364

Figure 5.2: Key indicators of the past five years of the magazine *PLOS ONE*.

JCR Impact Factor						
JCR Year ▼	MULTIDISCIPLINARY SCIENCES			BIOLOGY		
	Rank	Quartile	JIF Percentile	Rank	Quartile	JIF Percentile
2017	15/64	Q1	77.344	N/A	N/A	N/A
2016	15/64	Q1	77.344	N/A	N/A	N/A
2015	11/63	Q1	83.333	N/A	N/A	N/A
2014	9/57	Q1	85.088	N/A	N/A	N/A
2013	8/55	Q1	86.364	N/A	N/A	N/A

Figure 5.3: Impact factor of the past five years of the magazine *PLOS ONE*.

## 5.2.2 Selective in vitro and in silico butyrylcholinesterase inhibitory activity of diterpenes and rosmarinic acid isolated from *Perovskia atriplicifolia* Benth. and *Salvia glutinosa* L. - *Phytochemistry*

In this section we present the data related to the journal where the first article that forms part of this thesis *Selective in vitro and in silico butyrylcholinesterase inhibitory activity of diterpenes and rosmarinic acid isolated from Perovskia atriplicifolia Benth. and Salvia glutinosa L.* In the figures 5.4, 5.5 y 5.6 we present the quality indicators and the impact factor of the journal *Phytochemistry*.

<p><b>PHYTOCHEMISTRY</b>  ISSN: 0031-9422  PERGAMON-ELSEVIER SCIENCE LTD  THE BOULEVARD, LANGFORD LANE, KIDLINGTON, OXFORD OX5 1GB, ENGLAND  ENGLAND</p> <p><a href="#">Go to Journal Table of Contents</a>   <a href="#">Go to Ulrich's</a></p>	<p><b>Titles</b>  ISO: Phytochemistry  JCR Abbrev: PHYTOCHEMISTRY</p> <p><b>Categories</b>  BIOCHEMISTRY &amp; MOLECULAR  BIOLOGY - SCIE;  PLANT SCIENCES - SCIE;</p> <p><b>Languages</b>  Multi-Language</p> <p>18 Issues/Year;</p>
--	--

Figure 5.4: Title and data of the journal publishing the article *Selective in vitro and in silico butyrylcholinesterase inhibitory activity of diterpenes and rosmarinic acid isolated from Perovskia atriplicifolia Benth. and Salvia glutinosa L.*

Key Indicators													
Year ▾	Total Cites <a href="#">Graph</a>	Journal Impact Factor <a href="#">Graph</a>	Impact Factor Without Journal Self Cites <a href="#">Graph</a>	5 Year Impact Factor <a href="#">Graph</a>	Immediacy Index <a href="#">Graph</a>	Citable Items <a href="#">Graph</a>	Cited Half-Life <a href="#">Graph</a>	Citing Half-Life <a href="#">Graph</a>	Eigenfactor Score <a href="#">Graph</a>	Article Influence Score <a href="#">Graph</a>	% Articles in Citable Items <a href="#">Graph</a>	Normalized Eigenfactor <a href="#">Graph</a>	Average JIF Percentile <a href="#">Graph</a>
2017	30,812	3.186	3.065	3.041	0.509	212	17.6	10.9	0.01...	0.766	96.70	1.51...	71.414
2016	31,101	3.205	3.075	3.349	0.545	165	>10.0	>10.0	0.01...	0.875	96.97	1.90...	71.668
2015	30,508	2.779	2.605	3.218	0.762	281	>10.0	9.6	0.01...	0.818	92.17	1.83...	65.458
2014	29,581	2.547	2.376	3.278	0.466	236	>10.0	>10.0	0.01...	0.852	98.73	1.98...	60.322
2013	30,636	3.350	3.162	3.571	0.404	302	>10.0	>10.0	0.02...	0.912	97.35	2.31...	74.620

Figure 5.5: Key indicators of the past five years of the magazine *Phytochemistry*.

JCR Impact Factor						
JCR Year ▾	BIOCHEMISTRY & MOLECULAR BIOLOGY			PLANT SCIENCES		
	Rank	Quartile	JIF Percentile	Rank	Quartile	JIF Percentile
2017	124/293	Q2	57.850	34/223	Q1	84.978
2016	119/290	Q2	59.138	34/212	Q1	84.198
2015	140/289	Q2	51.730	44/209	Q1	79.187
2014	156/290	Q3	46.379	53/204	Q2	74.265
2013	108/291	Q2	63.058	28/199	Q1	86.181

Figure 5.6: Impact factor of the past five years of the magazine *Phytochemistry*.

### 5.2.3 Acetylcholinesterase inhibitory assessment of isolated constituents from *Salsola grandis* Freitag, Vural & Adıgüzel and molecular modeling studies on N-acetyltryptophan - *Phytochemistry Letters*

In this section we present the data related to the journal where the first article that forms part of this thesis *Acetylcholinesterase inhibitory assessment of isolated constituents from Salsola grandis* Freitag, Vural & Adıgüzel and molecular modeling studies on N-acetyltryptophan. In the figures 5.7, 5.8 y 5.9 we present the quality indicators and the impact factor of the journal *Phytochemistry Letters*.

**Phytochemistry Letters**  
 ISSN: 1874-3900  
 ELSEVIER SCIENCE BV  
 PO BOX 211, 1000 AE AMSTERDAM, NETHERLANDS  
 NETHERLANDS

[Go to Journal Table of Contents](#)   [Go to Ulrich's](#)

**Titles**  
 ISO: Phytochem. Lett.  
 JCR Abbrev: PHYTOCHEM LETT

**Categories**  
 PLANT SCIENCES - SCIE;  
 CHEMISTRY, MEDICINAL - SCIE

**Languages**  
 English  
 4 Issues/Year;

Figure 5.7: Title and data of the journal publishing the article *Acetylcholinesterase inhibitory assessment of isolated constituents from Salsola grandis Freitag, Vural & Adıgüzel and molecular modeling studies on N-acetyltryptophan*.

Key Indicators													
Year	Total Cites	Journal Impact Factor	Impact Factor Without Journal Self Cites	5 Year Impact Factor	Immediacy Index	Citable Items	Cited Half-Life	Citing Half-Life	Eigenfactor Score	Article Influence Score	% Articles in Citable Items	Normalized Eigenfactor	Average JIF Percentile
2017	2,025	1.575	1.393	1.547	0.373	255	3.6	9.4	0.00473	0.346	95.29	0.55231	38.557
2016	1,599	1.418	1.271	1.493	0.276	203	3.3	9.2	0.00444	0.348	96.06	0.50999	37.783
2015	1,222	1.353	1.194	1.451	0.338	260	3.2	9.3	0.00334	0.323	94.23	0.38093	33.350
2014	952	1.450	1.305	1.549	0.313	211	2.8	9.7	0.00285	0.342	99.05	0.31952	34.710
2013	681	1.542	1.385	1.521	0.182	143	2.4	9.7	0.00233	0.325	99.30	0.25663	36.864

Figure 5.8: Key indicators of the past five years of the magazine *Phytochemistry Letters*.

JCR Impact Factor						
JCR Year	CHEMISTRY, MEDICINAL			BIOCHEMISTRY & MOLECULAR BIOLOGY		
	Rank	Quartile	JIF Percentile	Rank	Quartile	JIF Percentile
2017	48/59	Q4	19.492	N/A	N/A	N/A
2016	47/60	Q4	22.500	N/A	N/A	N/A
2015	N/A	N/A	N/A	244/289	Q4	15.744
2014	N/A	N/A	N/A	242/290	Q4	16.724
2013	N/A	N/A	N/A	240/291	Q4	17.698

Figure 5.9: Impact factor of the past five years of the magazine *Phytochemistry Letters*.



### 5.2.4 Profiling Auspicious Butyrylcholinesterase Inhibitory Activity of Two Herbal Molecules: Hyperforin and Hyuganin C - *Chemistry & Biodiversity*

In this section we present the data related to the journal where the first article that forms part of this thesis *Profiling Auspicious Butyrylcholinesterase Inhibitory Activity of Two Herbal Molecules: Hyperforin and Hyuganin C*. In the figures 5.10, 5.11 y 5.12 we present the quality indicators and the impact factor of the journal *Chemistry & Biodiversity*.

**CHEMISTRY & BIODIVERSITY**  
 ISSN: 1612-1872  
 WILEY-VCH VERLAG GMBH  
 POSTFACH 101161, 69451 WEINHEIM, GERMANY  
 GERMANY (FED REP GER)  
[Go to Journal Table of Contents](#) [Go to Ulrich's](#)

**Titles**  
 ISO: Chem. Biodivers.  
 JCR Abbrev: CHEM BIODIVERS

**Categories**  
 BIOCHEMISTRY & MOLECULAR BIOLOGY - SCIE;  
 CHEMISTRY, MULTIDISCIPLINARY - SCIE;

**Languages**  
 English  
 12 Issues/Year;

Figure 5.10: Título y datos de la revista donde se ha publicado el artículo *Profiling Auspicious Butyrylcholinesterase Inhibitory Activity of Two Herbal Molecules: Hyperforin and Hyuganin C*.

Key Indicators													
Year	Total Cites	Journal Impact Factor	Impact Factor Without Journal Self Cites	5 Year Impact Factor	Immediacy Index	Citable Items	Cited Half-Life	Citing Half-Life	Eigenfactor Score	Article Influence Score	% Articles in Citable Items	Normalized Eigenfactor	Average JIF Percentile
2017	3,869	1.617	1.410	1.624	0.391	238	7.2	9.2	0.00434	0.362	98.32	0.50665	28.769
2016	3,465	1.440	1.192	1.662	0.211	185	6.6	9.8	0.00438	0.352	91.35	0.50341	29.468
2015	3,210	1.444	1.231	1.735	0.144	139	5.9	9.8	0.00615	0.429	85.61	0.70105	31.629
2014	3,059	1.515	1.337	1.686	0.217	152	5.4	>10.0	0.00612	0.392	93.42	0.68552	34.835
2013	3,193	1.795	1.587	1.957	0.331	181	5.0	10.0	0.00773	0.458	90.61	0.85214	40.655

Figure 5.11: Key indicators of the past five years of the magazine *Chemistry & Biodiversity*.

JCR Impact Factor						
JCR Year ▼	BIOCHEMISTRY & MOLECULAR BIOLOGY			CHEMISTRY, MULTIDISCIPLINARY		
	Rank	Quartile	JIF Percentile	Rank	Quartile	JIF Percentile
2017	244/293	Q4	16.894	102/171	Q3	40.643
2016	241/290	Q4	17.069	97/166	Q3	41.867
2015	237/289	Q4	18.166	90/163	Q3	45.092
2014	239/290	Q4	17.759	76/157	Q2	51.911
2013	223/291	Q4	23.540	63/148	Q2	57.770

Figure 5.12: Impact factor of the past five years of the magazine *Chemistry & Biodiversity*.

### 5.2.5 Selective *in vitro* and *in silico* cholinesterase inhibitory activity of isoflavones and stilbenes from *Belamcandae chinensis rhizoma* - *Phytochemistry letters*

In this section we present the data related to the journal where the first article that forms part of this thesis *Selective in vitro and in silico cholinesterase inhibitory activity of isoflavones and stilbenes from Belamcandae chinensis rhizoma*. In the figures 5.13, 5.14 y 5.15 we present the quality indicators and the impact factor of the journal *Phytochemistry letters*.

<p><b>Phytochemistry Letters</b>  ISSN: 1874-3900  ELSEVIER SCIENCE BV  PO BOX 211, 1000 AE AMSTERDAM, NETHERLANDS  <b>NETHERLANDS</b></p> <p><a href="#">Go to Journal Table of Contents</a>   <a href="#">Go to Ulrich's</a></p>	<p><b>Titles</b>  ISO: Phytochem. Lett.  JCR Abbrev. PHYTOCHEM LETT</p> <p><b>Categories</b>  PLANT SCIENCES - SCIE;  CHEMISTRY, MEDICINAL - SCIE;</p> <p><b>Languages</b>  English</p> <p>4 Issues/Year;</p>
--	---

Figure 5.13: Title and data of the journal publishing the article *Selective in vitro and in silico cholinesterase inhibitory activity of isoflavones and stilbenes from Belamcandae chinensis rhizoma*.

Key Indicators													
Year ▾	Total Cites <a href="#">Graph</a>	Journal Impact Factor <a href="#">Graph</a>	Impact Factor Without Journal Self Cites <a href="#">Graph</a>	5 Year Impact Factor <a href="#">Graph</a>	Immediacy Index <a href="#">Graph</a>	Citable Items <a href="#">Graph</a>	Cited Half-Life <a href="#">Graph</a>	Citing Half-Life <a href="#">Graph</a>	Eigenfactor Score <a href="#">Graph</a>	Article Influence Score <a href="#">Graph</a>	% Articles in Citable Items <a href="#">Graph</a>	Normalized Eigenfactor <a href="#">Graph</a>	Average JIF Percentile <a href="#">Graph</a>
2017	2,025	1,575	1,393	1,547	0.373	255	3.6	9.4	0.00473	0.346	95.29	0.55231	38.557
2016	1,599	1,418	1,271	1,493	0.276	203	3.3	9.2	0.00444	0.348	96.06	0.50999	37.783
2015	1,222	1,353	1,194	1,451	0.338	260	3.2	9.3	0.00334	0.323	94.23	0.38093	33.350
2014	952	1,450	1,305	1,549	0.313	211	2.8	9.7	0.00285	0.342	99.05	0.31952	34.710
2013	681	1,542	1,385	1,521	0.182	143	2.4	9.7	0.00233	0.325	99.30	0.25663	36.864

Figure 5.14: Key indicators of the past five years of the magazine *Phytochemistry letters*.

JCR Impact Factor						
JCR Year ▾	CHEMISTRY, MEDICINAL			BIOCHEMISTRY & MOLECULAR BIOLOGY		
	Rank	Quartile	JIF Percentile	Rank	Quartile	JIF Percentile
2017	48/59	Q4	19.492	N/A	N/A	N/A
2016	47/60	Q4	22.500	N/A	N/A	N/A
2015	N/A	N/A	N/A	244/289	Q4	15.744
2014	N/A	N/A	N/A	242/290	Q4	16.724
2013	N/A	N/A	N/A	240/291	Q4	17.698

Figure 5.15: Impact factor of the past five years of the magazine *Phytochemistry letters*.

### 5.2.6 Structure-based discovery of clinically approved drugs as Zika virus NS2B-NS3 protease inhibitors that potently inhibit Zika virus infection in vitro and in vivo - *Antiviral Research*

In this section we present the data related to the journal where the first article that forms part of this thesis *Structure-based discovery of clinically approved drugs as Zika virus NS2B-NS3 protease inhibitors that potently inhibit Zika virus infection in vitro and in vivo*. In the figures 5.16, 5.17 y 5.18 we present the quality indicators and the impact factor of the journal *Antiviral Research*.

<b>ANTIVIRAL RESEARCH</b> ISSN: 0166-3542 ELSEVIER SCIENCE BV PO BOX 211, 1000 AE AMSTERDAM, NETHERLANDS <b>NETHERLANDS</b> <a href="#">Go to Journal Table of Contents</a> <a href="#">Go to Ulrich's</a>		<b>Titles</b> ISO: Antiviral Res. JCR Abbrev: ANTIVIR RES  <b>Categories</b> PHARMACOLOGY & PHARMACY - SCIE; VIROLOGY - SCIE;  <b>Languages</b> English  12 Issues/Year;
---	--	---

Figure 5.16: Title and data of the journal publishing the article *Structure-based discovery of clinically approved drugs as Zika virus NS2B-NS3 protease inhibitors that potently inhibit Zika virus infection in vitro and in vivo*.

Key Indicators													
Year ▼	Total Cites <a href="#">Graph</a>	Journal Impact Factor <a href="#">Graph</a>	Impact Factor Without Journal Self Cites <a href="#">Graph</a>	5 Year Impact Factor <a href="#">Graph</a>	Immediacy Index <a href="#">Graph</a>	Citable Items <a href="#">Graph</a>	Cited Half-Life <a href="#">Graph</a>	Citing Half-Life <a href="#">Graph</a>	Eigenfactor Score <a href="#">Graph</a>	Article Influence Score <a href="#">Graph</a>	% Articles in Citable Items <a href="#">Graph</a>	Normalized Eigenfactor <a href="#">Graph</a>	Average JIF Percentile <a href="#">Graph</a>
2017	8,099	4.307	4.002	4.185	1.460	248	5.1	6.3	0.01...	1.294	97.18	2.05...	81.823
2016	7,138	4.271	3.920	3.845	1.121	206	5.3	6.6	0.01...	1.208	94.17	1.90...	83.145
2015	6,984	4.909	4.563	4.074	0.995	182	5.1	6.4	0.01...	1.248	80.77	2.06...	90.481
2014	6,290	3.938	3.576	3.788	0.851	195	5.0	6.3	0.01...	1.099	87.69	1.75...	78.984
2013	5,736	3.434	3.008	3.874	0.785	233	5.1	6.0	0.01...	1.028	73.82	1.51147	72.860

Figure 5.17: Key indicators of the past five years of the magazine *Antiviral Research*.

JCR Impact Factor						
JCR Year ▼	PHARMACOLOGY & PHARMACY			VIROLOGY		
	Rank	Quartile	JIF Percentile	Rank	Quartile	JIF Percentile
2017	32/261	Q1	87.931	9/35	Q2	75.714
2016	38/257	Q1	85.409	7/34	Q1	80.882
2015	22/255	Q1	91.569	4/33	Q1	89.394
2014	42/255	Q1	83.725	9/33	Q2	74.242
2013	58/256	Q1	77.539	11/33	Q2	68.182

Figure 5.18: Impact factor of the past five years of the magazine *Antiviral Research*.

### 5.2.7 Exploring African Medicinal Plants for Potential Anti-Diabetic Compounds with the DIA-DB Inverse Virtual Screening Web Server - *Molecules* (MDPI)

In this section we present the data related to the journal where the first article that forms part of this thesis *Exploring African Medicinal Plants for Potential Anti-Diabetic Compounds with the DIA-DB Inverse Virtual Screening Web Server*. In the figures 5.19, 5.20 y 5.21 we present the quality indicators and the impact factor of the journal *Molecules* (MDPI).

**MOLECULES**  
 ISSN: 1420-3049  
 MDPI  
 ST ALBAN-ANLAGE 66, CH-4052 BASEL, SWITZERLAND  
 SWITZERLAND

[Go to Journal Table of Contents](#)   [Go to Ulrich's](#)

**Titles**  
 ISO: Molecules  
 JCR Abbrev: MOLECULES

**Categories**  
 BIOCHEMISTRY & MOLECULAR  
 BIOLOGY - SCIE;  
 CHEMISTRY, MULTIDISCIPLINARY -  
 SCIE;

**Languages**  
 English

12 Issues/Year,  
 Open Access from 1997

Figure 5.19: Title and data of the journal publishing the article *Exploring African Medicinal Plants for Potential Anti-Diabetic Compounds with the DIA-DB Inverse Virtual Screening Web Server*.

Key Indicators													
Year	Total Cites	Journal Impact Factor	Impact Factor Without Journal Self Cites	5 Year Impact Factor	Immediacy Index	Citable Items	Cited Half-Life	Citing Half-Life	Eigenfactor Score	Article Influence Score	% Articles in Citable Items	Normalized Eigenfactor	Average JIF Percentile
2017	31,047	3.098	2.787	3.268	0.550	2,223	4.1	7.5	0.05...	0.631	84.98	6.50...	57.994
2016	23,361	2.861	2.643	2.988	0.445	1,720	4.1	7.3	0.04...	0.628	84.65	5.64...	72.034
2015	17,613	2.465	2.248	2.749	0.471	1,347	3.8	7.5	0.04...	0.579	83.52	4.72...	60.169
2014	13,592	2.416	2.231	2.791	0.307	1,286	3.7	7.5	0.03...	0.605	85.93	4.15...	62.931
2013	10,380	2.095	1.902	2.638	0.315	1,003	3.5	7.7	0.02...	0.553	86.64	3.14...	49.138

Figure 5.20: Key indicators of the past five years of the magazine *Molecules* (MDPI).

JCR Impact Factor						
JCR Year ▼	BIOCHEMISTRY & MOLECULAR BIOLOGY			CHEMISTRY, ORGANIC		
	Rank	Quartile	JIF Percentile	Rank	Quartile	JIF Percentile
2017	131/293	Q2	55.461	N/A	N/A	N/A
2016	N/A	N/A	N/A	17/59	Q2	72.034
2015	N/A	N/A	N/A	24/59	Q2	60.169
2014	N/A	N/A	N/A	22/58	Q2	62.931
2013	N/A	N/A	N/A	30/58	Q3	49.138

Figure 5.21: Impact factor of the past five years of the magazine *Molecules* (MDPI).

# Bibliography

- Bajusz, D., Rácz, A., and Héberger, K. (2015). Why is tanimoto index an appropriate choice for fingerprint-based similarity calculations? *Journal of Cheminformatics*, 7:20.
- Banegas-Luna, A.-J., Cerón-Carrasco, J. P., and Pérez-Sánchez, H. (2018). A review of ligand-based virtual screening web tools and screening algorithms in large molecular databases in the age of big data. *Future Medicinal Chemistry*, 10(22):2641–2658.
- Banegas-Luna, A. J., Imbernón, B., Llanes Castro, A., Perez-Garrido, A., Ceron-Carrasco, J. P., Gesing, S., Merelli, I., D’Agostino, D., and Perez-Sanchez, H. (2019). Advances in distributed computing with modern drug discovery. *Expert Opinion on Drug Discovery*, 14(1):9–22.
- Berthold, M. R., Cebron, N., Dill, F., Gabriel, T. R., Kötter, T., Meinl, T., Ohl, P., Thiel, K., and Wiswedel, B. (2009). Knime-the konstanz information miner: version 2.0 and beyond. *AcM SIGKDD Explorations Newsletter*, 11(1):26–31.
- Birks, J. S. (2006). Cholinesterase inhibitors for alzheimer’s disease. *Cochrane Database of Systematic Reviews*, (1).
- Boulware, S., Fields, T., McIvor, E., Powell, K., Abel, E., Vasquez, K., and MacLeod, M. (2012). 2,6-Dithiopurine, a nucleophilic scavenger, protects against mutagenesis in mouse skin treated in vivo with 2-(chloroethyl) ethyl sulfide, a mustard gas analog. *Toxicology and Applied Pharmacology*, 263(2):203–209.

- Brown, F. K. et al. (1998). Chemoinformatics: what is it and how does it impact drug discovery. *Annual Reports in Medicinal Chemistry*, 33:375–384.
- Budryn, G., Zaczyńska, D., Pałecz, B., Rachwał-Rosiak, D., Belica, S., den Haan, H., Peña-García, J., and Pérez-Sánchez, H. (2016). Interactions of free and encapsulated hydroxycinnamic acids from green coffee with egg ovalbumin, whey and soy protein hydrolysates. *LWT - Food Science and Technology*, 65:823–831.
- Cerón-Carrasco, J. P., den Haan, H., Peña-García, J., Contreras-García, J., and Pérez-Sánchez, H. (2016). Exploiting the cyclodextrins ability for antioxidants encapsulation: A computational approach to carnosol and carnosic acid embedding. *Computational and Theoretical Chemistry*, 1077:65–73.
- Citro, V., Peña-García, J., Den-Haan, H., Pérez-Sánchez, H., Del Prete, R., Liguori, L., Cimmaruta, C., Lukas, J., Cubellis, M., and Andreotti, G. (2016). Identification of an allosteric binding site on human lysosomal alpha-galactosidase opens the way to new pharmacological chaperones for Fabry disease. *PLoS ONE*, 11(10).
- Cohen, P. (2002). Protein kinases — the major drug targets of the twenty-first century? *Nature Reviews Drug Discovery*, 1(4):309–315.
- den Haan, H., José Hernández Morante, J., and Pérez-Sánchez, H. (2016). Computational evidence of a compound with nicotinic  $\alpha 4\beta 2$ -ach receptor partial agonist properties as possible coadjuvant for the treatment of obesity. *The preprint server for biology (bioRxiv)*.
- den-Haan, H., Fassih, A., Bueno-Crespo, A., Soto, J., Vegara-Meseguer, J., Montoro, S. and Pérez-Sánchez, H. (2015). Application of Modern Drug Discovery Techniques in the Context of Diabetes Mellitus and Atherosclerosis. *Drug Designing: Open Access*, 04(01).
- Drews, J. (2000). Drug discovery: a historical perspective. *Science*, 287(5460):1960–1964.



- Fahimeh Ghasemi, Alireza Mehri, Jorge Peña-García, Helena den-Haan, Alfonso Pérez-Garrido, Afshin Fassihi, and Horacio Pérez-Sánchez (2015). Improving activity prediction of Adenosine A2b receptor antagonists by machine learning methods. In *International Work-Conference on Bioinformatics and Biomedical Engineering*, pages 635–644, IWBBIO.
- Fleuren, E. D. G., Zhang, L., Wu, J., and Daly, R. J. (2016). The kinome 'at large' in cancer. *Nature Reviews Cancer*, 16(2):83–98.
- Futreal, P. A., Coin, L., Marshall, M., Down, T., Hubbard, T., Wooster, R., Rahman, N., and Stratton, M. R. (2004). A census of human cancer genes. *Nature Reviews Cancer*, 4(3):177–183.
- Germain, D. P. (2010). Fabry disease. *Orphanet Journal of Rare Diseases*, 5(1):30.
- Ghosh, S., Nie, A., An, J., and Huang, Z. (2006). Structure-based virtual screening of chemical libraries for drug discovery. *Current Opinion in Chemical Biology*, 10(3):194–202.
- Gramatica, P. (2007). Principles of qsar models validation: internal and external. *QSAR & Combinatorial Science*, 26(5):694–701.
- Gray, N. S. (2006). Drug discovery through industry-academic partnerships. *Nature Chemical Biology*, 2(12):649.
- Gross, S., Rahal, R., Stransky, N., Lengauer, C., and Hoeflich, K. P. (2015). Targeting cancer with kinase inhibitors. *The Journal of Clinical Investigation*, 125(5):1780–1789.
- Imbernón, B., Cecilia, J. M., Pérez-Sánchez, H., and Giménez, D. (2017). META-DOCK: A Parallel Metaheuristic schema for Virtual Screening methods. *The International Journal of High Performance Computing Applications*.
- Jerbi, J., Springborg, M., den Haan, H., and Cerón-Carrasco, J. P. (2017). S-adenosyl-methionine analogs as enhanced methyl donors: Towards novel epigenetic regulators. *Chemical Physics Letters*, 690:74 – 81.

- Jorge Peña-García, Alfonso Pérez-Garrido, Andrés Muñoz, Helena den-Haan, Baldomero Imbernón, José Pedro Cerón-Carrasco, Antonio Banegas-Luna, Jesús Soto, and Darius Mrozek (2016). ZincFetcher: a tool for easy compound filtering from ZINC database. In *4th International Work-Conference on Bioinformatics and Biomedical Engineering*, pages 343–351, IWBBIO.
- Jorgensen, W. L. (2004). The many roles of computation in drug discovery. *Science*, 303(5665):1813–1818.
- Khan, H., Zafar, M., Den-Haan, H., Perez-Sanchez, H., and Kamal, M. A. (2018). In-silico Studies of Isolated Phytoalkaloid Against Lipoxygenase: Study Based on Possible Correlation. *Combinatorial Chemistry & High Throughput Screening*, 21(3):215–221.
- Khanna, I. (2012). Drug discovery in pharmaceutical industry: productivity challenges and trends. *Drug Discovery Today*, 17(19-20):1088–1102.
- Khoury, G. A., Baliban, R. C., and Floudas, C. A. (2011). Proteome-wide post-translational modification statistics: frequency analysis and curation of the swiss-prot database. *Scientific Reports*, 1:90.
- Klaeger, S., Heinzlmeir, S., Wilhelm, M., Polzer, H., Vick, B., Koenig, P.-A., Reinecke, M., Ruprecht, B., Petzoldt, S., Meng, C., Zecha, J., Reiter, K., Qiao, H., Helm, D., Koch, H., Schoof, M., Canevari, G., Casale, E., Depaolini, S. R., Feuchtinger, A., Wu, Z., Schmidt, T., Rueckert, L., Becker, W., Huenges, J., Garz, A.-K., Gohlke, B.-O., Zolg, D. P., Kayser, G., Vooder, T., Preissner, R., Hahne, H., Tönisson, N., Kramer, K., Götze, K., Bassermann, F., Schlegl, J., Ehrlich, H.-C., Aiche, S., Walch, A., Greif, P. A., Schneider, S., Felder, E. R., Ruland, J., Médard, G., Jeremias, I., Spiekermann, K., and Kuster, B. (2017). The target landscape of clinical kinase drugs. *Science*, 358(6367):eaan4368.
- Kola, I. and Landis, J. (2004). Can the pharmaceutical industry reduce attrition rates? *Nature Reviews Drug discovery*, 3(8):711.

- Law, V., Knox, C., Djoumbou, Y., Jewison, T., Guo, A. C., Liu, Y., Maciejewski, A., Arndt, D., Wilson, M., Neveu, V., Tang, A., Gabriel, G., Ly, C., Adamjee, S., Dame, Z. T., Han, B., Zhou, Y., and Wishart, D. S. (2013). DrugBank 4.0: shedding new light on drug metabolism. *Nucleic Acids Research*, 42(D1):D1091–D1097.
- Lei, J., Hansen, G., Nitsche, C., Klein, C., Zhang, L., and Hilgenfeld, R. (2016). Crystal structure of zika virus ns2b-ns3 protease in complex with a boronate inhibitor. *Science*, 353(6298):503–505.
- Leidenheimer, N. J. and Ryder, K. G. (2014). Pharmacological chaperoning: a primer on mechanism and pharmacology. *Pharmacological Research*, 83:10–19.
- Lukacs, G. and Verkman, A. (2011). Cftr: Folding, misfolding and correcting the f508 conformational defect. *Trends in Molecular Medicine*, 18:81–91.
- Lyne, P. D. (2002). Structure-based virtual screening: an overview. *Drug Discovery Today*, 7(20):1047–1055.
- Manning, G., Whyte, D. B., Martinez, R., Hunter, T., and Sudarsanam, S. (2002). The Protein Kinase Complement of the Human Genome. *Science*, 298(5600):1912–1934.
- Mlakar, J., Korva, M., Tul, N., Popović, M., Poljšak-Prijatelj, M., Mraz, J., Kolenc, M., Resman Rus, K., Vesnaver Vipotnik, T., Fabjan Vodušek, V., et al. (2016). Zika virus associated with microcephaly. *New England Journal of Medicine*, 374(10):951–958.
- Müller, S., Chaikuad, A., Gray, N. S., and Knapp, S. (2015). The ins and outs of selective kinase inhibitor development. *Nature Chemical Biology*, 11(11):818–821.
- Orhan, I., Senol, F., Shekfeh, S., Skalicka-Wozniak, K., and Banoglu, E. (2017). Pteryxin - A promising butyrylcholinesterase-inhibiting coumarin derivative from *Mutellina purpurea*. *Food and Chemical Toxicology*, 109:970–974.
- Orhan, I., Senol Deniz, F., Trædal-Henden, S., Cerón-Carrasco, J., den Haan, H., Peña-García, J., Pérez-Sánchez, H., Emerce, E., and Skalicka-Wozniak, K. (2019).

- Profiling Auspicious Butyrylcholinesterase Inhibitory Activity of Two Herbal Molecules: Hyperforin and Hyuganin C. *Chemistry and Biodiversity*, 16(5).
- Pereira, A., Haan, H., Peña-García, J., Moreno, M., Pérez-Sánchez, H., and Apostolides, Z. (2019). Exploring african medicinal plants for potential anti-diabetic compounds with the DIA-DB inverse virtual screening web server. *Molecules*, 24(10).
- Pérez-Garrido, A., Helguera, A. M., Guillén, A. A., Cordeiro, M. N. D., and Escudero, A. G. (2009). Convenient qsar model for predicting the complexation of structurally diverse compounds with  $\beta$ -cyclodextrins. *Bioorganic & Medicinal Chemistry*, 17(2):896–904.
- Pérez-Sánchez, H., Rezaei, V., Mezhuyev, V., Man, D., Peña-García, J., den Haan, H., and Gesing, S. (2016). Developing science gateways for drug discovery in a grid environment. *SpringerPlus*, 5(1):1300.
- Peña-García, J., den Haan, H., Caballero, A., Imbernón, B., Cerón-Carrasco, J. P., Vicente-Contreras, A., and Pérez-Sánchez, H. (2016). GrantFinder, a web based tool for the search of research grant calls. In *4th International Work-Conference on Bioinformatics and Biomedical Engineering*, pages 326–333, IWBBIO.
- Powell, K., Boulware, S., Thames, H., Vasquez, K., and MacLeod, M. (2010). 2,6-dithiopurine blocks toxicity and mutagenesis in human skin cells exposed to sulfur mustard analogues, 2-chloroethyl ethyl sulfide and 2-chloroethyl methyl sulfide. *Chemical Research in Toxicology*, 23(3):497–503.
- Pérez-Sánchez, H., Peña-García, J., den Haan, H., Rodríguez-Schmidt, R., Cerón-Carrasco, J. P., Raposo, A. N., Bouarkat, M., Sabeur, S. A., and Díaz-Baños, F. G. (2016). HYDROWEB, an Online Tool for the Calculation of Hydrodynamic Properties of Macromolecules. In Ortuño, F. and Rojas, I., editors, *Bioinformatics and Biomedical Engineering*, Lecture Notes in Computer Science, pages 82–90, IWBBIO. Springer International Publishing.

- Qing, W.-G., Powell, K., Stoica, G., Szumlanski, C., Weinshilboum, R., and Macleod, M. (1995). Toxicity and metabolism in mice of 2,6-dithiopurine, a potential chemopreventive agent. *Drug Metabolism and Disposition*, 23(8):854–860.
- Rauf, A., Farooq, U., Khan, A., Hadda, T. B., Naz, S., Ibrar, A., Jehan, N., Cerón-Carrasco, J. P., Haan, H. d., Peña-García, J., Pérez-Sánchez, H., Khan, H., Ramadan, M. F., Abu-Izneid, T., Bawazeer, S., Rauf, A., Farooq, U., Khan, A., Hadda, T. B., Naz, S., Ibrar, A., Jehan, N., Cerón-Carrasco, J. P., Haan, H. d., Peña-García, J., Pérez-Sánchez, H., Khan, H., Ramadan, M. F., Abu-Izneid, T., and Bawazeer, S. (2017). Sedative and muscle relaxant activities of diterpenoids from *Phlomischema parviflorum*. *Revista Brasileira de Farmacognosia*, 27(5):636–640.
- Ricardo Rodríguez-Schmidt, Jorge Peña-García, Alfonso Pérez-Garrido, Helena den-Haan, Andrés Bueno-Crespo, José Pedro Cerón-Carrasco, Jesús Soto, Anil Thapa, and Jon Atli-Benediktsson (2016). A hybrid machine learning and molecular modeling methodology for the prediction of novel blood anticoagulants. pages 334–342, IWBBIO.
- Ripphausen, P., Nisius, B., and Bajorath, J. (2011). State-of-the-art in ligand-based virtual screening. *Drug Discovery Today*, 16(9-10):372–376.
- Sánchez-Linares, I., Pérez-Sánchez, H., Cecilia, J. M., and García, J. M. (2012). High-throughput parallel blind virtual screening using bindsurf. *BMC Bioinformatics*, 13(14):S13.
- Schenone, M., Dančák, V., Wagner, B. K., and Clemons, P. A. (2013). Target identification and mechanism of action in chemical biology and drug discovery. *Nature Chemical Biology*, 9(4):232.
- Schneider, G. (2010). Virtual screening: an endless staircase? *Nature Reviews Drug Discovery*, 9(4):273.
- Senol, F., Ślusarczyk, S., Matkowski, A., Pérez-Garrido, A., Girón-Rodríguez, F., Cerón-Carrasco, J., den Haan, H., Peña-García, J., Pérez-Sánchez, H., Do-

- maradzki, K., and Orhan, I. (2017). Selective in vitro and in silico butyrylcholinesterase inhibitory activity of diterpenes and rosmarinic acid isolated from *Perovskia atriplicifolia* Benth. and *Salvia glutinosa* L. *Phytochemistry*, 133:33–44.
- Shivakumar, D., Williams, J., Wu, Y., Damm, W., Shelley, J., and Sherman, W. (2010). Prediction of Absolute Solvation Free Energies using Molecular Dynamics Free Energy Perturbation and the OPLS Force Field. *Journal of Chemical Theory and Computation*, 6(5):1509–1519.
- Sánchez-Pérez, A., Muñoz, A., Peña-García, J., den Haan, H., Bekas, N., Katsikoudi, A., Tzakos, A. G., and Sánchez, H. P. (2015). DIA-DB: A Web-Accessible Database for the Prediction of Diabetes Drugs. In *Bioinformatics and Biomedical Engineering - Third International Conference, IWBBIO 2015, Granada, Spain, April 15-17, 2015. Proceedings, Part II*, pages 655–663.
- Tapia-Abellán, A., Angosto-Bazarra, D., Martínez-Banaclocha, H., de Torre-Minguela, C., Cerón-Carrasco, J. P., Pérez-Sánchez, H., Arostegui, J. I., and Pelegrin, P. (2019). Mcc950 closes the active conformation of nlrp3 to an inactive state. *Nature Chemical Biology*, 15(6):560.
- W Loo, T., Claire Bartlett, M., and Clarke, D. (2002). Introduction of the most common cystic fibrosis mutation (f508) into human p-glycoprotein disrupts packing of the transmembrane segments. *The Journal of Biological Chemistry*, 277:27585–8.
- Wild, D. J. and Wiggins, G. D. (2006). Challenges for chemoinformatics education in drug discovery. *Drug Discovery Today*, 11(9-10):436–439.
- Wu, P., Nielsen, T. E., and Clausen, M. H. (2015). FDA-approved small-molecule kinase inhibitors. *Trends in Pharmacological Sciences*, 36(7):422–439.
- Yar, M., Shahzadi, L., Farooq, A., Jalil Imran, S., Cerón-Carrasco, J. P., den Haan, H., Kumar, S., Peña-García, J., Pérez-Sánchez, H., Grycova, A., Dvorak, Z., and Vrzal, R. (2017). In vitro modulatory effects of functionalized pyrimidines and piperidine derivatives on Aryl hydrocarbon receptor (AhR) and glucocorticoid receptor (GR) activities. *Bioorganic Chemistry*, 71:285–293.

Yuan, S. Chan, J. Y. K. d.-H. H. P.-G. J. C.-C. J. and Pérez-Sánchez, H. (PCT/CN2017/088420, US 62491007 (2017). Patent pending). Zika virus protease inhibitors and methods of use thereof.

Yuan, S., Chan, J.-W., den Haan, H., Chik, K.-H., Zhang, A., Chan, C.-S., Poon, V.-M., Yip, C.-Y., Mak, W.-N., Zhu, Z., Zou, Z., Tee, K.-M., Cai, J.-P., Chan, K.-H., de la Peña, J., Pérez-Sánchez, H., Cerón-Carrasco, J., and Yuen, K.-Y. (2017). Structure-based discovery of clinically approved drugs as Zika virus NS2b-NS3 protease inhibitors that potently inhibit Zika virus infection in vitro and in vivo. *Antiviral Research*, 145:33–43.

Ślusarczyk, S., Senol Deniz, F., Woźniak, D., Pecio, Pérez-Sánchez, H., Cerón-Carrasco, J., Stochmal, A., den Haan Alonso, H., Matkowski, A., and Orhan, I. (2019). Selective in vitro and in silico cholinesterase inhibitory activity of isoflavones and stilbenes from *Belamcandae chinensis* rhizoma. *Phytochemistry Letters*, 30:261–272.